Final Report

Enhancement of FDOT's SERF Device and a Study of Erosion Rates of Rock, Sand, and Clay Mixtures using FDOT's RETA and SERF Equipment

BDK75 977-09
UF Project 00074057

Submitted by:

David Bloomquist, Ph.D., P.E.
Raphael Crowley, Ph.D., E.I.

Department of Civil and Coastal Engineering
University of Florida
Gainesville, Florida 32611

Developed for the

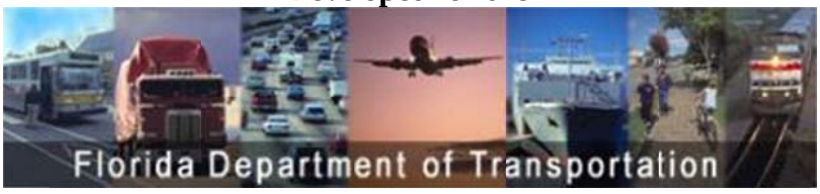

Rick Renna, P.E., Project Manager
October 2010

Disclaimer

The opinions, findings, and conclusions expressed in this publication are those of the author and not necessarily those of the State of Florida Department of Transportation.

SI (MODERN METRIC) CONVERSION FACTORS (from FHWA)

APPROXIMATE CONVERSIONS TO SI UNITS

SYMBOL	WHEN YOU KNOW	MULTIPLY BY	TO FIND	SYMBOL
LENGTH				
in	inches	25.4	millimeters	mm
ft	feet	0.305	meters	m
yd	yards	0.914	meters	m
mi	miles	1.61	kilometers	km
SYMBOL	**WHEN YOU KNOW**	**MULTIPLY BY**	**TO FIND**	**SYMBOL**
AREA				
in^2	square inches	645.2	square millimeters	mm^2
ft^2	square feet	0.093	square meters	m^2
yd^2	square yard	0.836	square meters	m^2
ac	acres	0.405	hectares	ha
mi^2	square miles	2.59	square kilometers	km^2
SYMBOL	**WHEN YOU KNOW**	**MULTIPLY BY**	**TO FIND**	**SYMBOL**
VOLUME				
fl oz	fluid ounces	29.57	milliliters	mL
gal	gallons	3.785	liters	L
ft^3	cubic feet	0.028	cubic meters	m^3
yd^3	cubic yards	0.765	cubic meters	m^3
NOTE: volumes greater than 1000 L shall be shown in m^3				
SYMBOL	**WHEN YOU KNOW**	**MULTIPLY BY**	**TO FIND**	**SYMBOL**
MASS				
oz	ounces	28.35	grams	g
lb	pounds	0.454	kilograms	kg
T	short tons (2000 lb)	0.907	megagrams (or "metric ton")	Mg (or "t")
SYMBOL	**WHEN YOU KNOW**	**MULTIPLY BY**	**TO FIND**	**SYMBOL**
TEMPERATURE (exact degrees)				
^oF	Fahrenheit	5 (F-32)/9 or (F-32)/1.8	Celsius	^oC
SYMBOL	**WHEN YOU KNOW**	**MULTIPLY BY**	**TO FIND**	**SYMBOL**
ILLUMINATION				
fc	foot-candles	10.76	lux	lx
fl	foot-Lamberts	3.426	candela/m^2	cd/m^2
SYMBOL	**WHEN YOU KNOW**	**MULTIPLY BY**	**TO FIND**	**SYMBOL**
FORCE and PRESSURE or STRESS				
lbf	pound force	4.45	newtons	N
lbf/in^2	pound force per square inch	6.89	kilopascals	kPa

APPROXIMATE CONVERSIONS TO ENGLISH UNITS

SYMBOL	WHEN YOU KNOW	MULTIPLY BY	TO FIND	SYMBOL
LENGTH				
mm	millimeters	0.039	inches	in
m	meters	3.28	feet	ft
m	meters	1.09	yards	yd
km	kilometers	0.621	miles	mi
SYMBOL	**WHEN YOU KNOW**	**MULTIPLY BY**	**TO FIND**	**SYMBOL**
AREA				
mm^2	square millimeters	0.0016	square inches	in^2
m^2	square meters	10.764	square feet	ft^2
m^2	square meters	1.195	square yards	yd^2
ha	hectares	2.47	acres	ac
km^2	square kilometers	0.386	square miles	mi^2
SYMBOL	**WHEN YOU KNOW**	**MULTIPLY BY**	**TO FIND**	**SYMBOL**
VOLUME				
mL	milliliters	0.034	fluid ounces	fl oz
L	liters	0.264	gallons	gal
m^3	cubic meters	35.314	cubic feet	ft^3
m^3	cubic meters	1.307	cubic yards	yd^3
SYMBOL	**WHEN YOU KNOW**	**MULTIPLY BY**	**TO FIND**	**SYMBOL**
MASS				
g	grams	0.035	ounces	oz
kg	kilograms	2.202	pounds	lb
Mg (or "t")	megagrams (or "metric ton")	1.103	short tons (2000 lb)	T
SYMBOL	**WHEN YOU KNOW**	**MULTIPLY BY**	**TO FIND**	**SYMBOL**
TEMPERATURE (exact degrees)				
^oC	Celsius	1.8C+32	Fahrenheit	^oF
SYMBOL	**WHEN YOU KNOW**	**MULTIPLY BY**	**TO FIND**	**SYMBOL**
ILLUMINATION				
lx	lux	0.0929	foot-candles	fc
cd/m^2	$candela/m^2$	0.2919	foot-Lamberts	fl
SYMBOL	**WHEN YOU KNOW**	**MULTIPLY BY**	**TO FIND**	**SYMBOL**
FORCE and PRESSURE or STRESS				
N	newtons	0.225	pound force	lbf
kPa	kilopascals	0.145	pound force per square inch	lbf/in^2

*SI is the symbol for the International System of Units. Appropriate rounding should be made to comply with Section 4 of ASTM E380.(Revised March 2003)

Technical Report Documentation Page

<table>
<tr><td>1. Report No.</td><td>2. Government Accession No.</td><td colspan="2">3. Recipient's Catalog No.</td></tr>
<tr><td colspan="2" rowspan="2">4. Title and Subtitle
Enhancement of FDOT's SERF Device and a Study of Erosion Rates of Rock, Sand, and Clay Mixtures using FDOT's RETA and SERF Equipment

BDK-75-977-09
UF Project 00074057</td><td colspan="2">5. Report Date
October 2010</td></tr>
<tr><td colspan="2">6. Performing Organization Code</td></tr>
<tr><td colspan="2">7. Author(s)
David Bloomquist, Raphael Crowley</td><td colspan="2">8. Performing Organization Report No.</td></tr>
<tr><td colspan="2" rowspan="2">9. Performing Organization Name and Address
Department of Civil and Coastal Engineering
365 Weil Hall
University of Florida
Gainesville, Florida 32611</td><td colspan="2">10. Work Unit No.</td></tr>
<tr><td colspan="2">11. Contract or Grant No.
BDK-75-977-09</td></tr>
<tr><td colspan="2" rowspan="2">12. Sponsoring Agency Name and Address
Florida Department of Transportation
605 Suwannee Street, MS 30
Tallahassee, FL 32399</td><td colspan="2">13. Type of Report and Period Covered
Draft Report
5/1/2008 – 10/31/2010</td></tr>
<tr><td colspan="2">14. Sponsoring Agency Code</td></tr>
<tr><td colspan="4">15. Supplementary Notes</td></tr>
<tr><td colspan="4">16. Abstract
The primary cause of bridge failure in the United States is scour, or erosion of bed material around the bridge's foundations. Over the years, equations and predictive methods have been developed to predict erosion depths around a bridge's substructure. The most effective of these predictive methods for situations where cohesive material, or earth material that is composed of clayey or rock-like elements, is present require the input of a parameter known as a sediment transport function. A sediment transport function is simply a relationship between flow conditions and erosion rate of the bed material in the absence of the structure. Theoretical methods exist for predicting sediment transport functions, but they are difficult to compute. Current design standards recommend measuring sediment transport functions in a laboratory. Until now, there has been some question as to how to do this properly. Work in this report helps to answer this question.</td></tr>
<tr><td colspan="2">17. Key Word
Erosion, laboratory testing, flume, shear stress, scour</td><td colspan="2">18. Distribution Statement
No restrictions.</td></tr>
<tr><td>19. Security Classif. (of this report)
Unclassified.</td><td>20. Security Classif. (of this page)
Unclassified.</td><td>21. No. of Pages
323</td><td>22. Price</td></tr>
</table>

TABLE OF CONTENTS

page

LIST OF TABLES

LIST OF FIGURES

EXECUTIVE SUMMARY

Scour is the primary cause of bridge failures in the United States. Although predicting scour depths for non-cohesive (sandy) bed materials is fairly well understood, much less is known about predicting scour depths when cohesive materials such as clays, sand-clay mixtures, and rock are present. Two semi-empirical methods exist for predicting scour depths. Both of these methods rely on the input of a sediment transport function. Current design guidelines recommend measuring sediment transport functions in a laboratory, but there has been some question as to how to do this properly.

To answer this question, a series of improvements and enhancements were made to the Sediment Erosion Rate Flume (SERF). A laser leveling system, a vortex generator, a shear stress measuring system, computer updates, and a sediment control system were designed. With the exception of the sediment control system, new updates functioned as designed. Using the new shear stress system, a series of tests were run to assess the proper way to measure shear stress in a flume-style erosion rate testing device. Results showed that the pressure drop method appears not to measure shear stress properly. A correlation was developed between bed shear stress and grain size that may provide a proper means of estimating shear stress in flume-style erosion rate testing device. A new material was developed for testing in both the SERF and the Rotating Erosion Testing Apparatus (RETA) to serve as a basis of comparison between the two instruments. Results were inconclusive because rock-like erosion described by the Stream Power Model appeared to dominate erosion. A database of results from the RETA was used to verify that it is measuring the correct erosion rate vs. shear stress relationships. Results appeared to show that for the special case where particle-like erosion dominates, the RETA appears to produce correct results. Results also indicate that when rock-like erosion is present, it is generally an order of magnitude lower than situations where particle-like erosion dominates. Further analysis of the database showed that there may be a correlation between material strength and erosion rate. Further research was aimed at generalizing erosion rate vs. shear stress relationships for sand-clay mixtures. A series of tests were conducted on a variety of sand-clay mixtures. Results showed hypersensitivity to the method in which the sand-clay mixtures were prepared. Rock-like erosion and particle-like erosion were present in most sand-clay mixtures

even though typical sand-clay mixtures would not typically be described as “rock-like materials.” Recirculating sediment during sand-clay testing indicated that suspended sediment in the SERF has little effect on bed shear stress.

CHAPTER 1
INTRODUCTION

1.1 Motivation for Research

In 1987, the Schoharie Creek Bridge on the I-90 Thruway corridor in upstate New York collapsed resulting in the loss of four cars, a truck, and most importantly 10 lives (Figure 1-1). The collapse of this bridge led to an investigation by the Federal Highway Administration (FHWA), where they found that the bridge collapsed because of the loss of support capacity of the bridge's footings due to scour (Trammel 2004).

Figure 1-1. Photograph of the Schoharie Creek Bridge Collapse

In 1989, largely as a result of the Schoharie Creek Bridge failure, the United States Geological Survey (USGS) and the Federal Highway Administration (FHWA) launched a cooperative study to monitor and assess the scour problem on bridges in the United States (Placzek and Haeni 1995). This study found that scour was a much greater issue than anyone had previously realized. The results of this study were two-fold: first, engineers for the first time began to realize how large of an issue scour was in the United States; secondly, the first edition of the Hydraulic Engineering Circular No. 18 (HEC-18) Evaluating Scour at Bridges was

published in 1991. This document was the first reliable method that engineers in the United States had for designing for bridge scour.

Shortly after the Schoharie Creek Bridge collapse in 1987, Murillo determined that from 1961 to 1976, 48 of 86 major bridge failures in the United States, or 56%, were the result of scour near the bridge piers (Murillo 1987). Other studies were conducted after Murillo's research to give even more credence to the scour problem, and some of these studies are cited in the latest edition, the 4th edition, of HEC-18. According to HEC-18, the most common cause of bridge failure is from scour (Richardson and Davis 2001). Although the Schoharie Creek Bridge collapse was one of the most publicized bridge failure of the 1980's, FHWA determined that during the floods of 1985 and 1987, 16 other bridges in New York and New England also failed because of scour. In 1985, 73 bridges were destroyed by floods in Pennsylvania, West Virginia, and Virginia. The 1993 floods in the Mississippi Basin caused 23 bridges to fail, and the total cost of these failures was estimated to be $15 million. Of these 23 bridges, over 80% of them failed because of scour. In 1994, flooding from Tropical Storm Alberto in Georgia caused scour damage to over 150 bridges resulting in damage costs of approximately $130 million (Jones et al. 1995). In 2004, Briaud launched another study to quantify the scour problem. He determined that there are 600,000 bridges in the United States and of these 600,000 bridges, one-third of them are scour critical. Over 1,000 bridges have sustained significant damage due to scour, and it costs approximately $50 million per year on average to keep up with this issue (Briaud 2004).

Because engineers had no method for scour design for so long, it is not surprising that the scour problem is so severe with regard to existing bridges. Now that HEC-18 exists, engineers are starting to get a better handle on the scour problem, and based on the data just presented, this is essential. The main downside though to HEC-18 is that several engineers – some engineers at the FDOT for example – believe that some of its guidelines for designing new bridges are overly conservative (Slagle 2006). The complaint of many engineers is that HEC-18 takes a reactionary approach with regard to design specifications for the scour problem (Trammel 2004). The goal of this report is to investigate some of these design specifications presented in HEC-18. Before getting into specifics however, the general concepts of scour as presented in HEC-18 will be discussed.

1.1 Scour Definitions

HEC-18 divides scour into four subcategories, general scour, aggradation/degradation, contraction scour, and local scour. When designing a structure over a waterway, an engineer is instructed to compute the amount of scour caused by each of these four components and add their total effects together to get the total net scour depth.

1.1.1 General Scour

General scour describes channel migrations, tidal inlet instability, or river meanders. It is different from other types of scour because it may not produce a net reduction in sediment at the bridge section. However, the bed elevation at a particular locus can be raised or lowered because of the channel migration. Manmade disruptions such as water redirection structures may contribute to general channel migration (Slagle 2006). General scour occurs at a much slower rate than other types of scour (cm per year vs. cm per storm event), it is generally better understood than other scour mechanisms, and it is not the focus of this report.

1.1.2 Aggradation/Degradation

Aggradation and degradation refer to long-term elevation changes due to natural or unnatural changes in the sediment system. Aggradation refers to deposition of sediment previously eroded from an upstream location while degradation refers to erosion of sediment due to a deficit of upstream sediment supply (Slagle 2006). These processes are also better understood than the remaining two scour mechanisms and are not discussed further in this report.

1.1.3 Contraction Scour

Contraction scour is a decrease in bed elevation in a channel caused by a reduction in cross sectional area of the channel. The cross sectional area of the channel may be reduced by either the presence of a structure such as a bridge pier or a natural obstruction such as a block of ice or debris. Flow rate is given as $Q = VA$ where V is the average flow velocity and A is the cross sectional area of the channel. Because of continuity, Q must be constant upstream and downstream from any obstruction within the channel. Therefore, when an obstruction is present, velocity must increase and the water moving through the channel must accelerate past the

obstruction. This increase in water velocity results in higher forces along the bed, and these higher forces result in greater bed shear stresses. Greater bed shear stresses in turn cause greater erosion rates, or scour, in the vicinity of the structure. Scour will continue under these conditions until a depth is reached where the bed shear stress reverts to sub-critical levels or the sediment deposition rate equals the sediment erosion rate (Richardson and Davis 2001). Work completed in this report can potentially be used to improve understanding of the contraction scour problem.

1.1.4 Local Scour

Local scour is the most complicated scour mechanism, because it is caused by a series of events that occur nearly simultaneously. Any obstruction in a waterway will cause flow dynamics in the direct vicinity of the structure to change. A pier will be used as a simple example to illustrate how these hydrodynamic changes affect the bed material in the vicinity of the structure.

A protruding pier in a free stream will cause a pile-up effect of water on its upstream face, which in turn will cause a downflow along this face. When water from the downflow reaches the bed, it spawns secondary flows, or horseshoe vortices, along the bed. The velocity of water within these vortices is often fast enough to exceed the critical velocity, or velocity for incipient motion of sediment particles, of the bed. Subsequently, a scour hole forms around the base of the pier. Scour will continue until the vortices weaken sufficiently such that either deposition rate equals erosion rate or the vortex velocity is less than the critical velocity of the bed material. Figure 1-2 and Figure 1-3 illustrate the process of local scour (Slagle 2006).

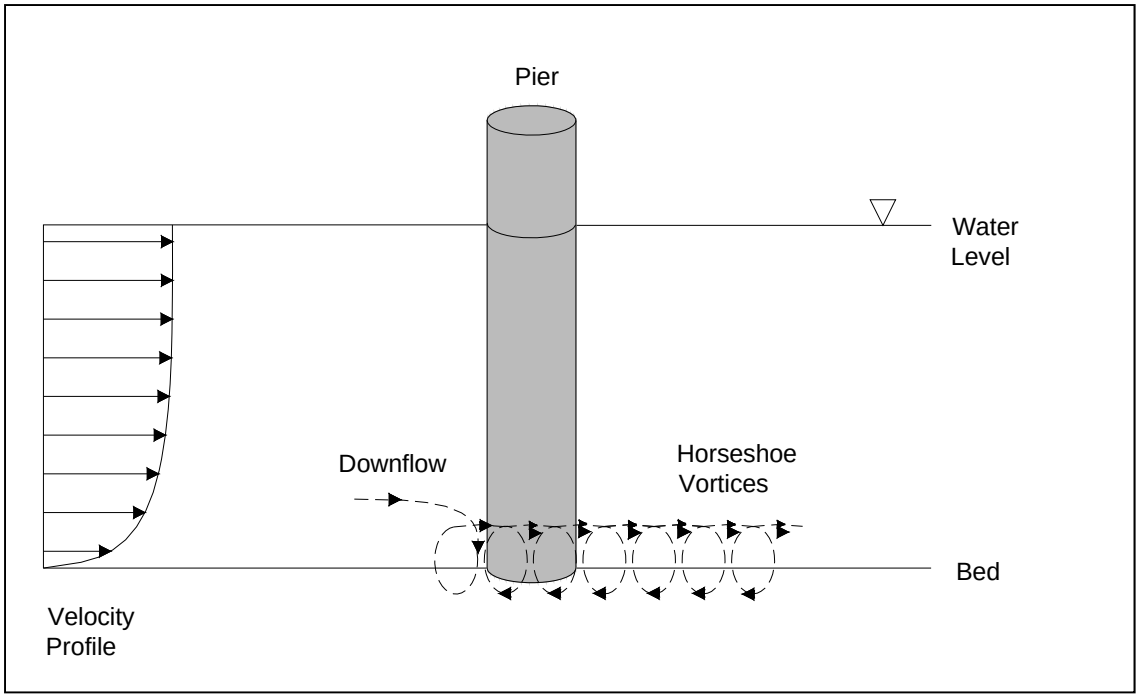

Figure 1-2. Beginning of local scour (Slagle 2006)

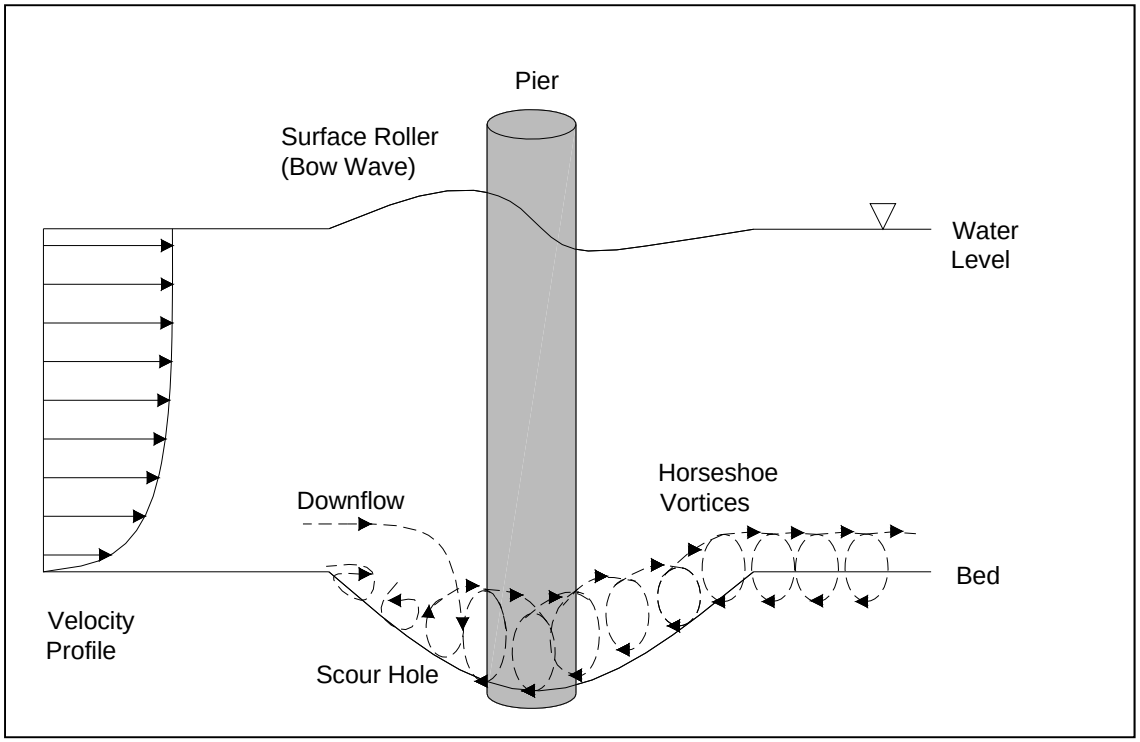

Figure 1-3. Local scour after some time has elapsed (Slagle 2006)

1.2Controversy Surrounding HEC-18

As mentioned in Section 1.1, when HEC-18 was introduced in 1991 it was the first document like it in the United States. Its importance cannot be overlooked or understated – for the first time, engineers had a reliable set of guidelines to use for designing a structure to withstand mechanisms associated with scour. Despite its benefits, HEC-18 has been somewhat controversial due to certain design guidelines that may be overly conservative. The scour problem is already so large, so problematic, and so expensive, that avoiding an overly conservative approach is necessary. If scour can be better understood, and if more accurate equations can be developed, overestimation of scour depths may be avoided. This result could be remarkable – millions of dollars could be saved every year in construction costs, or better yet, this money could be allocated to mitigate existing bridges that already have well-documented scour problems.

Much of the controversy surrounding HEC-18 stems from its approach with regard to computing scour for cohesive bed materials. Although cohesionless sediments such as sands will erode much faster than cohesive soils and rock, HEC-18 assumes that even bed materials that are resistant to scour will erode to the same depths as sands given enough time. The 4th edition of HEC-18 does cite the Briaud 2004 EFA-SRICOS method as an alternative for designing foundations on cohesive bed material, but according the HEC-18, Briaud found that clays erode to the same depth as sands eventually, and the EFA-SRICOS method should only be used under certain conditions. HEC-18 acknowledges that this finding may be overly conservative. Specifically it says:

> "The equations and methodologies presented in this manual, which predict the maximum scour depth in non-cohesive soil, may, in some circumstance be too conservative. The pier scour equation represents an envelope curve of the deepest scour observed during the various laboratory studies and field data." (Richardson and Davis 2001)

With regard to rock scour, HEC-18 gives Annandale's Erodibility Index Method (Annandale 2005) for predicting scour depths, but acknowledges that this method "needs further research."

In response to these controversies, Florida Department of Transportation (FDOT) has been sponsoring research in the area of cohesive scour and rock scour in the past ten years. FDOT has worked in conjunction with the University of Florida (UF) to develop experimental mechanisms for determining erosion rates of bed materials as a function of other bulk material

properties. Results from some of this research have been used in recent FDOT bridge designs. Although progress has been made in this area, more research needs to be done.

1.3Approach

As previously mentioned, HEC-18 cites the EFA-SCRIOS method as an alternative option when designing bridge foundations that rest on cohesive and rock-like beds. Integral to implementation of the EFA-SRICOS method is the ability to accurately obtain a relationship between erosion rate and shear stress. In 2003, Miller and Sheppard developed an analytical model for predicting scour hole depth for a non-cohesive soil. Although cohesive scour holes are shaped differently than non-cohesive scour holes (Ting et al. 2001), the EFA-SRICOS method, which is empirically based seems to agree in principle with the overall theme of the Miller Sheppard approach – namely that erosion rate, and in turn scour depth, should be a function of bed shear stress under particle-like erosion conditions. This agreement between the two methods, which were developed independently from one another, appears to be a positive sign and serves as a rudimentary indication that an erosion rate vs. shear stress relationship appears to be physically valid and useful.

In nature, this correlation of shear stress to erosion rate is important because there is a definitive relationship between stream velocity. In general, faster flow velocities produce larger bed shear stresses. Using modern computer models (for example, the EFA-SRICOS method uses a k-ε approach), bed shear stresses can be computed fairly accurately for a situation where water flows past a protruding pile or bridge pier. A k-ε model is a commonly used turbulence closure model that employs the use of a turbulent kinetic energy equation (the "k" component) and a turbulent dissipation equation (the "ε" component).

This relationship between stream velocity and shear stress is critical for implementation of either the EFA method or the Miller-Sheppard approach because if a designer has a stream hydrograph, a predictive time-series of stream velocities and corresponding shear stresses can be approximated. Given this time series of stream velocities, a corresponding time series of shear stresses can be determined using the shear stress-velocity relationship under natural conditions. With this shear stress information, final local scour depths can be computed – assuming the relationship between erosion rate and shear stress is known for the bed material in question.

This final step is where the aforementioned semi-empirical methods tend to struggle and where the crux of research for this report rests. To properly implement either alternative design approach, there needs to be a way to accurately measure shear stresses and corresponding erosion rates for an eroding bed material. Although this sounds simple, it is very complicated. The purposes of this report then are to:

1. Develop test equipment to measure erosion rates and shear stresses for a wide range of eroding bed materials.

2. Use these equipment upgrades and other analytical techniques to comment quantitatively on older methods for measuring these parameters by running a series of tests with the new equipment.

3. Use these new measurements and older results to determine if erosion rate can be related to any other existing common geotechnical parameters.

4. Use the new equipment to develop a series of erosion rate-shear stress curves for sand clay mixtures. Under natural conditions, it is rare to find a bed material that is purely cohesive or purely non-cohesive. Instead, usually sand is interspersed with clay particles or vice versa. Previous research has looked mostly to classify erosion rate-shear stress curves under conditions where a uniform material is present, but because this is rarely the case, erosion properties of mixtures is investigated.

1.4Methodology and Organization

To meet these goals, the following methodology was used:

1. An existing piece of equipment, the Sediment Erosion Rate Flume (SERF), was enhanced so that it could more accurately measure erosion rates and shear stresses for eroding bed materials.

2. A nearly-uniform material, Gator Rock, was developed so that it could be tested in the SERF and the Rotating Erosion Testing Apparatus (RETA). The original goal with the development of Gator Rock was to use it to directly compare the two devices. Although this direct comparison between the RETA and SERF did not go as planned, the development of Gator Rock is still significant.

3. A series of tests was conducted in the SERF where shear stress was measured for samples containing various uniform roughness. The results were compared with analytical shear stress estimates used by other flume style devices similar to the SERF such as the erosion function apparatus (EFA), and Sediment Erosion and Depth Flume (SEDFlume).

4. Extensive data analysis was conducted on an existing database where RETA results are contained. The goal was first to verify that the RETA was properly measuring erosion rate and shear stresses under particle-like erosion conditions. Once this was shown, the second goal was to find another geotechnical parameter that could be used to predict erosion rate.

5. A series of tests was conducted in the RETA on the new Gator Rock samples. Similar-style tests were concurrently conducted in the SERF. As discussed in (3), the direct comparison between the two devices did not go as planned. Still, results from this dataset are interesting, and they should be discussed. Additionally, tensile and compressive strength tests were run on the Gator Rock samples to determine the material's strength characteristics.

6. A series of tests was conducted in the SERF on sand-clay mixtures. Previously, the SERF was not usable when clay was present in the bed material because the old sample leveling devices – a series of ultrasonic probes – would penetrate into the sample. Because of the enhancements to the SERF discussed in (1), clay testing is now possible. Tensile strength, compressive strength, and density profile tests were also conducted on the sand-clay mixtures to try to explain (and eventually quantify) differential erosion rates that were observed both within the samples and from a sample-to-sample standpoint.

This report is organized in the following manner:

1. Chapter 2 presents an in-depth background discussion and a literature review.

2. Chapter 3 presents a summary and a discussion of the SERF including improvements and enhancements to the device completed as part of this report.

3. Chapter 4 presents a discussion on the shear stress tests that were conducted in the SERF.

4. Chapter 5 presents a discussion on the development of Gator Rock and preliminary tests with it.

5. Chapter 6 presents a discussion on RETA database analysis.

6. Chapter 7 provides a discussion on sand-clay tests in the SERF.

7. Chapter 8 provides a brief discussion regarding conclusions and recommendations for future work.

8. Appendix A chronicles the state-of-the art in sand scour prediction.

9. This report should be read in conjunction with its sister document, *Operation Manual for the Sediment Erosion Rate Flume Second Edition*, which provides an in-depth overview of the SERF, testing with the instrument, and all associated computer programs for the device.

CHAPTER 2
BACKGROUND AND LITERATURE REVIEW

2.1 Scour Depths in Non-Cohesive Soil

When design guidelines such as HEC-18 were being developed for scour, the non-cohesive problem was addressed first for two reasons. First, predicting scour or erosion is less complex under a non-cohesive condition than it when cohesive sediments are present because cohesive forces do not need to be taken into account. Secondly, if non-cohesive assumptions are used for cohesive soils, the result will be conservative because cohesive forces will only serve to slow erosion and decrease the equilibrium local scour depth. Therefore, even if non-cohesive materials are not well understood, non-cohesive equations can be used for design, and the structure's foundation will not fail.

Because of these reasons, when the scour problem was first being tackled, most research for predicting local scour focused on non-cohesive conditions. From this research, HEC-18 was developed (Richardson and Davis 2001). Using guidelines from these manuals, engineers can compute equilibrium scour depths for a variety of complex bridge piers under stream flow from any attack angle. Specifics for scour design from these manuals are presented in Appendix A.

2.2 Predicting Local Scour Hole Depth for Cohesive Soils and Rock

In Chapter 1, four different scour modes were briefly outlined – aggradation/degradation, general scour, contraction scour, and local scour. Local scour is the most complicated, most interesting, and often the most significant source of scour for bridge foundations. Most of HEC-18 involves predicting local scour depths. If the design guidelines presented in HEC-18 are to be modified for cohesive conditions, it is logical to start with methods for predicting local scour depths.

There are two known methods available for computing local scour depths for cohesive soils – the scour reduction method and a semi-empirical approach. Under the scour reduction method, scour depth is computed as if a foundation's bed material is non-cohesive. Then, a scour-reduction factor is applied, and the final equilibrium scour depth is computed. Under the

semi-empirical methods (of which there are also two), a more sophisticated approach is used where scour depth is estimated as a function of bulk material erosion rate.

To compute scour depth for rock, HEC-18 becomes somewhat muddled. HEC-18 briefly mentions that the erodibility index method (ERI) may be usable, but this method is not discussed in depth. Some qualitative techniques are presented for determining whether or not a rock may or may not erode, but as far as predicting an actual local scour depth, the only reliable method that is given is a permutation of the cohesive soil semi-empirical approaches where again bulk material erosion rate ultimately determines scour depth.

2.2.1 Colorado State University Tests (CSU 1991 - 1996)

From 1991 – 1996, tests were conducted at Colorado State University (CSU) to test the effects of sediment gradation and cohesion on scour development. During these tests, 20-non cohesive sediments and 10 cohesive sediment mixtures were tested in five flumes of varying sizes with nine different cylindrical pier sizes and seven different abutment protrusion lengths. Flumes for these tests were open-channel and filled with sediment such that as flow eroded the sediment, a scour hole could be measured. Molinas' synthesis report divides the tests into four sections (Molinas 2003):

1. Effects of gradation and coarse material fraction from pier scour tests.
2. Effects of gradation and coarse material fraction on abutment scour tests.
3. Effects of cohesion on pier scour tests.
4. Effects of cohesion on abutment scour tests.

Of particular interest are the portions of these tests pertaining to cohesion effects on pier scour.

2.2.1.1 Setup for CSU Tests

These tests were conducted in three flumes at CSU: the first flume was 2.4 m wide by 60 m long; the second flume was 5 m wide by 30 m long; and the third flume was 1.2 m wide by 12 m long. Circular piers of 0.15 m diameter were used with a constant approach depth of 0.24 m.

Velocity was measured in these flumes via a magnetic flow-meter, and approach velocity was found from depth and width integrated averages of vertical velocity profiles. Approach depth was determined from width and length-averaged values of water elevation. Scour depth

was measured during and at the end of each test by measuring the difference between minimum bottom elevation in the scour hole and maximum elevation away from the structure. Investigators at CSU used a combination of Montmorillonite clays and sand that had a median diameter of 0.55 mm and a gradation of 2.43 (Molinas 2003).

2.2.1.2 Results from CSU Tests

Results from the CSU tests, which were run for 16 hours, are presented in Figure 2-1.

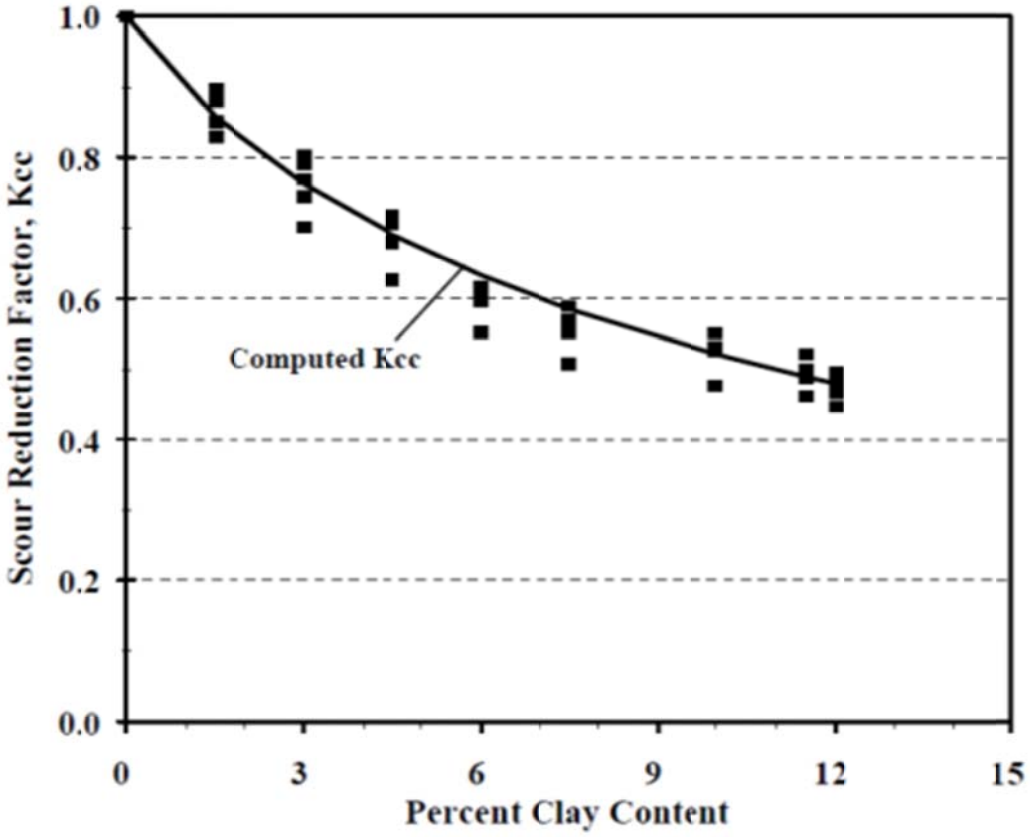

Figure 2-1. Results from CSU Pier Scour Study (Molinas 2003)

The best-fit trend line through this data was:

$$K_{CC} = \frac{1}{1 + \left(CC/11\right)^{0.9}} \tag{2-1}$$

where K_{CC} is a scour reduction factor to be applied to the sand-scour equations in HEC-18 and CC is clay content. Sand-clay mixtures with clay contents higher than 11% were found to be

dominated by initial water content and consolidation. Because these factors were not controlled in this round of tests, they were not included in finding the correction factor for clay content (Molinas 2003).

2.2.1.3 Concerns with the CSU Correction Factor

In his 2006 master's thesis, Slagle argues that the grain size standard deviation of 2.43 is probably too large for accurate testing. Grain size standard deviation was computed using Equation 2-2:

$$\sigma_g = \frac{1}{2}\left(\frac{D_{84}}{D_{50}} + \frac{D_{50}}{D_{16}}\right) \tag{2-2}$$

where *D*'s are the grain size (mm) at the particular percent passing

This relatively large grain size standard deviation is a concern because of the potential for armoring effects. Larger sand grain particles require stronger forces to incite incipient motion than smaller particles. At lower flow rates then, fine grained material is transported while larger particles are left in place. Eventually, these large particles settle into voids created by the smaller particles, and thus, an armoring layer develops along the top of the bed. When velocities increase in the channel, the armor layer will scour away. This will expose the smaller diameter particles and cause a faster erosion rate. The question then, is if the scouring resistance was truly due to cohesive forces or if it was a result of these artificially created armoring effects (Slagle 2006)?

The second area of concern with the CSU equation is with regard to recirculating flumes. Two of CSU's flumes allow sediment to erode and remain in the flow. The presence of sediments in the water column changes clear water conditions to live bed conditions. This may change the scour rate. These areas of concern gave credence to the notion that further investigation needed to be conducted to determine scour rates for sand-clay mixtures.

2.2.2 The EFA-SRICOS Method

Recall from Chapter 1 that HEC-18 does offer one alternative design approach for designing local scour depths for foundations built on cohesive soils and rock – the EFA-SRICOS

method. As explained in HEC-18, the EFA-SRICOS method is not written in its entirety; rather, HEC-18 offers an elementary version of this method.

2.2.2.1 HEC-18 Version of EFA-SRICOS Method

According to HEC-18, the EFA-SRICOS method may be used as an alternative approach for scour design when either rock-like or cohesive bed material is present. Under the HEC-18 version of the method, first statistical storm data is used to determine a hydrograph of stream flow conditions during the lifespan of the structure. Then, based on this hydrograph of flow velocity, Equation 2-3 is used to determine the shear stress on the stream bed:

$$\tau_{\max} = 0.0094 \rho V^2 \left[\frac{1}{\log \mathrm{Re}} - \frac{1}{10} \right] \tag{2-3}$$

where ρ is the density of water, V is the fluid velocity, and Re is the Reynolds Number.

Next, an engineer takes a soil sample of sediment at the foundation site. Then, using an erosion rate testing device (which will be discussed in Section 2.4.2), a relationship must be found between erosion rate and shear stress. Once erosion rate-shear stress relationship is known and the stream hydrograph is known, the final scour depths can be computed based on these two relationships.

2.2.2.2 Complete Version of EFA-SRICOS Method

The HEC-18 version of the EFA-SRICOS method is rather elementary, and in his papers, Briaud offers a more complete version of the method. The first step and second steps from both HEC-18 and Briaud's papers are the same. The engineer must compute a hydrograph of stream data and use Equation 2-3 to find shear stress as a function of time over the bridge's life cycle.

The next step in the complete EFA-SRICOS method however is different. Instead of simply using the erosion rate-shear stress relationship to find equilibrium scour depth, Briaud's full version of the method says that Equation 2-4 should be used to find the upper-limit "cap" on scour hole depth:

$$z_{\max} = 0.18 \mathrm{Re}^{0.635} \tag{2-4}$$

Equation 2-4 (which is in mm), is an empirical formula found from 43 different scaled model flume tests (Briaud et al. 1999). According to Briaud, this equation appears to be valid for both

sands and cohesive materials. Briaud also says that these equations are limited to conditions where a uniform soil is present, there is a constant velocity hydrograph, and the bridge pier is in deep water.

Once z_{max} has been computed, equilibrium scour depth is still found using the bed material's erosion rate, although in the complete version of the method, z_{max} is a parameter in the final scour depth expression:

$$z = \frac{t}{\frac{1}{\dot{z}} + \frac{t}{z_{\max}}} \tag{2-5}$$

2.2.2.3 EFA-SRICOS Setup Discussion

The presumptions behind the EFA-SRICOS method are two-fold. First, the EFA-SRICOS method presumes that an erosion rate testing device can accurately measure the erosion rate and estimate shear stress for an eroding sample. Although this sounds simple, it is not – particularly because shear stress is difficult to accurately determine. Different erosion rate testing devices and methods will be discussed in Section 2.2-4. Secondly, Equation 2-3 must be a valid means of relating site-specific shear stress to site-specific freestream velocity.

2.2.2.4 Discussion of Equation 2-3

Equation 2-3 was developed in the late 1990's using a computer model. In 1996, Chen et al. developed the CHIMERA-RANS model, and in 1997, Wei et al. applied it to a situation where water was flowing past a single cylindrical bridge pier over a flat bottom. The CHIMERA-RANS model is a Reynolds Averaged Navier Stokes (RANS) numerical model (Briaud 2004). Briaud's 2004 Transportation Research Board (TRB) report describes the details of the model:

> "First, the docompositional domain was divided into a number of smaller grid blocks to allow complex configuration and flow conditions to be modeled efficiently through the judicious selection of different block topology, flow solvers, and boundary conditions. The chimera domain decomposition technique was used to connect the overlapped grids

together by interpolating information across the block boundaries. The Reynolds stresses were evaluated using the two-layer turbulence model of Chen and Patel. The mean flow and turbulence quantities were calculated using the finite-analytical method of Chen, Patel, and Ju. The SIMPLER/PISO pressure-velocity coupling approached of Chen and Patel and Chen and Korpus was used to solve for the pressure field." (Briaud et al. 2004a).

The model that generates Equation 2-3 requires the input of initial conditions. Specifically, the initial Reynolds Number and Froude Number must be specified because they affect how the computational grid is generated. Additionally, the boundary conditions on surfaces and must be specified. From these initial conditions, the computer model computes an initial velocity profile based on the geometry and the mean velocity.

From this, it appears as though the CHIMERA-RANS model is an adequate method for estimating the maximum shear stress on a flat bottom if the initial conditions are correct. In Briaud's 2004 report, he indicated that a boundary layer of 0.06m was used for computer model runs, and that this was consistent with a 1997 study by Gudavalli (Briaud et al. 1999). To calibrate his computer model, Briaud used a dataset from a 1975 study by Hjorth (Figure 2-2).

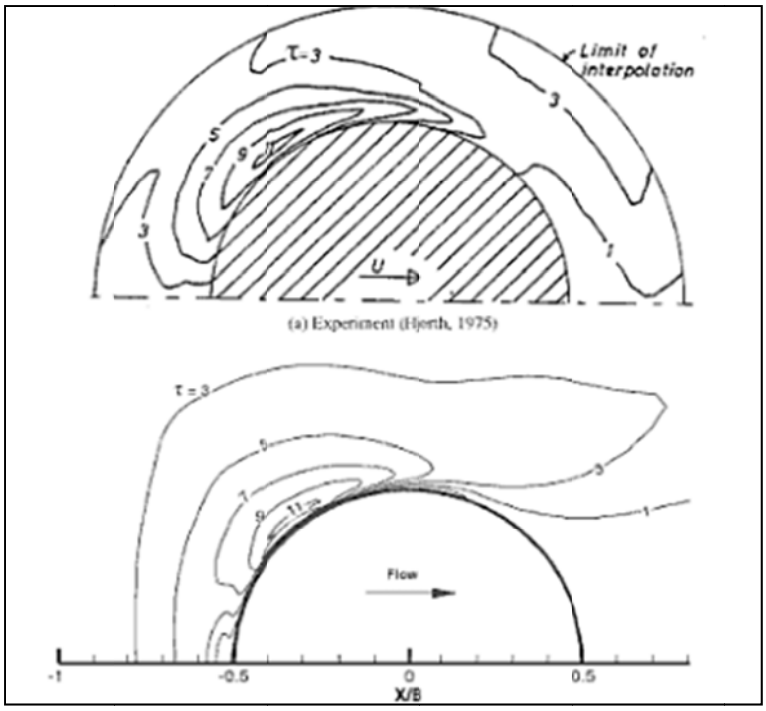

Figure 2-2. Comparison Between Hjorth's Results (Top) and Briaud's Computer Model (Bottom) (Briaud et al. 1999 and Hjorth 1975).

The most notable source of error with Briaud's model is that he is assuming a flat bottom and ignoring friction. His model uses a k-ε approach with a homogeneous eddy viscosity to model the Reynolds stresses (Wei et al. 1997). Because he is using a two-equation k-ε model, roughness is taken into account in the model with regard to the interface between the water column and the bed material, but roughness is only taken into account with regard to calibrating the model to Hjorth's results. Hjorth's test used a hot film probe that was flush to a flat flume bottom to measure the shear stress around the cylinder (Hjorth 1975).

Since Hjorth's test used a flat flume bottom with a flush hot film probe, and this was the dataset used to calibrate Briaud's model, it can be inferred that in a sense, roughness of bed material was not taken into account when Equation 2-3 was estimated. In other words, if shear stress was measured directly in a situation where there a circular cylinder surrounded by sand, it is possible that the stresses could be different. Research from Papanicolau et al. (2001), Roberts and Yaras (2005), Suntoyo and Tanaka (2008), and several others indicates that surface roughness can affect boundary layer propagation and development.

Discussion regarding surface roughness effects on boundary development is not the focus of this report however, and will not be discussed extensively. Instead, for the purposes of this paper, it must be understood that Equation 2-3 is a good approximation for maximum bottom shear stress based on a flat-bottomed k-ε model, but the usage of a model such as this may warrant some criticism, and it may be possible to improve this model. It is important to understand that this model is based on the hydraulic conditions under which the circular pile is subjected; it is theoretical in nature; and it may be limited because it was calibrated against a dataset that used a flat-bottom.

A misconception regarding this argument is that if Equation 2-3 was developed using a flat bottom, then shear stress within an erosion rate testing apparatus should also be computed or measured under flat conditions. This is incorrect because the shear stress vs. erosion rate curve developed using the EFA-SRICOS method is material dependent whereas the maximum shear stress computed from Equation 2-3 is material independent. It is irrelevant whether or not Equation 2-3 is used with cobbles, sand, silt, or clay as the bed material; the equation will give the same maximum shear stress based on hydrodynamics. Conversely, the erosion rate vs. shear stress curves that are generated during implementation of an erosion rate testing device are generated for a specific material. Cobbles will have a different erosion rate vs. shear stress curve

than coarse sand; coarse sand will have a different erosion rate vs. shear stress curve than fine sand, etc. Measuring both the erosion rate and the shear stress accurately for the specific material is essential in implementation of the EFA-SRICOS method.

2.2.3 The Miller-Sheppard Method

In 2003, Dr. D. Max Sheppard of UF and Dr. William Miller (Sheppard's former Ph.D. student) developed their own semi-empirical method similar to the EFA-SRICOS method (Miller 2003). Miller's method started with an idealized scour hole as shown in Figure 2-3, Figure 2-4, and Figure 2-5:

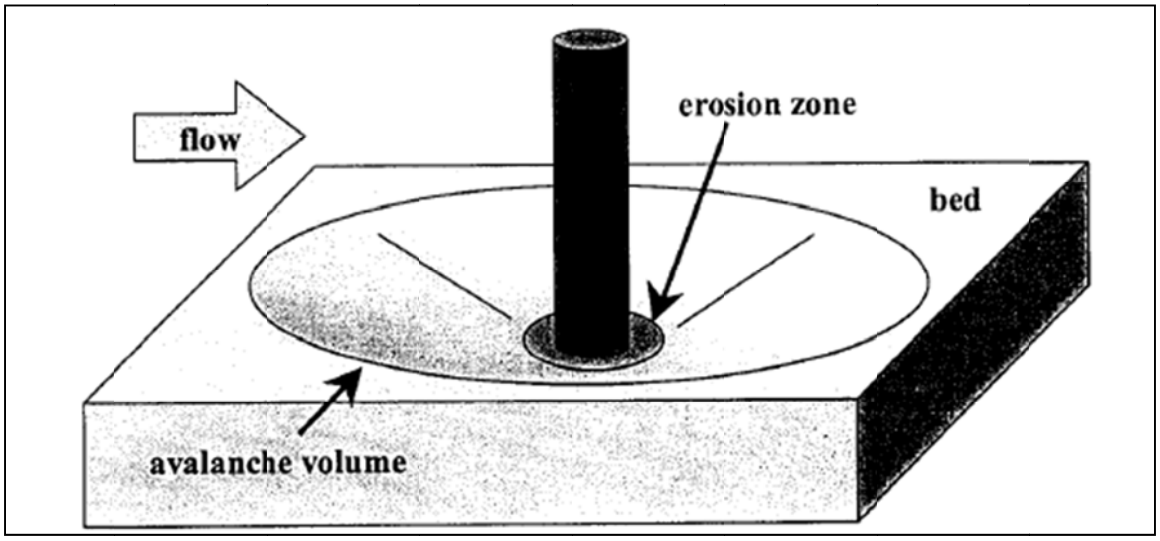

Figure 2-3. 3-D Idealized Scour Hole (Miller 2003)

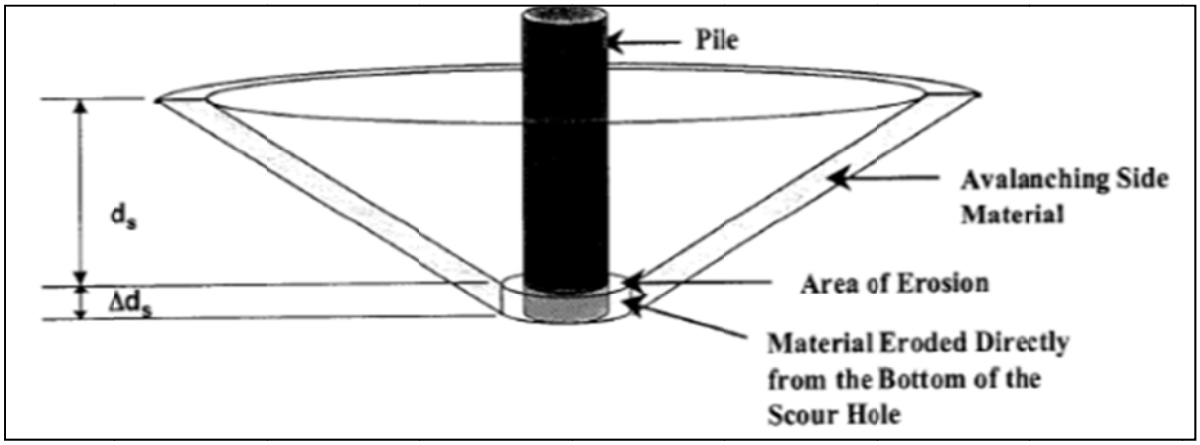

Figure 2-4. Definition Sketch from 3-D Ideal Scour Hole (Miller 2003)

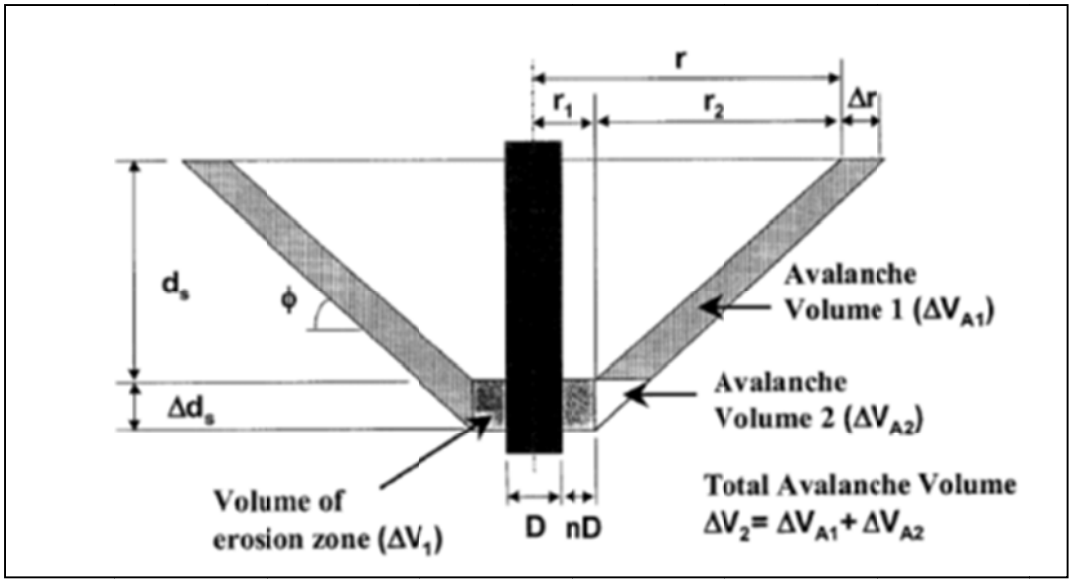

Figure 2-5. Second Definition Sketch from 3-D Ideal Scour Hole (Miller 2003)

Miller used these definition sketches to develop a volumetric expression where the depth of scour hole was found per unit time such that the avalanched volume of material back into the scour hole was taken into account. In other words, as a scour hole develops, some material will fall back into the hole (ΔV_{A1}), while at the same time, some material is eroded directly from the bottom of the scour hole (ΔV_{A2}). Both of these sediment quantities need to be taken into account to properly predict scour hole depth at each time step. Miller analysis resulted in Equation 2-6:

$$\frac{dV_x}{dt} = \pi(1-p)\frac{d(d_s)}{dt}\left[nD^2(1+n) + D(2n+1)\frac{d_s}{\tan\phi} + \left(\frac{d_s}{\tan\phi}\right)^2\right] \tag{2-6}$$

where p is the bed material's porosity, and other terms are defined in the definition sketches. The net volume rate of sediment transport is described by Equation 2-7 where w is the widths of area over which the sediment transport function acts.

$$\frac{dV_s}{dt} = Q_{out} = q_{out}w \tag{2-7}$$

Next, Miller looked a top view of the pile shown in the previous definition sketches (Figure 2-6):

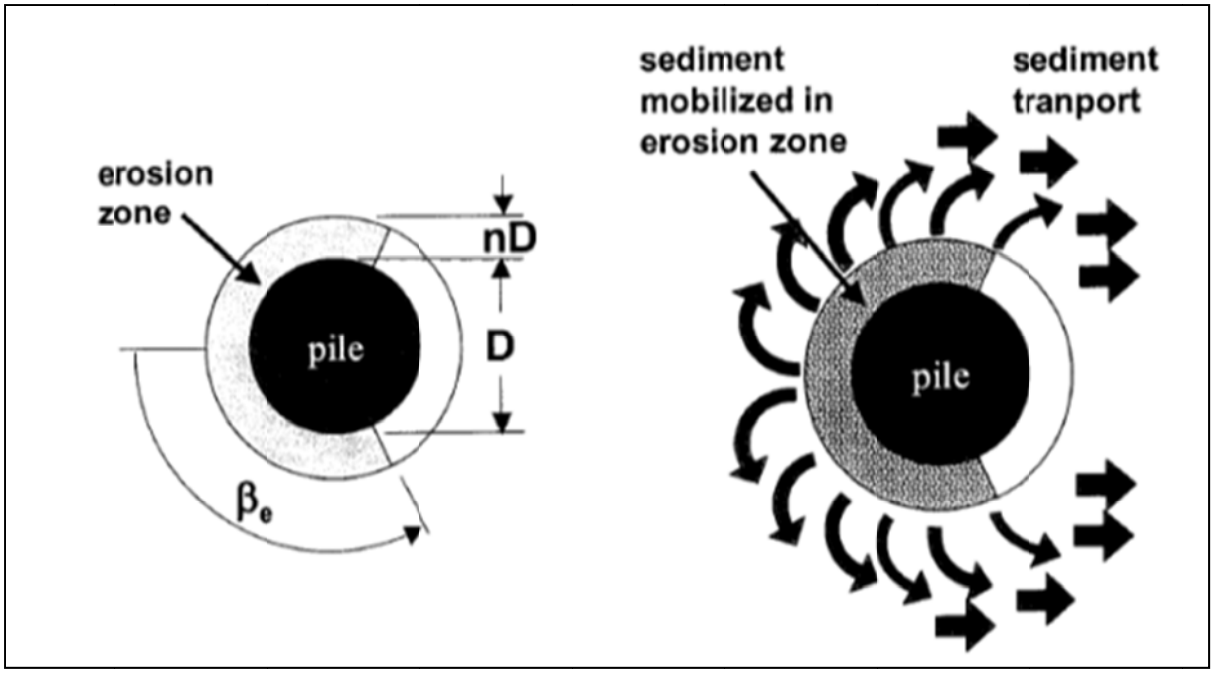

Figure 2-6. Top-View of Pile Definition Sketch

Miller used Figure 2-6 to incorporate pile width as a function of flow separation angle, β_e. Then, he non-dimensionalized scour depth such that $y = d_s/d_{se}$ where d_{se} is the total scour depth:

$$\frac{dy}{dt} = \frac{K_D q_{out}}{K(y)} \tag{2-8}$$

$$K_D = D(2n+1)\beta_e \tag{2-9}$$

$$K(y) = \pi(1-p)d_{se}\left[nD^2(1+n) + D(2n+1)\frac{d_{se}y}{\tan\phi} + \frac{d_{se}y^2}{\tan\phi} \right] \tag{2-10}$$

These equations assume that no sediment is introduced into the scour hole from upstream (clear water conditions). To generalize Equation 2-8 (make it usable under live-bed conditions), Miller introduced an input sediment transport term:

$$\frac{d(y)}{dt}K(y) = K_D q_{out} - q_{in}w \tag{2-11}$$

Miller assumes that input bed-load sediment falls into the scour hole and becomes part of the avalanched material while suspended material remains in suspension and passes over the scour hole. This results in the following equations:

$$\frac{dy}{dt} = \frac{K_D q_{out} - L(y)q_{in}}{K(y)} \tag{2-12}$$

$$L(y) = L_0 + L_1 y \tag{2-13}$$

$$L_0 = D(1 + 2n) \tag{2-14}$$

$$L_1 = \frac{2d_{se}}{\tan\phi} \tag{2-15}$$

Equation 2-8 and Equation 2-12 show that both under clear water and live-bed conditions, scour depth should be a function of a material's sediment transport function. Although Miller verified his model using non-cohesive results, from this derivation, it is clear that this model should also be valid when cohesive bed materials are present.

To apply his model, Miller relied on analytically based stochastic formulations from Meyer-Peter and Mueller (1948), Einstein (1950), Englund and Hansen (1972), Neilsen (1992), and Van Rijn (1992). Note that these sediment transport models use an average sediment diameter to determine sediment transport function (d_{50}). For a non-uniform material, these methods either need to be modified, or alternatively, the erosion rate-shear stress relationship can be measured directly.

Miller notes that the commonality among these different sediment transport models is that they are of the form $q=Cf(\theta)$ or alternatively some constant times a function of shear stress. Miller realized that finding the effective shear stress in a scour hole is not easy nor is it always measurable, but he assumed that the sediment transport constant would remain the same as the scour hole developed. Therefore, he expressed Equation 2-12 in terms of the sediment transport constant:

$$\frac{dy}{dt} = \frac{K_D C f(\theta') - L(y) q_{in}}{K(y)} \tag{2-16}$$

Then, he used a scour depth vs. time fit function from his results to determine dy/dt when $t = 0$, and from Sheppard's 2002 work, he found the initial bed shear stress required for scour to initiate. From this, he computed C, and based on this constant value of C, he was able to develop a time series of effective shear stress over the development of the scour hole. His results were of the form given in Figure 2-7:

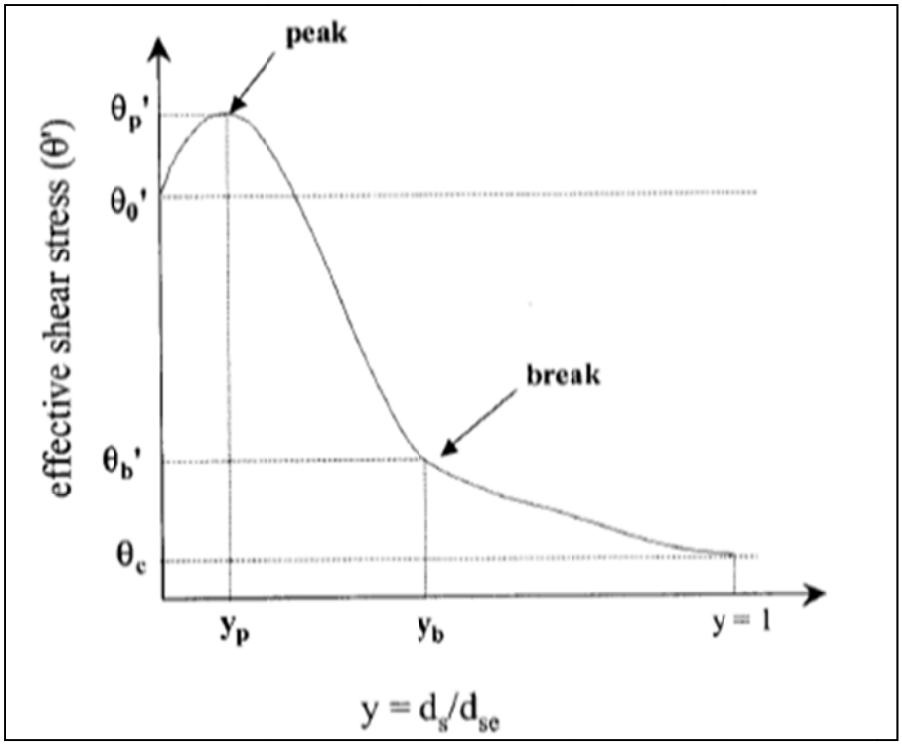

Figure 2-7. Effective Shear Stress vs. Scour Hole Depth

These curves show that as a scour hole develops, shear stress reaches a peak at y_p and a break at y_b. Miller used his results to develop a table where effective shear stress, the break point, and the peak point were determined as a function of velocity, sediment size, and pile diameter.

Miller's model is dependent on non-cohesive sediment because of his assumed scour hole shape. Work from Ting et al. (2001) indicates that for a cohesive soil, the scour hole generally will begin to form adjacent to the front edge of a protruding pile and extend some distance downstream from the pile face. The front edge of the idealized Miller scour hole, or the "avalanched volume" as labeled in Figure 2-3 will not develop because stiffer cohesive soils will resist falling into a developing hole. Still, according to Briaud and his equation for z_{max}, (Equation 2-4) ultimate scour depth should be the same regardless of sediment size. In other words, although the front portion of the scour hole may not avalanche into the hole, the maximum depth of the hole, which should occur at a point nearly adjacent to the protruding pile, should be similar.

According to this reasoning then, the shape of Miller's scour hole in Figure 2-3 should be a semi-circle rather than a circle, yet the depth at the front fact of the semi-circle should be same as

indicated through Miller's derivation. Although work in this report does not attempt to use Ting's work to develop a cohesive analytical solution similar to Miller's, in principle Miller's expression for scour hole development (Equation 2-16) should still hold true in the sense that scour hole development should be a function of the bed material's erosion rate.

2.2.4 Scour Depth for More Complex Structures

The preceding EFA-SRICOS method and the Miller-Sheppard approach for predicting scour depth are somewhat limited in that they are only valid for a single pile situation. When a bridge pier or foundation is more complex, methods presented in Section 2.2.2 and Section 2.2.3 need to be modified to fit these more complicated scenarios. Although Miller-Sheppard follow-up with more complex pier geometries could not be found, in the late 1990's and early 2000's, Briaud did perform more research. Briaud developed an empirical dataset so that his EFA-SRICOS method could be used for more complicated foundations.

Briaud used Equation 2-4 and Equation 2-5 as a starting point, and his hypothesis was that correction factors could be developed where τ_{max} and z_{max} from these two equations could be modified for more complex pier geometries. This approach assumes that effect of one parameter (for example, attack angle) is independent from the effects from another parameter (for example, pier shape). This approach is common; it is the same approach used in the sand-scour equations in HEC-18. Briaud's equations for complex piers are given in Equation 2-16 and Equation 2-17:

$$\tau_{\max} = k_w k_{sp} k_{sh} k_{\alpha} \left(0.094 \rho V^2 \left[\frac{1}{\log\left(\frac{VB'}{\upsilon} \right)} - \frac{1}{10} \right] \right) \tag{2-16}$$

$$z_{\max} = K_w K_{sp} K_{sh} \left(0.018 \left(\frac{VB'}{\upsilon} \right)^{0.635} \right) \tag{2-17}$$

Shallow water correction factors are given in Equation 2-18 and Equation 2-19:

$$K_w = \begin{cases} 0.85 \left(\frac{H}{B} \right)^{0.34} & H/B < 1.62 \\ 1 & H/B > 1.62 \end{cases} \tag{2-18}$$

$$k_w = \frac{\tau_{\max}}{\tau_{\max(deep)}} = 1 + 16 e^{-\frac{4H}{B}} \tag{2-19}$$

where H is the height of the water and B is the width of the piers. For the case of closely spaced piers, the spacing correction factors are given by Equation 2-20 and Equation 2-21:

$$K_{sp} = \frac{W_1}{(W_1 - nB)} \tag{2-20}$$

$$k_{sp} = \frac{\tau_{\max}}{\tau_{\max(\text{single})}} = 1 + 5e^{-\frac{1.1S}{B}} \tag{2-21}$$

where W_1 is the width of the channel without the piers n is the number of piers, and S is the spacing between piers. For the case of different shaped piers, the shear stress correction factor is given by Equation 2-22 where L is the width of the pier. The scour depth correction factor is given by HEC-18. Briaud's tests were on square-nosed piers, so he used a K_h value of 1.1. For piers of other shapes, Briaud recommends using the same K_h factors prescribed in HEC-18.

$$k_{sh} = -1.15 + 7e^{-4\frac{L}{B}} \tag{2-22}$$

Finally, for the case of flow from a different angle, α, Briaud used the pier projected width, B', (the same B' as in HEC-18) to evaluate this condition. Even with B' defined however, introduction of an attack angle coefficient, k_α was still necessary for shear stress:

$$B' = L\sin\alpha + B\cos\alpha = B\left(\frac{L}{B}\sin\alpha + \cos\alpha\right) \tag{2-23}$$

$$k_\alpha = \frac{\tau_{\max}}{\tau_{\max(0\text{ degree})}} = 1 + 1.5\left(\frac{\alpha}{90}\right)^{0.57} \tag{2-24}$$

2.3 Analytical Methods for Determining Erosion Rate-Shear Stress Relationships

Based on the preceding discussion on the aforementioned semi-empirical methods and Slagle's 2006 argument regarding the CSU equations, in recent years research has looked not to define the scour-hole proper as a function of bed material, but rather use either a method similar to the Miller-Sheppard approach or the EFA-SRICOS approach as a standard for overall scour depth and fit one of these two models to a generalized scour scenario. At their core, these two models require the same input parameter – an erosion rate vs. shear stress relationship. Logically then, the goal of research should not be to define scour depth, but it instead should be to define

an erosion rate-shear stress relationship and if possible, generalize this relationship to other geotechnical parameters.

There are two methods to determine this erosion rate-shear stress relationship. On one hand, as discussed in the last section, engineers can take Briaud's approach and try to fit analytical sediment transport models to the problem. There is a significant advantage to this approach. These models are based on physics and analytical reasoning, and as such, results from these models can be used in a generalized scour situation for any bed material in which the models' assumptions are valid. In this section, a brief analysis will follow of several analytical models, while in Section 2.4 analysis of the other method for determining an erosion rate-shear stress relationship will be discussed – measuring this parameter directly using an erosion rate-shear stress testing device.

2.3.1 Particle-Like vs. Rock-Like Erosion and Shields (1936)

In 1936, Shields argued that for a coarse sediment, there should be a shear stress, τ_c that would represent the shear stress that caused incipient motion of bed material. This shear stress could be drawn as a function of bed roughness, or the roughness Reynolds Number, Re_* such that:

$$\frac{\tau_c}{gd(\rho_s - \rho)} = f^n(\mathrm{Re}_*) \tag{2-25}$$

$$\mathrm{Re}_* = \frac{u_* d}{\nu} \tag{2-26}$$

$$u_* = \sqrt{\frac{\tau_c}{\rho}} \tag{2-27}$$

Although Shields' original data only corresponded to sands, over the years (following Mantz 1977), his data points have been extended to cover the fine sediment regime. An extended Shields Diagram is presented in Figure 2-8:

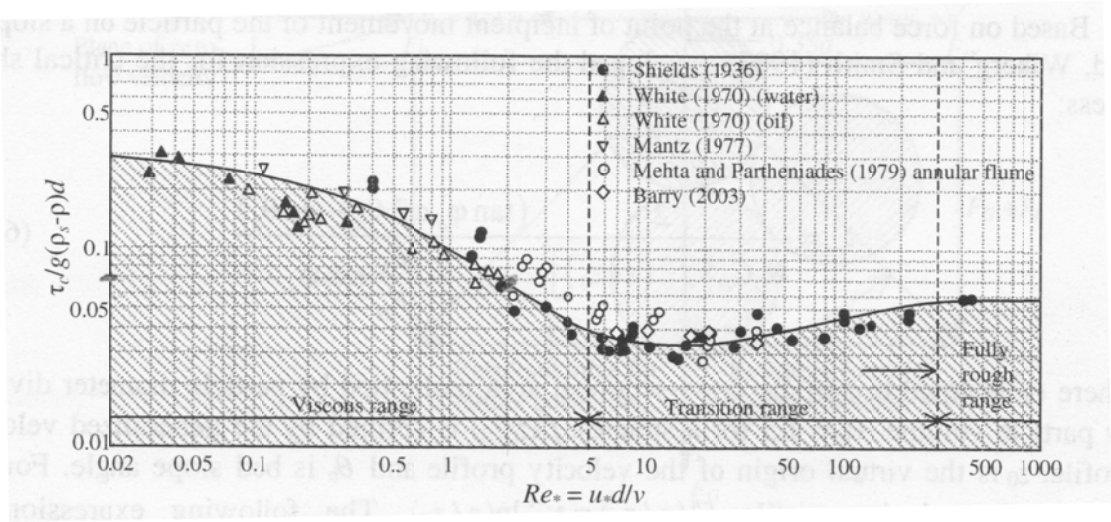

Figure 2-8. Extended Shields Diagram (Mehta 2007 and Mantz 1977)

The essential component of Shields' work is his critical shear stress assumption. Shields assumed that during an erosion event, erosion would only be caused by a small tug or pull on a few particles on a material lattice. It can be shown that if this is the case, erosion must correspond only to the Shields parameter given in Equation 2-25. This erosion mode will be defined as particle-like erosion.

For non-cohesive sediments, this is true, but for cohesive sediments and rock, another erosion mode exists. For cohesive material such as sand-clay mixtures and stiff rock-like materials, this slight tug or pull on the exterior rock-like face sometimes does little in terms of net-overall erosion. Rather, erosion under these conditions is instead governed by the fluctuating normal force component on the material's face and localized density/roughness/cracking in the rock or sand-clay lattice.

When Miller used analytical sediment transport equations to calibrate his model, he only considered the particle-like erosion mode. Under rock-like conditions, it may not be possible to find erosion rate as a strict function of shear stress. Under this scenario, Equation 2-12 is still valid, while Equation 2-16 is not because it would not be possible to define a sediment transport constant when the governing component of sediment transport was a normal forcing parameter. Still, for certain sand-clay mixtures, certain cohesive sediments, and some rock-like materials, particle erosion is present, and methods for finding both critical shear stress and sediment transport functions (erosion rate-shear stress relationships) should be discussed in some detail.

First, critical shear stress will be discussed, then methods for determining erosion rate-shear stress curves will be examined.

2.3.1.1 Einstein (1943) and Christensen (1975)

In 1943, Einstein developed an expression for critical shear stress, τ_c of a cohesive bed material based on a stochastic method (Einstein 1943):

$$\bar{\tau}_c = \theta_{cr}(\gamma_x - \gamma)d_e \tag{2-28}$$

where d_e is the effective grain size, γ_s is the specific weight of the sediment, γ is the specific weight of water, and θ_{cr} is the Shield's parameter, or parameter for incipient motion. Although Einstein developed his own Shield's parameter, in 1975, Christensen modified Einstein's equation and developed Equation 2-29 based on a probability distribution for erosion:

$$\theta_{cr} = \frac{\alpha_1}{\alpha_2}\frac{1+S_u^2}{\cot\varphi + 0.556\left[\ln\left(1+\frac{10.4}{r}\right)\right]^2}\frac{1}{(1+nS_u)^2} \tag{2-29}$$

where r is the roughness/grain-size ratio defined as the equivalent sand roughness, k_s divided by d_e, S_u is the dimensionless value of the standard deviation of the velocity fluctuation, σ defined by σ_u/u_{bar}, u_{bar} is the average velocity, n is the normalized velocity fluctuation u'/s_u, u' is the velocity fluctuation component, and α_1 and α_2 are shape factors. Christenson found that S_u = 0.164 and n = 3.09 which corresponded to the probability of erosion Pr = 0.001 which was related to the Gaussian distribution of u' (Mehta 2007).

2.3.1.2 Wiberg and Smith (1987)

Wiberg and Smith developed their own relationship for critical shear stress in the late 1980's. Their expression centered around the argument that when dealing with a mixed bed, there are two length scales that need to be dealt with – the diameter of particle size that will be eroded and the roughness of the surrounding bed. In other words, when dealing with a heterogeneous bed, a smaller particle may erode first, but the flow velocity is dependent on the size of the larger particles surrounding the smaller particle. To grapple with this scaling problem, Wiberg and Smith introduced a Φ factor into their equations because they argue that the particle failure angle changes for a mixed bed. In other words, it would be easier for a large

particle to roll over a bed that consisted of smaller particles than it would be for a small particle to roll over a bed that consisted of larger particles (Barry 2003). An expression from Miller and Byrne (1966) was used to quantify Φ. Wiberg and Smith's critical velocity equation and Φ equation are given by:

$$\tau_{cr} = \frac{2}{C_D \alpha_3} \frac{1}{\left[f^2\left(\frac{z}{z_0}\right)\right]} \frac{\tan\Phi\cos\theta_b - \sin\theta_b}{1 + \frac{F_L}{F_D}\tan\Phi} \tag{2-30}$$

$$\Phi = \cos^{-1}\frac{d/k_s + z_0}{d/k_s + 1} \tag{2-31}$$

Where a_3 is a parameter for grain geometry, $f^2(z/z_0)$ is derived from the expressions for drag and lift coefficient (Equation 2-32 and Equation 2-33), z is the height above the bed, z_0 is the bottom roughness parameter, q_b is the bed slope, d is the particle diameter, and k_s is the length scale for bed roughness.

$$F_D = \frac{1}{2} C_D \rho \bar{u}^2 A \tag{2-32}$$

$$F_L = \frac{1}{2} C_L \rho \bar{u}^2 A \tag{2-33}$$

In these expressions, A is the cross-sectional area of the particle, C_L is the lift coefficient, C_D is the drag coefficient, and ρ is the density of water.

To find the bottom roughness parameter, an expression for the velocity profile is necessary. Wiberg and Smith used Reichardt's 1951 expression which gives a transition between the viscous sub-layer and the logarithmic flow above (Schlichting 1979, Barry 2003).

$$u(z) = u_* \left[\frac{1}{\kappa} \ln\left(1 + \kappa z^+\right) - c\left(1 - e^{-z^+/11.6} - \frac{z^+}{11.6} e^{-0.33 z^+}\right)\right] \tag{2-34}$$

$$z^+ = \frac{u_* z_0}{\nu} = \frac{R_* z}{k_x} \tag{2-35}$$

$$z_0^+ = \frac{u_* z_0}{\nu} = \frac{R_* z_0}{k_s} \tag{2-36}$$

$$R_* = \frac{u_* k_s}{\upsilon} \tag{2-37}$$

where ν is the kinematic viscosity of water and R_* is the roughness Reynolds Number.

2.3.1.3 Dade and Nowell (1991)

Dade and Nowell sought to develop a relationship for critical shear stress for a cohesive or mixed bed that was independent of inter-particle cohesion forces (Barry 2003). Their expression for critical shear stress is given in the Equation 2-38:

$$\tau_{cr} = \frac{40\rho\upsilon^2}{\tan\Phi d^2}\left[\sqrt{\frac{g\rho'_s\, d^3 \tan^2\Phi}{240\rho\upsilon^2}\left(1+3(1-\cos\Phi)\frac{\tau_b}{g(\rho_s-\rho)d}\right)}+1-1\right] \tag{2-38}$$

where τ_b is the mud interfacial mud shear stress, g is the acceleration due to gravity, Φ was found to be 65^o, and previous terms have already been defined.

2.3.1.4 Dade et al. (1992)

The purpose of this investigation was to find an expression for critical shear stress that included the effects of cohesion. This approach was similar to Weiberg and Smith's approach except that Dade et al. included a cohesion term. The resulting expression for the Shield's parameter is given in the following equations:

$$\theta_{cr} = \frac{1}{\Xi}\left[\frac{5X}{\tan\Phi}\frac{\sqrt{\frac{4}{X}-3}-1}{1-X}\right]^2 \tag{2-39}$$

$$\Xi = \frac{g(\rho_s-\rho)d^3}{\rho\nu^2} \tag{2-40}$$

$$X = \Xi\left(1+\frac{F_A}{W_b}\right)\frac{\pi}{4800 b_1}\tan^3\Phi \tag{2-41}$$

where b_1 is a shape factor, Z is the Yalin (1972) parameter F_A is the magnitude of the inter-particle force, and W_b is the immersed weight of the particle grain. The ratio of immersed weight to inter-particle force is obtained from Equation 2-42 (Barry 2003):

$$\frac{F_A}{W_b} = 3b_2(1-\cos\Phi)\frac{\tau_y}{g(\rho_s-\rho)d} \tag{2-42}$$

2.3.1.5 Mehta and Lee (1994)

In 1994, Mehta and Lee developed their own relationship for critical shear stress by using a balance between angle of repose, drag force, buoyant weight, and lift force as their starting point rather than using the F factor that was employed by Christensen and Dade et al. Their starting point, Equation 2-43 led to the development of Equation 2-44 for critical shear stress:

`

$$\tan\varphi = \frac{F_D}{W_b + F_c + F_L} \tag{2-43}$$

$$\frac{\tau_c}{g(\rho_s - \rho)d} = \frac{\alpha_3 \tan\varphi}{\alpha_1 + \alpha_2 \tan\varphi} + \frac{F_c \tan\varphi(\alpha_1 + \alpha_2 \tan\varphi)}{g(\rho_s - \rho)d^3} \tag{2-44}$$

$$\tau_x = \alpha_4(\phi_a - \phi_{ac})^{\beta} \tag{2-45}$$

Equation 2-45 was developed from an evaluation of previous laboratory tests where α_4 and β are sediment-specific constants. The advantage of this approach is that the Shields parameter is easily recognizable on the left hand side of the equation.

2.3.1.6 Torfs et al. (2000)

Torfs took Equation 2-43 from Mehta and Lee and noticed that it was only applicable for erosion of a bed material of single-sized particle grains. Torfs sought to characterize entrainment within a fine-coarse sediment mixture by size, d_m and density, ρ_s. Everything else remains the same as it did in Equation 2-43, except that the cohesive force, F_c must be replaced with F_m, or the force representing the effects of both cohesion and the influence of inter-bedded grains. The result is:

$$\tau_c = \left[\frac{\alpha_{3cg} \tan\phi_{cg}}{\alpha_{1cg} + \alpha_{2cg} \tan\phi_{cg}} + \frac{K'\zeta(\phi_v - \phi_{vc})^{\xi}}{g(\rho_s - \rho)d_m}\right] g(\rho_s - \rho)d_m \tag{2-46}$$

where ϕ_{vc} is the fine solids volume fraction, ϕ_v is the threshold value of ϕ_{vc} below which the bed becomes fluid-like, ξ and ζ are coefficients that depend on bed composition and levels of consolidation, and a_3 is the shape factor related to d_m. d_m is the characterization diameter, analogous to the effective diameter, D_* from the FDOTBSM except that d_m refers to particle size. The critical aspect of this equation is the inclusion of *K'* which is included to quantify increases or decreases in critical shear stresses due to the presence of fine materials. If *K'* = 0, it implies

that there are no fine materials; an increasing *K'* signifies a greater presence of fine materials and a corresponding higher critical shear stress.

2.3.1.7 Sharif (2002)

In 2002, Sharif developed his own model for critical shear stresses of cohesive soils. Sharif concluded that developing an all-inclusive model was not practical and instead, in his work three different models were created. The first model was for pure clays, the second model was for mixed beds with low clay content and the third model was for mixed beds with high clay content.

For the case of a mixed bed with high clay content, Equation 2-47 provides an expression for critical shear stress. In this equation, ρ_{sn} is the density of the non-cohesive particle, ρ_{sc} is the density of cohesive particles, d_{nc} is the diameter of non-cohesive particles, f_c is the weight fraction of cohesive particles, ρ_d is the bulk density of the bed, ξ is the magnitude of the force between cohesive and non-cohesive particles, θ is the Shields parameter, d_c is the average diameter of cohesive particles, α_{vc} and α_{vn} are shape factors for cohesive particles, and α_{sn} is an area shape factor for non-cohesive particles.

$$\tau_{cn} = g(\rho_{sn} - \rho)d_n\theta + \frac{18\alpha_{sn}\xi\theta}{\alpha_{vc}\alpha_{vn}\pi d_n d_c^2 \rho^2 \rho_{sc}^2}\left(\frac{f_c\rho_d\rho_{sn}}{\rho_{sn} - f_n\rho_d}\right)^3 \tag{2-47}$$

Equation 2-47 was developed by setting up a force balance between a single non-cohesive particle and a cohesive sediment bed. The equation for critical shear stress of a pure clay bed, Equation 2-48, was developed by creating a force balance for separation of aggregates from the bed itself. In this equation, ρ_{ag} is the density of aggregates, ζ is the average force between cohesive particles, θ is the Shields parameter, and k_1 and k_2 are coefficients based on floc diameter.

$$\tau_{ca} = \frac{k_1 g\theta}{(\rho_{ag} - \rho)^{k_2 - 1}} + \frac{18\rho_{ag}\theta\xi}{\pi\alpha_{vc}d_c^2\rho_{sc}} \tag{2-48}$$

Equation 2-49, the model for mixed beds with low clay content, was developed under the assumption that critical shear stress under these conditions would be dominated by non-cohesive particles and aggregates. Then, Sharif assumed that each component of critical shear stress – the

aggregate component and the non-cohesive component – would govern critical shear stress based on the average area along the failure plane covered by each of these materials.

$$\tau_{ch} = \tau_{cn} A_{nb}^{b_b} + \tau_{ca} A_{ab}^{b_a} \tag{2-49}$$

where A_{nb} is the area of non-cohesive particles, A_{ab} is the area of cohesive aggregate, and b_n and b_a are experimentally determined coefficients.

2.3.1.8 Critical Shear Stress Discussion

The previous section was a brief summary of a number of expressions that can define the critical shear stress for a bed material analytically. This critical shear stress parameter is useless as means of estimating scour depths if it cannot somehow be correlated to erosion rate. This advance forward began in the 1960's with Partheniades and has been improved since then.

2.3.1.9 Partheniades (1962)

In the early 1960's Partheniades was conducting tests on mud from San Francisco Bay, and he noticed that cohesive sediment eroded much differently from non-cohesive sediment. Partheniades discovered that unlike sand, equilibrium scour depths are not reached when live-bed conditions develop. In other words, with sand, eventually a scour hole gets to the point where rate of deposition equals rate of erosion as sand particles are eroded and redeposited within the domain of the hole. Mud on the other hand appears to harden until eventually the floc shear strength can withstand the shear stress that is applied to it.

Using this rationale, Partheniades took the stochastic approach used by Einstein to develop a relationship for critical shear stress. The resulting equation, Equation 2-50, gives erosion rate as a function of bed shear stress (Figure 2-9).

$$E = k_1 \left[1 - \frac{1}{2} \left(\operatorname{erf} \left(\frac{1}{\sqrt{2}} \omega \right)^{\frac{k_2}{\tau_b} - 2}_{\frac{-k_2}{\tau_b} - 2} \right) \right] \tag{2-51}$$

where erf is the error function, and k_1 and k_2 are experimentally determined coefficients that equal 0.036 and 1.61 respectively (Mehta 2007).

In 1974, Ariathurai used empirical data to develop Equation 2-51, which is a straight-line approximation of the trend shown by the Partheniades equation.

$$E = M\left(\tau_b - \tau_c\right) \tag{2-51}$$

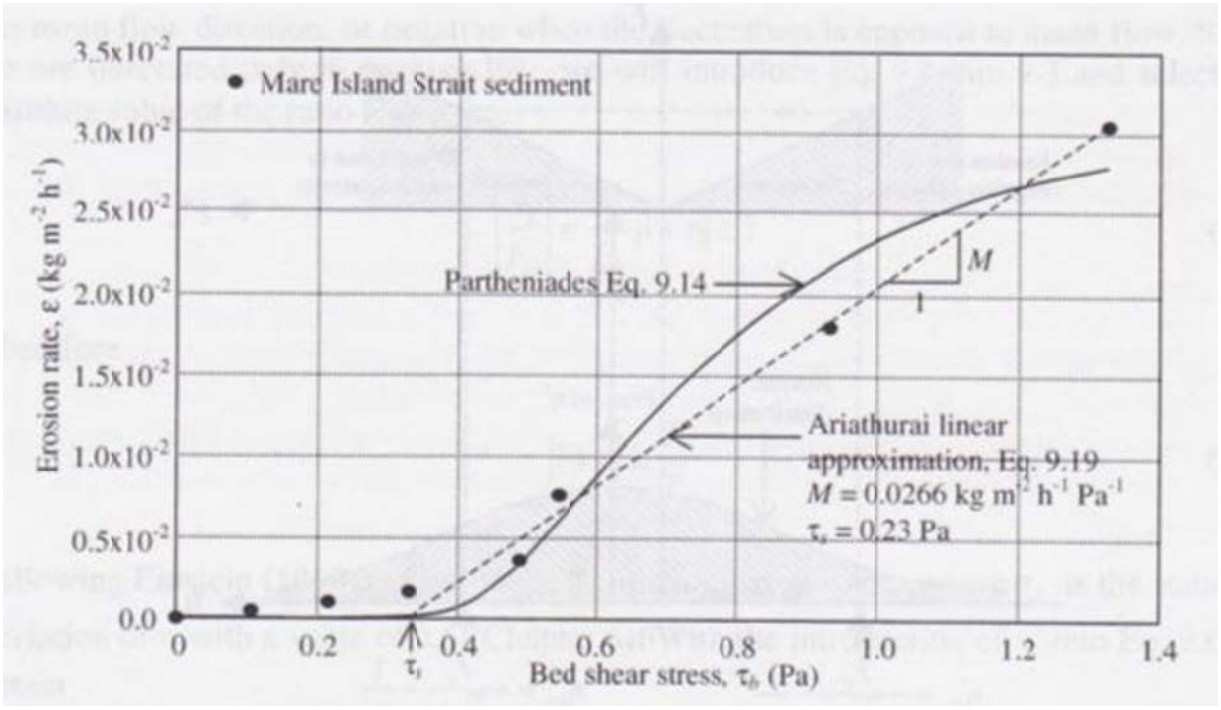

Figure 2-9. Ariathurai-Partheniades Relationship for Erosion vs. Shear Stress (Mehta 2007)

This equation is extraordinarily significant because of its overall form. Equation 2-51 shows that for a cohesive bed material under particle-like erosion conditions, erosion rate should be a function of the deficit between critical shear stress and bed shear stress – or the same form that Miller saw during his analysis.

2.1.1.10 Christensen (1975)

In parallel with his work on critical shear stresses for cohesive beds, Christensen also developed an expression for average shear stress on a sediment bed:

$$\bar{\tau}_b = C_D \rho \frac{\bar{u}^2}{2}\left(1 + \left(\frac{\sigma_u}{\bar{u}}\right)^2\right) \tag{2-52}$$

2.3.1.11 McLean (1985)

In 1985, McLean developed an energy balance between potential energy of an entrained particle and bed shear stress. This resulted in an expression for erosion rate of eroding bed particle, or Equation 2-53:

$$E = M_e \frac{\tau_b - \tau_c}{\tau_c} \tag{2-53}$$

According to Mehta, this relationship was actually first proposed by Kandiah (1974) based solely on empirical results. This equation also resembles the Partheniades equation and the Ariathurai equation, and serves as further evidence that quantifying erosion rates as a function of shear stress should be a valid method for predicting scour depths under particle-like conditions.

2.3.1.12 Van Prooijen and Winterwerp (2008)

In 2008, Van Prooijen and Winterwerp argued that knowledge regarding the stochastic nature of the turbulent boundary layer has increased. Therefore, the probability density function (PDF) is now known more accurately than before when Einstein, Christensen, and others were conducting their research. Using the same approach as Hofland and Battjes (2006) and data from Obi et al. (1996), a new PDF was developed for bed shear stress:

$$p(T) = \frac{\alpha}{2\sqrt{2\pi T^*}} \exp\left[-\frac{1}{2}\left(\sqrt{T^*} - \delta\right)\right] \tag{2-54}$$

where T is given by the dimensionless parameters:

$$\omega = \frac{u_b}{\sigma_u} \tag{2-55}$$

$$\delta = \frac{u_u}{\sigma_u} \tag{2-56}$$

$$T = \frac{\tau_b}{\rho \sigma_u^2} = \omega |\omega| \tag{2-57}$$

$$T^* = \alpha T - \beta \delta^2 | \tag{2-58}$$

and ω is the dimensionless near-bed velocity, δ is the dimensionless mean velocity, and T is the dimensionless shear stress. Parameters are scaled with σ_u or the standard deviation of near-bed velocity. The factors α, β, and δ were fitted to match Obi's 1996 data such that α = 1.75, β = 0.83, and δ = 3.1.

The result of this is that the Gaussian distribution assumed by Einstein in 1950 and used by Partheniades in 1962 became skewed slightly to the left. When applied to the Ariathurai expression, a formula for erosion rate is given:

$$\frac{E}{M\rho\sigma_u} = \frac{-T_c^* + \delta^2 + 1}{2\alpha} + \frac{\sqrt{T_c^*} + \delta}{\alpha\sqrt{2\pi}} \exp\left(-\frac{T_c^*}{2} + \delta\sqrt{T_c^*} - \frac{\delta^2}{2}\right) + \frac{\delta^2 + 1 - T_c^*}{2\alpha} \text{erf}\left(-\sqrt{\frac{T_c^*}{2}} + \frac{\delta}{\sqrt{2}}\right) \quad (2\text{-}59)$$

Results from Equation 2-59 are presented in Figure 2-10 and compared with Ariathurai's relationship.

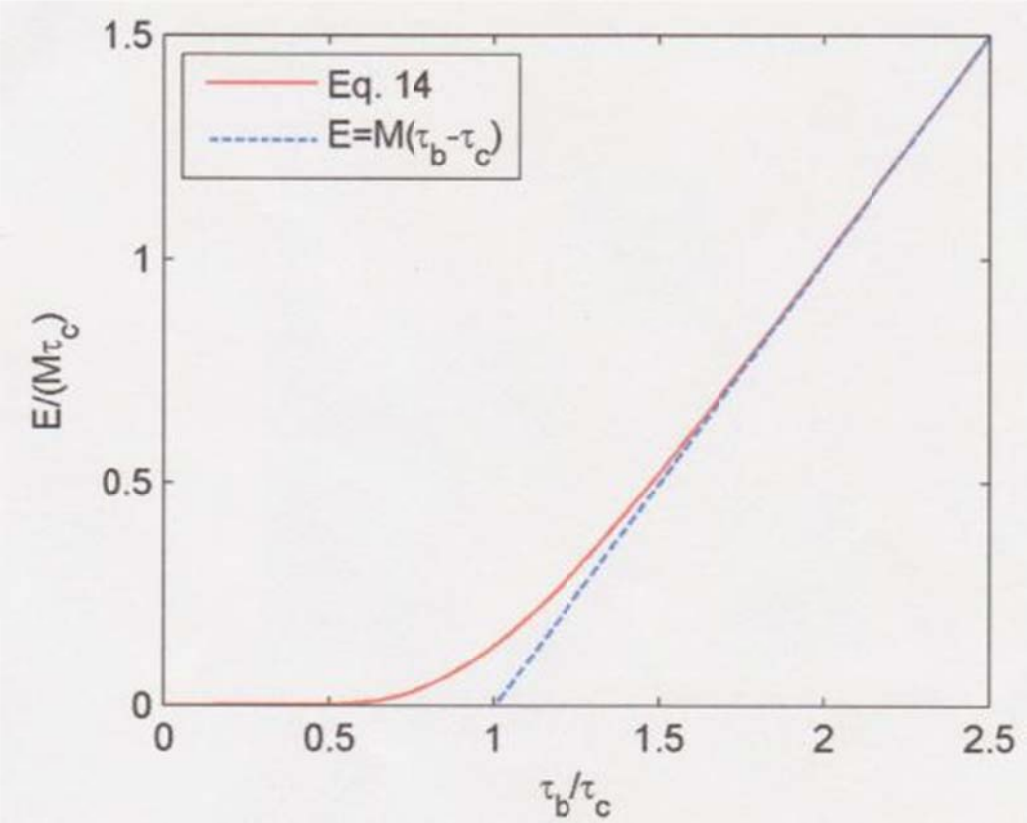

Figure 2-10. Results from Modification of Partheniades Equation (Van Prooijen and Winterwerp2008)

Because Equation 2-59 is not convenient for use in numerical models, a three-piece third order polynomial was developed:

$$\frac{E}{M\tau_c} = \begin{cases} 0 \text{ if } \frac{\tau_b}{\tau_c} < 0.52 \\ -0.144\left(\frac{\tau_b}{\tau_c}\right)^3 + 0.904\left(\frac{\tau_b}{\tau_c}\right)^2 - 0.823\left(\frac{\tau_b}{\tau_c}\right) + 0.204 \\ \left(\frac{\tau_b}{\tau_c} - 1\right) \text{if } \frac{\tau_b}{\tau_c} > 1.7 \end{cases} \quad (2\text{-}61)$$

Where *M* is Ariathurai's coefficient. Note that even here, erosion rate is parameterized via critical shear stress-bed shear stress function.

2.3.2 Analytical Methods for Determining Rock Erosion

At present, engineers do not have a comprehensive quantitative understanding of what occurs during rock-like erosion events where the fluctuating normal force component on the rock-face is a more significant erosion source than the shear stress tug or pull that acts against the rock surface. As mentioned in the preceding section, during particle-like erosion events, a critical shear stress can usually be defined where below this threshold no erosion occurs. With rock and materials that obey rock-like erosion characteristics, this shearing threshold does not appear to exist. There has been limited analytical work completed in this area, and most of it is still unable to accurately predict erosion rates.

2.3.2.1 Cornett et al. (1994) and Henderson (1999)

According to Cornett et al. (1994) and Henderson (1999), erosion of rock may not be directly related to shear stress because erosion occurs along a rock's internal fracture plane, and this may be driven by hydrodynamic pressures within the fracture. Figure 2-11 was proposed by Cornett, Henderson, and Kerr (2001) as a possible explanation for erosion of rock:

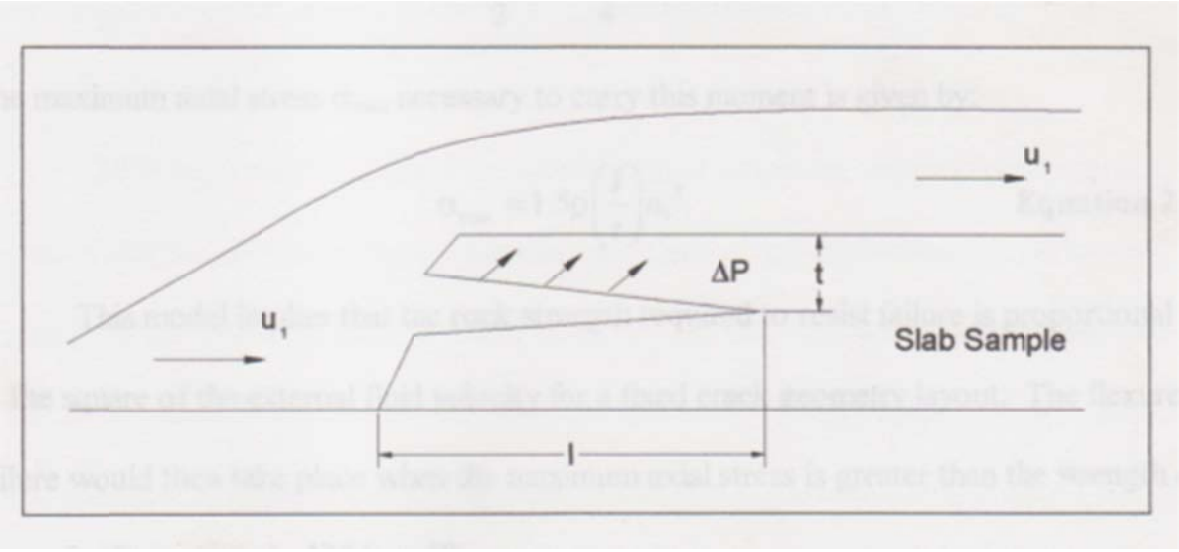

Figure 2-11. Definition Sketch for Rock Fracture (Henderson 1999)

In this sketch, the crack, which is a stagnation point, of length *l* and height *t* is subjected to a steady flow of velocity *u*. Bernoulli's equation can be applied to this scenario such that the pressure difference between the crack and the external flow can be expressed:

$$\Delta P = \frac{\rho}{2}\left(u_1^2 - u_2^2 + 2gt\right) \approx \frac{\rho u_1^2}{2} \tag{2-62}$$

This pressure differential is the velocity head that acts to open the crack, and fracture occurs when the pressure within the crack exceeds rock strength. The bending moment, *M* in the rock above the crack base can also be written (Equation 2-63), and the maximum axial stress to carry the moment can be expressed (Equation 2-64) (Henderson 1999).

$$M = \frac{l^2}{2}\Delta P = \frac{\rho l^2 u_1^2}{4} \tag{2-63}$$

$$\sigma_{\max =} = 1.5\rho\left(\frac{l u_1}{t}\right)^2 \tag{2-64}$$

Equation 2-64 implies that to failure resistance is proportional to the square of free-flowing fluid velocity. Note that this expression deviates from the shear-based expressions presented in Section 2.3.1.

2.3.2.2 Stream Power Method

In 2003, Bollaert developed the only known quantitative analytical method for predicting erosion for a jointed rock mass. Bollaert argues that rock masses are jointed, and as such erosion is most likely to occur along the joints or cracks in the material lattice. Bollaert set up a force balance between the pulsating normal forces along the rock face that result from flow along the rock surface:

$$\int_0^{\Delta t}\left(F_{up} - F_{down} - W_g - F_{s1} - F_{s2}\right)dt = mv_{\Delta t} \tag{2-65}$$

where F_{up} and F_{down} are the total upward and downward impulses causes by fluctuating pressures on top of a rock block, W_g is the submerged weight of the rock block, and F_{s1} and F_{s2} are the resistive shear forces (friction forces) that develop along the rock block's side faces as it is being lifted up out of the material matrix.

Bollaert solved this force balance for the case where a jet of water pours into a plunge pool. Based on analytical reasoning, the height at which the rock block will be lifted up is given by:

$$h_{up} = \left[2\left(\frac{x_b + 2z_b}{c} \right) \right]^2 \frac{1}{2g x_b^4 z_b^2 \rho_x^2} \left[C_I \phi \gamma \frac{V_j^2}{2g} x_b^2 - (\gamma_s - \gamma) x_b^2 z_b - F_{sh} \right]^2 \quad (2\text{-}66)$$

where x_b is the width of the rock block, z_b is the height of the rock block, c is the pressure wave celerity of water, g is the acceleration due to gravity, ρ_s is the density of the rock block, V_j is the jet velocity into the plunge pool, $\gamma_s = \rho_s g$, $g = \rho g$ where ρ is the density of water, F_{sh} is the sum of shear forces acting on the rock block, and C_I is the dynamic impulsion coefficient. Based on experimental results for a jet entering a plunge pool, the dynamic impulsion coefficient was found as a function of pool depth (Y) and jet diameter (D_j):

$$C_I = 0.0035\left(\frac{Y}{D_j} \right)^2 - 0.119\left(\frac{Y}{D_j} \right) + 1.2 \quad (2\text{-}67)$$

Based on these equations, one can compute the height to which an eroding rock mass will move from its matrix. If the ratio between h_{up} and z_b is greater than 1.0, the rock segment will likely erode. If this ratio is between 0.5 and 1.0, the rock may erode or it may not depending on ambient flow conditions. If this ratio is between 0.1 and 0.5, the rock block will probably vibrate but remain in place and not erode. If this ratio is less than 0.1, the rock block will remain in place.

Bollaert intended this model to be used under conditions similar to a dam spillway. However, it may be possible to develop a similar model for use under local scour conditions. When local scour is present, the force balance shown in Equation 2-65 is the same as it would be when water is entering a plunge pool. The vertical forces are caused by the horseshoe vortices instead of the jet velocity while the resistive forces remain the same. If this is the case, then it appears as though the fluctuating normal stress impulse along a rock's surface during a local scour event should play a role in determining the rock's erosion rate.

2.4 Empirical Methods for Measuring Scour and Erosion in Cohesive Soils and Rock

Most of these aforementioned analytical expressions for erosion in cohesive soils and rock contain a high number of governing parameters. Trammel (2004) argues that it is unrealistic to develop accurate predictive correlations based on these variables. Trammel also cites Mehta who says that the cost of evaluating this high number of parameters is often prohibitively high.

Because of this, Trammel argues that pure empirical methods for predicting erosion rate-shear stress relationships should be explored. Slagle (2006) agrees with Mehta's and Trammel's assessments, and he also advocates the use of pure empirical erosion rate-shear stress relationships for use in the EFA-SRICOS or a method similar to the Miller-Sheppard scour models.

2.4.1 Erosion Rate-Shear Stress Standards for Rock

HEC-18, the state-of-the-art in rock erosion and rock scour is empirically based, but even still most results in this design manual are strictly qualitative. A series of simple guidelines are presented where an engineer can pseudo-determine whether or not a given rock or rock-like material will erode. Specifically, four categories of analysis are recommended to qualitatively determine how a rock-face will react to changing flow conditions resulting from a foundation (Richardson and Davis 2001):

1. Geologic, geomorphologic, and geotechnical analyses
2. The July, 1991 memorandum from the FHWA titled "Scourability of Rock Formations"
3. Flume tests to determine the resistance of rock to scour
4. Erodibility Index procedure

2.4.1.1 Geologic, geomorphologic, and geotechnical analyses (Richardson and Davis 2001)

To determine the geologic parameters used for design, HEC-18 says that extensive rock coring should be used. The cores should be subjected to standard field classification and soil mechanics tests. The geologic formation on which the bridge is to be constructed needs to be determined and mapped. The geomorphology of the site needs to be determined and related to the erodibility of the foundation material. The long-term stability of the stream or waterway needs to be estimated, studied, and related to these geomorphological parameters. Additionally, erosion should be made if the erodibility or scourablity of the rock is unknown.

2.4.1.2 July 1991 FHWA "Scourability of Rock Formations" (Gordon 1991)

According to Trammel, because numerous bridge foundation failures have occurred as a result of rock or rock-like scour, in 1991, the FHWA developed an interim guidance document to assess rock scourability by using empirical methods and testing procedures. Trammel says that these procedures are provided as a guideline until results from ongoing research permit more accurate evaluation procedures for estimating a design scour depth (Gordon, 1991 and Trammel 2004).

According to the memorandum, no single rock index property will properly predict whether or not a rock will scour. Rather, different rock scours for different reasons. For example, a rock may have a high bearing capacity and be very hard, but when water passes over it, it may erode rather quickly. The memorandum encourages designers to use a combination of the following seven methods to assess scourability until more qualitative procedures become available (Gordon 1991):

1.) Subsurface Investigation
2.) Geologic Formation/Discontinuities
3.) Rock Quality Designation (RQD)
4.) Unconfined Compressive Strength, q_u
5.) Slake Durability Index (SDI)
6.) Soundness
7.) Abrasion

Subsurface Investigation

The subsurface investigation portion of the memo simply provides guidelines for the type of borehole pattern to be used when preparing to build a bridge foundation. At minimum, a 3.3 m core length of material below the footing should be obtained and subjected to the remaining six examinations (Gordon 1991).

Geologic Formation/Discontinuities

In general, the 1991 memo says that rock cores with one or fewer fractures per foot should indicate that the rock is of good quality and may resist scour. High rock fracture rates (five or six fractures per foot) qualitatively appear to indicate a poor quality rock that may be scourable (Gordon 1991).

Rock Quality Designation (RQD)

RQD is a modified computation of percent rock core recovery that reflects the relative discontinuity of the rock. The 1991 memo says that rock cores with an RQD less than 50 should be considered to be soil-like and therefore at a high risk of scour (Gordon 1991).

Unconfined Compression Strength

According to the 1991 memo, qualitatively as compressive strength, q_u, increases, bearing capacity increases and scourability decreases. The memo says that there is only a generalized correlation between scourability and compressive strength.

Slake Durability Index (SDI)

The SDI test is a test used on metamorphic rock and sedimentary rock like slate and shale. In general, a low SDI number indicates a highly erodible material. The 1991 memo says that an SDI value lower than 90 indicates that the rock could be highly scourable (Gordon 1991).

Soundness

Soundness is measured by soaking the rock in a magnesium or sodium sulfate solution for twelve hours. Generally, the less sound the rock, the more scourable it will be, but specifically, the 1991 memo says nothing regarding what "less sound" means relative to "more sound" (Gordon 1991).

Abrasion

The 1991 memo cites the Los Angeles Abrasion Test as the method to use for measuring this parameter. Qualitatively, the less a material abrades, the less it will scour, and materials with loss percentages greater than 40 should be considered highly erodible (Gordon 1991).

Discussion of 1991 Memorandum

The above-mentioned memorandum is highly qualitative; there is no definitive point where an engineer can say that a material will or will not erode based on the information given here. Further, this memo was released in 1991; it is nearly twenty years old and there is not yet a

better, more quantitative method for estimating or establishing an erosion rate of a rock or rock-like bed material that can be used in design.

2.4.1.3 Erodibility Index Method (Annandale et al. 1996)

The Erodibility Index Method (ERI) was developed by Annandale, and it identical to Kirsten's Excavatability Index (Richardson and Davis 2001). It is used to quantify the relative ability of a non-uniform earth material to resist erosion. Figure 2-12 provides a definition sketch for the erodibility index method:

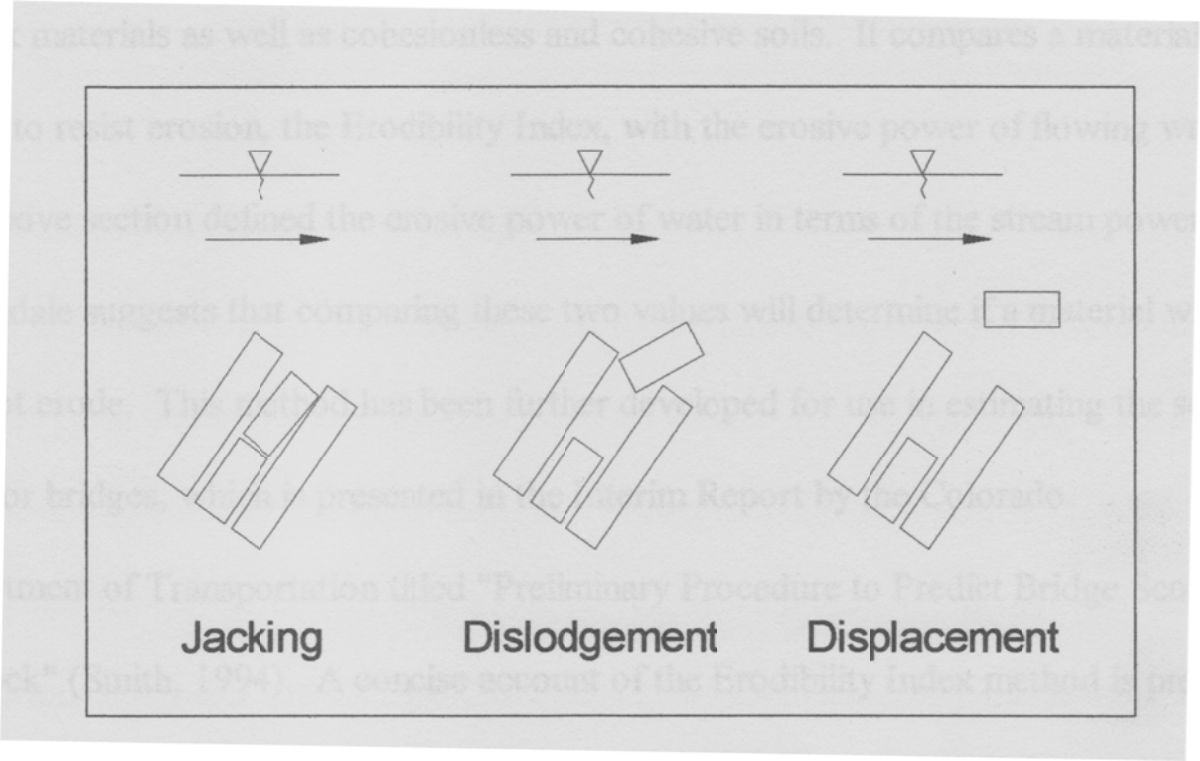

Figure 2-12. ERI Definition Sketch (Henderson 1999)

Water along the bed experiences turbulence, and Annandale suggests that this turbulence causes a pressure gradient that progressively "jacks" rock material from its initial position. Once removed, the material then becomes dislodged and displaced.

In the ERI, a material's ability to withstand erosion, K_h, which is identical to Kirsten's ripability index, is defined:

$$K_h = M_s K_b K_d J_s \tag{2-68}$$

such that M_s is the mass strength number, K_b is the particle or block size number, K_d is the discontinuity or inter-particle bond strength, and J_s is the relative ground structure number. The mass strength number is determined from the material strength of an intact sample of rock without regard to geologic heterogeneity. The particle or block size number is a factor that represents the rock mass quality. The bond strength factor represents the relative strength of discontinuities and it is made by visual observations. The ground structure number relates the shape of material particles to the direction of free-stream flow (Henderson 1999)

Tests were conducted at the Turner Fairbank Highway Research Center's (TFHRC) Hydraulics Laboratory to find a relationship between stream power and scour depth so that a practical application of the ERI could be used for scour prediction. HEC-18 says that based on these tests, although a relationship between ERI and stream power appears feasible, more research is still needed (Richardson and Davis 2001). This evaluation was made before development of Bollaert's Stream Power Model.

2.4.1.4 Flume Tests (Richardson and Davis 1991)

Appendix M of HEC-18 says that samples should be subjected to flume tests to see if they erode. This conclusion is interesting, as it is the same conclusion that is drawn from Appendix L for cohesive sediments. Under cohesive scour conditions, the semi-empirical approaches discussed in Section 2.3 may be applied, and in principle, these methods should be usable when rock is present as well. This ultimately means that for either cohesive sediments or rock, the same method – flume tests (or similar erosion rate testing devices) – are the most effective solution for determining a material's erosion rate-shear stress curve.

2.4.2 Erosion Rate Testing Devices

In principle, the idea of using a flume or a similar erosion rate testing devices appears as though it should be straight-forward. However, like most variables pertaining to the scour problem, implementation of a properly working erosion rate testing device is not as easy as it sounds. The following is a summary of a number of erosion rate testing tests that have been conducted in recent years. Although not every device mentioned was designed to capture erosion rate-shear stress relationships specifically, this discussion highlights the evolution of erosion rate testing devices.

2.4.2.1 Nalluri and Alvarez (1992)

In 1992, Nalluri and Alvarez ran a study to identify the influence of cohesive sediment on erosion of a mixed bed. Tests were conducted in a 154 mm wide open channel and a 302 mm diameter pipe. Their study led to three important conclusions. First, even a low level of cohesive material (and subsequently cohesion) can increase the critical shear stress (and critical velocity required to move a non-cohesive particle). Secondly, sand size has no effect on the critical shear stress of a cohesive sediment. Third, for a given sand, an optimum sand-clay mixture could be achieved where critical shear stress was maximized.

2.4.2.2 Mitchener and Torfs (1996)

In 1996, Mitchener and Torfs synthesized a series of laboratory data from a variety of different types of erosion tests to try to quantify the erosion rates of sand-mud mixtures. After analysis of these data sets, a number of interesting conclusions were drawn:

1. The addition of even a little bit of mud to sand affects the critical shear stress of the mixture.

2. If enough mud is added to sand, the entire mixture behaves as if it was a mud, and these results agree with earlier results by Dade and Nowell.

3. The addition of mud to clays also decreases the erosion rate of sand/clay mixtures compared to what the erosion rate would have been had the mud not been present. Inversely, the addition of sand to mud increases the erosion rate of the mixture.

4. A recommendation was made to further investigate the relationships between erosion parameters (critical shear stress and erosion rates) and bed roughness from 0% sand to 100% sand.

Mitchener and Torfs tried to develop a relationship between erosion rate and bulk density and critical shear stress as well. This relationship is presented in Figure 2-13, while relationships between erosion rate, shear stress, and critical shear stress are presented in Figure 2-14 and Figure 2-15.

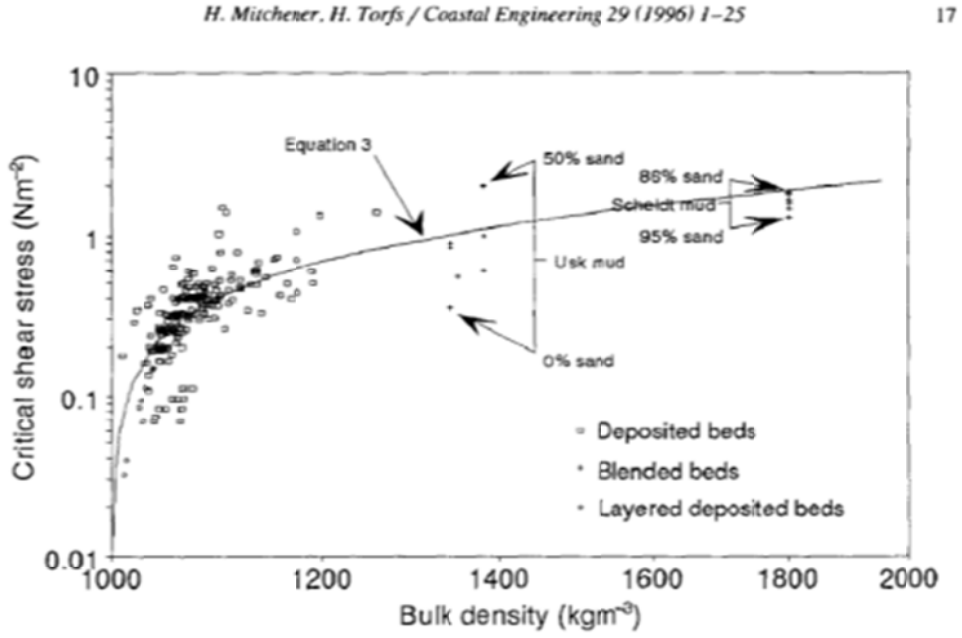

Fig. 9. Critical shear stress for erosion against bulk density for artificially created mixed sediment beds.

Figure 2-13. Relationship between bulk density and critical shear stress (Mitchener and Torfs 1996)

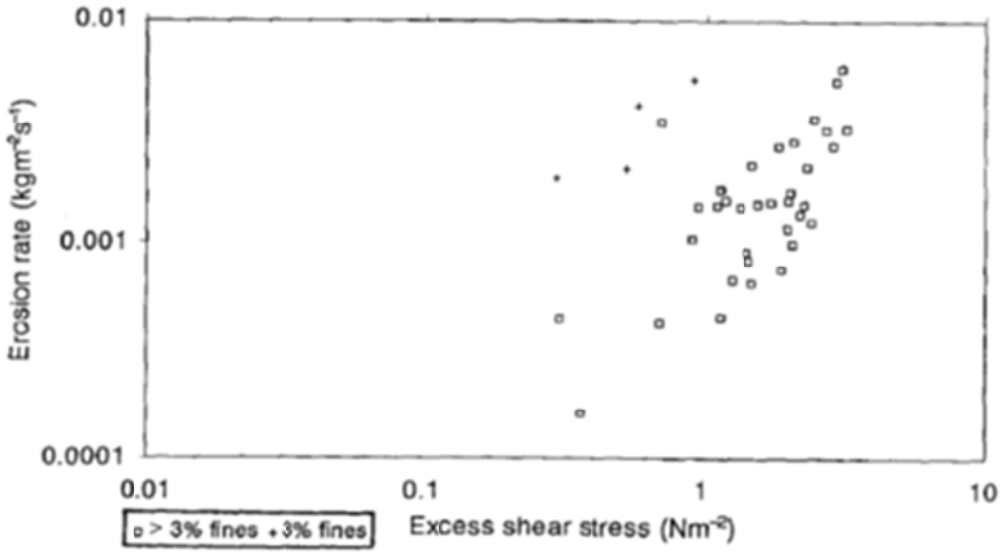

Figure 2-14. Erosion Rate vs. Excess Shear Stress Relationships (Mitchener and Torfs 1996)

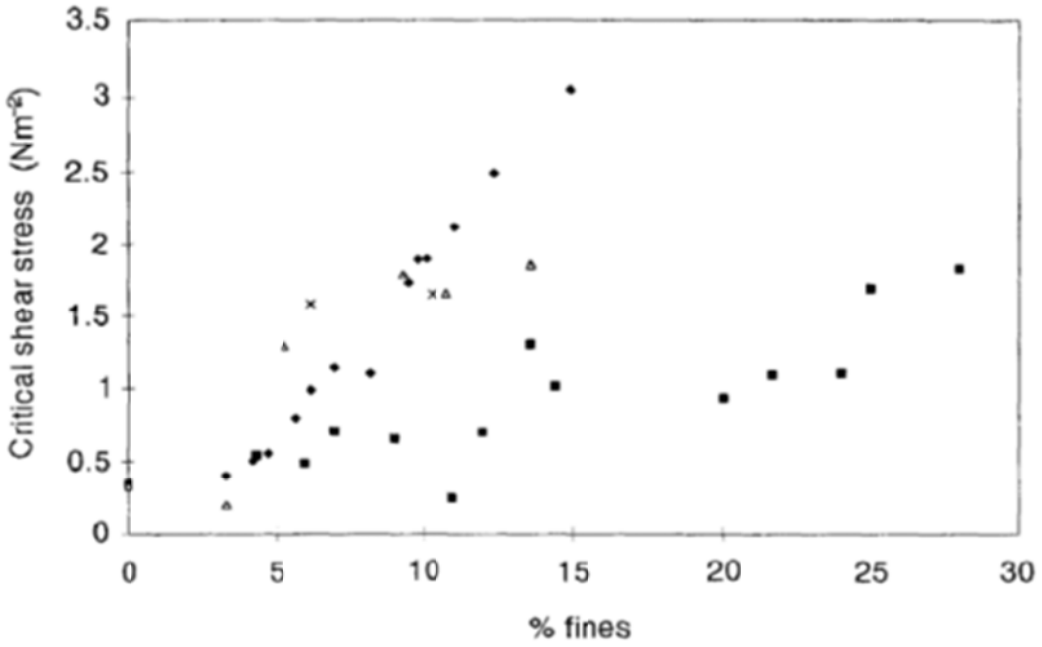

Figure 2-15. Critical Shear Stress vs. % Fines Relationships (Mitchener and Torfs 1996)

2.4.2.3 Panagiotopolous et al. (1997)

Panagiotopolous sought to further study the effects of clay content on a non-cohesive bed. His results suggest that critical shear stresses increase with increased clay content while erodibility decreases with increased clay content. He identified two specific regimes:

1. For sand/clay mixtures where there was less than 30% clay present, there is a slight increase in the critical shear stress for the bed material.

2. For sand/clay mixtures where there was more than 30% clay present, erosion rate decreases.

According to Barry (2003), these results agree with Dyer (1986) and Raudkivi (1990).

Additionally, this study found that if the critical stress was not exceeded for a sand/clay mixture, or if u was less than u_c, and then the velocity was to be slowly increased, critical shear stress would also increase as a result of this pre-critical flow. This was expected because even though the critical velocity was not met at these lower speeds, grains or aggregates that did not satisfy the threshold criterion adjusted to more stable positions within the bed. The implication here is that when tests are run in the EFA or the SERF, velocities need to be selected randomly

when erosion rates are measured. If velocities are not selected randomly, the erosion-rate testing apparatus will under-predict the erosion rate for a given shear stress.

2.4.2.4 SEDFlume (McNeil et al. 1996, Jepsen et al. 1997)

In 1996, McNeil wanted to find the erosion rates and associated shear stresses of fine grained bed materials. His motivation was environmental, not structural; his goal was to see if there was there potential for contaminants at the bottom of rivers to resuspend themselves during large-scale storm events.

To investigate this issue, McNeil developed the Sediment Erosion at Depth Flume or SEDFlume. At the time, SEDFlume was unique because it allowed for in-situ testing of bed materials. According to McNeil, previous laboratory designs by their nature disturbed the sediment that they tested; McNeil cites Fukuda and Lick (1980), Mehta, et al. (1982), Tsai and Lick (1988), and MacIntyre et al. (1990) as examples of laboratory flumes that disturb the samples that they are testing (McNeil et al. 1996).

A sketch of the original SEDFlume schematic is presented in Figure 2-16. An undisturbed sample is loaded into the SEDFlume and a piston is placed below the sample. Then, water was pumped through the 2 cm by 10 cm flume from a 120 gallon reservoir tank. As the water passed over the sample, the sample eroded, and as the sample eroded, the piston was raised so that the sample was level with the bottom of the bed (McNeil et al. 1996).

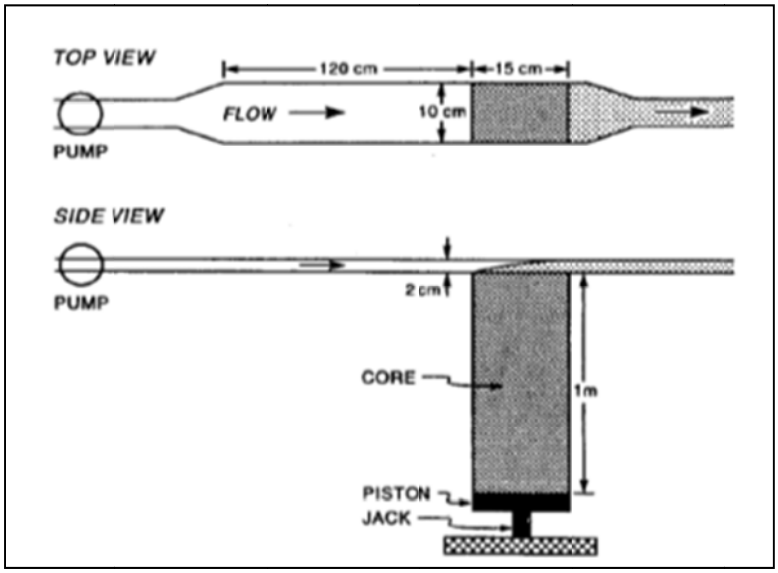

Figure 2-16. Original Schematic Diagram of SEDFlume

The mechanism for raising the piston (and subsequently the sample) into the flume was operator dependent. The research technician was charged with watching the sample erode and advancing the sample into the flume with a 1/3 hp motor. One had to have experience using the device to know when to turn on the motor, how fast to raise the piston, etc.

Shear stresses in the SEDFlume were estimated using Prandtl's Universal Law of Friction. For a rectangular duct with smooth surfaces, Equation 2-69 can be derived:

$$\frac{1}{\sqrt{\lambda}} = 2.0\log\left[\frac{UD\sqrt{\lambda}}{\upsilon}\right] - 0.8 \tag{2-69}$$

$$D = \frac{2hw}{h+w} \tag{2-70}$$

$$\lambda = \frac{8\tau}{\rho U^2} \tag{2-71}$$

where λ is the friction factor defined by the Darcy-Weisbach equation given in 2-71, U is the freestream velocity, D is the hydraulic diameter defined by equation 2-70, ν is the kinematic viscosity of water, h is the height of the duct, w is the width of the duct, and τ is the shear stress on the four walls of the duct. These three equations can be combined to find shear stress as an implicit function of freestream velocity. To measure freestream velocity, a paddlewheel flowmeter was used (McNeil et al. 1996).

As shown here then, the SEDFlume did not measure shear stresses directly; rather, shear stresses were implied as a function of freestream velocity. The assumption behind the usage of these equations then is that the shear stress on the walls of the flume approximates the shear stresses seen by the eroding sample and that the SEDFlume is hydraulically smooth. In his paper, McNeil says that he uses a relationship between shear stress and flow rate for a hydraulically smooth flow (Figure 2-17).

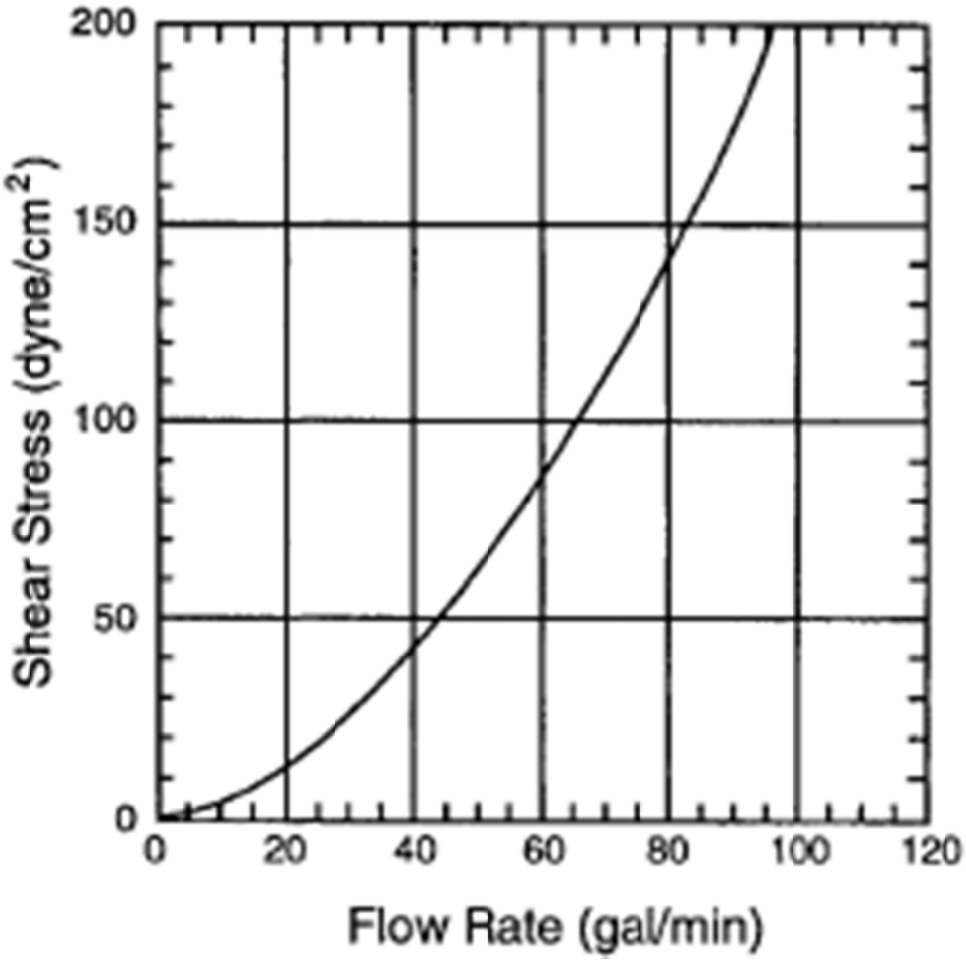

Figure 2-17. Flow Rate vs. Shear Stress Relationship (McNeil et al. 1996)

Measurements of erosion rates were conducted on a series of samples from the Trenton Channel of the Detroit River from 1993 – 1994. McNeil organized erosion rates as a function of both core depth and shear stress. An example of McNeil's results is presented in Figure 2-18:

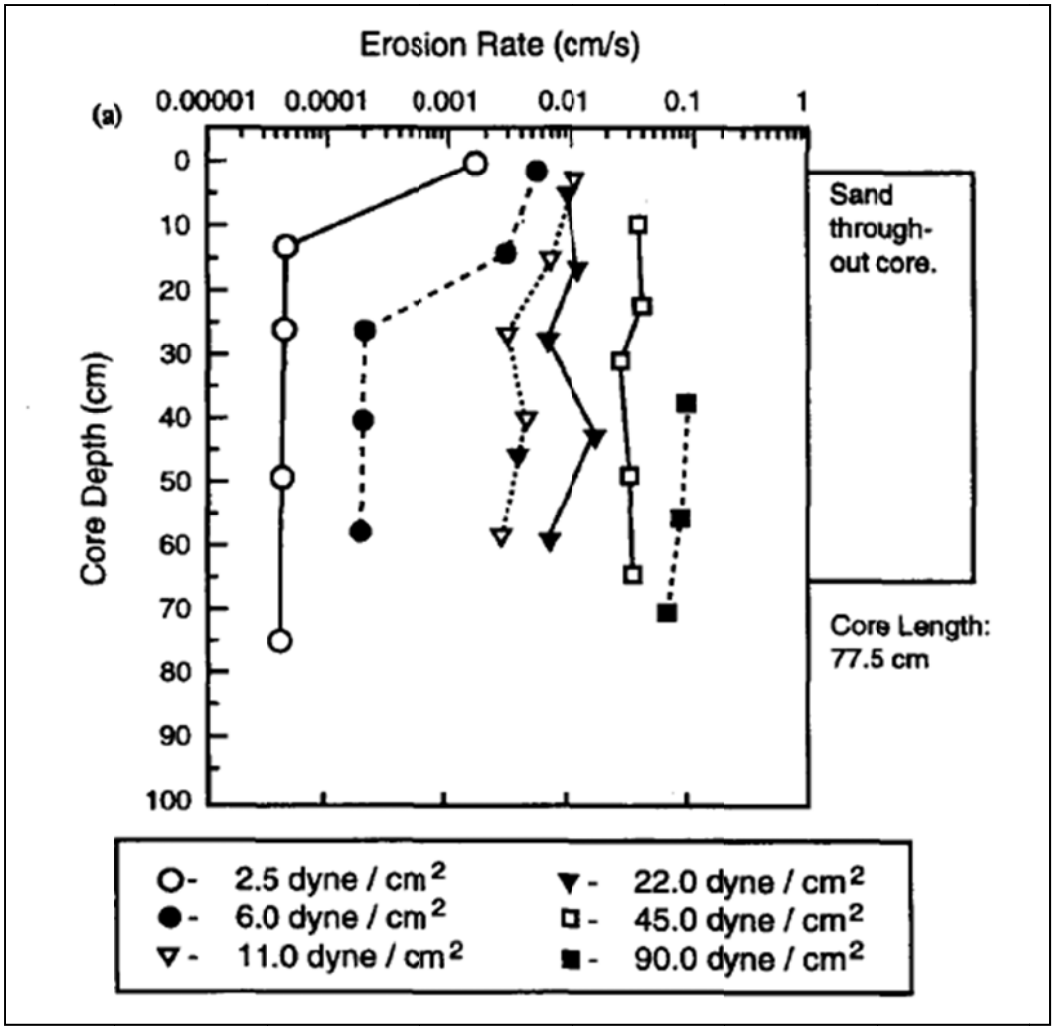

Figure 2-18. Example of SEDFlume Results (McNeil et al. 1996)

McNeil's results show that as shear stress increases, erosion rate also increases, and they imply another interesting phenomenon. As depth increases for a given shear stress, it appears that erosion rates level off. Consider that McNeil was dealing with cohesive sediments. As depth increases for a cohesive sediment, it is likely that consolidation of these sediments increases. As consolidation increases, it is likely that material strength, or cohesive strength, of the sediments increases. If this is true, then his results imply that material strength also plays a role in determining the erosion rate of his bed materials.

In 1997, Jepsen, Roberts, and Lick extended McNeil's work. They ran a series of tests to determine erosion rate and critical shear stress as a function of bulk density for bed particles from the Detroit River in Michigan, the Fox River in Wisconsin, and a slough near Santa Barbara, California. Their results show that for a given shear stress, erosion rate is a unique

function of bulk density and erosion rate decreases as bulk density increases (Jepsen et al. 1997). This appears to imply a further dependence between erosion rate and material strength because as density increases, materials become more compacted. As materials become more compacted, their cohesive strength should increase. Shear stress estimation still utilized a flat-bottom Darcy-Weisbach frictional coefficient.

In 2003, the SEDFlume was enhanced so that it could produce oscillatory flows. The new device was named the SEAWOLF and it was used to measure erosion rates of quartz sand under these oscillating conditions. To predict shear stress under oscillating conditions, an effective shear stress for wave motion is estimated. Then, this effective shear stress is transferred to erosion rate-shear stress relationships from unidirectional flow to yield a prediction for erosion rate under wave conditions (Jepsen et al. 2003).

2.4.2.5 ASSET (Roberts et al. 2003)

In 2003, Roberts et al. developed the second generation of the SEDFlume. The motivation behind this research was that although the SEDFlume was useful for measuring sediment erosion rate properties, it only measured bulk erosion rates. The SEDFlume gave no information regarding the transport mode of eroded materials – i.e. bedload vs. suspended load. The Adjustable Shear Stress Erosion and Transport (ASSET) Flume was designed to determine the bedload fraction of eroding sands.

The ASSET was similar to the SEDFlume, but its dimensions were slightly larger. While the SEDFlume was 2 cm tall by 10 cm wide, the ASSET was 5cm high by 10.5 cm high. The ASSET was designed with a bedload trap positioned 1 m downstream from the eroding sample (Figure 2-19). Sand caught in the bedload trap during a test was the bedload fraction from that run (Roberts et al. 2003).

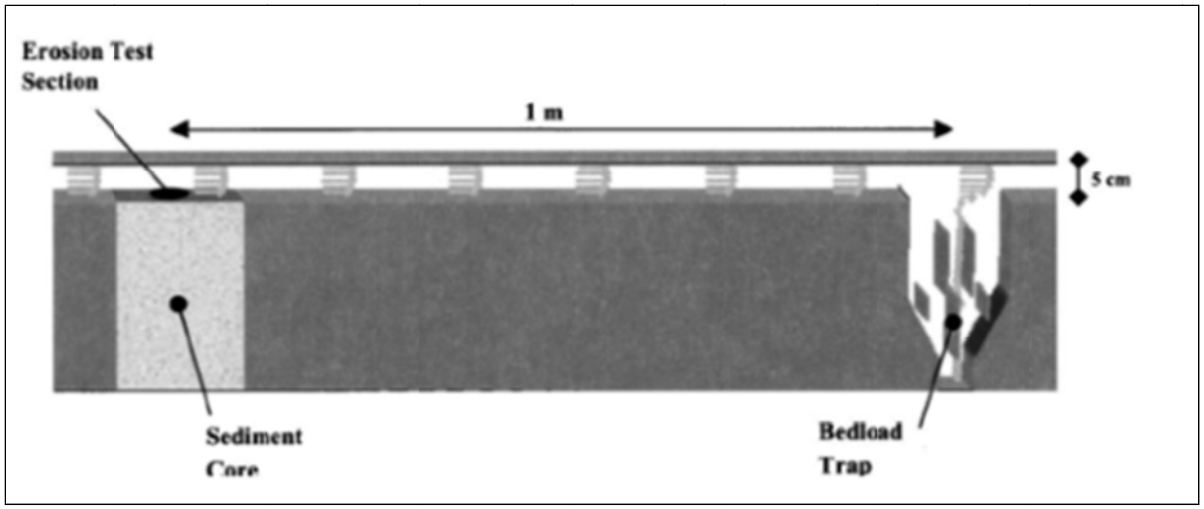

Figure 2-19. Original Schematic of the ASSET (Roberts et al. 2003)

The ASSET used the same method as the SEDFlume for estimating shear stresses on an eroding sample – Equation 2-69, Equation 2-70, and Equation 2-71. Results from the ASSET show that bedload fraction is a function of both particle size and shear stress (Figure 2-20). Because the focus of this study was on determining bedload, no information was given regarding total erosion rate as a function of shear stress.

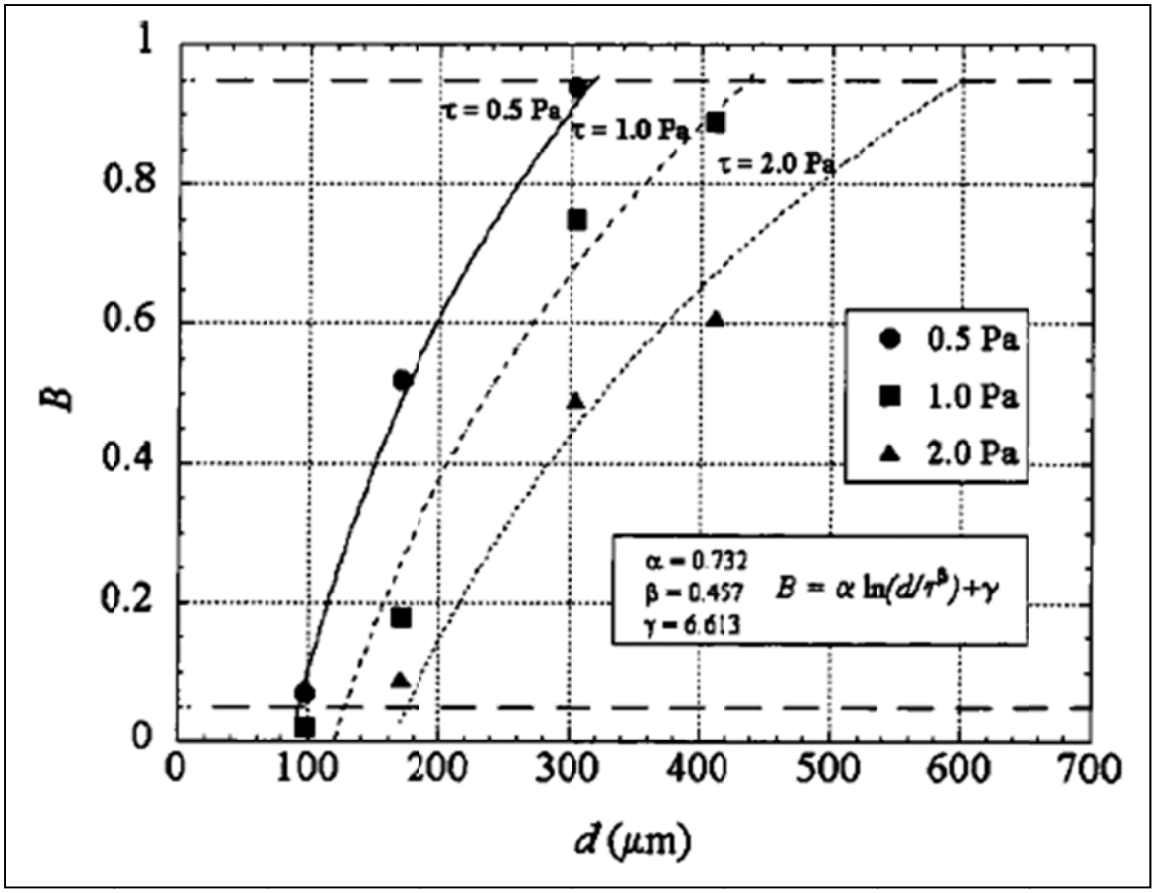

Figure 2-20. Results from ASSET Tests (Roberts et al. 2003)

Roberts mentions that some qualitative work was done in the ASSET with cohesive sediments. Although no hard data is given in his paper, he notes that cohesive sediments often do not erode as individual particles; rather, cohesive sediments erode as aggregates, or flocs (Roberts et al. 2003).

2.4.2.6 EFA (Briaud et al. 1991-2004)

The EFA-SRICOS method has been discussed at length in terms of the initial requirements necessary for its implementation. In preceding discussion regarding the EFA-SRICOS method, it was assumed that it would be possible to determine a shear stress-erosion rate relationship.

The principle behind the EFA is similar to principles behind both the ASSET and the SEDFlume. In fact, the EFA and the ASSET/SEDFlume/SEAWOLF apparatuses were developed independently from one another. A sample is loaded into the flume through the

bottom, and as water passes over the sample, the sample is advanced into the flume. Through this mechanism, erosion rate is measured directly.

Similar to the ASSET and the SEDFlume, the advancement mechanism of the EFA (Figure 2-21) was also conducted via visual inspection. According to the EFA testing procedure, the sample is to be loaded into the flume such that it protrudes into the flume 1 mm (Figure 2-22); presumably this protrusion into the flume is recommended so that visual inspection is easier.

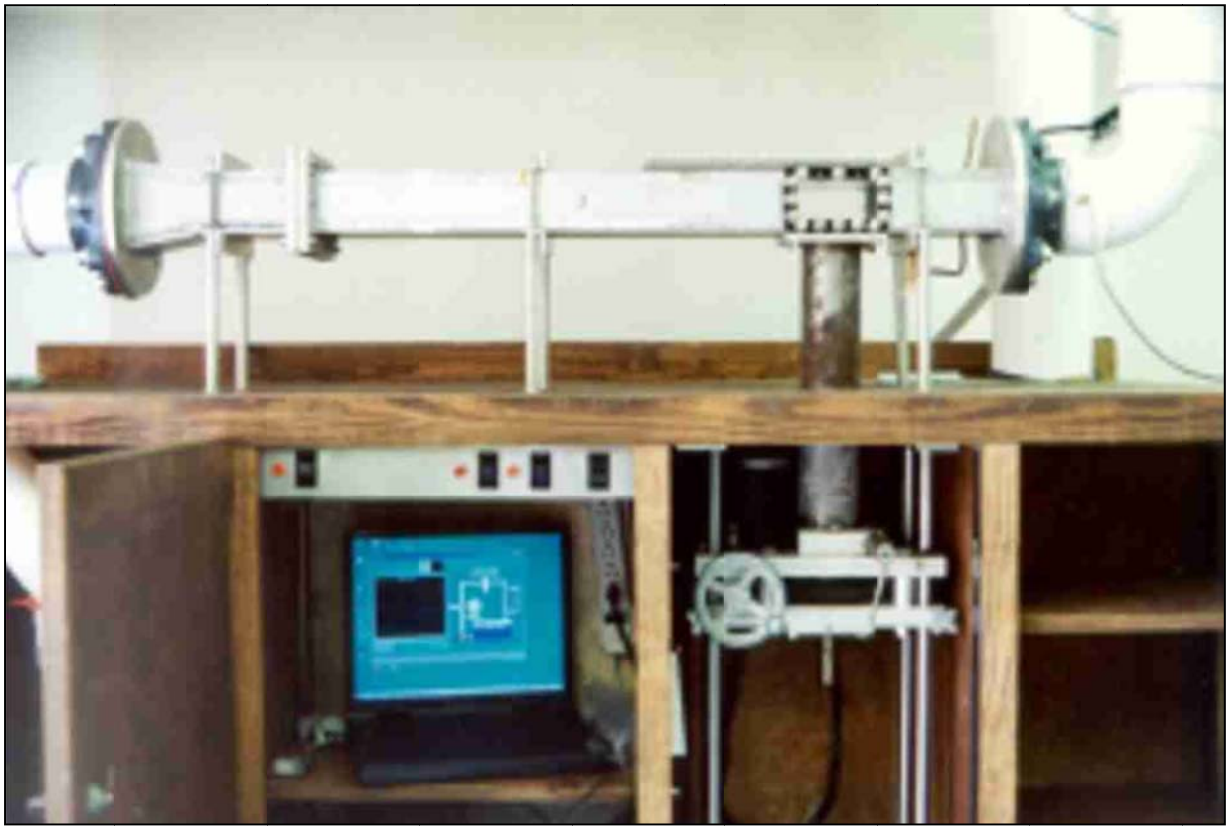

Figure 2-21. Photograph of the EFA (Briaud et al. 2010)

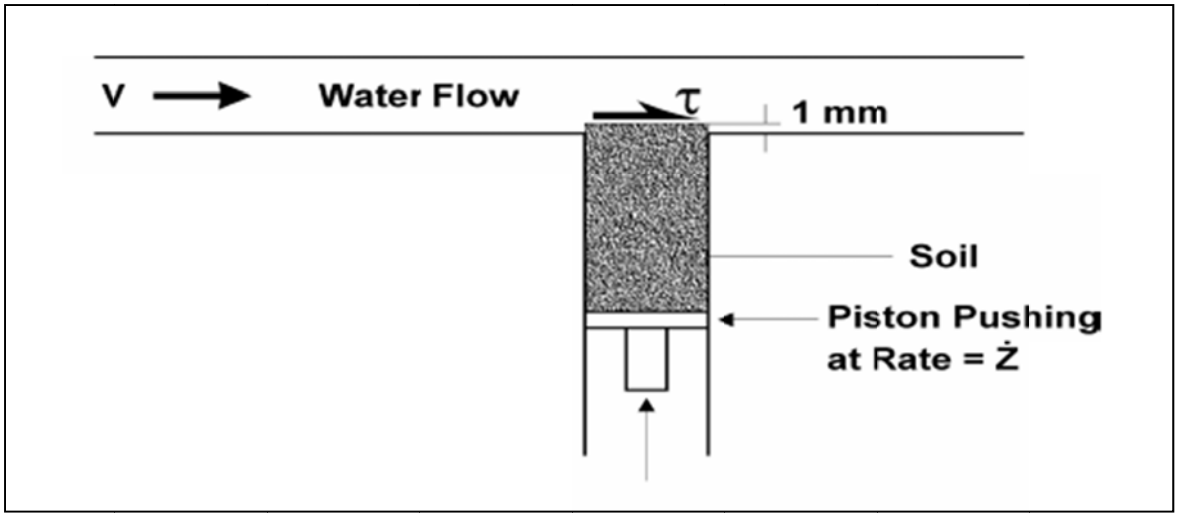

Figure 2-22. Schematic of 1 mm EFA protrusion into flume (Briaud et al. 2010)

As of the date of the last known EFA publication (2004), the EFA estimates shear stress by using a Moody chart (Figure 2-23).

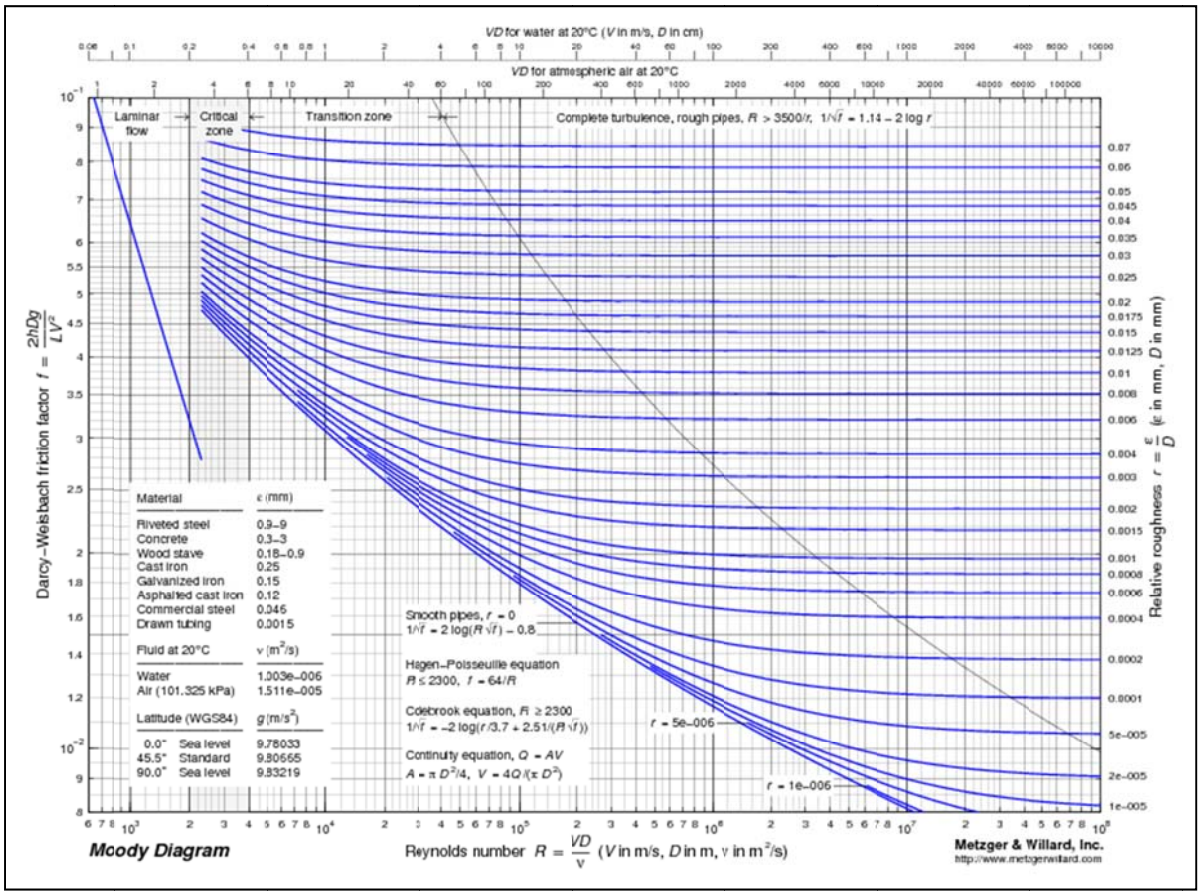

Figure 2-23. An example of a Moody Diagram (Briaud et al. 2010)

Shear stress is approximated by finding a friction factor from the Moody diagram and then using the friction factor to approximate shear stress with the following equation:

$$\tau = \frac{1}{8} f \rho v^2 \tag{2-72}$$

where τ is the shear stress, f is the friction factor, ρ is the density of water, and ν is the kinematic viscosity of the water.

Like other erosion rate testing devices, the EFA does have drawbacks, and erosion rate-shear stress data from it has been criticized in the past. First, the EFA's method for shear stress estimation has been questioned (for example in Annandale 2005). Friction factor estimation from the Moody Diagram depends on selection of the correct roughness factor or roughness height. If the relative roughness of an eroding sediment can be properly estimated, the Moody Diagram method may work properly, but selecting the correct relative roughness for a bed material is not straight forward. In his work, Briaud does not indicate what value for relative roughness he is using during EFA shear stress estimates, nor does he indicate how any roughness coefficient is calibrated in his flume. Further, the Moody diagram was developed from tests with pipes of uniform roughness. The EFA does not have a uniform roughness. The side walls and top of the EFA's rectangular duct are smooth while the false bottom in which the sample projects itself into the flume is rough. Annandale (2005) says that because of this, using a uniform roughness coefficient from a Moody diagram is incorrect.

The second possible oversight with regard to the EFA is that the sample protrudes into the flume 1 mm. If the sample is protruding into the flume, it will be subjected to both normal stresses and shear stresses. Because of the addition of a normal stress, the sample will erode faster than it would if it was subjected to only a shear stress. It appears then that for a given shear stress as estimated upstream using a Moody Diagram (or more explicitly a given velocity, as velocity is the only quantity that is actually measured during the test), erosion rates would be overestimated. This overestimation of erosion rates for a given shear stress would lead to conservative equations. Conservative equations are better than non-conservative equations, but if the erosion rate data from the EFA could be improved, it may be possible to avoid over designs.

The third possible issue associated with the EFA-SRICOS method is the same discussed with both the ASSET and the SEDFlume in that these devices rely on visual inspection to

advance the sample into the flume. They are also operator dependent, and reproduction of results may be difficult.

2.4.2.7 RETA (Henderson 1999 Kerr 2001 and Slagle 2006)

Preceding erosion-rate testing devices that were used to estimate shear stresses and measure erosion rates of cohesive material were designed similarly: a flume was used to flow water over an advancing sample, and a theoretical relationship used to estimate the shear stress on it. In 2001, The Rotating Erosion Testing Apparatus (RETA) was designed to measure erosion rates and shear stresses of a intact bed material as an alternative design.

The RETA (Figure 2-24) approaches the problem differently than traditional bottom-loaded flume designs. Instead of flowing water over a sample, in the RETA a sample is loaded into an annulus filled with water (Figure 2-25 and Figure 2-26). The annulus spins around the sample which creates a shear stress, which in turn causes the sample to erode (Figure 2-27). Before the sample is loaded, a hole is drilled through it, a rod is attached through the center of the sample, and the sample rod is attached to a torque cell (Figure 2-28). Rather than inferring shear stress from theoretical equations that describe shear stress on the flat walls of a flume, the torque cell measures the shear stresses directly (Kerr 2001).

Figure 2-24. Photograph of the RETA (Sheppard et al. 2006a)

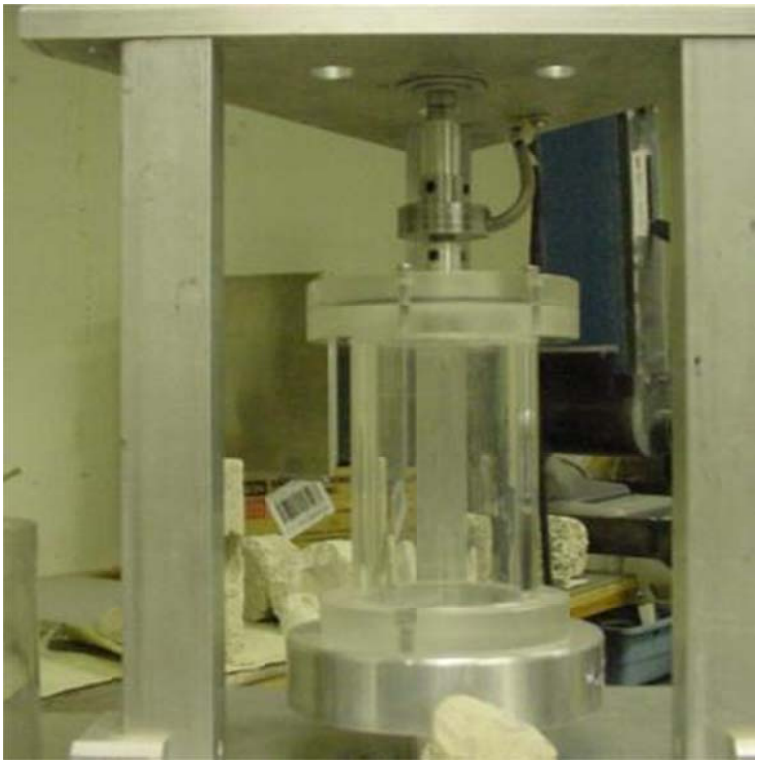

Figure 2-25. RETA Sample Annulus (Sheppard et al. 2006a)

Figure 2-26. RETA Sample Annulus (Close-up) (Sheppard et al. 2006a)

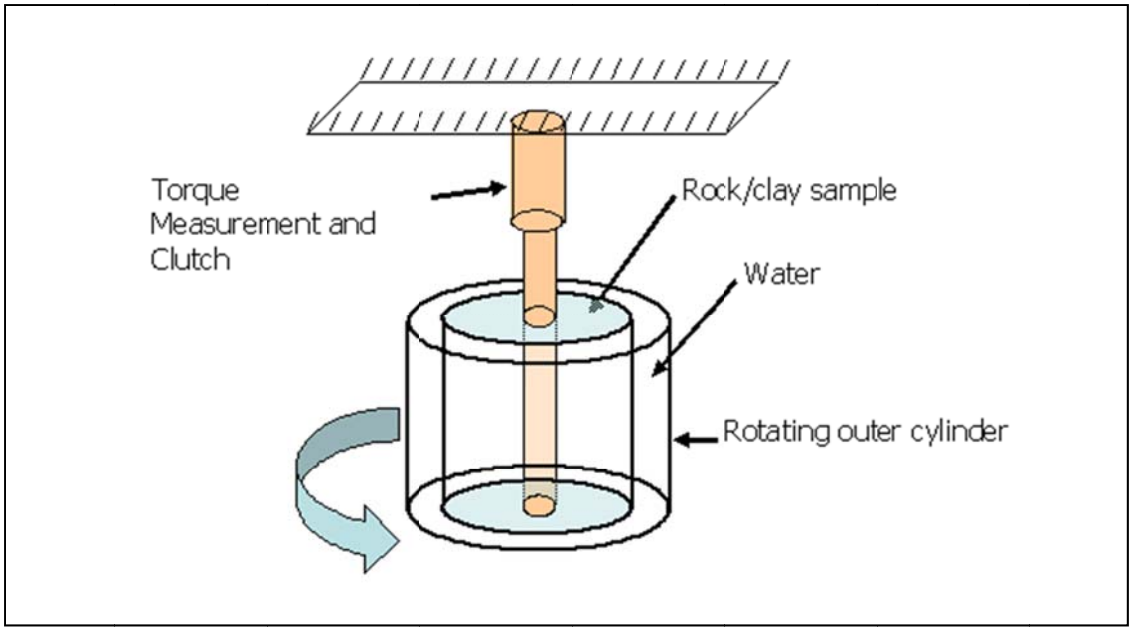

Figure 2-27. Schematic Diagram of RETA (Sheppard et al. 2006a)

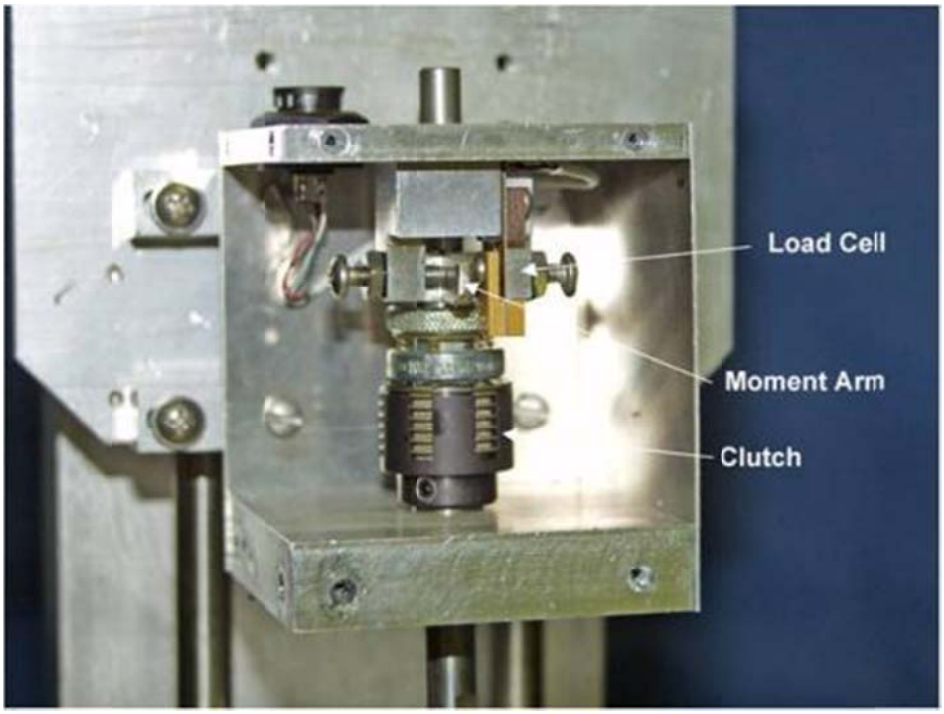

Figure 2-28. Photograph of Torque Cell in RETA (Sheppard et al. 2006a)

Figure 2-29. Photograph of Rock Sample in RETA (Sheppard et al. 2006)

Figure 2-30. Top View of RETA (Sheppard et al. 2006)

The torque cell measures torque on the entire sample as the rotating cylinder spins around it. To convert the torque measurement to shear stress, Equation 2-73 is used. To find the total erosion rate, Equation 2-74 is applied. In these equations, R is the radius of the sample, L is the length of the sample, T is the torque measured from the torque cell, E is the erosion rate, Δm is the amount of mass removed during the test, and D is the duration of the test. Standard RETA tests are specified to be run for 72 hour increments (Sheppard et al. 2006a).

$$\tau \equiv \text{Average Shear Stress} = \frac{T}{2\pi R^2 L} \tag{2-73}$$

$$E = \frac{\Delta m}{2\pi\rho RLD} \tag{2-74}$$

The most obvious advantage to RETA testing is that shear stress is measured directly, but this technique is not without criticism. Because the gap between the sample and the annulus' walls is small, the size of turbulence-induced vortices in the flow regime between the sample and the annulus wall may be different for the same average shear stress. In other words, under rock-like erosion conditions where the normal force impulse to the rock face is the dominant erosion mode, the fluctuating normal stress component to the material face will be different than it would be in nature.

There are other pitfalls in using average shear stress along a vertical plane to represent the shear stress on the sample. The RETA presumes uniform erosion; in reality, when rock is subjected to RETA testing, sometimes chunks of the material often erode at one time. This "chunking" and "pitting" mechanism can produce localized shear or normal stresses along the sample face that are higher than the uniform component. This is in turn can produce more chunking, which in turn can produce even greater localized shear stresses, etc. These localized stresses cause localized higher erosion rates, yet a value for average erosion rate is the goal. Because erosion rate is measured by simply measuring the mass of the sample at the end of the test and subtracting this mass from the total mass at the beginning of the test, these localized variations can cause inaccurate average erosion rate results.

This pitting or chunking mechanism implies the presence of rock-like erosion, and while shear stress is measured directly in the RETA, normal stress is not. As shown in Section 2.3, when rock-like erosion dominates, erosion rate is probably not a strict function of shear stress.

The third criticism with the RETA is that because the fluid around the sample is being spun, the sample is subjected to torque or moment action. Kerr (2001) and Slagle (2006) both argue that this behavior would lead to slightly more conservative equations and is therefore acceptable. Critics, particularly those who would label the equations in HEC-18 as "overly conservative" would argue that because there is no quantitative date to support the claim that this moment action leads to only "slightly conservative results," one cannot be sure how overly conservative the RETA is (Kerr 2001). Because of these concerns, there has been a goal in recent years to correlate RETA results to results from another erosion-rate testing apparatus.

RETA Results

Tests in the RETA were conducted by both Kerr in 2001 and Slagle in 2006. Kerr's tests were preliminary; the focus of his work was development and calibration of the instrument. Slagle's work on the other hand was more comprehensive. First, Slagle conducted a series of RETA tests on limestone taken from the Jewfish Creek Bridge on US 1 in near Key Largo, FL. Like Briaud, Slagle developed curves for erosion rate vs. shear stress (Figure 2-31). However, Slagle, after discussion with Bloomquist, hypothesized that erosion rate of a rock may also be a function of material strength. He presented one graph of particular interest (Figure 2-32) in his Master's Thesis that shows Jewfish Creek limestone behaving with some dependence on cohesion.

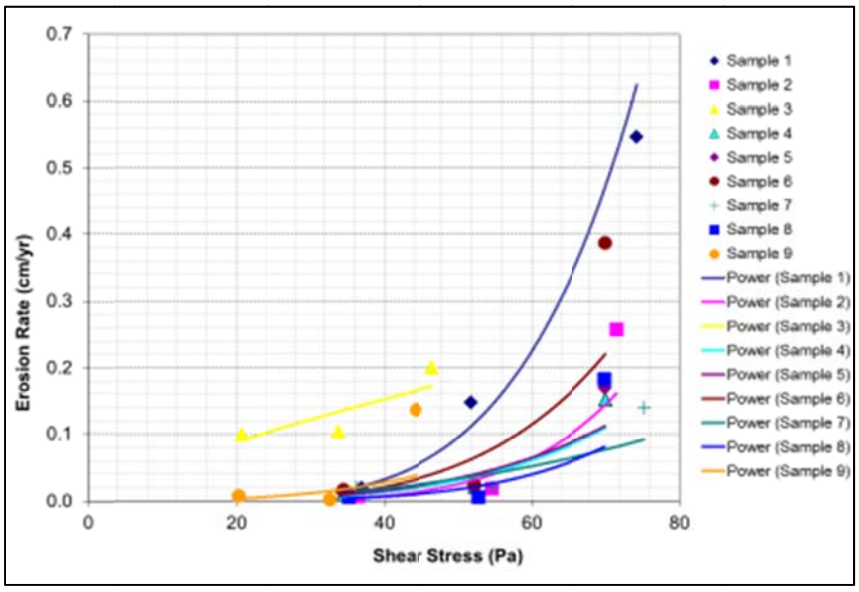

Figure 2-31. Relationship between shear stress and erosion rate for different Jewfish Creek Limestone samples (Slagle 2006)

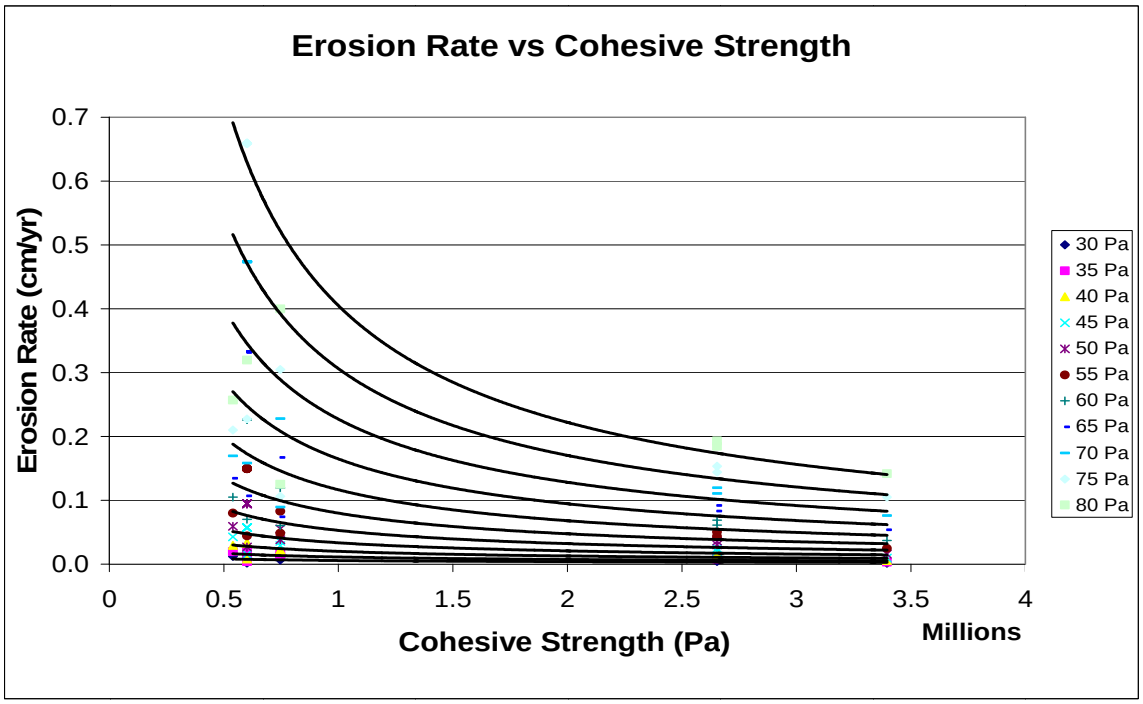

Figure 2-32. Relationship between cohesion and erosion rate for different shear stresses from Jewfish Creek Limesonte data set (Slagle 2006)

Cohesion may be derived from two Mohr's Circle using simple geometry. Figure 2-33 provides a definition sketch:

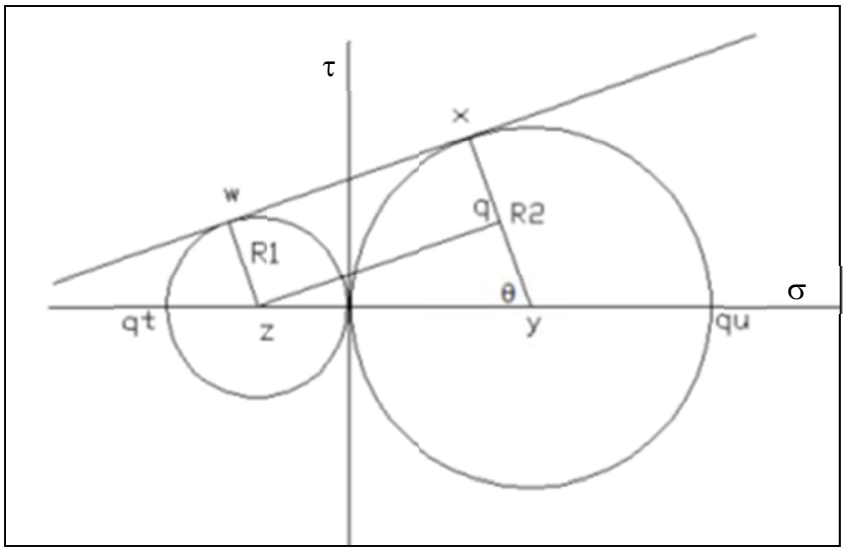

Figure 2-33. Definition sketch for Cohesion Derivation

If one examines triangle *zqy*, the cosine of the angle, θ, and the sin of the angle can be defined:

$$\cos\theta = \frac{R_2 - R_1}{R_2 + R_1} \tag{2-75}$$

$$\sin\theta = \frac{2\sqrt{R_1 R_2}}{R_2 + R_1} \tag{2-76}$$

If a perpendicular line is then drawn from point *x* perpendicular to the x-axis, a new triangle will be apparent, and the length of the perpendicular distance from point *x* to the x-axis can be shown to be $R_2\sin\theta$. Furthermore, the slope of line *wx* must be the same as the slope of line *zq*, and it must equal $-x\cot\theta$.

Next, coordinates are transferred such that the new y-axis now sits at the center of Circle 2. From above, the equation of line *wx* through the new coordinate system must be:

$$y' = \frac{R_2}{\sin\theta} - x\cot\theta \tag{2-77}$$

Cohesion is defined as the point where line *wx*, the line tangent to both the Mohr's Circle for axial strength (circle 1) and the Mohr's Circle for compressive strength (circle 2) crosses the x-axis. Setting *x* in Equation 2-77 equal to R_2 and using Equation 2-75 and Equation 2-76 yields the following expression:

$$y' = \frac{R_2 R_1}{\sqrt{R_1 R_2}} \tag{2-78}$$

Substituting q_u and q_t, or the compressive and axial strength definitions respectively, yields:

$$y \equiv C = \frac{1}{2}\sqrt{q_u q_t} \tag{2-79}$$

where *C* is the cohesion.

Figure 2-32 appears to indicate that erosion rate may be a function of shear stress and cohesion, but Slagle's results are limited. This figure is the only graph that he presents that shows this relationship. More work needs to be done to determine whether this dependence on cohesion is simply a coincidence that was found for Jewfish Creek Limestone or whether this dependence on cohesion can be extrapolated to other materials. Work by Briaud et al. (1999) suggests that erosion rate is not a function of any geotechnical properties and therefore he recommends his site-specific EFA-SRICOS method. In a 2002 discussion piece, Hanson and Simon agree with Briaud's assessment (Hanson and Simon 2002).

On the other hand, if one examines the definition of a Mohr's circle, the vertical axis represents shear stress while the horizontal axis represents normal stress. If erosion is caused by a simple shearing action, then the normal stress – or value along the Mohr's circle x-axis – should be close to zero. This would lead directly to the y-intercept, or the cohesion point. If Slagle's apparent relationship between erosion rate and cohesion can be proven, it may contradict Briaud's assessment and provide an alternative means for predicting erosion rates of bed materials. Slagle's relationship implies that under the conditions that he studied, shear stress was dominant.

Slagle's other results from the RETA focused at finding erosion rates of Gator Rock (Section 2.5). For now, it is sufficient to say that Gator Rock is a material that is designed to be uniform in its properties. Slagle did this run of tests presumably to compare RETA results with SERF (Section 2.4.2.9) results, but instead of running the same shear stresses in each instrument, he used the RETA to measure results with a low shear stress and the SERF to measure results with a high shear stress.

Slagle argued that because his erosion rate curves followed the same trends when he combined instrumental results, it proved that both instruments were measuring erosion rate and shear stresses correctly and that the RETA had been verified. This argument is questionable because there are significant "gaps" between the data sets. For example (Figure 2-34), there are no readings between approximately 40 Pa and approximately 70 Pa.

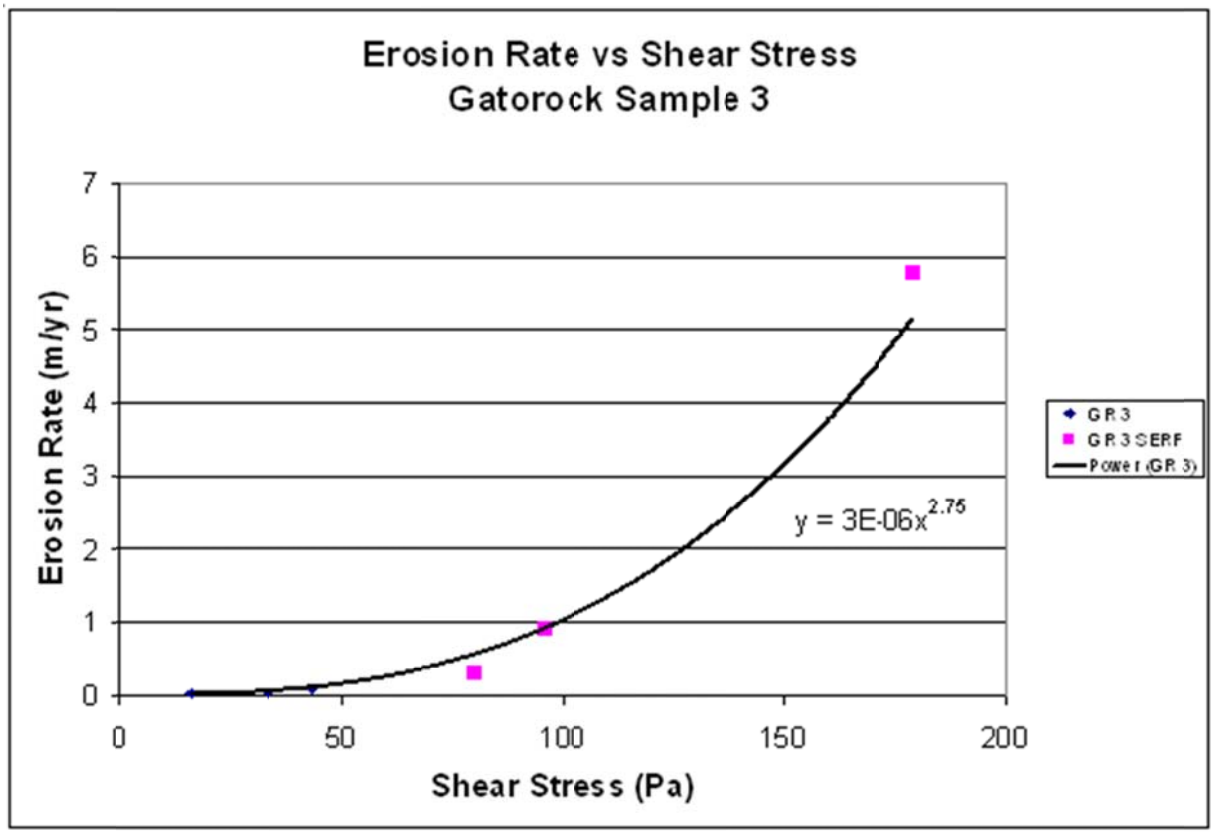

Figure 2-34. Typical results from Slagle's Gator Rock tests. The pink data points are from the SERF and the blue data points are from the RETA (Slagle 2006)

This data gap is typical for most of Slagle's tests. Slagle only ran one test where there was an overlapping shear stress data point. Although this data point did match in both the RETA and the SERF, one point is not enough to say that results from the RETA are proven to be the same as they would have been using a more traditional erosion rate testing device. Slagle also discussed issues with Gator Rock non-uniformity in his thesis. Although a graph of Gator Rock erosion is presented here, there no data could be found that verified near uniform erosion in the RETA. As discussed, a fundamental assumption behind the RETA is that samples will erode uniformly; if they do not, it is difficult to rely on the results, and hard to say what is being measured.

2.4.2.8 Barry et al. (2003)

In 2003, Barry ran a series of tests to determine how critical shear stress of a sand-clay mixture varied based on clay content. Testing was conducted in a recirculating flume, a Schultz

ring tester, and a RETA (although as of 2003, the RETA was called the "Simulator of Erosion Rate Function," or "SERF").

Barry concluded that as clay particles were added to the mixture, critical shear stress first decreased to some value, ψ_{min}, then steadily increased beyond this ψ_{min} threshold. Barry developed a shear resistance model for clay lubrication, to explain this behavior of ψ_{min} but it performed poorly when compared to experimental results. Barry blamed the analytical model's failure on the fact that the model predicted a clay layer that was much smaller than the asperities in the sand. Although this round of tests is excellent for providing critical shear stresses as a function of clay content, it did not measure erosion rates of these materials.

2.4.2.9 SERF (Trammel 2004, Slagle 2006, Kerr 2001)

The SERF (Figure 2-35 and Figure 2-36) was designed over a number of years at the University of Florida in parallel with development of the RETA. The goal during design was to construct a traditional flume-designed erosion-rate testing device. Although it was to be similar to the devices developed and used by Professor Wilber Lick at the University of California at Santa Barbara (the ASSET, SEDFlume, and SEAWOLF) it would contain significant improvements. It should be emphasized that these devices were all developed independently from the EFA. According to Braiud, development of the EFA began in the 1990's, while Lick's devices were starting to be developed during the 1980's (McNeil et. al 1996, Briaud 2010).

Figure 2-35. Photograph of the SERF (Side View) (Trammel 2004)

Figure 2-36. Top View of the SERF (Original Design) (Trammel 2004)

The SERF is a rectangular recirculating flume that is driven by two 1000-gpm pumps (Figure 2-37). The flume's cross-sectional dimensions are 1.75 inches by 8.00 inches. Along its length, the flume is designed so that a 4 inch Sch.80 pipe feeds into the rectangular section through a tapered 1 foot transition region. Beyond the transition region is a 1 foot section of rectangular flume that is equipped with a flow straightener. Total length of the rectangular section of the flume is 10 feet. Flow rates in the flume can reach approximately 2000 gpm. An eroding sample section is located in the center of the rectangular portion of the flume (Figure 2-38).

Figure 2-37. Pumps used to drive water through the SERF (Trammel 2004)

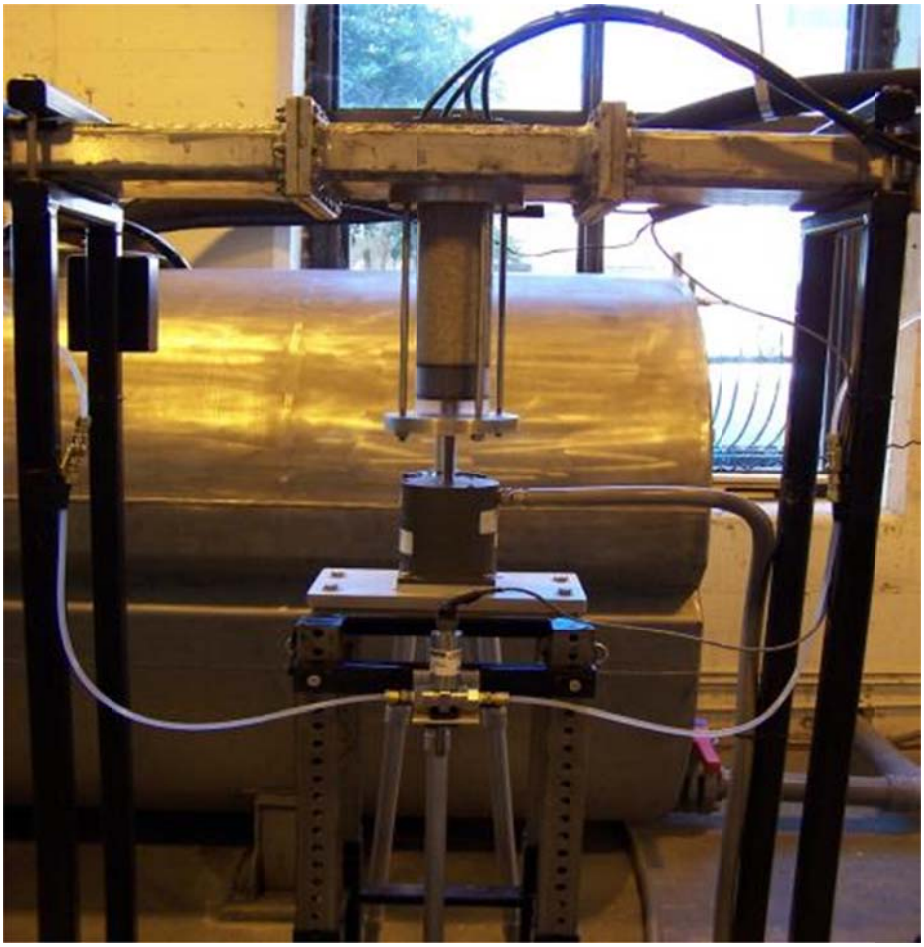

Figure 2-38. Eroding Sample Section of the SERF (Trammel 2004)

The first goal of the design of the SERF was to remove operator dependency from testing. Recall that during an EFA test, the sample is to protrude into the flume 1 mm, the sample is to be eroded, and then the sample is advanced again. Advancement procedures with the EFA (and previous devices) were conducted manually. With the SERF, its designers hoped to take the operator out of the equation; instead a computer would decide when a sample was to be advanced into the flume. Although the SERF is equipped with a viewing port (Figure 2-39), unlike the EFA whose port is used by the operator on when to advance the sample. Instead, the SERF's port was installed so that a video camera can keep a record of erosion testing.

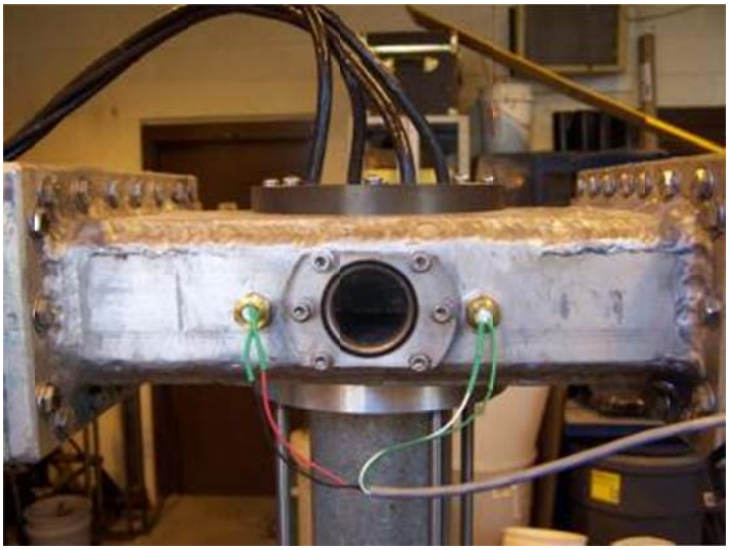

Figure 2-39. Viewing Window on SERF (Trammel 2004)

Trammel, Bloomquist, Sheppard, Kerr, and several others designed the SERF so that sample advancement would be automated. On the top of the flume, an array of ultrasonic depth sensors was mounted so that it could consistently monitor the distance between the top of the flume and the top of the sample (Figure 2-40 and Figure 2-41). The sample was placed in a cylinder with a piston on its bottom, and the piston was advanced via an electric stepper motor. Both the stepper motor and the ultrasonic depth sensor array were programmed into a feedback loop with one another. If the sample's position deviated by more than 0.5 cm from where it should have been, it was advanced (or retracted). This feedback mechanism marks a breakthrough in erosion-rate testing devices because this was the first time that sample advancement had been automated.

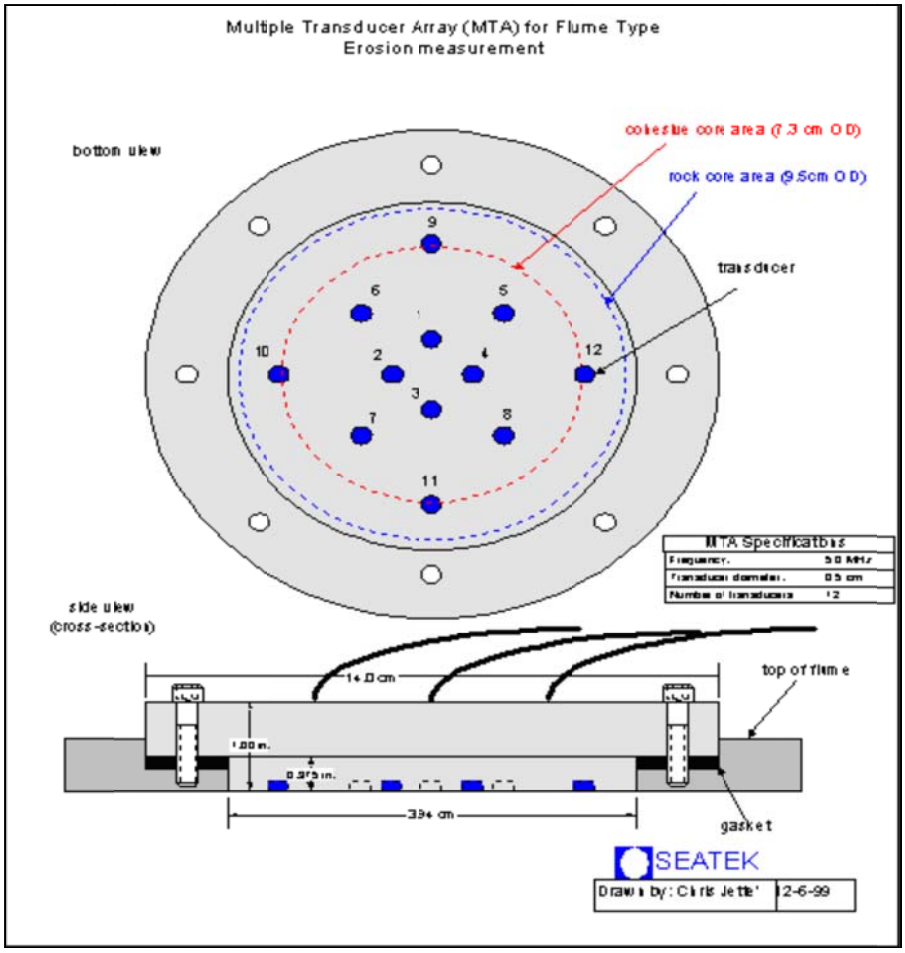

Figure 2-40. Schematic Drawing of Ultrasonic Ranging System (Trammel 2004)

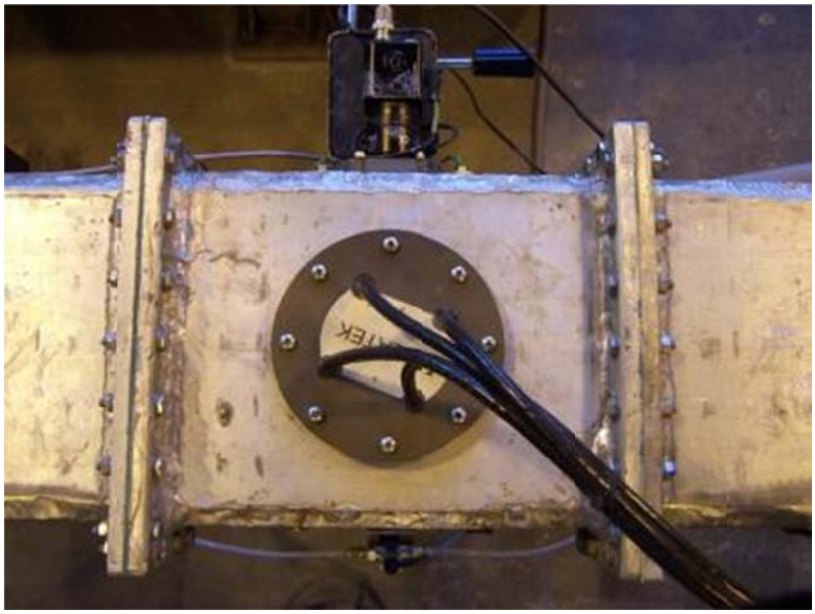
Figure 2-41. Top View of Ultrasonic Depth Sensor on SERF (Trammel 2004)

As originally designed, the SERF, like the EFA, was not capable of measuring shear stresses directly on a sample. However, instead of using a strictly theoretical approach where velocity is correlated to shear stress, the SERF used a pressure drop measurement to infer the shear stresses on the sample. From continuity, given a control volume of fluid in a closed flume, the shear stress along the flume walls should balance the pressure gradient within the flume. Put another way:

$$\tau(2l + 2w)L = \Delta plw \tag{2-80}$$

where τ is the shear stress along the flume walls, l is the cross-sectional width of the flume, w is the cross-sectional height of the flume, and Δp is the difference in pressure along an arbitrary flume length, L. Rearranging (Trammel 2004):

$$\tau = \frac{\Delta plw}{(2l + 2w)L} \tag{2-81}$$

This expression assumes that shear stress along the flume walls is representative of the shear stress across the face of the sample. It also assumes that the sample is large enough to increase the average pressure drop relative to what the pressure drop would have been under smooth conditions.

The SERF was specifically designed to maximize the likelihood of achieving a uniform velocity profile over the eroding test section. Because velocity profiles cannot currently be measured, it is important to understand the flow dynamics associated with flow in a rectangular duct so that the likely distribution of the velocity profile can be better understood. Therefore, an investigation on flow in rectangular ducts was conducted.

In 1998, Rokni et al. developed a numerical model to study flow in a rectangular duct, and Results were verified in an experiment. Results from Rokni are presented in Figure 2-42 and Figure 2-43.

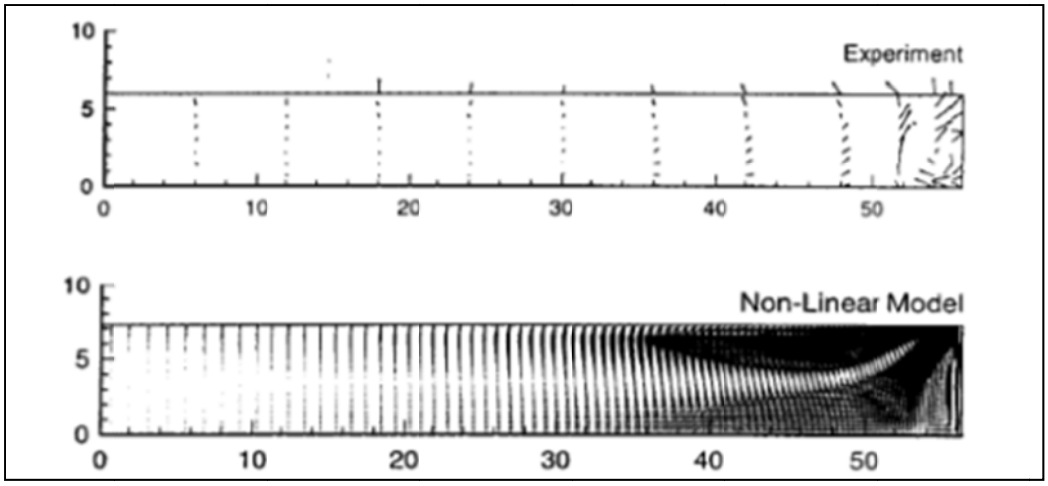

Figure 2-42. Rokni's Results

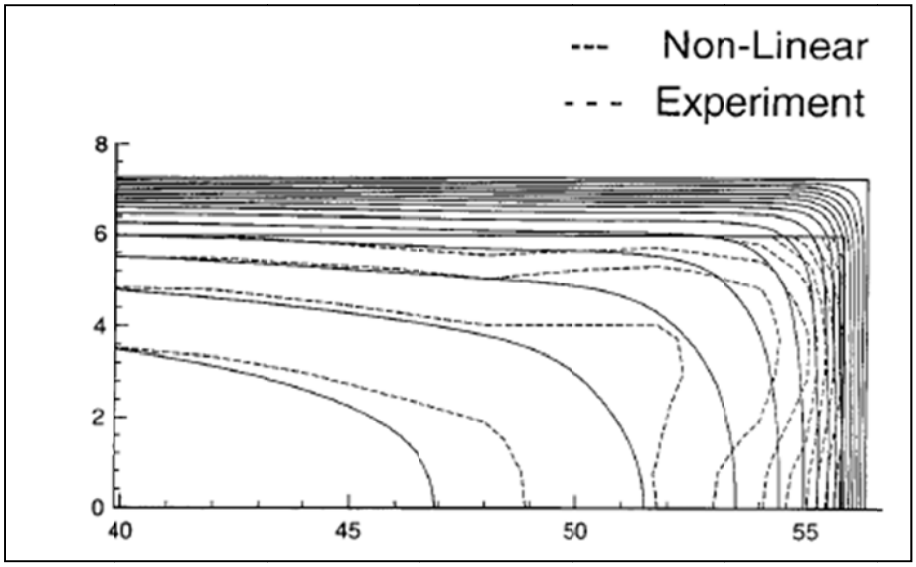

Figure 2-43. Comparison Between Rokni's Experimental and Numerical Results

Several other numerical and experimental studies were conducted in rectangular ducts including Cokljat et al. (1996), Gessner and Emery (1980), Naimi and Gessner (1993), and Melling and Whitelaw (1976). These analyses were also studied to determine flow characteristics in rectangular ducts although their results are not presented in this report.

In 2004, Trammel ran a series of tests in the SERF, and he developed curves that correlated shear stress to erosion for a sand and a clay material that was obtained from Jackson County, FL. In 2006, Slagle's tests (as previously mentioned) were used to extrapolate RETA results to higher values for shear stress. Typical results from Slagle have already been presented; typical results from Trammel are presented in Figure 2-44:

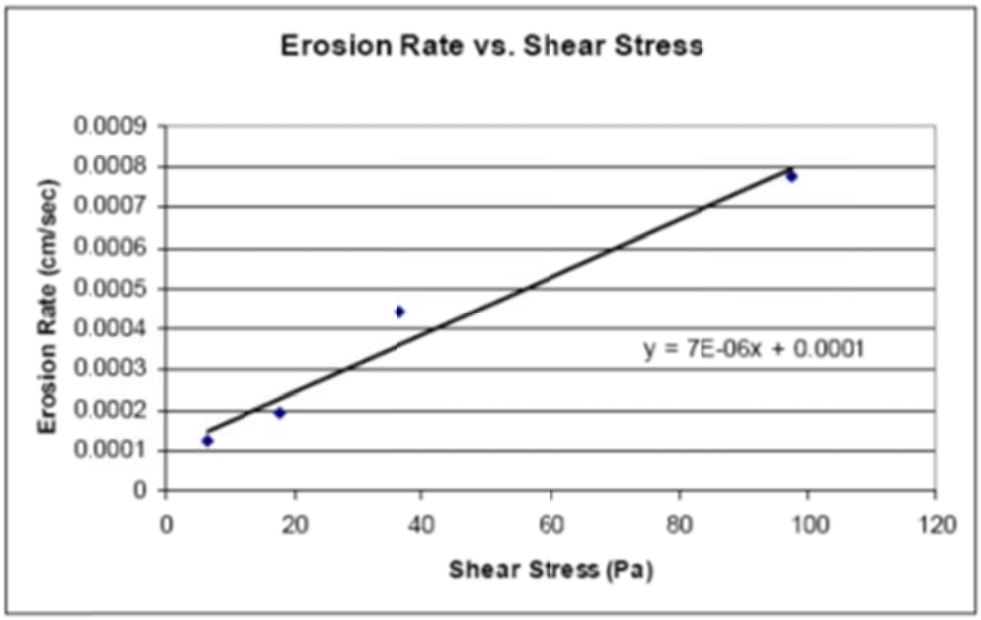

Figure 2-44. Trammel's Results for Cohesive Material from Jackson County, FL (Trammel 2004)

Although in principle, the SERF is well designed, there were several issues in its operation. First, the ultrasonic depth array, the centerpiece of the device's design, was prone to errors. During tests with cohesive materials, the ultrasonic pulses from the depth array were found to penetrate into the samples and return incorrect bottom measurements (Slagle 2006). These instrument errors caused the stepper motor (and sample) to advance (or retract) uncontrollably. The net result was a ruined test.

Secondly, during longer tests, the water temperature within the closed SERF system would rise quickly because the pumps generate significant amounts of heat. Figure 2-45 shows an example of this temperature rise often seen during long tests.

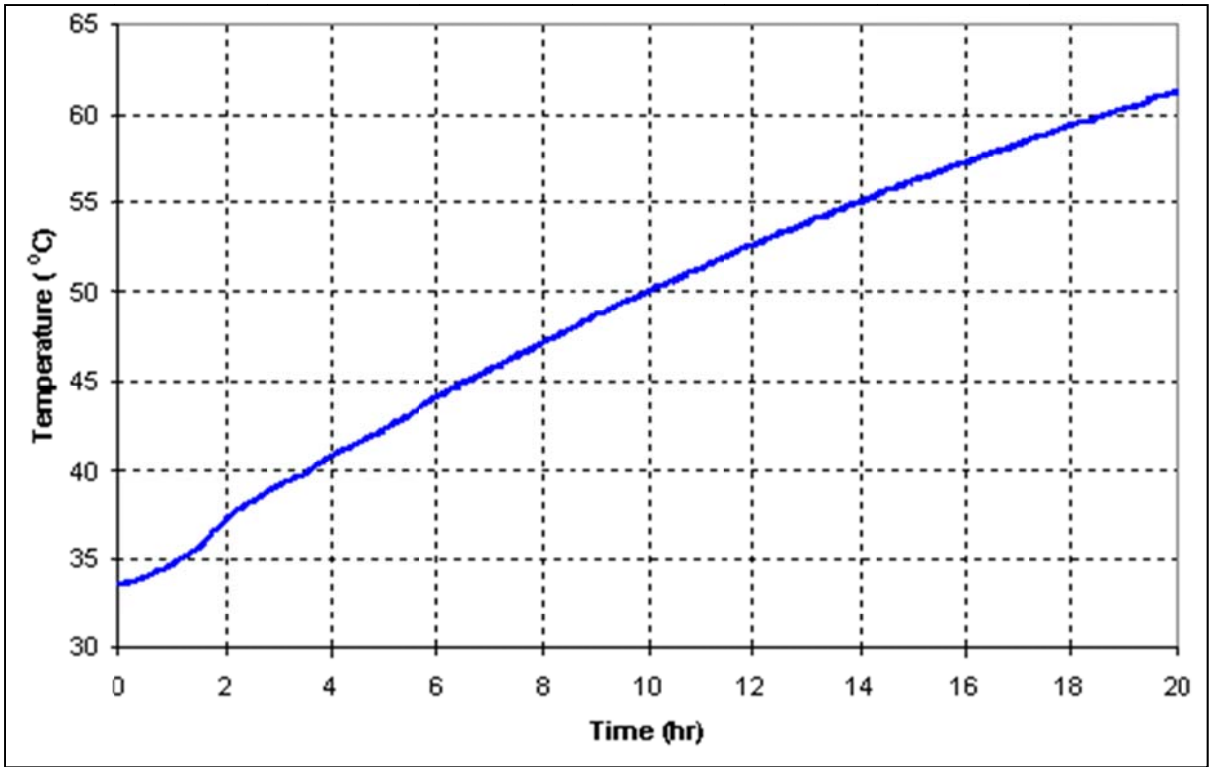

Figure 2-45. Graph of Typical Temperature Rise During Longer SERF Tests (Slagle 2006)

This rise in water temperature was problematic for two reasons. First, the speed of sound is dependent on temperature; a temperature rise causes sound waves to speed up. When the temperature rose, the ultrasonic depth array was calibrated for the "old" temperature, and as time went on, it produced incorrect results and caused the sample to uncontrollably advance (or retract). Secondly, there was a fear that high temperatures could break the depth sensor and the pressure transducers. These issues aside, in nature, a temperature flux of ~+2^{o}C per hour are not seen.

The final issue that was seen during SERF testing has already been discussed: the inference of shear stress on the sample from the pressure drop on the flume's walls. Because no verification could be provided from these pressure drop readings, one could argue that this was the weakest element of the SERF tests. A direct measurement of shear stress would be better.

Despite these issues, at the time of its construction the SERF was one of the a valuable upgrade when compared with other erosion rate testing devices. Although the ultrasonic depth array wasn't without its limitations, when it was working properly it did provide reproducible results. These limitations are readily apparent however, and hence can be improved.

2.5 Gator Rock

Gator Rock has been mentioned briefly at several points throughout this background section. A discussion of Gator Rock will follow in the subsequent section, while a discussion of a new method of creating Gator Rock will be presented in Chapter 5.

2.5.1 Gator Rock: A Brief History and Description

Gator Rock was originally developed at the University of Florida by Niraula (2004) for use in centrifuge testing. Niraula's motivation for research was to develop new T-Z curves for the FB-Pier bridge modeling system, and he needed a uniform, homogeneous, material that could be subjected to centrifuge testing. A T-Z curve is a non-linear spring used in FB-Pier that transfers load from a foundation's pile/shaft to the soil/rock on which the pile rests. Niraula argued that Florida limestone is subject to high variability, and variability could not be tolerated in his study (Niraula 2004). However, he needed a material that would behave similarly to Florida limestone in terms of strength – therefore, Gator Rock was invented.

To create Gator Rock, Niraula dried crushed limestone for 72 hours, and then he mixed water, and Portland cement with the limestone aggregate. Three water contents were mixed, and axial and compressive strength tests were run on two samples from each of the three batches. According to Niraula, these batches showed good repeatability during these strength tests. Niraula indicates that tests were repeated three to five times, although he does not indicate the standard deviation among tests nor does he indicate the percent difference between the tests.

2.5.2 Extension of Gator Rock to Flume Tests

As previously discussed, since the inception of the RETA, there has been a desire to verify that experimental results from it are the same as they would have been in another erosion-rate testing apparatus. There are two levels of verification possible in the RETA:

1.) Does the RETA reproduce traditional flume-style (devices similar to the SERF) results for a material that is homogeneous?
2.) Does this change for a material that has been developed in layers like a sedimentary rock?

Before the second question can be answered, the first one must be addressed because if the RETA cannot even produce similar results for a completely uniform material, chances are small that it will be possible to reproduce results for a nonhomogeneous material. To answer this question via a direct comparison, a material needed to be either located or engineered that was hearty enough to withstand the moment forces associated with rotating RETA water and maintain its structural integrity on its own. However, the material could not be so resistant to erosion that it completely resisted eroding forces. The material had to erode uniformly top-to-bottom; in other words, it had to be nearly homogeneous.

2.5.3 Gator Rock 2.0

Slagle (2006) and his advisor Bloomquist proposed using a material like Niraula's Gator Rock because from Niraula's experience, Gator Rock exhibited nearly uniform characteristics. Although Niraula's Gator Rock was constructed using a relatively high water-to-cement ratio, Slagle and Bloomquist reasoned that they could increase this ratio and thereby make a weaker material such that this newer version of Gator Rock, Gator Rock 2.0, was easily erodible. The original version of Gator Rock would not erode in the RETA.

Slagle attempted mixing batches of this new version of Gator Rock at various water-to-cement ratios. He used Niraula's specifications during the mixing procedure, but he increased his water content. When Slagle's samples had cured, they visually appeared to be uniform, but when he subjected them to RETA testing, he saw that Gator Rock 2.0 did not erode uniformly. Instead, the tops of the samples eroded much faster than the bottom of the samples. An example of a Gator Rock 2.0 sample after RETA testing is presented in Figure 2-46.

Figure 2-46. Eroded Gator Rock 2.0 Sample. Note that top section has eroded more than bottom.

Slagle and Bloomquist attributed this differential erosion rate to capillary processes during the mixing procedure. The Gator Rock slurry was mixed while it was wet and allowed to sit and dry for 28 days. While it was drying, Bloomquist reasoned that capillary forces in the water caused water from the bottom of the Gator Rock mold to move up through the sample as it was curing. Meanwhile, the heavier materials – particularly the crushed limestone – sank to the bottom of the molds. In effect, after 28 days what happened was that there was more water at the top of the mold and the curing sample than there was at the bottom. Conversely, there was more crushed limestone and Portland cement in the bottom of the sample than there was in the top. The result was the formation of Gator Rock that was nonhomogeneous in erosion, and the top of each sample was much weaker and easily erodible than the bottom of the sample. Erosion results from this batch of Gator Rock are what is presented in Slagle's thesis.

Gator Rock 2.0 did visually appear to be uniform, and if it had been subjected to strength testing, it may have exhibited near uniform break-patterns like Niraula's. Recall from the discussion on rock scour (Section 2.3) that strength properties of rock do not necessarily correlate to erosion properties of rock. The behavior of Gator Rock 2.0 is an example where a material appeared to be homogeneous but under erosion it did not behave as such. It would have been interesting to see axial and compressive strength results from this batch of Gator Rock, but none exist.

2.5.4 Gator Rock 3.0

Bloomquist and Slagle's response to this phenomenon was to design a new curing procedure for the Gator Rock. Instead of allowing the Gator Rock to sit while it was curing, they proposed using a rotisserie to slowly spin the sample as it was drying. The hope that was by spinning the sample slowly this capillary forcing mechanism could be averted and a uniform sample would be created.

The rotisserie method for curing Gator Rock did prevent capillary action from occurring during curing, but it still did not produce a uniform Gator Rock sample. Because the sample was spinning during curing, the centrifugal forces associated with this caused separation between the Portland cement and the crushed limestone. The lighter particles were sucked to the outside of the mold while the heavier particles remained in the center of the mold.

Although descriptions of RETA tests from this batch of Gator Rock are non-existent, one can easily speculate as to what would have happened. During the beginning of a RETA test, erosion would have been fast relative to erosion rates at the end of the RETA test. On average, an erosion rate could be computed over the entire domain, but a time series of erosion would have showed a continuously decreasing trend. Meanwhile, during a SERF test, the sides of the sample would have eroded much faster than the center of the sample. The resulting eroded sample would have resembled a small "hump." The middle of the sample would have hardly eroded at all, while the sides would have eroded. The end-product would have resembled an upside-down V-shape or a cone. These results would not have been an acceptable means of calibrating the RETA and SERF devices either.

2.5.5 Need for Better Gator Rock

Based on the above discussion, it is clear that there was still a need for a material that is strong enough to withstand RETA testing, soft enough to erode, and homogeneous enough to erode uniformly. Chapter 5 will discuss a new version of Gator Rock, Bull Gator Rock (or Gator Rock 4.0) that meets these criteria.

CHAPTER 3
ENHANCEMENTS AND IMPROVMENTS TO THE SEDIMENT EROSION RATE FLUME

3.1 Introduction

As discussed in Chapter 2, when originally built, the Sediment Erosion Rate Flume (SERF) was designed to be one of the most advanced erosion rate-testing devices in the world. Still, the issues with the device outlined in Chapter 2, prevented the device from being as accurate as one might need when developing shear stress-erosion rate relationships for use in the Sheppard-Miller method or the EFA-SRICOS method. The specific issues with the flume have already been described in detail, but to summarize, testing was limited because of the following factors:

1. When cohesive sediments were used, the ultrasonic pulses from the ultrasonic ranging system (SEATEK) often penetrated into the samples.
2. Water temperature in the flume increased over longer-durations tests.
3. Shear stress was not measured directly; rather it was inferred via a pressure drop.

In addition to fixing these issues with the SERF, another goal of this study was to make the flume operable for two more sets of experimental conditions:

1. The first goal was to strictly control recirculating sediment as it passes through the flume so that clear water vs. live bed conditions could be more precisely regulated and isolated from one another.
2. The second goal was to study the effects of upstream artificially induced vortices on both shear stress and erosion rate development.

This chapter discusses the improvements, enhancements, and additions made to the SERF to solve the original issues associated with testing and meet the new experimental goals for this project.

3.2 Laser Leveling System

The ultra-sonic pulse sample penetration problem was introduced in Chapter 2. To combat this issue, in the past, researchers like Slagle, who was actually the only previous researcher to use cohesive sediment in the SERF, only had one option – to input an artificial depth value in the

motor feedback loop program. The depth from the top of the flume to the top of the sample should be 4.92 cm. When Slagle tested cohesive material with the SEATEK (ultra-sonic ranging system) and the SEATEK returned depth values that deviated from the correct 4.92 cm reading, his solution was to tell the computer to use a different comparative depth. So, for example if on average the sand-clay mixture was returning a level value of 5.20 cm, this was used as the basis for comparison.

There were a several issues associated with this procedure. If Slagle was going to use the user-defined input parameter to level his samples, he would have standardized his testing procedure. Slagle's recommendation when experimenting on a sample that is experiencing ultrasonic penetration is essentially to run the SEATEK while the flume is running, and observe what the SEATEK return values should have been. A better method would have been to run the SEATEK for a specified time length while the sample was level with the flume bottom and pump speed was low (to prevent erosion). Then, SEATEK data would be recorded, an average would be taken, and this quantity would be used as the user-defined input value. Slagle does not explain why he did not use this method, but further analysis shows that even doing this would have not worked.

Experience with the SERF shows that at higher flow rates, return pulse timing yields a greater depth than it would have yielded at a slower flow rate. At first, this result appeared puzzling since the SEATEK should work independently from flow speed. This is because at higher flow rates, erosion rates are higher as well. Although a filter was added to the device (to be discussed in Section 3.5), the filter was unable to keep up with rapid cohesive erosion. The filter was also incapable of removing fine material from suspension such that when clayey samples eroded, there was often tiny clay flocs present in the water column.

When the ultrasonic pulses hit a sample (and potentially penetrate it), the presumption is that they are traveling in a straight line. As the pulses get deflected or diffracted, the time that it takes the pulses to return to their source increases. When more material is in suspension, as it is at higher flow rates because of recirculating material, the pulses will get deflected or diffracted more frequently. This causes a slightly slower pulse return time, which in turn translates into an apparent deeper SEATEK reading. Combine this with penetration effects, and it's obvious that a user-defined solution cannot work. To set up this condition quantitatively, one would have to run the SERF at a certain flow speed and continuously manually level off the sample with the

flume bottom. Then, the SEATEK return values would be recorded, averaged, and the correct user-defined depth would be known. Lastly, the test could be repeated such that the feedback mechanism, not user control, would govern sample advancement.

With this procedure, one of the SERF's advantages is eliminated because development of the flow speed vs. user-defined depth correlations would be dependent on operator input. Under these conditions then, the SERF would in effect be the same as the EFA, the ASSET, or the SEDFlume. Secondly, this procedure would double the amount of time it takes to obtain a dataset. The manual advancement step in the previous procedure would have produced its own erosion rate shear stress curve.

It is also likely that for a given flow speed, user-defined depth would have changed dynamically with time. In other words, as a sample erodes, more of the eroded portion of the sample recirculates back through the SERF. As this occurs, sediment concentration in the water column increases, which in turn causes a greater scatter frequency over the course of the test. In other words, if at the beginning of the test the SEATEK output a depth of 5.10 cm, by the end of the test due to the increase in particle concentration, the SEATEK would output a higher depth such as 5.30 cm.

Even if this could be accounted for, this ignores the fact that different sand-clay compositions yield different penetration depths. For example, penetration into a 25% sand sample is different from penetration into a 75% sample. To calibrate this procedure would require the development of an increasingly complicated set of curves and correction factors, and even with this, would likely not work as expected.

One goal of this project was to make the SERF capable of testing sand-clay materials. Because the SEATEK cannot be used as a stand-alone system when cohesive sediment is used, something else needed to be invented and installed. There are two ways to measure whether or not a sample is level with the flume bottom. The SEATEK approach involves a top-down design where measurements from a fixed point above the sample determine whether or not the sample needs to be advanced. The second approach – a flushness approach – had not yet been tried.

The simple analogy to a flushness approach is the safety for a garage door opener. The safety is designed such that at one end of the garage door, a laser is aimed at a corresponding photoelectric sensor at the other side of the door. If the photoelectric sensor can see the laser, it must mean that the path for the garage door is clear, and the door is allowed to operate. If the

sensor cannot see the laser, then something is blocking the laser's path. Under these conditions, a voltage is sent back through a feedback loop with the garage door opener's motor, and the motor is not allowed to operate until this voltage switch is on – or until the laser is no longer blocked.

A similar design to this was installed in the SERF. Using miniature fiber-optics, a series of three lasers and three corresponding photoelectric sensors were installed along the top of the flume's bottom wall (Figure 3-1). Diameter of the lasers and photoelectric sensors were 1.50 mm. Signals from the photoelectric sensors are amplified so that a light signal can be read even when the flume is full of water (Figure 3-2). Output from the amplifiers is sent through a control box, into the computer's SCC-2345 analog signal processor, to the computer's PCI-6310 card, and to the Labview control program.

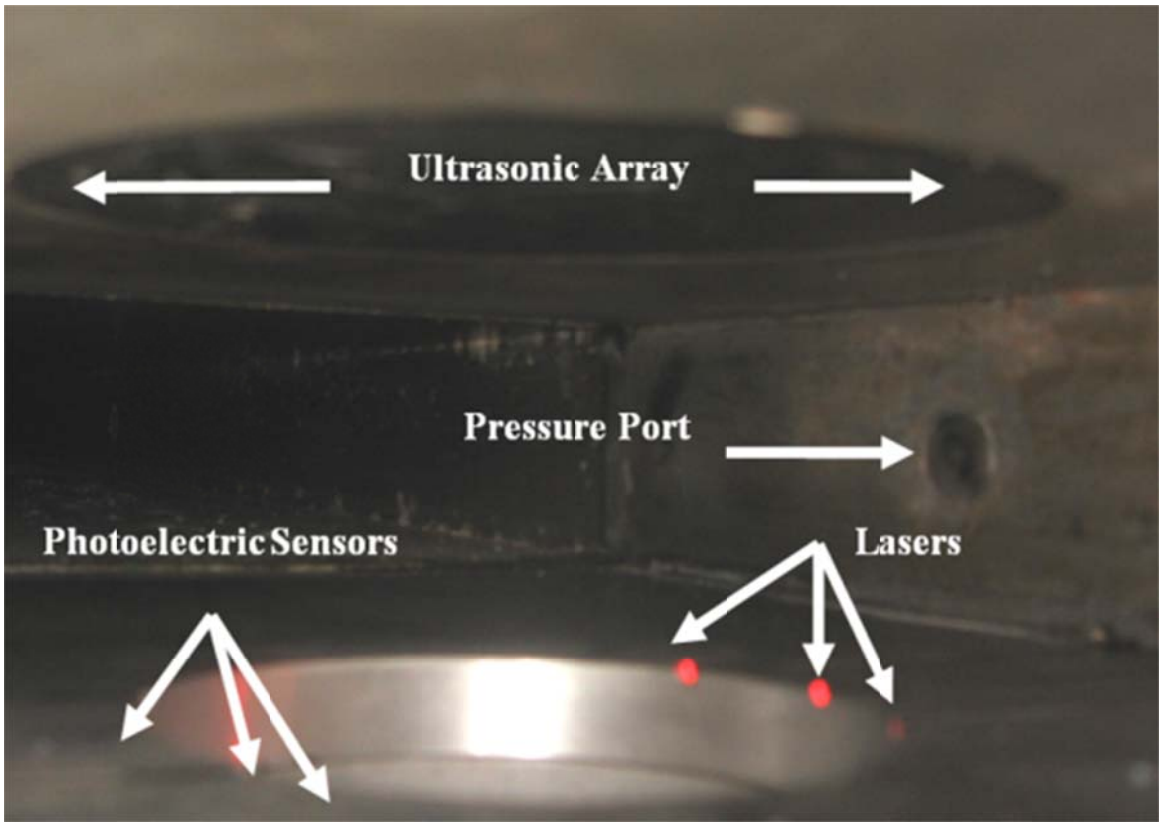

Figure 3-1. Photograph of Laser Leveling System (the third laser is blocked by the camera angle)

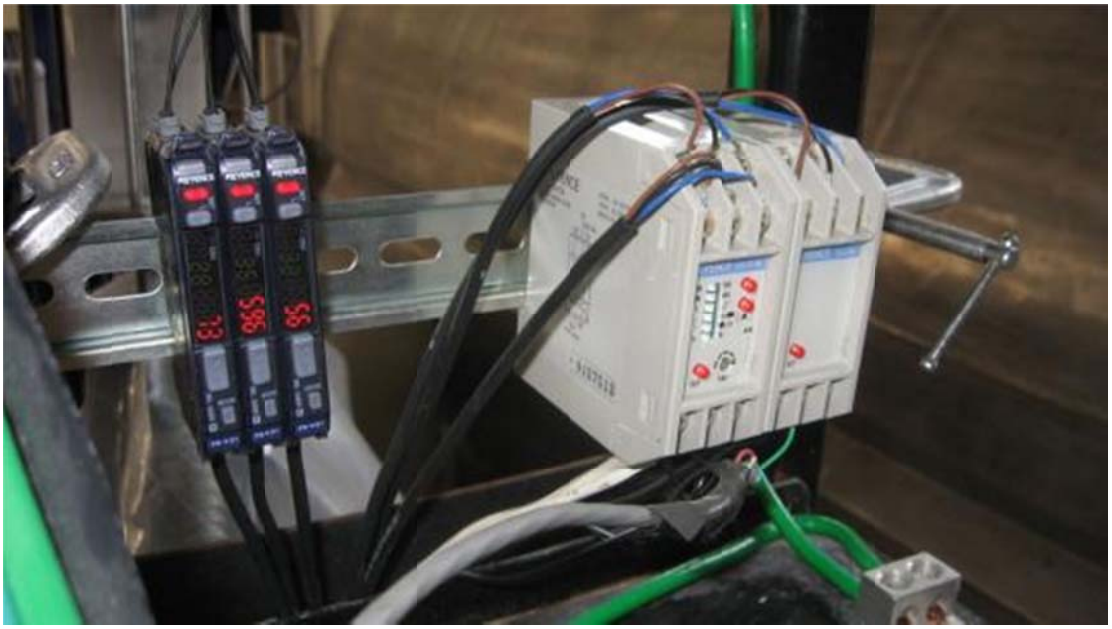

Figure 3-2. Photograph of Amplifiers and Control Boxes for the Laser Leveling System

Using the same principles as the garage door opener, if a laser-photoelectric sensor pair is blocked, it must be blocked by the sample. Under these conditions then, the motor will not move. When the laser-photoelectric sensor pair becomes uncovered, it must mean that the sample needs to be advanced. Qualitative testing with the laser-photoelectric sensor pairs before SERF installation showed two things:

1. This system would work under cloudy water conditions that would be seen during sand-clay erosion testing.

2. This system would be able to provide a recess resolution of approximately half the laser diameter – or approximately 0.75 mm.

The second point is discussed in some detail. When the lasers are operating, the motor will not move until all of them (if AND logic is used) or some of them (if OR logic is used) are uncovered. Only when the correct combination of lasers is uncovered will a sample advance. The advancement minimum then – 0.75 mm – becomes the associated error with this design. In other words, when the lasers are engaged, the sample cannot advance unless at least 0.75 mm of material has eroded from it. The SEATEK was slightly more precise as it would cause advancement/retraction with a depth deviation of 0.5 mm. This design error is of the same order of magnitude as the SEATEK, and smaller waterproof lasers could not be found.

Although three lasers were used during this study due to budget limitations, it is easy to see how to idealize this design. Often, samples in the SERF erode non-uniformly. For example,

certain sand clay mixtures exhibit erosion characteristics where their front face erodes much slower than their back edge. Rather than using three lasers spaced at a certain interval, the most effective design for a laser leveling system would be to install a continuous laser array and corresponding photoelectric sensors. This would eliminate the AND logic vs. OR logic question and instead allow a certain percentage of eroding sample length to determine sample advancement. Implementation of this complete system would not have fit within this project's budget constraints however, and therefore was economically not feasible. When implemented, the laser system as installed worked as it was designed. Due to differential erosion rates, the lasers were programmed such that OR logic was used. Therefore, if two of the three lasers became uncovered, the sample advanced.

Although the primary purpose of the laser leveling system was to allow for cohesive sediment testing, another valuable aspect of the system is that when non-cohesive sediments are used in the SERF, it can be used as a redundant check in conjunction with the SEATEK. Although not as common as with cohesive sediments, when sands are tested at high flow rates, sometimes sand particles can be seen recirculating back through the flume. As with clays, recirculation causes SEATEK errors, but with the implementation of the lasers, these errors can be reduced. During non-cohesive testing then, instead of using the SEATEK or the lasers as independent systems, the following feedback algorithm was programmed:

1. Check to see if the middle laser and either the front or back laser is uncovered.
2. Read depth from SEATEK.
3. If the correct laser sequence is uncovered and the SEATEK says that top-depth is greater than 0.5 mm, record the SEATEK depth deviation.
4. Move sample required amount.
5. Go back to (1)

This laser leveling system is the only known system like it in an erosion rate testing device, it has helped to reduce the number of SEATEK errors when non-cohesive sediments are present, and it has allowed the SERF to be used for testing cohesive materials. The introduction of the laser leveling system is the most significant upgrade made to the SERF during this project.

3.3 Temperature Control System and Temperature Patch for SEATEK

Besides the SERF's initial inability to test cohesive materials, the next issue with the device was the temperature rise during longer tests discussed in Chapter 2. Because of the speed of sound's dependence on water temperature, the temperature rise caused the SEATEK to malfunction and could have caused damage to the SEATEK. The SEATEK gets hot as it sends ultrasonic pulses and it is dependent on a steady stream of water to cool itself. If the water gets too hot, the SEATEK will be damaged. Also, a temperature rise during tests is not typical in nature and should be avoided.

To combat against temperature rises during tests, a temperature control device was installed. There were several designs that were considered when designing the temperature controlling apparatus. For example, there is a chilled water line that runs through Reed Lab (where the SERF was built), and there was talk at one point about running a cooling coils of that line into the reservoir tank. This design was ultimately rejected because there was a less expensive, more efficient option.

Eventually, the final cooling method was developed using a water chiller. There were two options for water chiller design. The first option involved sending flow through the SERF (2,000 gpm during max capacity) through the chiller so that it could be cooled. However, a chiller with 2,000 gpm capacity is prohibitively expensive, and it was not feasible with the budget constraints of the project.

The second chiller option was to install a cooling device in parallel with the SERF pumps. Although the temperature rise in the SERF is large over a 24-hour time scale, over a one-hour time span it is actually relatively small. Temperature only rises approximately $2^{o}C$ per hour during maximum capacity flow conditions. Because of this, it was possible to design a chiller that was just large enough to keep up with that degree of temperature rise at a much lower flow rate. A 6-ton chiller was installed in parallel with the primary pumps and powered by an internal 30-hp pump (Figure 3-3).

Figure 3-3. Water Chiller

The RTS-603 Rite Temp Water Chiller runs at a flow rate of approximately 30 gpm, and it is capable of removing 72,000 BTU/hr. of heat. Because the temperature in the SERF reservoir tank rose at approximately 2°C/hr., the following calculation was conducted to make sure that the 6-ton chiller could keep up with the temperature rise:

$$1100\,\text{gal} * \frac{62.4\,\text{lb}}{\text{ft}} * \frac{0.1337\,\text{ft}^3}{1\,\text{gal}} = 9{,}177 * 1.5\,(\text{S.F.}) * 3.6^{\circ}F\ (\text{temp rise}) \sim 50{,}000\,\text{BTU/hr.req'd.}$$

As shown here, the 6-ton chiller is oversized by approximately 30% even with a safety factor of 2.0 built into the calculation. Although a five-ton chiller could have done the job (max capacity of 60,000 BTU/hr.) the chiller was oversized for two reasons. First, the 6-ton chiller wasn't much more expensive than the five-ton chiller. Secondly, the six-ton chiller is capable of cooling water in the tank more quickly. This means that the six-ton chiller's compressor will

shut off more often and it will not have to run constantly. Because the chiller is not continually running, it will save electricity and it will lessen the chance that the chiller could break.

To confirm that the chiller was the proper size, a cooling test was conducted in the SERF reservoir tank. Figure 3-4 shows the results of the test.

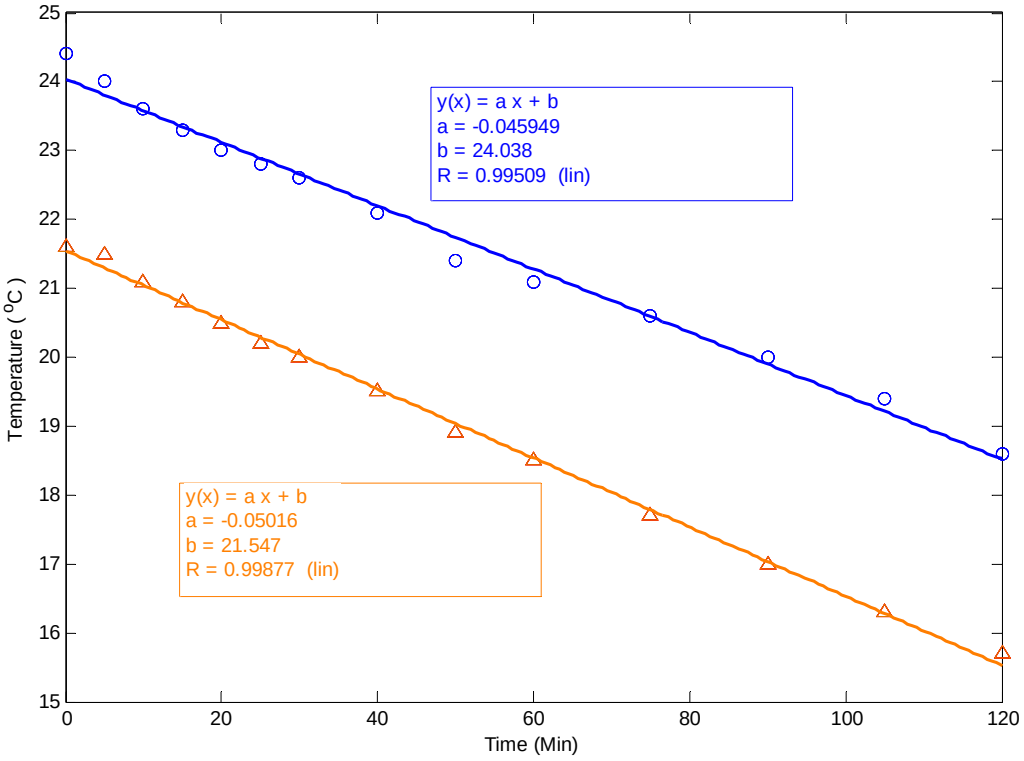

Figure 3-4. Temperature Drop after Water Chiller Installation

As demonstrated, the chiller is capable of producing a temperature drop of approximately 3.0°C/hr. and temperature in the tank appears to respond to the relationship given by Equation 3-1:

$$T_f = -0.05t + T_i \tag{3-1}$$

where t is the time in minutes and T_i is the initial temperature.

Once the water chiller had been installed, the SERF was capable of running longer-duration tests. This was essential for testing of rock-like materials because these tests often take 24-hours or more.

Once the temperature had been regulated, the SEATEK feedback loop was studied one more time. In the past, getting the SEATEK up and running was cumbersome from a computing

standpoint. Previously, SERF users were required to open a serial connection with HyperTerminal or TeraTermainal, input a water temperature, and start a data run. Then, the experimenter would close HyperTerminal, start the control program that was written in Labview, and every time the Labview program ran through another loop, it would read output data from the SEATEK on the serial port.

The obvious problem with this method is that water temperature is only being fed to the SEATEK once at the beginning of the test. The temperature control system can effectively regulate temperature to +/-2^{o}C, yet even within this range, the SEATEK is supposed to be accurate within 0.5 mm. Because the speed of sound in water is so dependent on water temperature, if the SEATEK does not know the exact water temperature precisely, it will output a depth value that is incorrect.

A thermocouple had been installed in the SERF, but had not been incorporated into a feedback loop with the SEATEK. The presence of the thermocouple makes it possible to program the actual temperature to the SEATEK in real-time. A patch was written in Labview for the control program so that before the SEATEK takes a depth reading, it first is given a temperature reading from the thermocouple so that it knows what the correct ultrasonic pulse return time should be at that temperature. Although a quantitative analysis of error reduction was not conducted after installation of this temperature patch, qualitatively it appears that when the SEATEK is used as a stand-alone system now, particularly at low flow speeds, the sample appears to say more level with the flume's bottom. SERF computer programs including the new control system with the temperature patch are presented in the operations manual.

3.4 New Shear Stress System

As discussed in Chapter 2, other flume-style erosion-rate testing devices such as the EFA, the ASSET, the SEDFlume, and the original SERF did not measure shear stress on an eroding sample directly. Rather, shear stress was inferred in a few different ways. The EFA inferred shear stress from a Moody diagram; the ASSET and the SEDFlume inferred shear stress from a relationship obtained from the Darcy-Weisbach equation; and the SERF used a pressure drop relationship to infer shear stress.

When these other flumes were developed, the technology did not exist to measure shear stress directly. While some of these approximating methods are accurate, and some of them are

not, there was no way to quantify which were better than the others. To definitively answer how to properly measure shear stress in a flume-style erosion rate testing device, three sets of improvements were made to the SERF.

3.4.1 Shear Stress Sensor

The issue with measuring shear stress in devices like the SERF in the past stemmed from the inability to accurately measure shear stresses of small magnitudes. In the SERF, at high flow rates, a relatively high the shear stress is 100 Pa (0.015 psi) while typically at lower flow rates shear stresses are around 10 Pa (0.0015 psi). These stress values are much too small to be picked up accurately by most commercial strain gauges or pressure sensors.

From 2003 through 2007, researchers at the Turner Fairbank Highway Research Center were conducting research on the pressure flow scour problem, and they sought to correlate scour depth below a submerged bridge deck with bed shear stress. Kornel Kerenyi from the TFHRC worked with Hans Prechtl of Elektat in Austria to develop a device that was sensitive enough to measure small scale forcing associated with wall shear stresses in an open flume. During their research from 2003 through 2007, researchers at the TFHRC and Prechtl developed three generations of sensors that could measure wall shear stresses. Each new generation was an improvement over the previous design, and by 2007, their open channel design was excellent.

When talk of improving the SERF began, it was logical to go to Prechtl and develop a device that was capable of measuring wall shear stresses in a closed flume or rectangular duct. A new shear stress sensor was designed and developed that works in rectangular closed ducts (Figure 3-5).

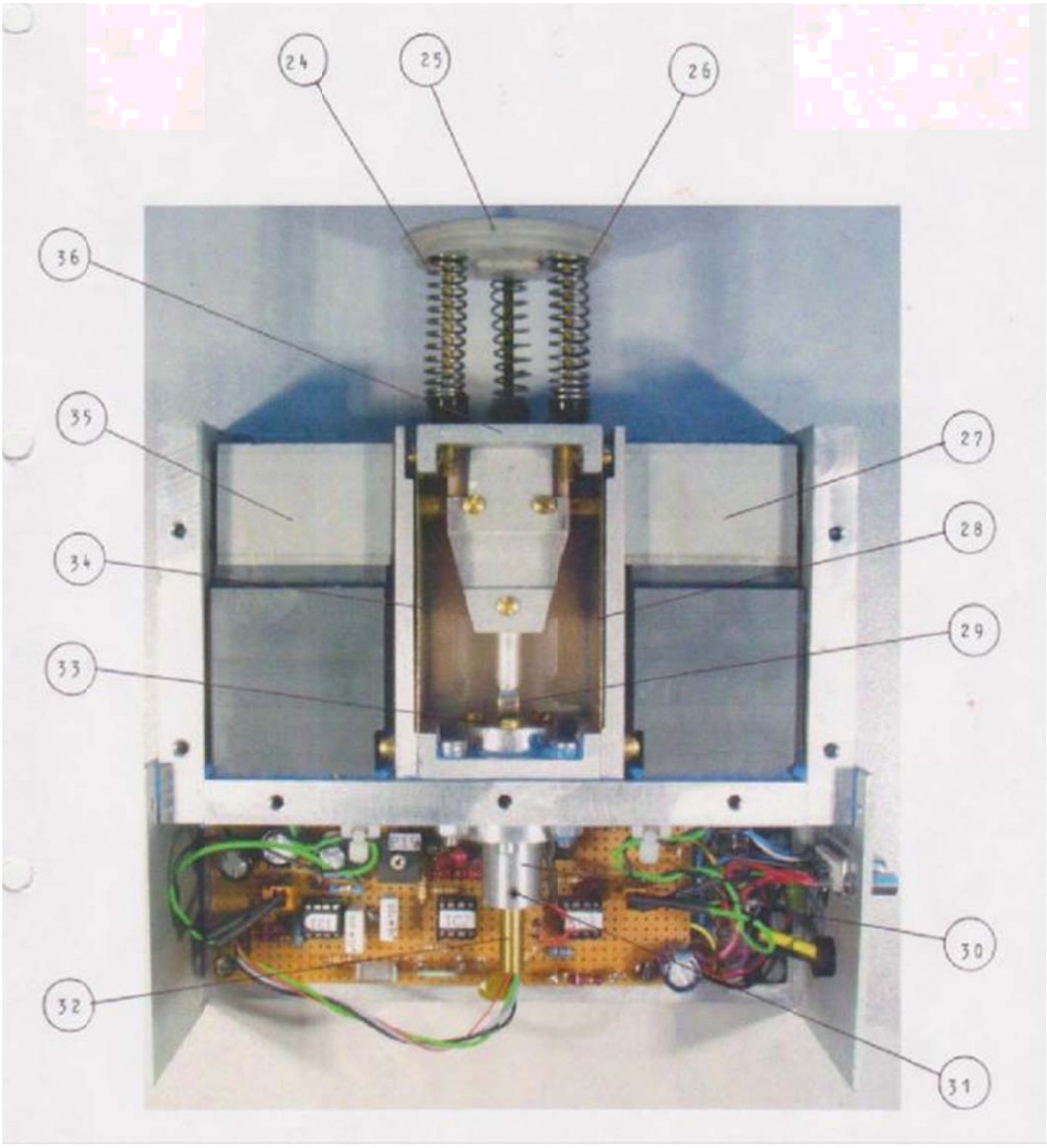

Figure 3-5. Inner Components of the Shear Stress Sensor

In the new shear stress sensor, a 50 mm disk (25) is attached to the top of a movable plate with three springs (24 and 26). The movable plate is attached to the base of the sensor using two

bronze leaf springs (28 and 34). Because bronze is so elastic, there is little friction with regard to platform movement. As water passes over the disk, the disk deflects a small amount, and in turn, the platform (36) will deflect. On the underside of the platform, a magnet (29) is mounted above a Hall Sensor (33). On the upstream and downstream face of the underside of the sensor, a brass rod is mounted and attached to two more magnets. Around these upstream and downstream magnets, an electrical solenoid is installed.

When the platform deflects, the Hall sensor reads the deflection reading and sends a signal to the upstream solenoid (35) so that the solenoid magnetizes enough to pull the platform back to its resting position. This feedback loop runs constantly, and an output voltage is sent from the deflection solenoid, through an amplifier (Figure 3-6), and to the SERF's analog signal control box based on the amount that the solenoids had to magnetize to move the disk back to equilibrium.

To calibrate the device, a signal can be sent from the control box, through the amplifier, and to the downstream solenoid (27) so that it magnetizes a specified amount. In response to this small deflection, the Hall sensor-upstream solenoid feedback loop will react, and voltage can be correlated to shear stress accurately. The shear stress sensor is capable of measuring stress differences on the order of 0.02 Pa ($3x10^{-6}$ psi).

The TFHRC sensors only used a Hall sensor to measure the initial deflection of the disk; there was no solenoid to move the disk back to equilibrium. Because of this, any presence of grit, bubbles, or turbulence in the sensor caused errors with the shear stress reading. The dual-solenoid design allows deflections of only 5 μm, and because the parts in the sensor move such a small amount, the potential for errors is lower. Figure 3-7, Figure 3-8, and Figure 3-9 are provided to give an overview of the new flume arrangement including the shear sensor, pressure transducers (Section 3.3.2), and sample section.

Figure 3-6. Shear Stress Sensor Amplifier

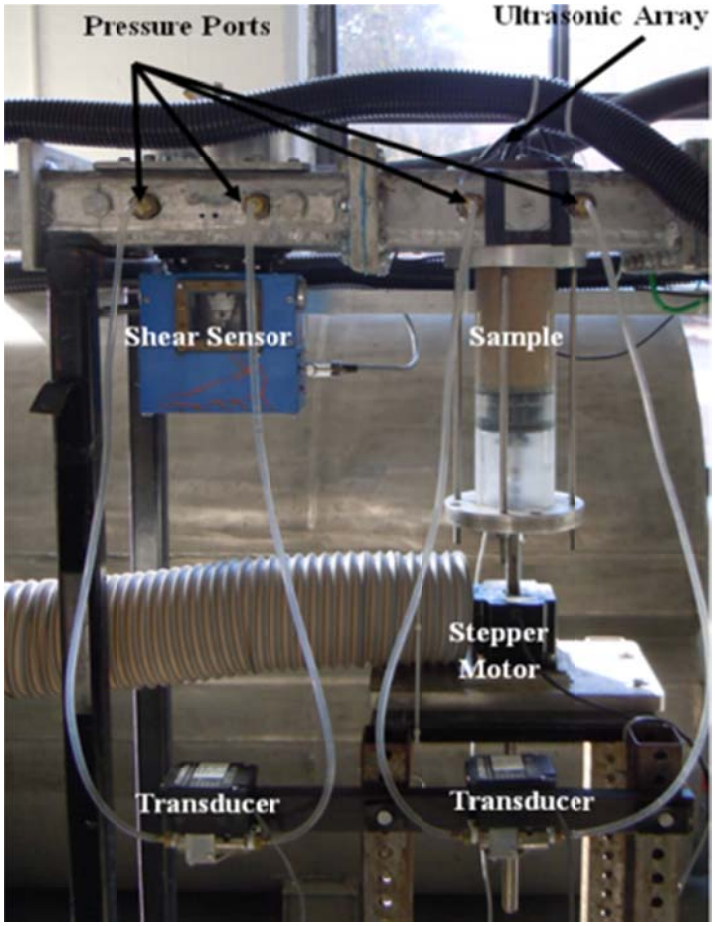

Figure 3-7. Close-up of Shear Sensor, Transducers, and Sample

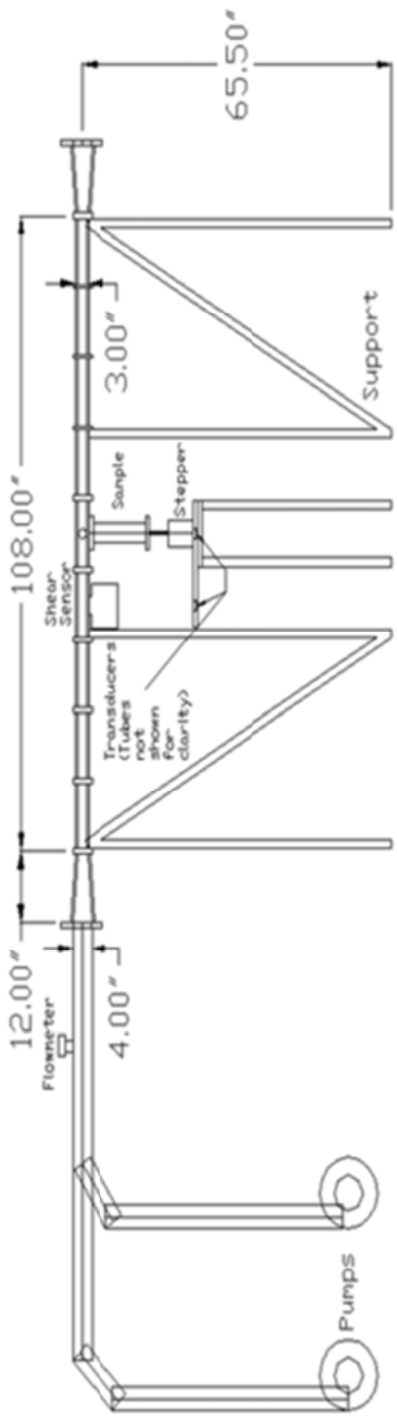

Figure 3-8. Schematic of new SERF setup

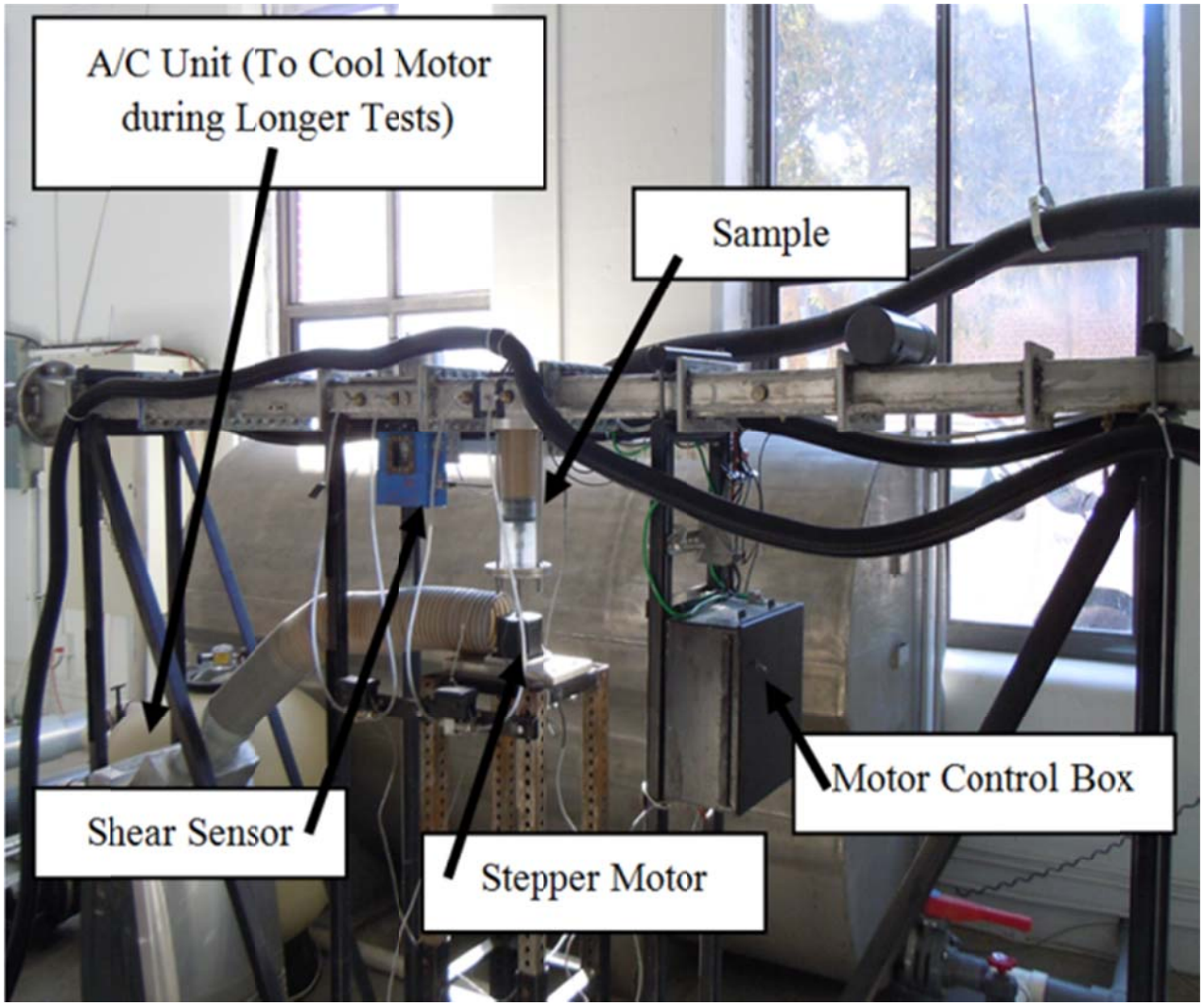

Figure 3-9. Photograph of SERF (upstream looking downstream)

3.3.2 New Pressure Transducers

The second shear stress system enhancement that was made to the SERF was the installation of a set of new pressure transducers. When the flume was originally designed (Trammel 2004), pressure difference upstream and downstream from the sample was measured with a transducer with a range of +/- 2.5psi (14,000 Pa). The accuracy of this device was 0.02% times its range which equals 5.2 Pa. When one examines the formula for converting pressure difference along a flume's walls to shear stress:

$$\tau = \frac{\Delta p l w}{(2l + 2w)L} \tag{3-2}$$

and uses an order of magnitude argument, it becomes obvious that measuring a pressure differential with 5.2 Pa accuracy could be better. In this equation, l = 4.44 cm, w = 20.32 cm, and L = 10.16 m. Substituting into Equation 3-2, τ is accurate to +/-0.50 Pa, which is well below the accuracy of the shear stress sensor.

In 2006, Slagle tried to improve the accuracy of the device by installing a differential pressure transducer that had a range of +/-10 inches of water (+/- 2450 Pa). This improved the accuracy of shear stress estimations from the pressure drop to +/-0.0891 Pa. Although Slagle's improvement gave more accurate shear stress data, the drawback was that the new sensors were ultrasensitive to over pressurizing and they often broke due to operational error. Often, a hose would be connected that was too long, and as a result, the membrane inside the sensor would snap or "pop" causing the sensor to break. This mistake happened often, and every time it happened, a new sensor would need to be purchased.

Slagle had the right idea when improving the accuracy of his pressure sensors, he chose sensors from Sensotec that had little over pressurization tolerance. During this project, the most effective aspects from Slagle and Trammel's design were combined. A new sensor system was purchased from Omega Engineering, and these sensors were capable of withstanding over pressurization forces of approximately 50 psi., while their range was accurate to +/-0.02% of 0.5 psi (3447 Pa). Although slightly less accurate than Slagle's sensor, they do not break as often, and they are close to the accuracy of Slagle's. Two sensors and four pressure ports were installed in the SERF. The first set of taps was installed upstream and downstream from the sample section while the second set of taps was positioned upstream and downstream from the shear stress sensor. The motivation behind this setup originally was to use the sensors as a "check" of the shear stress sensor, but as Chapter 4 will discuss, this may not be the most effective solution because inferring shear stress from a pressure drop may not be correct.

3.4.3 Paddlewheel Flow meter

The third shear stress system improvement that was made was the installation of a paddlewheel flow meter. In 2004, Trammel measured SERF velocity using an ultrasonic velocity flow meter (Figure 3-10), but ultrasonic flow meters are not accurate enough. Trammel's velocity correlation appeared incorrect physically – it was logarithmically distributed

which implies that for a low pump frequency, a negative velocity should ensue – so operators knew that it was questionable. To properly evaluate the Briaud Moody Diagram method and the Flat Wall method for estimating shear stress, an accurate velocity vs. pump speed distribution was required. When the first round of tests were conducted, investigators tried to use Trammel's velocity correlation in the Colebrook Equation (which describes the Moody Diagram to be discussed in Chapter 4) and Flat Wall equations, but results were such were even under flat conditions, the equations predicted shear stresses that were 10 times lower than actual readings from the shear stress sensor.

These results indicated that the velocities appeared to be incorrect, so an Omega FBP151 paddlewheel flow was installed to measure velocities accurately. This flow meter outputs a 4 – 20 mA analog signal, and has a maximum flow velocity of 30 fps. According to its manufacturer, it is accurate to +/-1% F.S. The flow meter has a digital display along its top, and different flow ranges can be selected to improve its accuracy. With the installation of the new flow meter, a new velocity-pump frequency correlation was developed and used on existing data to compute the velocity in the SERF (Figure 3-11).

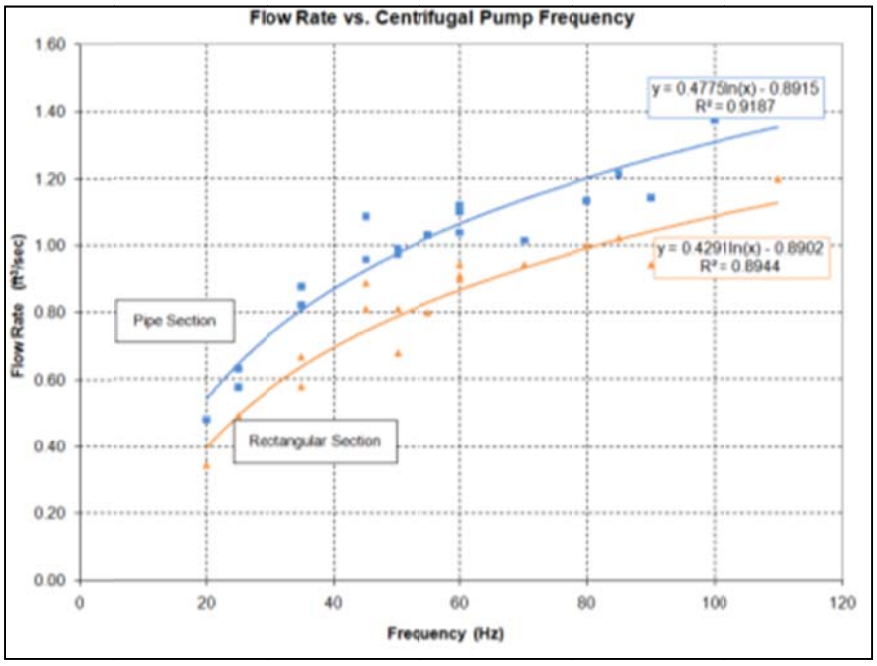

Figure 3-10. Trammel's Original Flow Rate vs. Pump Frequency

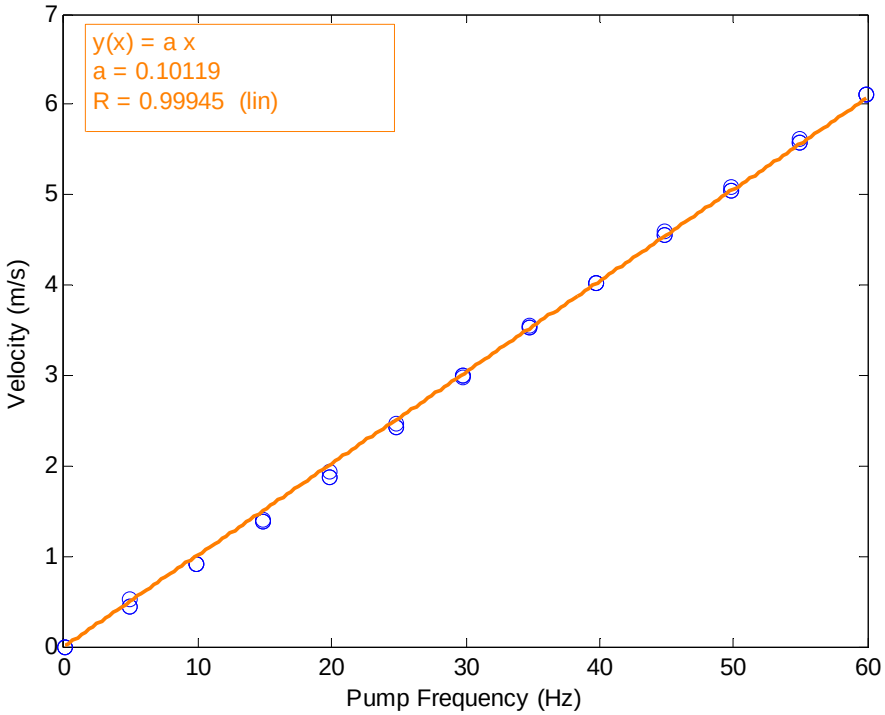

Figure 3-11. New Pump Frequency vs. Velocity Curve

3.5 Sediment Control System

As discussed in the introduction to this chapter, another goal of this project was to design a series of devices for the SERF such that suspended sediment in the water column could be strictly controlled. When a clear-water test was to be conducted in the flume, previously eroded sediment must be removed from the device. Conversely, sometimes investigators would want to run a test that simulated live-bed conditions. If live-bed conditions were to be analyzed, another device was to be designed to inject sand into the device. The sand concentrations coming from the sand injector would be highly regulated so that the sediment concentration variable could be isolated from other variables in the erosion problem. Two devices were designed to be used in this sediment control system, but unfortunately the failure of one of these devices precludes final installation of the other.

3.5.1 Filter System

Like the temperature rise problem, the recirculating eroded sediment (both sand and cohesive material) issue was examined from two approaches. On one hand, water could be

pumped through a filter at its maximum 2,000 gpm flow rate to insure that suspended sediment was removed from it. On the other hand, an independent filtering mechanism could be installed in series with the water chiller to act as a secondary system – similar to the way in which a swimming pool or a hot tub works.

Because of budget constraints, the second option was chosen. While the independent system design worked well with the water chiller, it did not work well with the filter. During a day of testing, particularly with sand-clay mixtures, visual observation showed that as testing continued, water became cloudier. Although quantitative measurements of sediment concentration were not conducted, qualitatively, by the end of a full day of testing, the camera could not see the eroding sample from its viewing port. This means that there was less than 10 cm of visibility in the flume.

At first, it was assumed that this cloudiness was the result of suspended clay flocs in the water column. Eventually, after a day of testing the flume was emptied as it was after every day of testing, and as water exited the flume five-gallon bucket samples of water were taken. Material was allowed to settle out of suspension, and as the eroded material settled, the resulting residue showed that sand and clay had stuck together to form sand-clay flocs. These sand-clay flocs were suspended in the water column during testing, and they were the causing some of the cloudiness in the water column.

This is not to say that the filter did nothing to help. After each round of testing, the reservoir tank was emptied, refilled with clean water, the filter was backwashed, and then the tank was filled again. Backwashing the filter revealed even cloudier (qualitatively) water than the dirty water that drained from the tank after a day of testing. It appears that the filter was doing some work in terms of removing suspended sediment from the water column, but after a day of extensive SERF testing (approximately four samples were tested per day), the filter simply could not keep up with the sediment influx rate. Whereas the smaller water chiller could keep up with a 2^{o}C temperature rise, the filter could not keep up with particle concentrations rising to 0.50g/L over the course of five hours of testing ([~500 g of solid material per sample*four tests per day] divided by1,100 gallons[4,164 L] = 0.48 g/L). Or, put another way, the sand filter could not keep up with sediment concentration increases of 0.1 g/L per hr.

The pump that drives the filter runs at approximately 30 gpm. Therefore, assuming uniform mixing, it would take the filter approximately 37 minutes to filter the water in the

reservoir tank. If this were the case, then breaks between tests to change the sample, reset the computer program, analyze data, etc. should have given the filter enough time to clean the tank's water. Because visually it was not happening, either:

1. The filter cannot filter fine enough particles out of the water.
2. Water in the reservoir tank is not being uniformly mixed.

It is difficult to isolate which of these two possibilities presented the largest problem with filtration, although because the installed filter was a sand filter, it is likely that it was unable to remove the small diameter particles from suspension. Still, even if a finer filter was used, it is unclear whether or not it would have any effect as much of the particulate that drained from the reservoir tank after testing was sandy.

Because of the filter's failure during sand-clay tests, results from the latest round of sand-clay tests in the SERF may be subject to the same criticism as results from the CSU tests. This was a disappointing development during testing, and it was not anticipated when the filter was installed.

The second issue that is caused by the sand filter's failure is that the highly regulated sand injection system could not be installed in the SERF. Adding another source of sand to the device without proper filtering would allow even more sediment to cycle back through the flume. Even without the introduction of another sediment source, it is impossible to say how sediment concentration is changing with time. Within the context of a flume run, suspended sediment concentration is continually changing. Adding another source of sediment would further skew the results and not produce valid data because it would be impossible to isolate sand concentration as a variable.

The third concern from the filter system's failure is that if the SERF is allowed to run with high sediment concentrations in the water, the pumps will eventually be compromised. The centrifugal pumps require a clean water source. If sand is moving through them at high flow speeds, the net effect is that the pumps' impellers are, in effect, being sand-blasted. Introduction of a sand injector would only serve to exacerbate the issue.

Although the SERF has been operable since Trammel started his work in 2002, this latest round of tests is the only time when the device was used extensively under high erosion conditions. Analysis of Slagle's work shows that his data points with the SERF are limited. Most of Slagle's work involved RETA testing. When Slagle did use the SERF, erosion rates

were low and the device could not be used for long periods of time (because of the temperature rise). Therefore, during Slagle's tenure at UF, the SERF frequently sat idle. Even with this down-time, when this project began, one of the flume's primary pumps was already damaged – presumably because of recirculating sediment. Fortunately this damage was only to the pump's seal, and repair was relatively inexpensive. If an impeller had to be replaced though, the cost could be prohibitively expensive and shut the SERF down for the foreseeable future.

Because of this, a decision was made to limit the dataset as much as possible. The necessity to do this though was disappointing and unexpected both because it precluded the installation of the sand injector and because it meant that the datasets generated would not be as extensive as they might have been.

3.5.2 Sand Injector

This project was conducted such that additions and improvements were designed and built before testing began. This was done to streamline the project and make things more efficient. Thus, if the sand injector, laser system, filter system, and chiller system could be designed and built at the same time in parallel with one another, then installation could happen simultaneously, and testing could follow. However, since the filter performed so poorly, work with on the aforementioned sand injector had been completed before testing began.

The limitation is that it cannot be installed because it currently cannot be used. However, when a proper filter is added to the SERF, the sand injector is ready to be put into operation. The sand injector must operate in a continuous stream under clear conditions. To do this, a 4 inch diameter PVC feedscrew was designed and built by Carleton Helical Technologies. The feedscrew was installed inside a 10 inch PVC reservoir and a 4 inch PVC pipe was extended down the screw length. The 10 inch PVC reservoir is filled with sand, and as the feedscrew turns, it feeds sand up the 4 inch PVC pipe into the PVC section of the SERF.

Although initially attempts were made to use a larger reservoir (a 55-gallon drum for example), these larger vessels were unable to withstand water pressure during operation. According to Sferrazza and Williams (2002), above a threshold pressure of approximately 14 psi, a 55 gallon drum will likely fail. Because it would be filled with water, this failure would not be explosive. Instead, a seal would break, and water would leak from it. The SERF, at higher flow rates, produces up to 20 psi, and the goal was for the sand injector to be usable at any flow rate.

Therefore, eventually the 55-gallon drum was abandoned in favor of the smaller 10 inch PVC pipe reservoir.

The sand injector's feedscrew is connected to a variable speed motor control. Although the motor control is not currently hooked up to the SERF control computer (this step was skipped since the sand injector was not installed), in the future this upgrade should be made so that the motor can be computerized.

To regulate sand entering the SERF, the sand injector rests on four, 250-lb capacity load cells (Figure 3-12). Before a test is conducted, the weight of the sand injector will be known. During testing, the sand injector weight will decrease, and after testing, the final weight will be known. By measuring the amount of mass lost, researchers will precisely know the quantity of sand that was injected.

Figure 3-12. Sand Injector Load Cell Mounts

Because the load cells need to slightly deflect so that they can output a weight signal, two expansion joints were installed at either end of the sand injector (Figure 3-13). These expansion joints allow for 0.5 in of deflection, which is less than the deflection of the load cell mounts. A photograph of the completed sand injector is presented in Figure 3-14.

Figure 3-13. Sand Injector Expansion Joints

Figure 3-14. Completed Sand Injector

Because the sand injector was not installed, it could not be calibrated. However when a proper filter is added to the SERF, it can be easily installed and calibrated.

3.6 Vortex System

Besides sediment control, there was another new scenario under which the SERF was to be run – the scenario where vortices are generated in the flume upstream from the eroding sample or shear stress sensor. These vortices do not mimic the horseshoe vortex. The vortex generator is instead designed such that the presence of an upstream obstruction generates a turbulent wake region (or vortex region) behind the obstruction. This newly formed turbulent flow regime may affect erosion rate.

To create this vortex obstruction, a circular cylinder was selected because flow past circular cylinders has been studied extensively, and flow patterns in the cylinder's wake region are fairly well understood. From experience at the TFHRC, in flume tests, blockage should less than 20% of the flume's cross-sectional area (Crowley 2007). Because the goal was to generate the largest wake region possible, the maximum cylinder size was chosen. The SERF height is 1.75 in., so the maximum horizontal cylinder that could be used was approximately 3/8 inch to ensure that blockage requirements were met.

To design the height of the cylinder properly so that full in-tact vortices were produced, research was conducted on flow fields around circular cylinders near a wall. Because the eroding test section is loaded into the flume from the bottom, the goal was to generate vortices as close to the bed as possible. According to Sumer and Fredsoe (2006), when a cylinder is placed near a wall, the flow around the cylinder changes compared to how it would look if the wall was not present. Among the changes to the flow patterns around a cylinder, the most important for the SERF is that vortex shedding becomes suppressed for gap ratio values smaller than approximately $e/D = 0.3$, where e is the gap between the bottom of the cylinder and the wall and D is the cylinder's diameter. Diagrams of gap-ratio effects on vortex generation are presented in Figure 3-15.

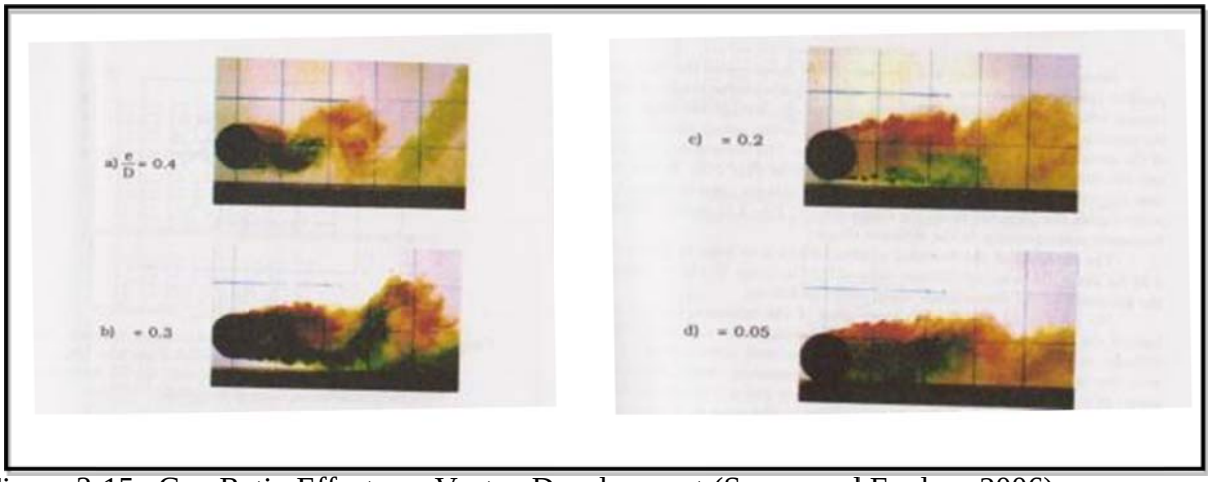

Figure 3-15. Gap Ratio Effects on Vortex Development (Sumer and Fredsoe 2006)

Because the diameter of the cylinder is fixed at 0.375 inches due to blockage requirements, the minimum gap that could be used to achieve a gap ratio of 0.3 is 0.104 inches. Because this is a non-standard size and because generally speaking, a larger gap means a larger wake region, this value was slightly expanded so that the design gap for the vortex generator would be 0.125 inches. This results in a gap ratio of 0.33 which is acceptable.

Once the cylinder and the gap had been properly sized, the Strouhal Number was used to predict the number of vortex oscillations that will occur. Past tests in the SERF have shown that erosion does not occur below a Reynolds Number of ~$3x10^2$, and based on a 2,000 gpm max volumetric flow rate limit, the largest Reynolds Number that will ever be present in the SERF is ~$4.5x10^4$. Within these ranges, the Strouhal number (Equation 3-3 and Figure 3-16) should stay fixed at approximately 0.2.

$$St = \frac{f_v D}{U} \tag{3-3}$$

In Equation 3-3, f_v is the vortex shedding frequency, D is the cylinder's diameter, and U is the water velocity. Therefore, at low flow rates, vortices should be produced at approximately 0.7 Hz, at high flow rates, approximately 70 Hz, and in between this upper and lower limit, a Strouhal analysis can be conducted to predict the vortex shedding frequencies at each velocity.

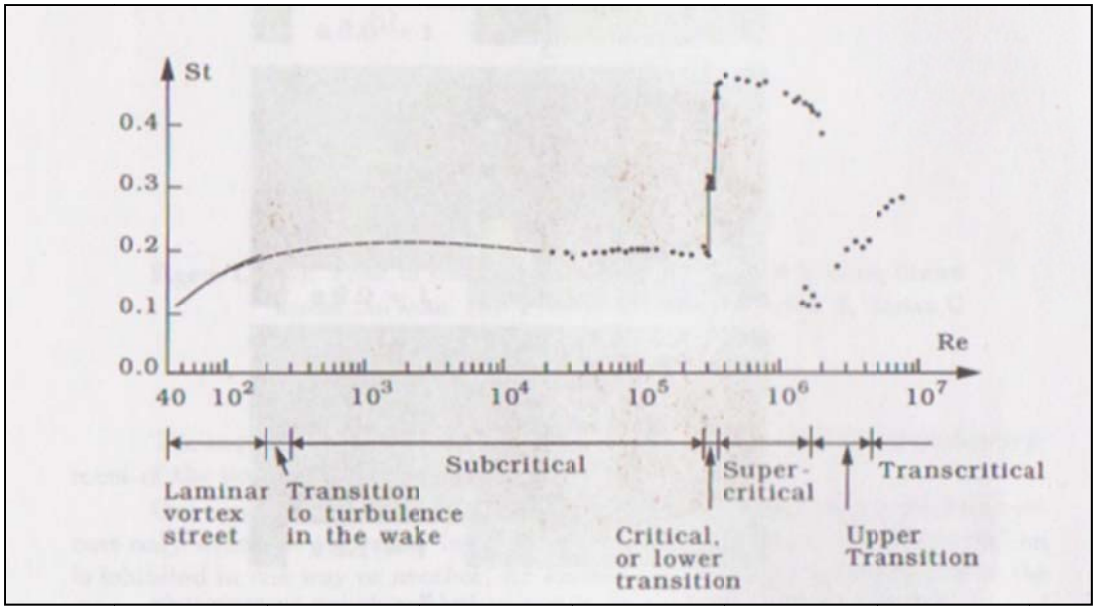

Figure 3-16. Graph of Strouhal Number vs. Reynolds Number

Analysis was conducted to determine the relative expected size of the vortices induced by the cylinder when they reach the test section and the sample section, but little research has been done in terms of characterizing vortex size specifically as a function of distance downstream from the cylinder. Rather, the bulk of research in flow past a circular cylinder has involved qualitative measurements for the characteristics of the vortex street with quantitative work focusing on drag and lift forces on the protruding structure.

The vortex generator was installed so that the protruding cylinder was easily removable. A photograph of the newly installed vortex section is shown in Figure 3-17. Water velocities in the SERF were first estimated using Trammel's curves, but when the flow meter was installed, the calculations were updated to account for the more accurate velocity measurements.

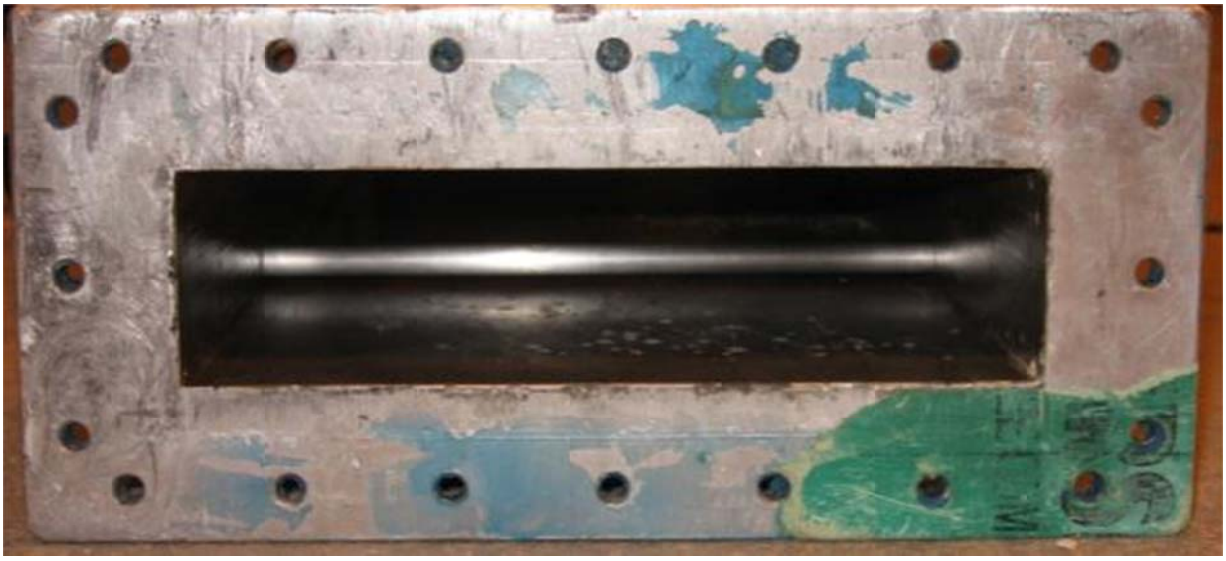

Figure 3-17. Vortex Generator installed in SERF (looking into flume)

3.7 Miscellaneous Other Enhancements to the SERF

Other than the major additions, enhancements, and improvements to the SERF, several other minor changes were made to the device. First, to accommodate the new components, the Labview computer program that runs the SERF was rewritten. When this project was started in 2007, the latest version of the computer program had numerous bugs, not intuitive and slower than it should have been. Although its original designers did an adequate job of integrating the device with Labview, more could have been done. Because of this, when the new systems were integrated it made more sense to simply rewrite large sections of Labview code rather than create patches to piece together the existing program.

A full discussion of the command modules of the SERF is presented in the operations manual, but in brief, the new version of the program allows the user to turn on or turn off any of the twelve crystals in the SEATEK, the entire SEATEK array, the laser system, the shear sensor, the pressure transducers (one or both of them), and the Servo-motor. The pump, which had been controlled with a digital display device that was independent from the computer, has been integrated with the GUI.

Because of the advanced computer integration of the SERF, a system was set up where the device could be controlled remotely. To operate the flume now, a user needs to load a sample, set up the instrument, and then periodically check on it from time to time to make sure

everything is operating properly. If something malfunctions, the pump, the motor, and the entire system can be stopped remotely. This capability is advantageous during longer testing (24 hours or more) of rock specimens. Even with this capability though, computers were used to create soft-limit switches for the motor so that if something were to go malfunction, the SERF should shut down autonomously.

Along with the need to rewrite the entire SERF computer system came a need to revamp the method in which the device captures and records video. The original method involved the use of a VCR or a Hi-8 recorder. The Hi-8 device was converted to a DVR with networking capabilities so that the operator can now operate the computer, see inside the flume, record video, and review video remotely.

3.8 Summary of SERF Improvements and Brief Discussion

In summary, the following components improvements and enhancements were made to the SERF:

1. Laser Leveling System installed
2. Temperature Control System
    a. Water Chiller installed
    b. Temperature Control Patch written
3. Shear Stress System
    a. Shear Stress Sensor installed
    b. Pressure Transducers installed
    c. Paddlewheel Flowmeter installed
4. Suspended Sediment Control System
    a. Sand Filter built and installed
    b. Sand Injector built
5. Vortex Induction System
6. Miscellaneous Improvements
    a. Computer code updated and rewritten

b. Computer operating system updated

c. Video capture system updated

Because of the improvements and enhancements made to the SERF, the testing procedures had to be changed. The last version of instructions for SERF testing appeared in Trammel's (2004) thesis, and is out of date. New testing procedures can be found in the operations manual. Also included in the operations manual are a series of steps that can be used for troubleshooting malfunctions in the device and a discussion on the new computer programs for SERF control.

These improvements and enhancements to the SERF are significant and they make the SERF unique when compared with other erosion-rate testing devices. The device was already unique because of its ultrasonic depth sensor-stepper motor feedback loop, but the addition of these components have move the SERF even further ahead of these other devices in terms of precision and sophistication. There are no other known devices like it in the world that have these computerized capabilities.

CHAPTER 4
ESTIMATIONS AND MEASUREMENTS OF SHEAR STRESSES ON AN ERODING BED MATERIAL IN FLUME-STYLE EROSION RATE TESTING DEVICES

4.1 Executive Summary

With the installation of the new shear stress system as described in Chapter 3, a method was finally available for measuring shear stress directly in a closed rectangular duct and comparing results with previous methods for estimating shear stresses in a flume. Tests were run in the SERF for varying bed roughness (grain sizes) and at a range of velocities to determine the accuracy of shear stress estimates using a pressure drop. Tests showed that large particles can cause higher shear stresses than the returned computed value using a pressure drop. As particle sizes become smaller, the pressure drop method for estimating shear stress becomes increasingly more accurate. Relationships were developed for shear stress as a function of particle size and compared with flat-walled results from the Darcy Weisbach equation and results obtained using the Colebrook Equation (Moody Diagram) as specified in the EFA. For large grain sizes, the flat-walled assumption provides poor results. The EFA's method for estimating shear stress works better than the flat-wall assumption and the pressure drop if a calibration is developed for absolute roughness based on flume-specific dimensions. When upstream vortices are artificially induced in the flow field, bed shear stress decreases sharply for a smooth bottom, while shear stress for rough bottoms remains similar to shear stresses under non-vortex conditions.

4.2 Review of Relevant Background

Recall from Chapter 2 that the method for estimating shear stresses in rectangular closed flumes like the SERF, the EFA, the ASSET, and the SEDFlume relied on estimation techniques. Shear stress in the ASSSET, the SEDFlume, and the SEAWOLF used the Darcy Weisbach Equation and a hydraulically smooth assumption to estimate shear stress. In the EFA, friction factor was obtained from a Moody Diagram, the Darcy Weisbach Equation was used, and shear stress was estimated. Originally in the SERF, a pressure drop was measured and a force balance was used to solve for shear stress as a function of head differential.

Recall from Chapter 2 that the ASSET, SEDFlume, and SEAWOLF use equations 4-1, 4-2, and 4-3 to estimate wall shear stress. These devices make a smooth-wall assumption, and consequently, the friction factor can be solved implicitly.

$$\frac{1}{\sqrt{f}} = 2.0 \log\left[\frac{\bar{u}D\sqrt{f}}{\upsilon}\right] - 0.8 \tag{4-1}$$

$$D = \frac{2hw}{h+w} \tag{4-2}$$

$$f = \frac{8\tau}{\rho \bar{u}^2} \tag{4-3}$$

In the EFA, Briaud et al. estimate shear stress using Equation 4-3, but their friction factor, *f*, is not solved for using Equation 4-1. Instead, a Moody Diagram is used to estimate this parameter. The Moody Diagram can be described by the Colebrook equation:

$$\frac{1}{\sqrt{f}} = -2.0 \log\left[\frac{k_s / D}{3.7} + \frac{2.51}{\mathrm{Re}\sqrt{f}}\right] \tag{4-4}$$

where k_s is the absolute roughness height, *D* is the hydraulic radius of the rectangular duct, and *Re* is the Reynolds Number (Eq. 4-5) with respect to hydraulic radius.

$$\mathrm{Re} = \frac{\bar{u}D}{\nu} \tag{4-5}$$

When examining a cross section of any erosion rate test flume, it becomes clear that the walls' roughness are not constant. On three sides of the flume, smooth walls are present, but along the bottom of the flume, a sample with a different roughness is present. Because the Colebrook Equation and Moody Diagram solve for average friction factor, and these methods rely on surface roughness, the question becomes which surface height to use when doing these calculations. Unfortunatley, Briaud does not say what value for k_s in his calculations. The goal of this portion of this study was to develop a relationship for k_s as a function of grain size in the SERF.

Once this question can be answered under steady flow conditions, the next question is how the presence of vortices affects bed-imposed shear stress (and particle-like erosion since $E = f(\tau)$). To study the effects of bed shear stress under vortex conditions, the vortex generator was

installed upstream from the shear stress sensor and shear stress measurements were made under vortex conditions using both the pressure drop and shear stress sensor method.

4.3 Experimental Setup

The SERF operations manual provides in-depth details of how to run a shear stress test in the SERF, but in brief, the procedure that was used for this study proceeded as follows:

1. Experimental discs were prepared for the SERF using the "synthetic" disc preparation method. Crushed limestone was sieved so that particles of 5 diameters – 2.0 mm, 1.0 mm, 0.5 mm, 0.25 mm, and 0.125 mm were isolated from one another. Then, a 50 mm diameter acrylic disc was coated with epoxy and particles from one of the five batches were attached to the front face of the disc. A flat disc was also prepared.

2. An experimental disc was loaded into the shear stress sensor and leveled with the flume bottom.

3. The shear stress sensor was calibrated such that there was a linear relationship between output voltage and shear stress. For example, an output voltage of 10 V indicates a shear stress of 100 Pa; an output voltage of 3 V indicates a shear stress of 30 Pa.

4. Water was run through the SERF to pressurize it, and the pressure transducers were bled to remove any bubbles from their hoses or nozzles. Once the transducers were bled, a 10 second, 1 kHz pressure reading burst was taken at no flow so that a "zero-point" for data analysis could be established.

5. Water was run through the SERF at varying flow rates. Flow rates ranged from 0 m/s to 6 m/s. Data was recorded from the pressure transducers, the shear stress sensor, and the paddlewheel flowmeter at a 1 kHz sampling frequency.

6. Pressure readings were converted to shear stresses using the following relationship:

$$\tau = \frac{\Delta p l w}{(2l + 2w)L} \tag{4-6}$$

   which is based on a force balance between wall shear stress and an upstream and downstream pressure gradient. Velocity readings were used to compute shear stresses using Equation 4-1 through Equation 4-6.

7. Steps 2 – 6 were repeated for each experimental disc and the flat disc. The result was the development of a relationship between velocity and shear stress for a pressure drop reading, a velocity reading, and a shear stress sensor reading for a given sediment size. Each test was repeated at least four times.

8. A gage pressure transducer was attached to one of the SERF's pressure ports. Normal stress readings were measured at the specified flow rates.

9. Shear stress tests were repeated with the vortex generator installed. Since the paddlewheel flowmeter was installed upstream from the vortex generator, average velocity readings did not change. Therefore, only the pressure drop and shear stress sensor readings were compared with one another.

4.4 Experimental Results and Discussion

4.4.1 Pressure Drop

Tests were first conducted on a flat disc to compare the pressure drop method for estimating shear stress with actual measurements. The first issue with testing was that significant noise was present in the pressure transducer signal. While small pressure differential voltage fluctuations were expected (10^{-3} V) relatively high pressure differential pressure voltage fluctuations were observed (10^{-1} V). Spectral analysis was conducted on the de-meaned signal from the pressure transducers (Figure 4-1), to determine why these fluctuations were occurring.

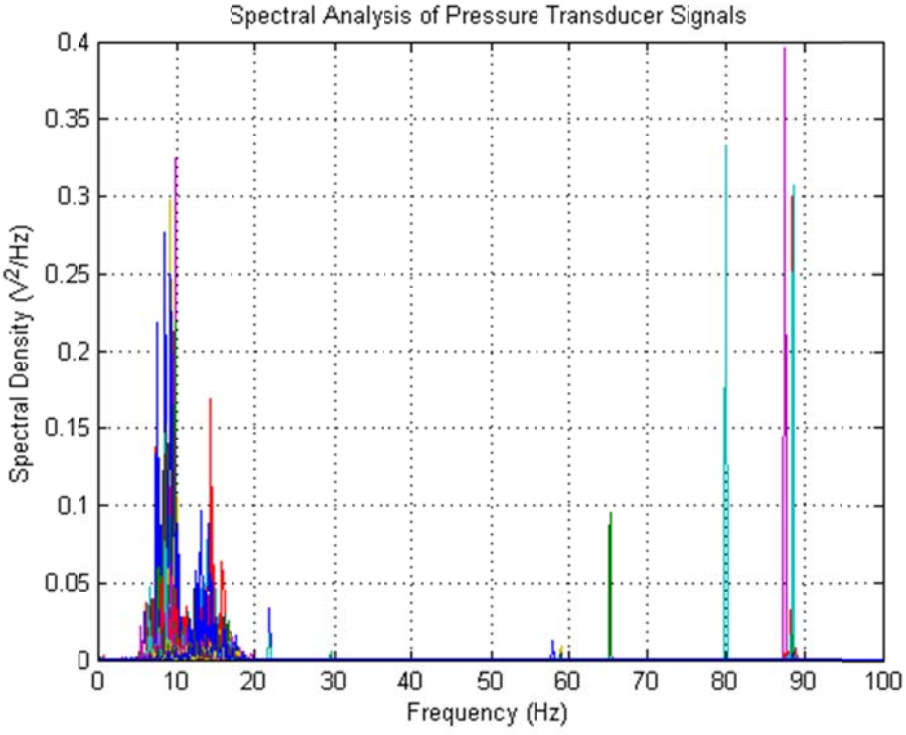

Figure 4-1. Spectral analysis of de-meaned pressure transducer voltages

As shown in this graph, there are several noticeable peaks in pressure readings between 5 Hz and 20 Hz. The 65 Hz spike is electrical noise (120 VAC produces this) and the 80 Hz and 90 Hz spike were only present on a few data runs. These are probably due to bubble development at higher flow rates and can be ignored. The focus then became determining what the 5 Hz – 20 Hz spike was.

Because shear stress readings were availabe from the sensor, it was possible to find what the oscillating frequency of the shear stress should have been based on the sensor data by performing another spectral analysis of shear measurements. Results of this are presented in Figure 4-2.

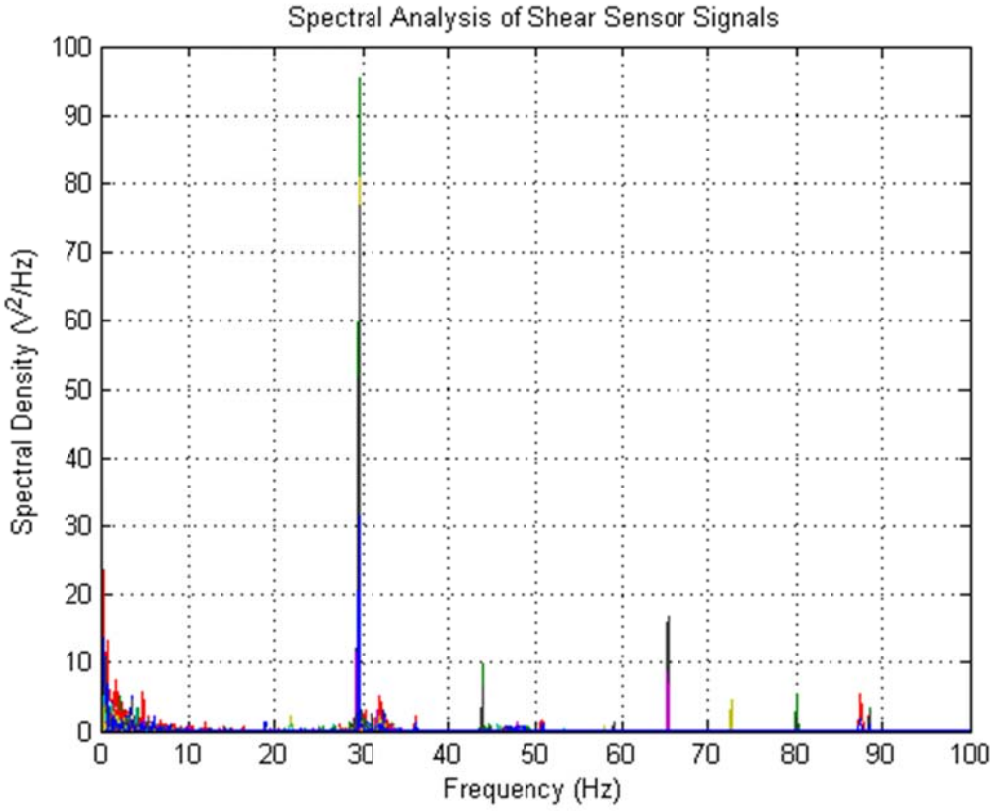

Figure 4-2. Spectral analysis of de-meaned shears stress sensor measurements.

As shown here, the shear stress sensor shows a large spike at approximately 30 Hz. This is most likley the resonant frequency of the sensor itself. Recall that the shear stress sensor oscillates back and forth on its leaf springs. When the sensor is knocked, or water flows over it, it will oscillate at its own fundamental frequency, and this is probabaly what is causing the 30 Hz

spike. If the true frequency of shear stress readings was at 30 Hz, a similar peak should be seen in Figure 4-1 because frequency should correspond to pressure. Although the correct pressure differential may not necessarily produce the correct shear stress, one would expect pressure fluctations and shear stress fluctuations to be similar. This relationship does not exist as demonstrated in these two figures. Therefore, the true data from the shear stress sensor is most likely the block of data seen in the Figure 4-2 spectograph that lies below 10 Hz. This can be confirmed by isolating the 30 Hz signal using a bandpass filter and plotting a time series of filtered data. The results from this are shown in Figure 4-3:

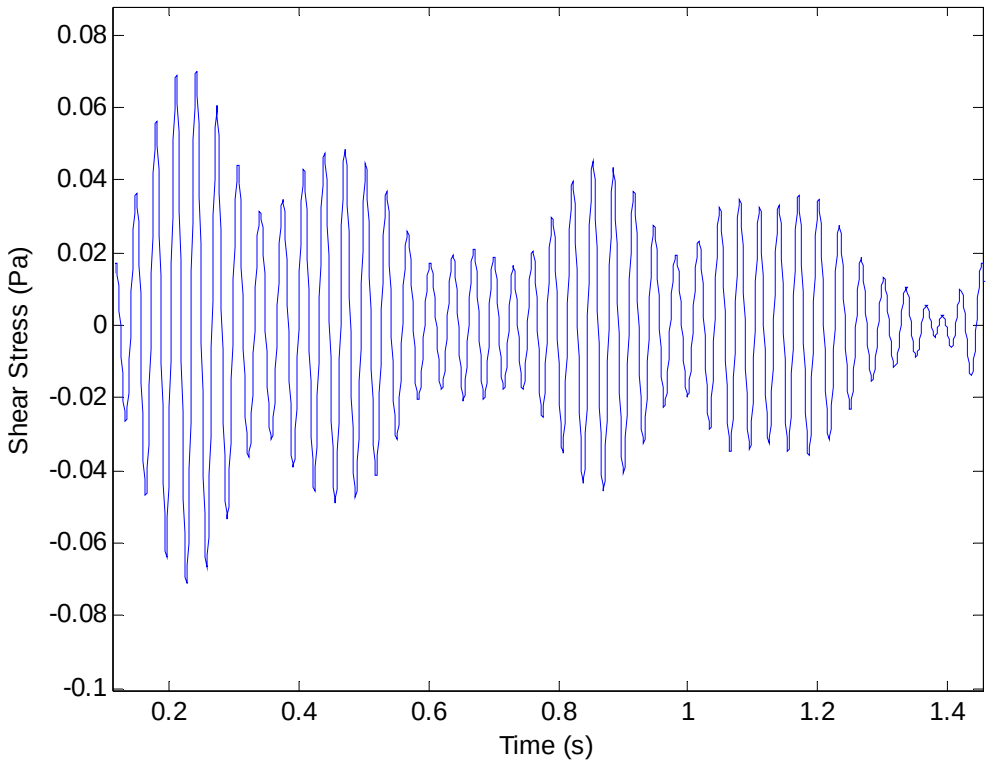

Figure 4-3. The 30 Hz data block from the shear stress sensor showing shear stress difference from the mean

The same technique used to isolate the 30 Hz data block from the shear stress sensor was used to look at the 5 - 20 Hz spike. Specifically, a 5 Hz – 20 Hz 4th order Butterworth bandpass filter was designed where this data block would be isolated, and another time series was plotted with transdcuer filtered data. Results from this are shown in Figure 4-4.

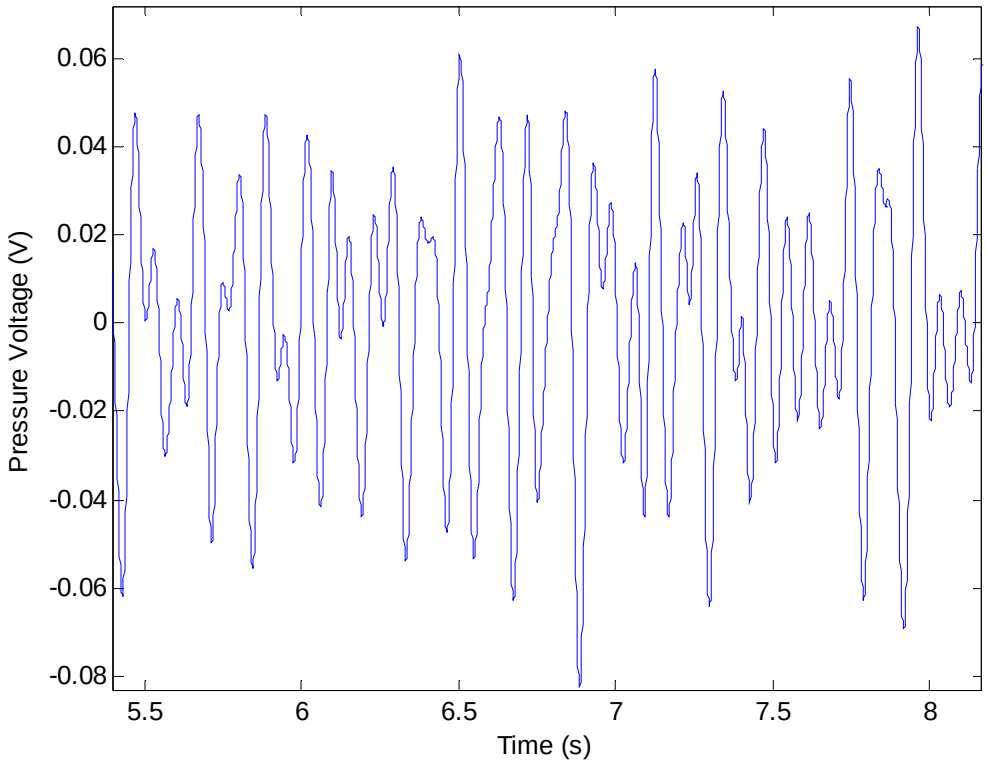

Figure 4-4. 4 Hz – 20 Hz data block from pressure transducer showing voltage difference from the mean

As shown here, the 5 Hz – 20 Hz data block oscillates at approximately 0 V. This data block then is not the actual signal that needs to be captured. Rather, it is some vibratory mode that is aliasing the signal. The next thought was that flume vibration may be causing this fluctuation. Two tests were conducted to rule this out. First, a test was designed where the pressure transducers were turned on, wired, and hooked up to the SERF. Then, the control valves from the flume tubing to the transducer were closed so that water could not cause a pressure differential on the transducer's membrane. The signal from the pressure transducers then would be the vibratory mode of the flume. Results from this round of tests are presented in Figure 4-5.

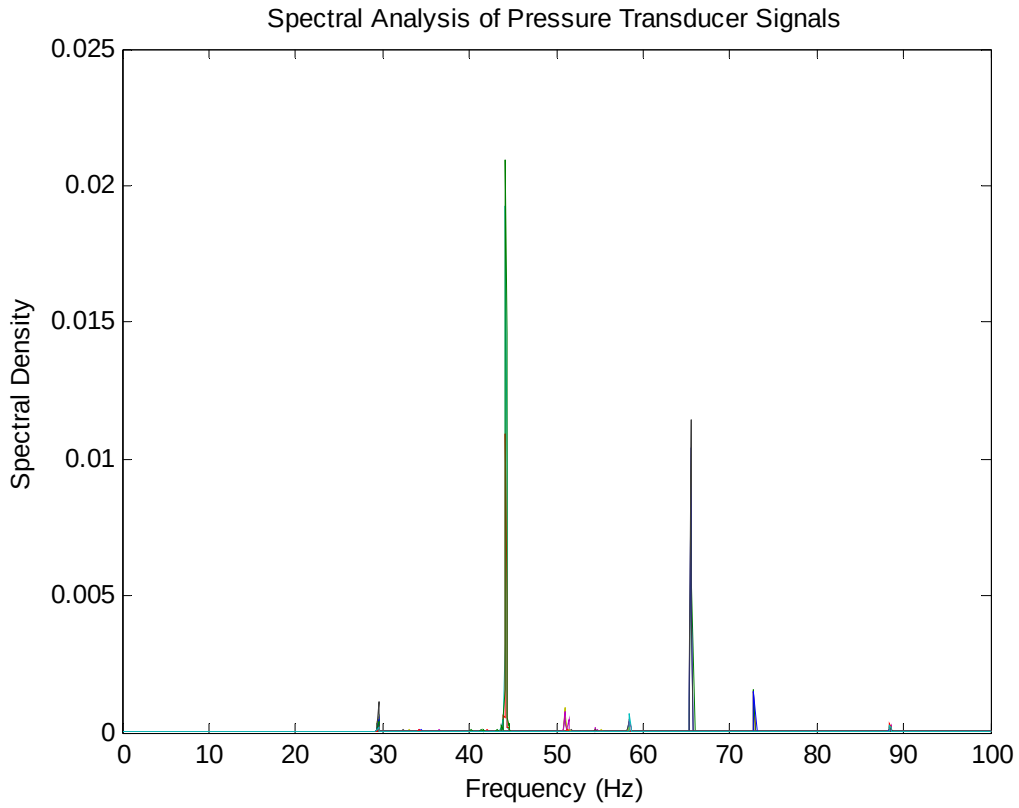

Figure 4-5. Spectral analysis of free-vibratory flume test voltage measurements

As shown in this graph, there is no peak between 5 Hz and 20 Hz. Therefore, the 5 Hz to 20 Hz signal must not be caused by flume or pump vibrations. The ~45 Hz spike only occurs in one dataset and is not repeated. This could be due to a number of factors – an air conditioning unit turning on, a fan blowing, someone using another piece of electrical equipment in the lab, etc. Because it is not repeated and it is not present under flow conditions, it was ignored. Again, the 65 Hz spike represents electrical noise.

To further confirm that the 5 Hz to 20 Hz vibration must be a "real" signal and not caused by pump or vibrational noise, the pressure transducer was removed from the SERF frame and attached to the external frame that holds the sample into place. Doing this eliminated most vibrations from the transducer. Data was taken at three flow rates because this data was taken concurrently with Gator Rock tests, and a spectral analysis was conducted (Figure 4-6). Although only three flow rates are used for this analysis, these results are expected to be typical.

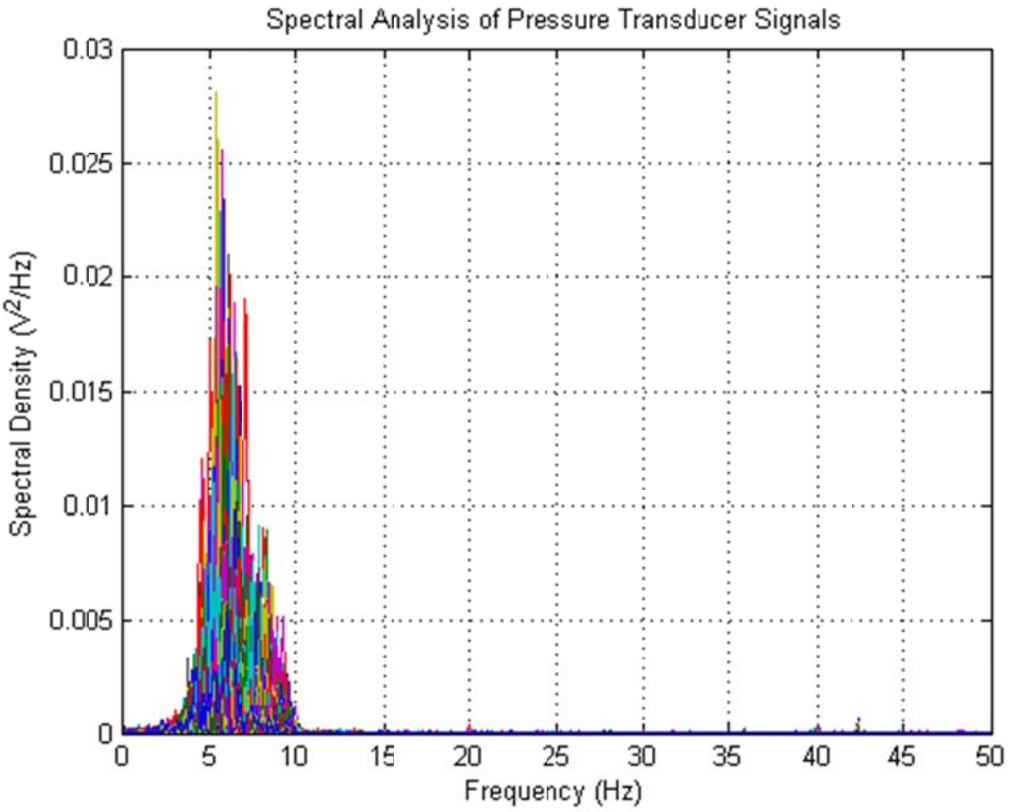

Figure 4-6. Spectral analysis of free-vibratory flume test with sensor on new frame

The combination of Figure 4-4, Figure 4-5, and Figure 4-6 show two things:

1. Flume vibrations are not the cause of the 5 Hz – 20 Hz spike in pressure transducer data.

2. The 5 Hz – 20 Hz signal is a "real" measurement. Because the gage pressure in the SERF is several orders of magnitude higher than the pressure difference, it was thought that the normal stresses were causing this fluctuation in pressure difference. A gage sensor was set up to measure normal forces (Figure 4-7), and a spectral analysis of these readings was conducted (Figure 4-8).

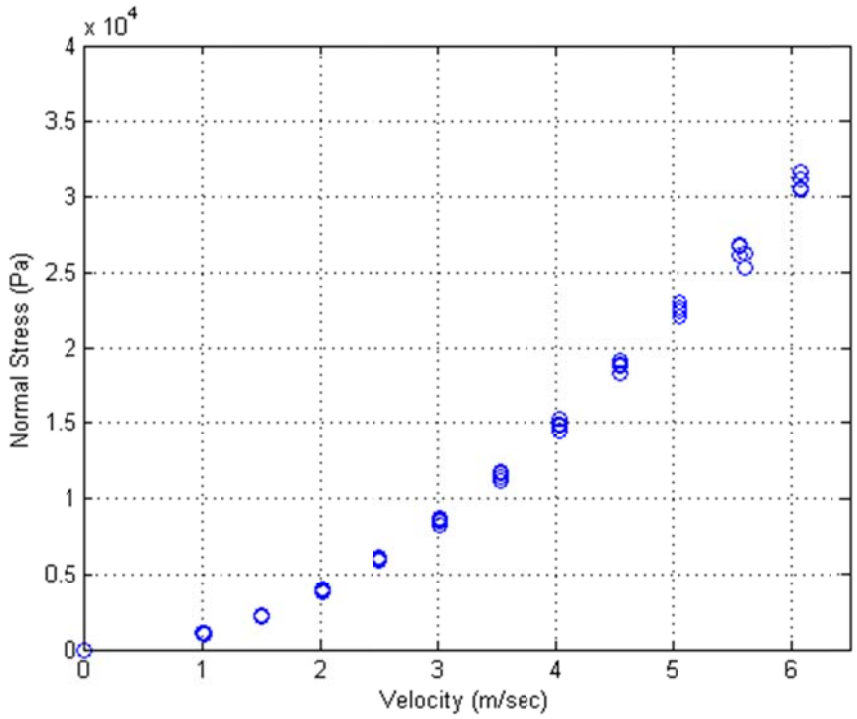

Figure 4-7. Average normal stresses in the SERF

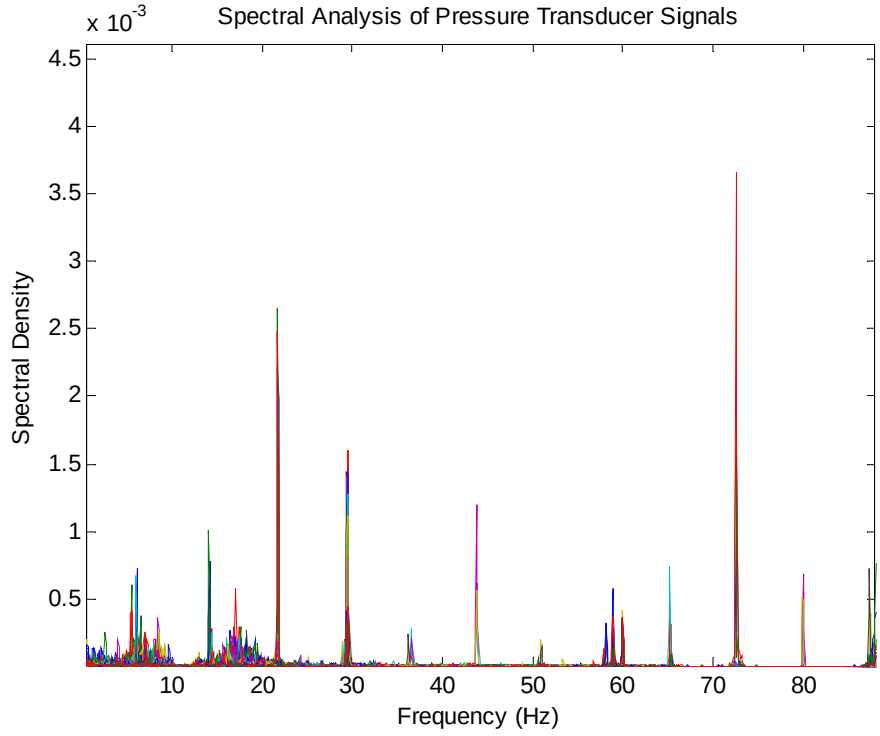

Figure 4-8. Spectral analysis of normal stresses

Figure 4-7 confirms that normal stresses in the SERF are four orders of magnitude higher than pressure differences while Figure 4-8 shows that normal pressure in the flume does not oscillate at 5 Hz – 20 Hz. There is a small frequency spike between 5 and 20 Hz, but it is several orders of magnitude smaller than the frequency spike seen with the pressure differential readings.

Pressure transducers are accurate up to 0.25% FS. For measuring normal stress in the SERF, a 30 psi transducer was selected because of the high pressures associated with high flow rates, and this sensor is only accurate to 0.075 psi. Conversely, the differential pressure transducers have a range of 0.5 psi, and they are accurate to 0.00125 psi. The 5 – 20 Hz signal from the differential transducers has a maximum magnitude of +/- 0.1 V from the mean. This corresponds to a pressure difference of 0.02 psi, which is much lower than the pressure fluctuation that can be accurately picked up with the gage pressure sensor. The pressure differential readings are then "real" and they are small – too small to be detected by a gage pressure sensor. If a gage sensor were attached, it would fail because the pressure is too high. These fluctuations must be attributed to normal stress fluctuations because they cannot be attributed to anything else. Relative to the normal stress scale, $O(10^4)$, these fluctuations are small, but relative to the scale required for shear stress, $O(10^0)$, they are large.

Data was collected over a 10 s time interval at a frequency of 1 kHz, and then averaged over the time domain. Because the 5 Hz – 20 Hz frequency band averages to zero, for the purposes of averaging, it could be ignored. If one wanted to eliminate this noise band, it would be possible using a longer flume length, but modifications would be required. Pressure could be measured higher upstream and further downstream than it currently is measured. Currently the pressure difference is only measured +/-2 inches from the sample because the goal is to isolate the sample's effect on pressure difference. With the flume's present setup, if the pressure ports were spaced further apart, a larger portion of the pressure difference would be caused by the flume walls, while a smaller relative portion of the pressure differential would be caused by the eroding sample roughness. On average then, a higher portion of the overall average shear stress would be computed from walls – thereby theoretically throwing the calculation for shear stress across the face of the sample off even further.

The word "theoretically" is used in the preceding paragraph because the rationale behind the original spacing of the SERF pressure ports was to space them close to the sample so that the sample's effects on pressure differential would be maximized. In other words, pressure ports

were spaced just upstream and just downstream from the sample because the sample is rougher than the flume walls. The rougher sample should produce an overall higher pressure differential effect on its respective flume portion. As pressure ports are spaced further from the sample locus, there will be more flat flume area relative to the amount of rough sample area (which must remain constant). This increase in relative smooth area should cause the pressure differential to behave more like a "smooth" pressure differential and less like a "rough" pressure differential.

Unfortunately, even with close pressure port spacing, the sample's effect on pressure differential (and subsequently shear stress) was minimal. To illustrate this, a series of discs with different uniform grain sizes – 2 mm, 1 mm, 0.5 mm, 0.25 mm, and 0.125 mm – were prepared by sieving crushed limestone through several ASTM standard sieves and gluing these particles to 50 mm shear stress sensor discs. Prefabricated 50 mm discs acrylic discs with a predrilled hole through the center were purchased, attached to the shear stress sensor and the SERF run at varying flow rates. Spectral analyses for these rough discs were similar to spectral analyses presented for flat discs and will not be repeated. Namely, there are zero-mean pressure fluctuations in the device that are probably caused by a small-scale axial stress fluctuation. Comprehensive results of different diameter tests will be presented in Section 4.4.2 so that they can be compared with analytical methods for estimating shear stress, but with respect to estimating shear stress via the pressure transducer, Figure 4-9 is an illustration of what is happening in the SERF.

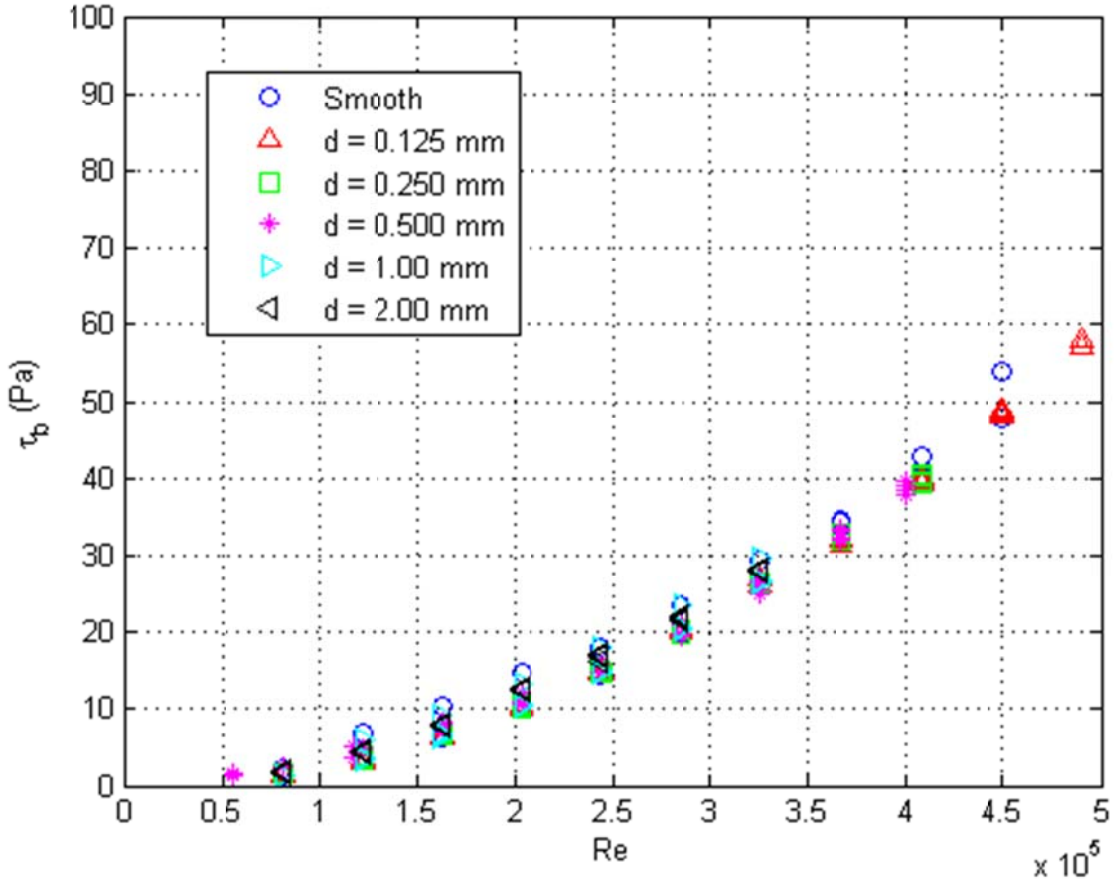

Figure 4-9. Shear stress estimates from pressure differential in SERF

As roughness of the shear stress sensor's disc changed from smooth under flat conditions to rough under large sediment conditions, the shear stress estimate from the pressure transducers did not change. It appears as though the sample area relative to the flat flume wall area is too small to see a noticable effect on average pressure difference in the flume. Figure 4-9 can be constrasted with Figure 4-10 to show the actual shear stress measurements across the face of the sample from the shear stress sensor. Figure 4-10 shows that as roughness (sediment size) increases, shear stress increases signficinatly. Therefore, using a pressure drop to estimate shear stress for a rough sample would underestimate the actual shear stress conditions because on average, the pressure drop is influenced more by the contributing area of the flat wall cross sectional area than it is by the rough sediment disc cross sectional area.

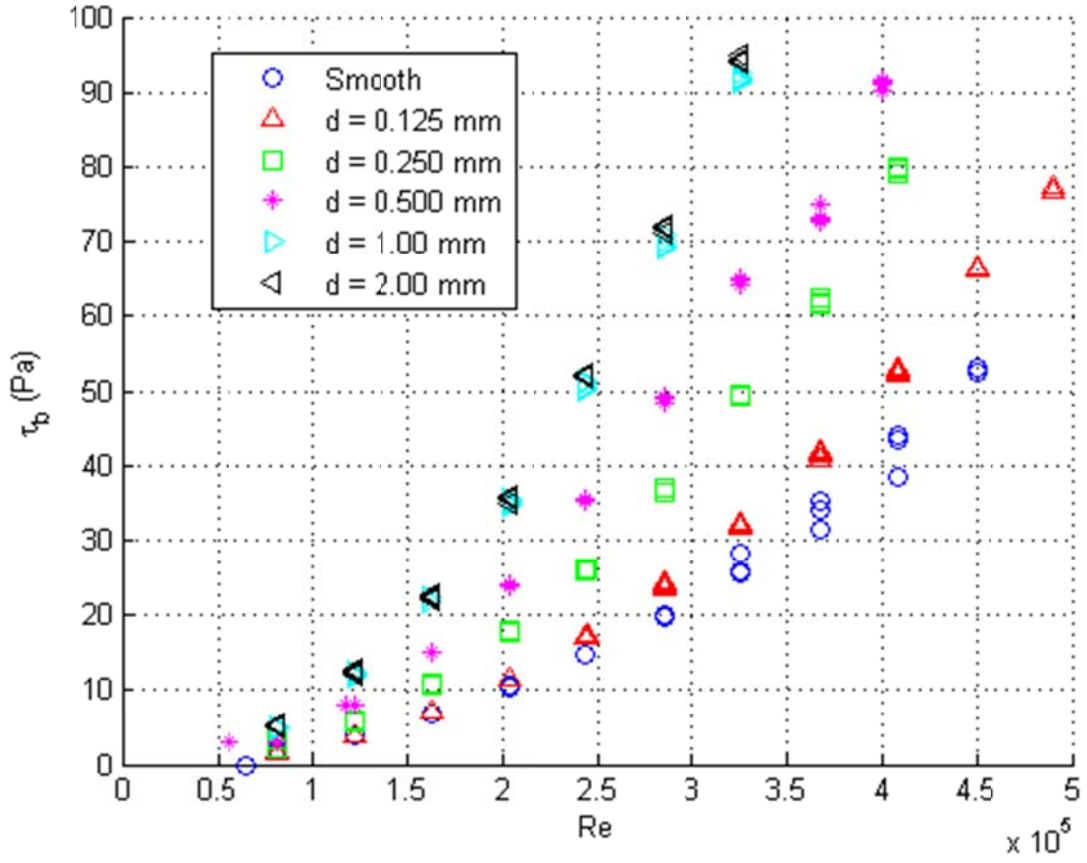

Figure 4-10. Shear stress measurments from the SERF's shear sensor

If one wanted to use a pressure differential to estimate shear stress, it would be possible if conditions in the SERF were different. Nikraudese originally estimated shear stress in pipes by measuring pressure differences; his results led to development of the Moody Diagram. In Nikraudese's tests, his pipes were uniformly coated with sediment so that pressure differential must be governed by rough pipe walls. A similar technique could be used to predict shear stresses in a flume like the SERF – wall inserts would need to be constructed where different size diameter sediments were used. This would provide accurate pressure drop readings. However, in its present setup, because the SERF has flat walls and because the area of the test section (and shear sensor) is so small relative to the area of the flat walls, estimating shear stress from a pressure drop will not produce accurate results.

The implications of this for previous SERF tests are interesting. Several erosion rate-shear stress curves have already been developed for materials that should not be considered flat (Gator

Rock in particular). Because of this, the shear stresses used in development of these curves must be too small, and should be modified.

4.4.2 Analytical Methods

Once the question of shear stress estimation using a pressure drop had been assessed, the other methods for estimating shear stress were investigated. The ASSET, SEDFlume, and SEAWOLF estimate shear stress by assuming smooth walls. To evaluate the EFA method (Colebrook Equation), results from the shear stress sensor were used to solve Eq. 4-4 for k_s (Fig. 4-11). The expression developed here was used to then to solve Eq. 4-4 for shear stress. Results were plotted and compared with actual shears stress readings and computations using a smooth wall approximation (Fig. 4-12) and non-dimensionalized (Fig. 4-13).

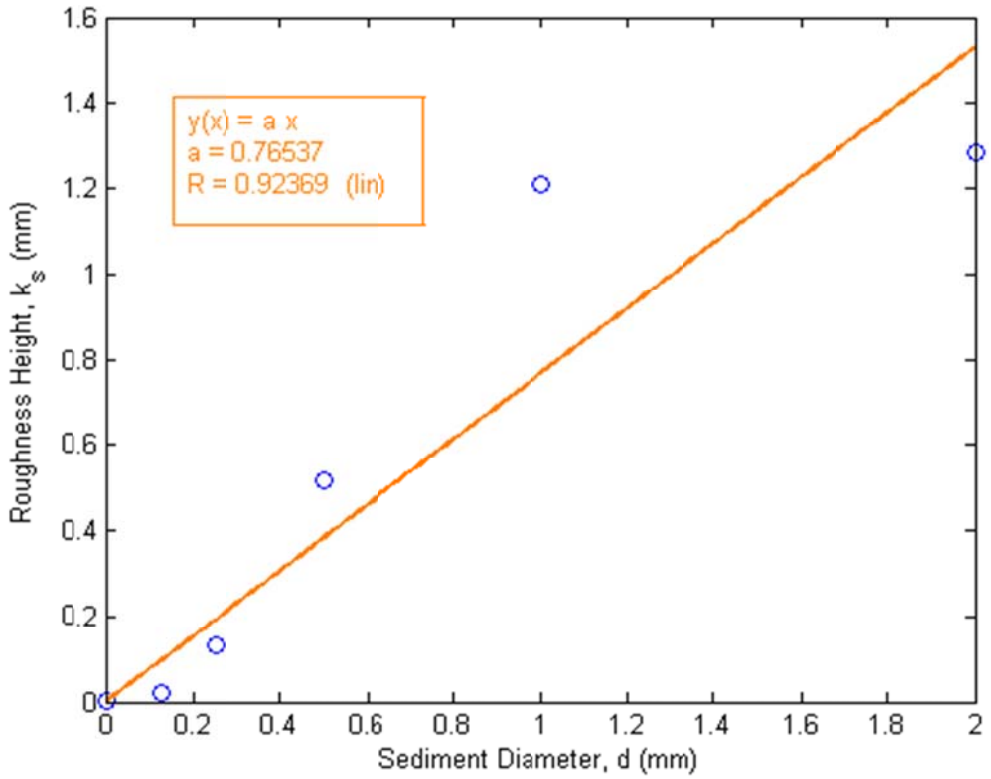

Figure 4-11. Absolute Roughness Height, k_s as a Function of Sediment Diameter, d

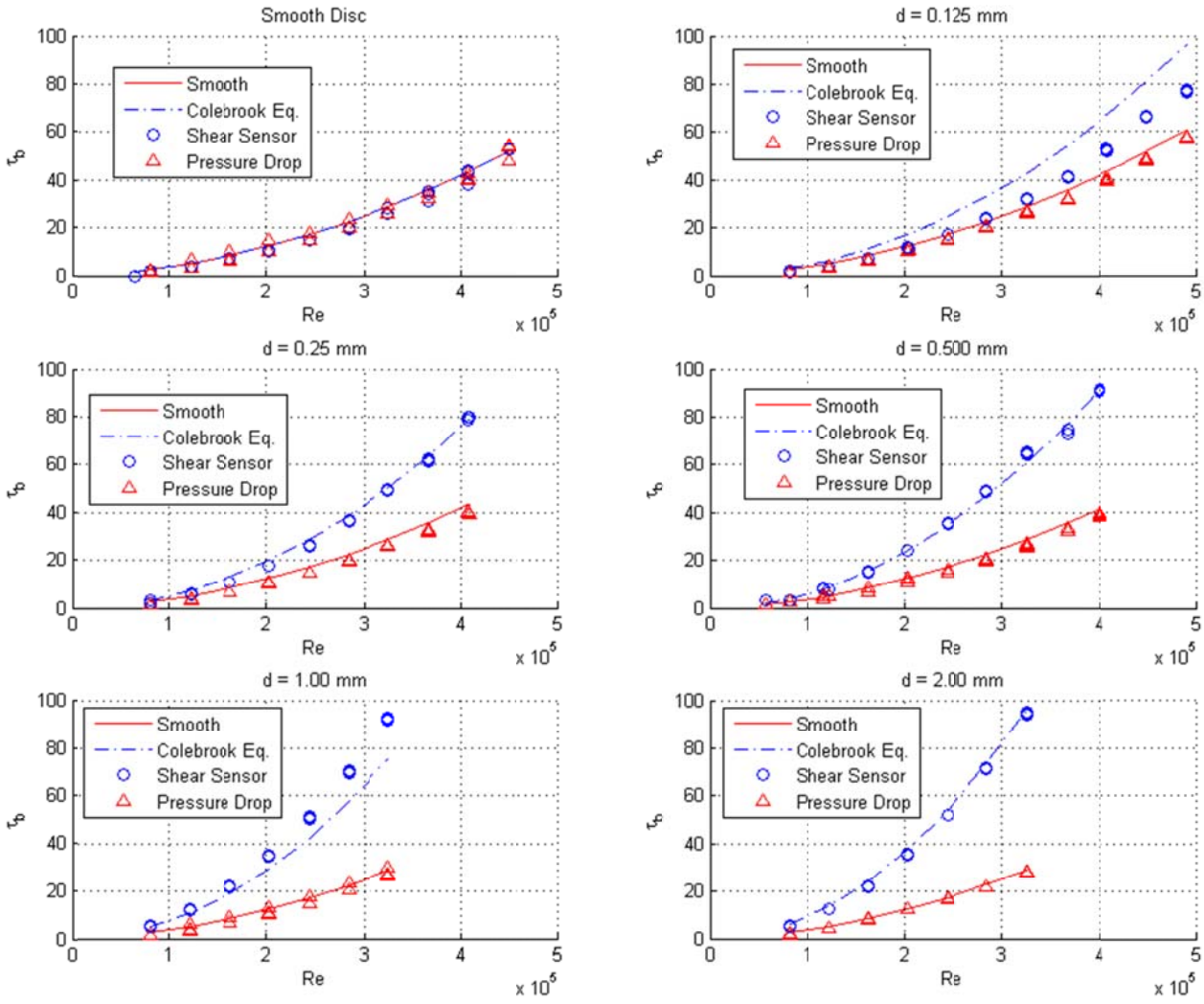

Figure 4-12. Shear stress as a function of flume Reynolds Number using actual data, the smooth wall approximation, pressure drop data, and the Colebrook Equation approximation from the relationship developed in Fig. 4-11.

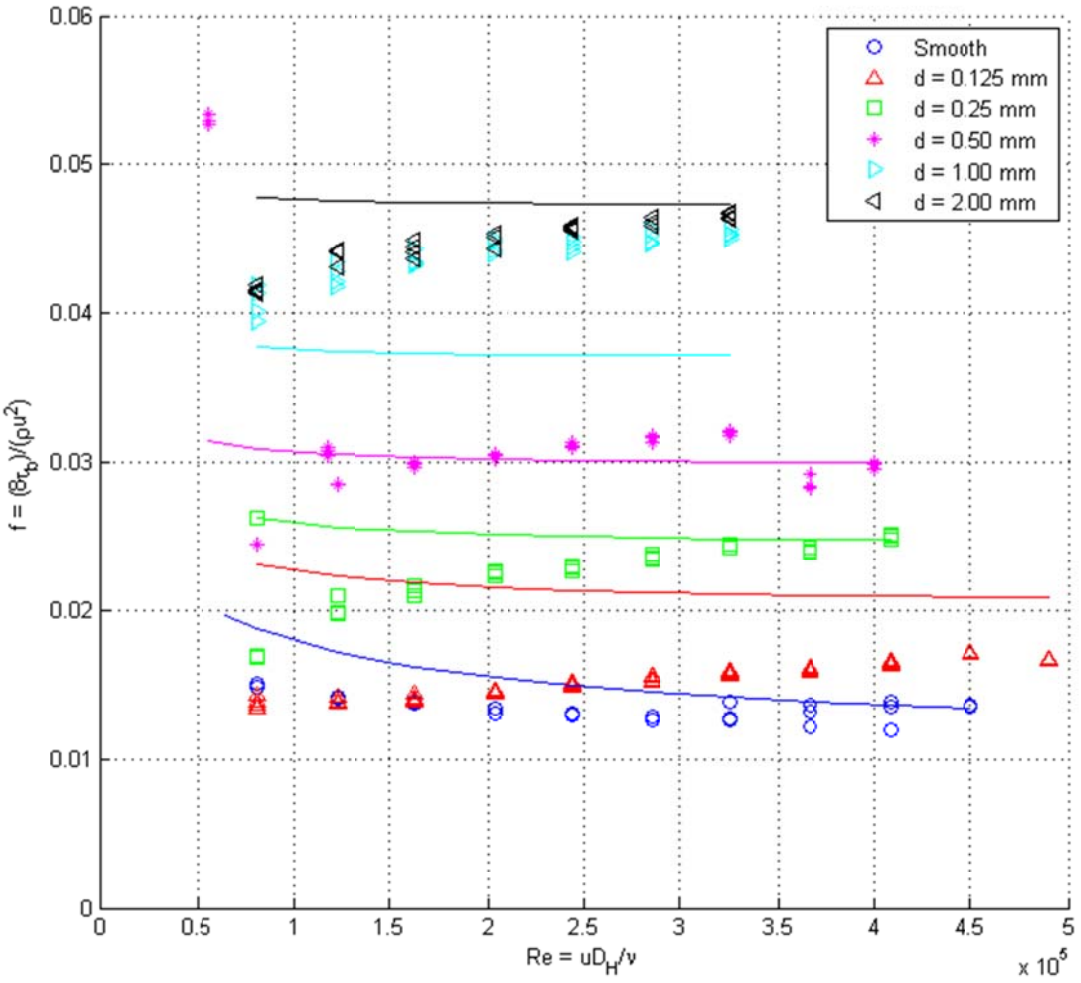

Figure 4-13. Combined Non-Dimensionalized Results From Colebrook Equation, Shear Readings, and Smooth-Wall Assumption

These figures illustrate four observations:

1. As sample-disc sediment size changes, results from the pressure drop computation do not appear to be affected.

2. Using a pressure drop to estimate shear stresses for a rough sample (compared to the smooth flume walls) will underestimate shear stresses. This under prediction increases as roughness increases.

3. The Colebrook Equation is the most accurate alternative technique if a roughness height of 0.76 times the sediment diameter is used.

4. Even though the Colebrook Equation appears to be a valid method for estimating shear stress, it still produces some error (Fig. 4-14).

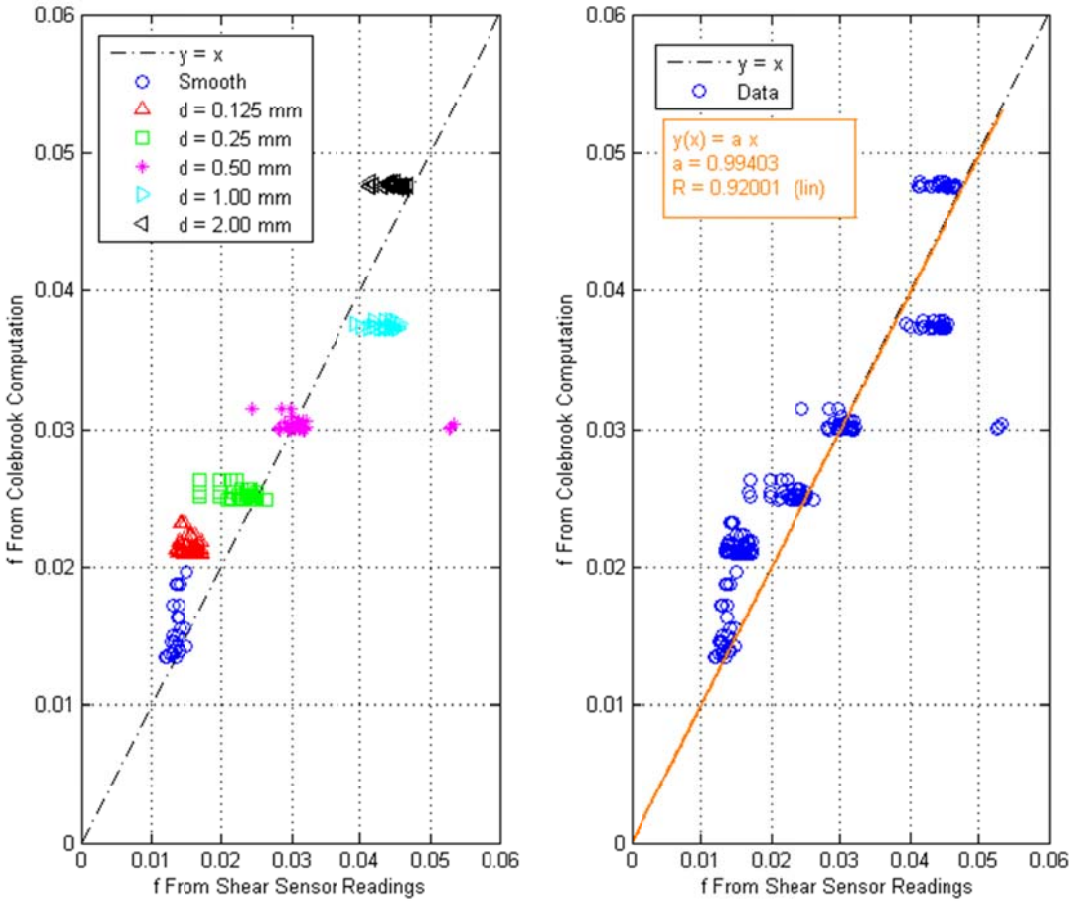

Figure 4-14. Friction factor, *f* from sensor readings and using Colebrook Equation Approximation

While data shows that it appears to be possible to calibrate the Colebrook Equation to SERF shear sensor readings, one must be careful when attempting to generalize results and extrapolate them to use with other instruments. The 0.7654 computed calibration factor should be interpreted as "instrument-specific" because the SERF's hydraulic radius was used to conduct the computation. If another instrument with a different hydraulic radius was used, a different relationship between roughness height and sediment diameter would most likely follow. This is due to the difference between the relative area the sample occupies compared with area of the duct on which smooth walls are present.

To generalize results further, a more in-depth analysis was conducted. Following intermediate fluid mechanics, given flow between two stationary plates (or within a duct), a wall friction coefficient, C_f can be defined:

$$C_f = \frac{2\tau}{\rho \overline{u}^2} \tag{4-7}$$

For the case of a flume-style erosion rate testing device, analytical reasoning dictates that it should be possible to quantify C_f as a function of the ratio between sediment diameter and flume height:

$$C_f = f\left(\frac{d}{h}\right) \tag{4-8}$$

In other words, as the ratio between grain size and flume height increases, shear stress should similarly increase. Frictional coefficients were computed from data and plotted as a function of the ratio shown in Eq. 4-8 (Fig. 4-15).

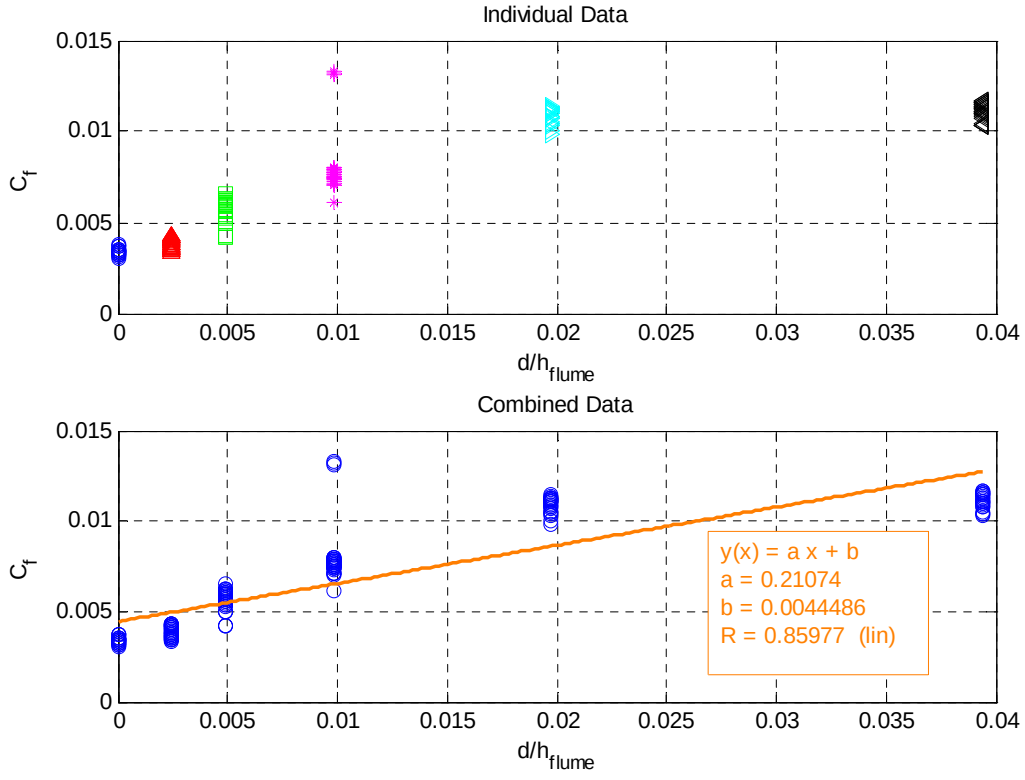

Figure 4-15. Wall friction coefficient as a function of grain size-flume height ratio

Fig. 4-15 may prove to be the most useful result presented in this study because it may provide a method for solving for shear stress in the case of a generalized erosion rate testing device. Further research should be conducted to verify that this correlation is valid for rectangular ducts of different heights since only the SERF was used to develop this correlation.

4.4.3 Vortex Conditions

Another goal of this study was to determine how the introduction of vortices influences erosion rate-shear stress curves. As discussed in the literature review, for particle-like erosion there is both a theoretical basis for quantifying erosion rate as a function of shear stress and a history of empirical relationships between these two parameters. When investigating the effects of vortices, preliminarily, it appears as though the vortex itself should not be studied, especially since at present a velocity profile cannot be measured in the SERF. Rather, the effect of the vortex on average shear stress should be studied, and because erosion rate is a function of shear stress, erosion rate effects of vortices would follow.

Preceding tests on uniform diameter experimental discs were repeated with the SERF's vortex generator installed. Results are presented in Figure 4-16, Figure 4-17, and Figure 4-18.

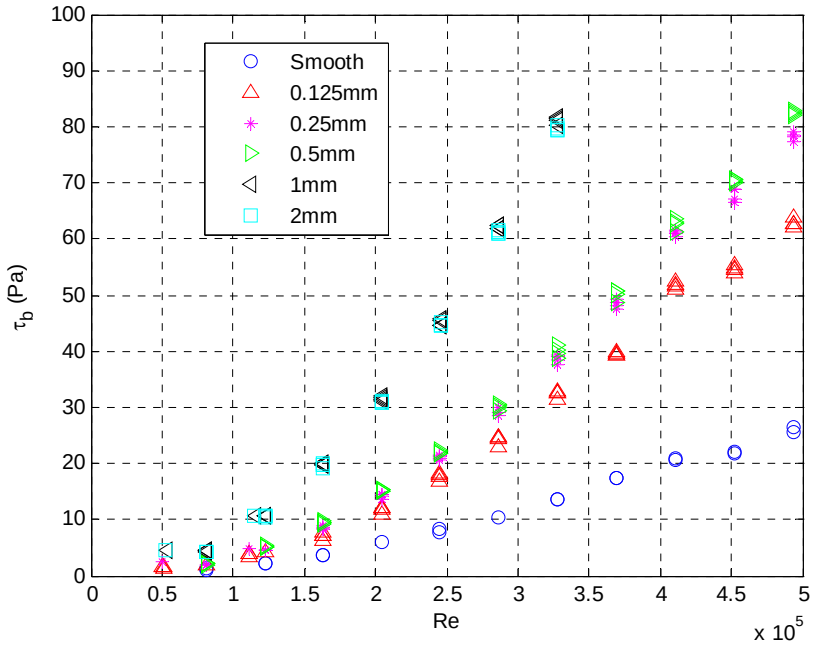

Figure 4-16. Combined Shear Stress Sensor Data under Vortex Conditions

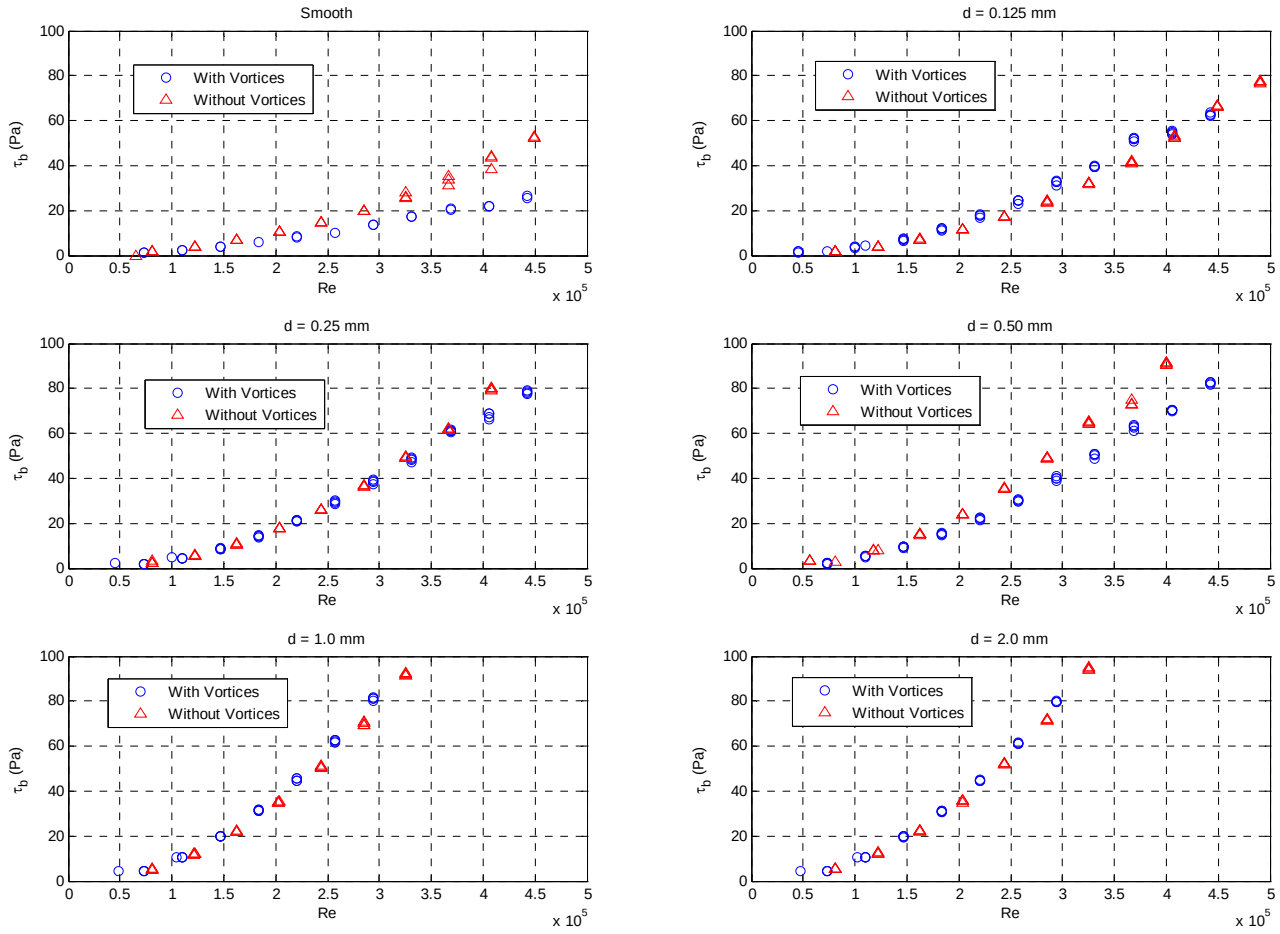

Figure 4-17. Shear stress comparison between vortex and non-vortex conditions

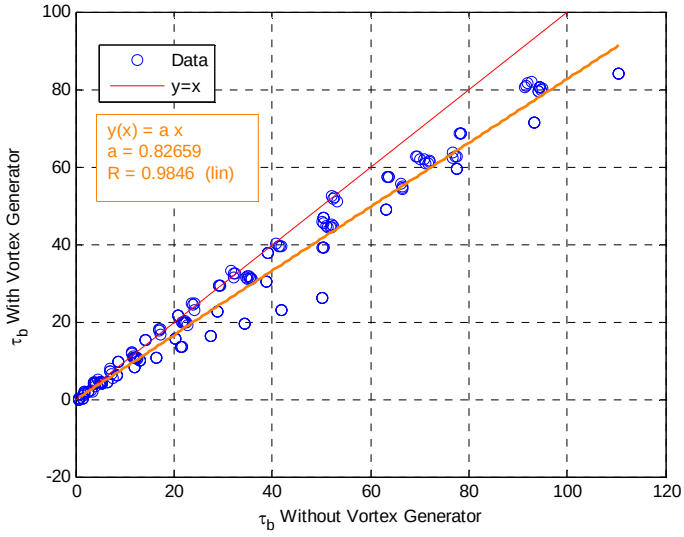

Figure 4-18. Shear stress comparison between vortex and non-vortex conditions (results plotted against one another)

As shown in these figures, in general, upstream vortices in the SERF appear to have a small effect when compared to non-vortex conditions. At higher velocities, the vortex generator appears to cause slightly lower shear stress. This seems logical because as velocity increases, the effective wake distance should similarly increase.

There also appears to be a particle-size dependency on vortex effects such that as surface roughness decreases, the effect of vortices increases. Qualitatively, this particle-dependency on vortex effects makes sense. Large particles are going to produce their own vortices, and introducing a large upstream vortex (wake region) should have a minimal effect when compared with the effects of the vortices caused by the roughness of the sample. Conversely, small particles will not produce large vortices on their own. Therefore, they are more affected by the shearing action of water against their surface and less affected by vortex-particle interaction. As such, when a large upstream vortex is induced in the SERF, its net effect from the perspective of a small particle is simply to retard the flow in the direct vicinity of a small particle, thereby decreasing the net overall shearing action against it. Large particles on the other hand are more affected by local vortex affects, and a small net-retardation of the flow will produce little shear stress effect.

Because in general vortex induction lowers shear stress, and because particle-like erosion rate is intrinsically tied to shear stress, under vortex conditions, particle-like erosion rate should decrease proportionally with shear stress. This could be useful under field conditions where a large obstruction is directly upstream from a bridge pier (a large pipe for example). The design shear stress may be able to be reduced by a factor proportional to particle size. To be conservative however, even under vortex conditions, non-vortex shear stress (and erosion rates) should be used until field verification of this can be made.

4.5 Recommendations and Conclusions

In summary, from this it appears as though the shear stress question in the SERF has been solved. The following are recommendations and conclusions from this study:

1. For a rough sample, a pressure drop may not be used to estimate shear stress because it will under predict actual shear stress conditions. However, the pressure drop method may be acceptable for relatively smooth samples.

2. For a smooth sample, the method used in the ASSET, SEDFlume, and SEAWOLF may be used to predict shear stress.

3. For a rough sample, the ASSET/SEDFlume/SEAWOLF method should not be used because it will under predict shear stress.

4. For a rough sample, the EFA method may be used, but an absolute roughness curve should be computed. Because a shear sensor would be required to develop the calibration curve, the purpose for using this method becomes defeated.

5. If the actual roughness is not known it appears to be possible to correlate shear stress to sediment diameter using a friction coefficient.

6. Vortices appear to have a small overall effect on average shear stress development.

7. For large particles, upstream vortices have a minimal effect.

8. For small particles, upstream vortices have a larger effect, and they generally reduce net overall average shear stress.

4.6 Future Work and Limitations

The equivalent roughness concept may help future flume-style shear stress testing. This can be viewed similarly to equivalent diameters for bridge piers as presented in the FDOT bridge scour manual. In other words, even though a rock core or sand-clay mixture may not have a specific grain size associated with it from a bulk sense (as would be common with natural samples), it may be possible to measure its surface roughness and assign an equivalent grain size that can be used to predict the shear stress from a Moody Diagram.

Although not in the scope of this project, there is a device at UF called AIMS that can measure the roughness of a series of concrete cores using high resolution cameras. The AIMS can be modified so that it can measure the roughness of rock cores or sand-clay samples. As demonstrated in this chapter, it appears that shear stress in a flume-style erosion rate testing device can be correlated to grain size. If equivalent roughness can be defined, it may be possible to predict shear stress for a sample using Fig. 4-15.

It is important to note that conclusions developed in this study assume that the sample roughness does not vary during testing. If roughness does change, using a separate shear stress measuring technique, a Moody Diagram, or a friction coefficient is no longer appropriate. Erosion tests on cohesive sediments often show differential erosion rates across the sample, i.e., where the upstream face erodes faster than the downstream edge or vice-versa. Under these conditions, bulk sample roughness should not be governed by a uniformly-rough assumption

since locally, the surface roughness height of the sample varies. In other words, when a large chunk of material fails to erode, the sample on average has a different roughness height than it would have had if the sample had eroded uniformly. Under these conditions, assuming that the sample's surface eroded nearly uniformly from front-to-back is incorrect. Using the techniques outlined in this paper to infer the average shear stress then would also be incorrect since the roughness height does not equal the roughness height of a uniformly rough disc. Further research is needed to develop a device that measures erosion rate and shear stress simultaneously under these conditions.

CHAPTER 5
DEVELOPMENT AND TESTING WITH A NEARLY UNIFORM, HIGHLY ERODIBLE, SYNTHETIC ROCK-LIKE MATERIAL TO BE USED FOR CALIBRATING EROSION-RATE TESTING DEVICES

5.1 Executive Summary

Because of questions in comparing Rotating Erosion Test Apparatus (RETA) results with more traditional flume-style erosion rate test devices results, attempts were made to develop a nearly uniform material to serve as a direct comparison medium between these different instruments. A new material, Bull Gator Rock, was developed using similar principles to older Gator Rock designs. While older versions of Gator Rock were mixed with water, Bull Gator Rock was mixed dry and water was added to the mix later through capillary action. Two different rounds of Bull Gator Rock mix were developed. The first round showed excellent compressive and tensile strength test results. Erosion results in the RETA and the Sedimentary Erosion Rate Flume (SERF) were mixed. Cement content and water content were increased, and a second round of Bull Gator Rock was produced. Because of aggregate variability, strength tests were not repeatable. Erosion tests showed the presence of rock-like erosion, although a promising result from one round of testing showed the potential for a particle-dominated erosion scenario. Eventually, researchers realized that for a direct RETA-to-flume style device comparison, an extensive dataset was required.

5.2 Review of Relevant Background

Because the RETA measures erosion on a rock core or Shelby tube's sides instead of on its top surface, people have questioned whether or not results from these erosion tests were the same as they would have been had a more traditional flume-style device been used instead. When this project began, the first thought was that the most effective way to verify that the RETA was to directly compare RETA results to results from a flume-style device. The Sediment Erosion Rate Flume (SERF) was used as the flume-style device in this study. To perform this comparison, a suitable material was needed for testing in both instruments.

Finding a naturally occurring material that is erodible in both the SERF and the RETA is not as easy as it sounds. Any material to be tested in both devices needs to have enough internal strength to withstand moment forces associated with the RETA. Materials like soft clay and compacted sands will often crumble during RETA testing, and these results are useless when trying to compare the two devices. Despite this internal strength criterion, the material to be tested in both devices also needs to be highly erodible. Any material to be tested in both devices must be nearly uniform. A non-uniform sample will become obvious during a RETA test, as one localized section of the sample will erode faster than another section. The material tested in both devices must also be uniform from another standpoint – from sample to sample. Repeatability of erosion and strength test data is important because if one can differentiate one sample from another, any results coming from a comparison will be meaningless.

Because of these stringent criteria for testing a material in the RETA and the SERF, work to compare results from the two devices in the past has focused on the use of synthetic materials. Niraula's (2004) Gator Rock was used as a starting point because previous researchers, particularly Slagle (2006) indicated that he believed Gator Rock could serve as a proper material for testing in both instruments. Although the original version of Gator Rock was too strong, Slagle believed that by raising the water content, he could create a nearly uniform material that was strong enough to withstand RETA testing while still eroding.

As discussed in Chapter 2, Slagle's original attempt to create Gator Rock was problematic. He mixed water, crushed limestone, and cement in the appropriate proportions, and allowed the samples to cure for 28 days. Then, the samples were subjected to RETA testing.

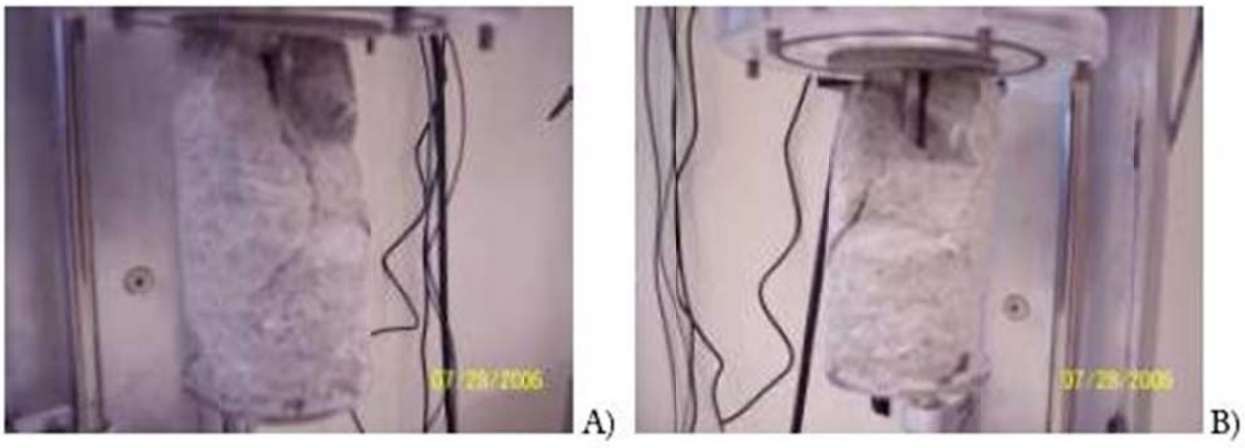

Figure 5-1. Examples of old-style Gator Rock after RETA testing (Shah 2009)

As shown, Slagle noticed that erosion was definitively non-uniform (Figure 5-1). Instead of uniform erosion, he observed that the tops of his samples eroded much more quickly than the bottoms. This phenomenon can be explained rather easily. The crushed limestone-water-cement slurry that was used to make his Gator Rock was mixed wet and water content was high. During curing, the samples were placed on the ground right-side up, and while this happened, because of the high water content, water worked its way up through the limestone-cement matrix because of capillarity. Over the 28 day curing time, a higher amount of water was present in the tops of the samples compared to the amount of water in the bottoms of the samples. This higher water content caused the tops of the samples to be much weaker than the bottoms of the samples, and as a result, differential erosion occurred.

As discussed briefly in Chapter 2, as a result of this water differential, Slagle tried another technique to make Gator Rock (Gator Rock 3.0 from Chapter 2). He next developed a rotisserie (Figure 5-2) so that the samples would spin while they were curing.

Figure 5-2. Slagle's Rotisserie

Spinning the sample during curing did stop capillary action from occurring during curing, but it may have created another issue. During curing, particles in the slurry should separate due to the spinning rotisserie's centrifugal forces such that smaller pieces of aggregate would be spun

to the outside of the molds while larger aggregate should remain concentrated in the samples' center. When looking at the sample from the top, the middle of the sample had a higher concentration of large aggregate than the outside of the sample. Although from top-to-bottom the sample may have been uniform, from side-to-side the sample was not. Top-to-bottom uniformity is essential for RETA testing, but side-to-side uniformity is vital for SERF testing. Because of the different types of heterogeneity, these Gator Rock samples could not be used either. In his 2006 thesis, Slagle discusses the issues with Gator Rock testing, and he cites non-uniformity as a constant source of concern. He does not specifically say how his samples were heterogeneous, but from the mechanisms just described, one can infer how it must have happened.

As of 2006, no known material had been developed that was appropriate for a SERF-vs.-RETA comparison. In this study, another attempt was made to create a new version of Gator Rock that would meet the stringent material criteria for SERF-RETA tests and that could be easily and inexpensively mass-produced.

5.3 Theory Behind Bull Gator Rock

In this study, a new tactic was used to construct Gator Rock. The rotisserie idea was abandoned, and instead, researchers looked to take advantage of the water's capillarity. Because capillary action occurs slowly, researchers hypothesized that cement and crushed limestone could be mixed dry, the dry mix could be placed in a specific amount of water, and over time, the water would work its way up through the sample much like it did during the first attempt to make Gator Rock. As the water worked its way through the sample slowly, a new, nearly uniform Gator Rock specimen should be created.

In principle this mixing technique had the potential to have the opposite effect as the original Gator Rock recipe. Because the Gator Rock sample was mixed dry, and water was added to it from the bottom, one could argue that the bottom of the sample would entrain more water than the top of the sample. If capillary forcing of the water was not higher than the force of gravity, indeed, this argument would make sense. A smaller quantity of water could be transferred to the top of the sample while a larger quantity of water would remain at the sample's bottom. However, during the original attempt to make Gator Rock, the opposite was seen. The tops of the samples, not the bottoms were locally the weakest. Therefore, it was known that

capillary forces in the crushed limestone-cement matrix were relatively high, and researchers thought that this dry-mix technique would produce a nearly uniform sample.

5.4 Procedure for Construction of "Bull Gator Rock"

The following procedure for development of Bull Gator Rock was developed by Crowley, Bloomquist, and Shah; it was originally presented in Shah's Honor's Thesis in 2009, but since then, some modifications have been made to the process. The finalized process in presented below:

1. Crushed limestone was obtained from the Whitehurst Company's mine in Newberry, FL (FDOT Reference No. 34-104), and oven dried for 72 hours.

2. Dried material was sieved through a standard ASTM No. 10 sieve to eliminate cobbles and larger pieces of aggregate.

3. 4 inch molds were cut from standard PVC pipe. For RETA testing, completed Gator Rock samples must have a final diameter of 2.40 inches while for SERF tests, samples must have a final diameter of 2.30 inches. Therefore, when samples were prepared for use in the RETA, standard 2.5 inches SCH 40 pipe was used; when samples were prepared for use in the SERF, standard 2.5 inches SCH 80 PVC pipe was used.

4. Micro filter paper was glued to the molds' bottoms and the molds' sides were coated with prestress mold release to prevent the samples from sticking to the molds' sides.

5. Water-cement ratios were chosen for the Bull Gator Rock batches. Then the appropriate amounts of water, cement, and water were determined using the following formulas:

$$M_{Limestone} = \left(\frac{\%LS}{\%LS + \%C} \right) M_{Total} \tag{5-1}$$

$$M_{Cement} = \left(\frac{\%C}{\%LS + \%C} \right) M_{Total} \tag{5-2}$$

$$M_{/Water} = \left(\frac{\%W}{1 - \%W} \right) \left(M_{Limestone} + M_{Cement} \right) \tag{5-3}$$

In these equations, *%LS* is the percentage limestone per batch, *%C* is the percentage cement per batch, and *%W* is the percentage water per batch. To estimate M_{Total} or the total mass of the entire Gator Rock batch, a mold was filled with crushed limestone, rodded, and weighed to determine the approximate total mass of substance that could be fit into a mold. Then, this weight was multiplied by the number of samples to be made. For example, if 40 samples were to be made, and the mass of crushed limestone that would fit inside of a mold was

approximately 475 g (which was typical for a SCH 40 mold), then M_{Total} = (40*475 g) = 19 kg.

6. A cement mixer was cleaned and dried. Limestone and cement were added to the mixer in the appropriate quantities. To prevent fines from escaping during mixing, a plastic bag was used to seal the cement mixer. The cement mixer was turned on, and mixing lasted for 10 minutes.

7. Molds were prepared.

8. First, an empty mold was weighed.

9. A collar was secured over the mold, and the dry mix was poured into the mold.

10. When the cement-limestone mix was approximately 2.5 inches from the top of the collar, pouring ceased, and the sample was gently leveled.

11. A plastic disc was placed in the 2.5 inches void to seal the contents of the mold. The disc was included so that during vibrating, the fines would not escape.

12. Samples were placed on a shake table with a 3.6 kg mass resting over each sample's plastic disc. The shake table was set to a speed of 2 and allowed to run for 8 minutes. This insured a densely packed dry mix.

13. The collar was removed, and pressure was applied to the plastic disc. Excess material was scraped from the top of the mold using a screed. The sample (with the mold) was weighed.

14. During SERF tests, it is useful to have an anchor to hold the sample to the piston. During high flow rates in the flume, the pressure differential caused by high velocities in the flume causes the sample to be "sucked" to the flume's top. For samples to be used in the SERF then, a 2.5 inch x 0.25 inch diameter bolt was inserted into the dry-mix. A 1.0 inch pilot hole was first manually drilled, the bolt was inserted, and the void was back-filled and tampered by hand.

15. Because RETA testing requires the presence of a 0.25 inch hole through the sample, for samples that were to be used for RETA testing, a 0.25 inch aluminum bar was coated with Prestress Release and driven through the samples. This step was added because drilling through a Gator Rock specimen with a drill press may cause the sample to crack. A similar technique to the technique used in (10) was used to insert these rods into the samples.

16. Samples were placed in buckets to allow for curing. The appropriate amount of distilled water was weighed and placed into each curing container. Each bucket was sealed to prevent evaporation during curing. Originally, plastic wrap and Duct Tape were used to seal the buckets, but later, buckets were replaced with Ziploc containers with air-tight lids.

17. Samples were allowed to cure for 28 days.

5.5 First Gator Rock Mix

5.5.1 Mix Compositions

During this project, two different versions of Gator Rock were created. The first version of Gator Rock was based on Niraula's 2004 original mixing procedure. According to Niraula, when he changed water-cement ratios, he fixed his water content at 20%, and he varied the cement content (Table 5-1).

Table 5-1. Niraula's Original Gator Rock Water-Cement Ratios

Batch Number	% Limestone	% Cement	% Water
I	75	5	20
II	72.5	7.5	20
III	70	10	20

Slagle did not indicate which water-cement ratios he used during his tests. Because Niraula was the only other available reference for Gator Rock, the same thing was done, and water content was fixed at 20%. To make samples weaker than Niraula's, cement content was reduced while Limestone content was increased (Table 5-2).

Table 5-2. Water, Cement, and Limestone Composition for First Round Bull Gator Rock Mix

Batch Number	% Limestone	% Cement	% Water
1	77	3	20
2	76	4	20
3	75	5	20
4	76	6	20
5	77	7	20

Before mixing, four random limestone aggregate samples were taken and sieved so that a grain size distribution could be produced. If random samples showed repeatability and regular uniformity, it was thought that there would be a better chance to insure that results from one sample could be compared with results from another sample. As shown (Figure 5-3) the four random grain size distributions were close to one another.

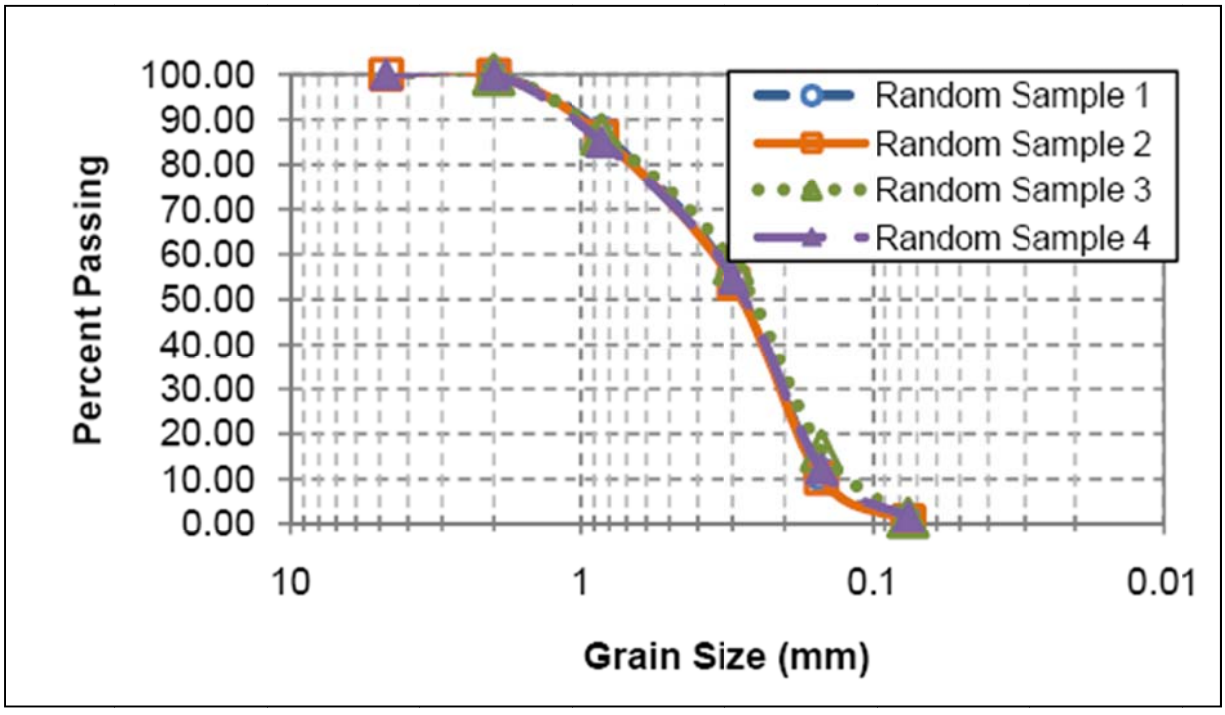

Figure 5-3. First Round of Bull Gator Rock Grain Size Distributions (Shah 2009)

5.5.2 Strength Tests

After curing had been completed, a random set of Bull Gator Rock samples were selected for tensile and compressive strength testing. Two samples from each batch were used in each test. Results from tensile and compressive strength tests were used to compute cohesion for each batch of Gator Rock according to the formula derived in Chapter 2:

$$C = \frac{1}{2}\sqrt{q_u q_t} \tag{5-4}$$

where q_u is the material's compressive strength and q_t is the material's tensile strength. Results from this round of tests are given in Figure 5-4:

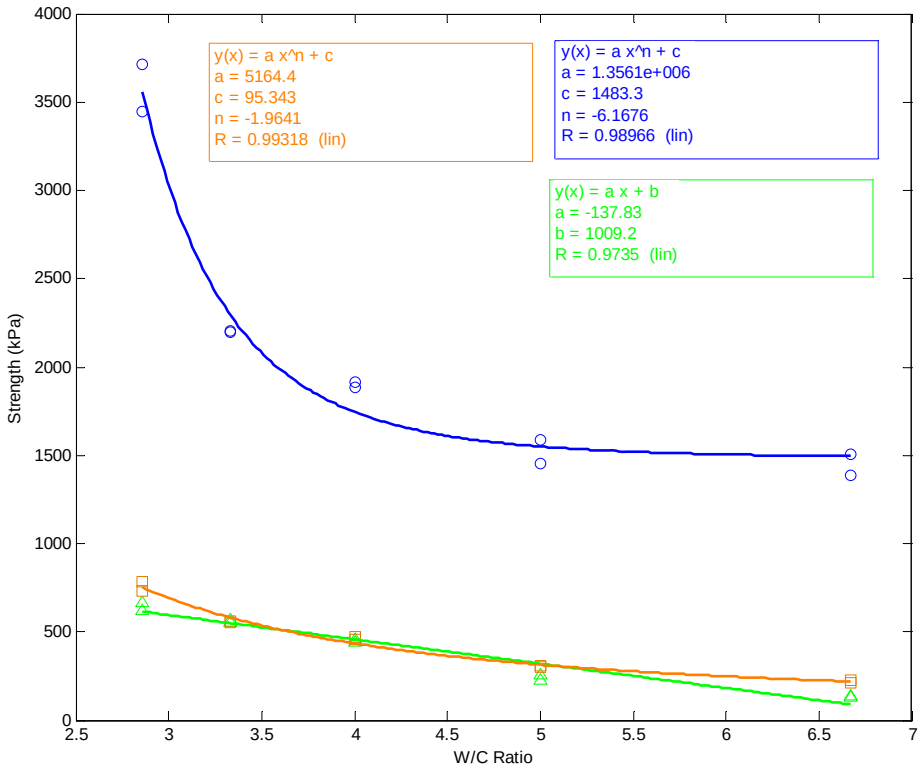

Figure 5-4. Strength Test Results from First Round of Bull Gator Rock Mixes. The orange line is cohesion; the green line is from compressive strength; the blue line is tensile strength.

As shown in Figure 5-3, repeatability from sample to sample of the same batch was excellent. Average percent difference between one sample and another of the same batch during tensile strength testing was 5.86%. Maximum difference from one sample to another during

tensile strength testing was 12.86% (Batch 2); the minimum difference was 2.00% (Batch 1). The standard deviation of percentage difference between samples of the same batch was 4.37%.

During compressive strength, the average percent difference between samples of the same batch was 5.25%. The maximum difference from one sample to another of the same batch during compressive testing was 9.09% (Batch 2); the minimum difference was 0.22% (Batch 4). The standard deviation of percent difference between samples of the same batch was 3.95%.

5.5.3 RETA Tests

RETA tests were conducted at the FDOT State Materials Office (SMO). Testing followed the standard RETA testing procedure. The only difference between RETA tests conducted during this study and typical RETA tests was that because the Gator Rock samples were artificially created and allowed to cure in molds, their side-walls were abnormally smooth. Therefore, before each test, the Gator Rock samples were slightly machined so that approximately 0.1 inches of material was removed from their smooth surface. This artificial procedure roughened the surfaces slightly. Overall, RETA tests produced mixed results.

5.5.3.1 First Round of Tests on First Batch of Gator Rock in RETA

The first round of samples that were tested produced encouraging results. Dan Pitocchi (2010), the SMO's lab technician who oversees FDOT RETA tests, indicated that these Bull Gator Rock samples were the best Gator Rock samples that he had ever worked with because from top to bottom, they appeared to erode uniformly. Unlike Slagle's samples (Figure 5-3) there were not obvious weaker sections on either the tops or the bottoms of the samples (Figure 5-5, Figure 5-6, and Figure 5-7).

Figure 5-5. Batch 1 Bull Gator Rock after RETA 24-hr. RETA Test (Shah 2009)

Figure 5-6. Batch 2 Bull Gator Rock after RETA 24-hr. Test (Shah 2009)

Figure 5-7. Batch 3 Bull Gator Rock after RETA 24-hr. Test (Shah 2009)

During the first round of testing, quantitative results showed what was expected in terms of an erosion rate-shear stress relationship. Generally, as shear stress increased, erosion rate increased (Figure 5-8, Figure 5-9, and Figure 5-10).

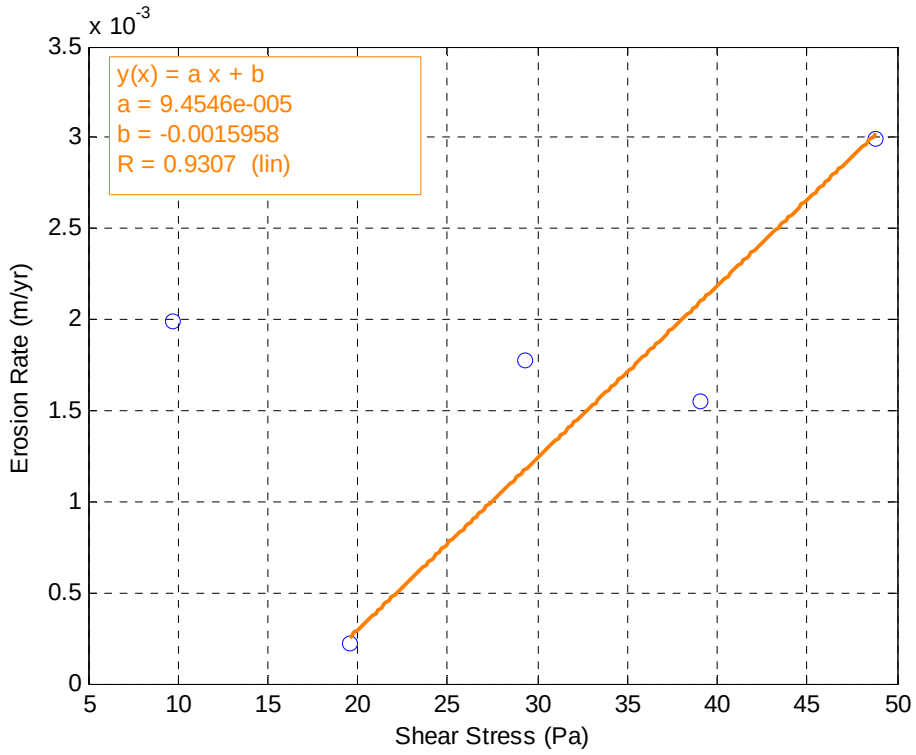

Figure 5-8. RETA Results From Batch 3, Round 1

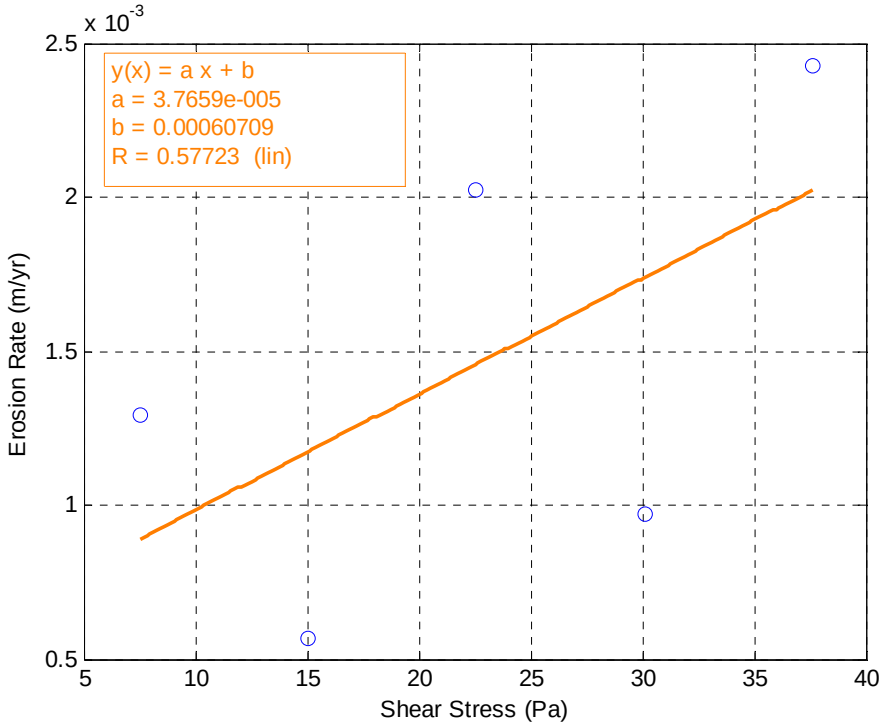

Figure 5-9. RETA Results from Batch 4, Round 1

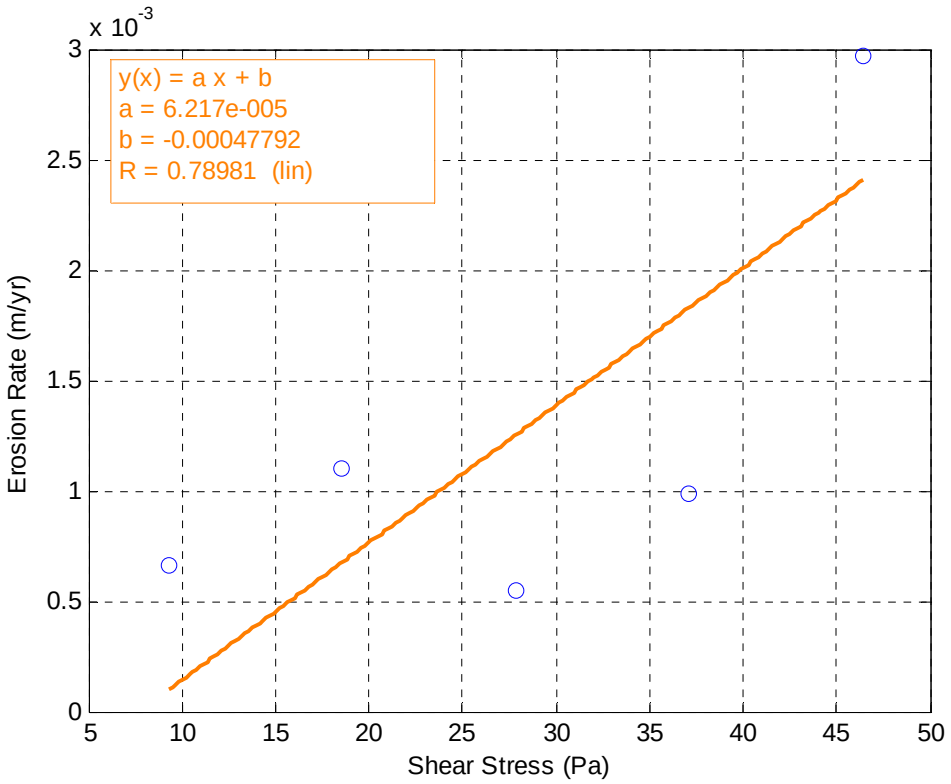

Figure 5-10. RETA Results from Batch 5, Round 1

As shown in these figures, a best-fit line was fit to each dataset using linear regression. As shown in Figure 5-8, the 10 Pa data point is higher than most other data points. Often, when a RETA test begins, RETA operators run the lowest shear stress first and increase the stress every specified time period (24-hours for these tests). Recall that as part of preconditioning, these samples were slightly machined. The standard RETA testing procedure calls for a quick wash of the material before data is taken. During the wash a high shear stress is used to remove any loose particle or debris from the sample. Then, RETA's annulus is emptied, cleaned, and the data run begins.

This washing technique does remove some loose particles from the sample. However, if erosion is rock-like, which for Gator Rock it may be, then this washing technique also serves to loosen or weaken some grains within the sample matrix. During the sample's first prolonged exposure to stresses – normal or shear – these loosened pieces of material will also break off over time. Therefore, during a 24-hour test, one should expect that some of the looser, exterior particles that comprise the sample will fall from it. In other words, although the wash removes

some loose pieces of the material, it loosens some others weaker particle bonds, and over the course of 24-hours of cyclical loading, it is likely that these relatively loose materials also fall from the sample's surface.

This is important because it explains why the first data point in Batch 3 is so high. During the first portion of the erosion test, most relatively loose material is removed from the face of the Gator Rock. Because the RETA does not continually measure erosion as a function of time, it is impossible to say how to define the "first portion" of the test, but the argument is that after a certain amount of cyclical loading on the surface of the rock face, most of the relatively loose material will eventually fall from it. What is left then is a more uniform material in terms of the particle-pack density. Because of this rationale, when fitting a line to the Batch 3 data, the first point was ignored.

Another encouraging thing regarding this first round of RETA tests is that they showed some qualitative relationship between material strength and erosion rate. Intuitively it appears that stronger materials should erode more slowly. HEC-18 makes this generalization, but does not give any quantitative method for correlating material strength to erosion properties. The reason that Batch 1 and Batch 2 data are not shown in this dataset is that Batch 1 and Batch 2 both failed before the end of the test. The Batch 1 sample failed at a 10 Pa shear stress while the Batch 2 sample failed at a 20 Pa shear stress. Batch 3, Batch 4, and Batch 5 stood up to the entire gambit of tests. If erosion rate was a function of material strength, as material strength increases, $dE/d\tau$ should decrease. While generally this is the case, this is probably not enough to draw any conclusive correlations.

Even with this disclaimer, limited analysis was conducted to try to draw a correlation between cohesion and erosion rate for these Gator Rock sample (Figure 5-11). Interestingly, this figure shows that there may be some correlation between these two parameters, and most interestingly, erosion rate appears to level off near zero above a cohesion value of 500 kPa. Because this graph shows cohesion vs. erosion rate, it was possible to use the Batch 1 and Batch 2 failed samples in its computation.

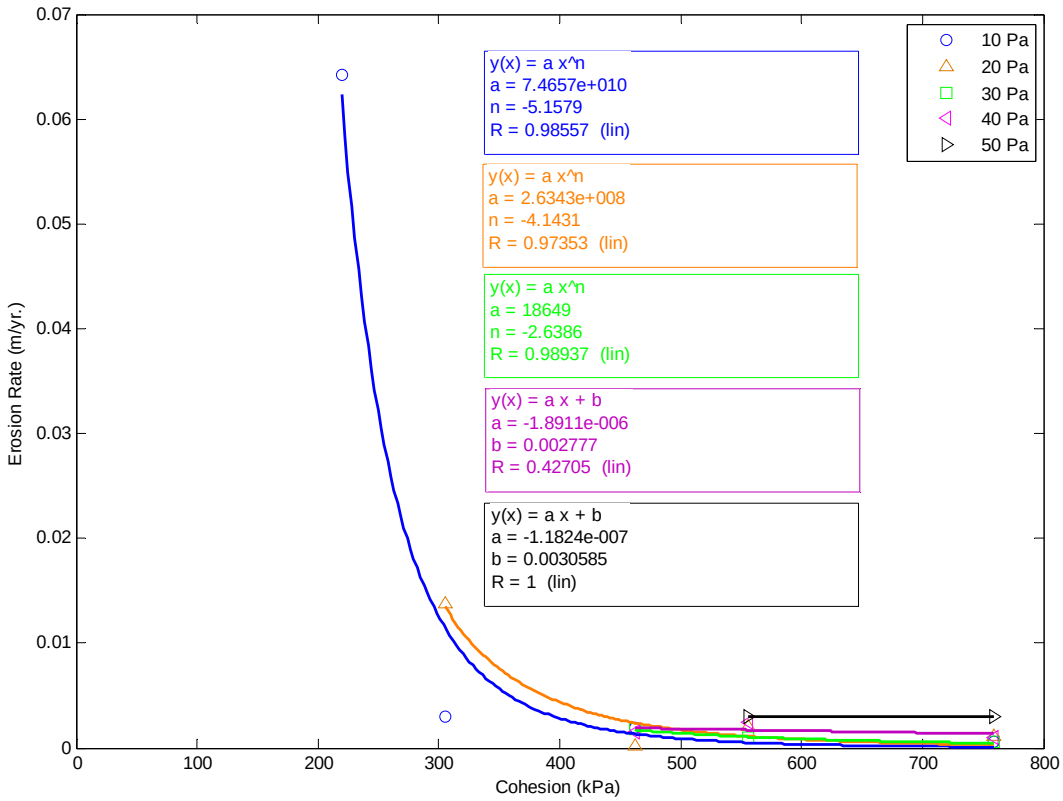

Figure 5-11. Cohesion vs. Erosion Relationship for First Round of Gator Rock Samples

5.5.3.2 Second Round of Tests on First Batch of Gator Rock in RETA

After the initial promising tests with Bull Gator Rock, a second series of tests was conducted on different samples from the same corresponding Bull Gator Rock batches. The goal of this series of tests was to produce some repeatability between the first dataset and a new dataset. If erosion results from both sets of data were similar, one could conclude that from a sample-to-sample perspective, the Bull Gator Rock was behaving as designed. If this second round of tests was able to produce the expected results, it would mean that Bull Gator Rock responded predictably to erosion and that because of this it could be used as a basis of comparison with the SERF. Unfortunately, during the second round of tests, samples behaved much differently than they behaved during the first data run. Results from the second round of Bull Gator Rock tests are presented from Figure 5-12 through Figure 5-16:

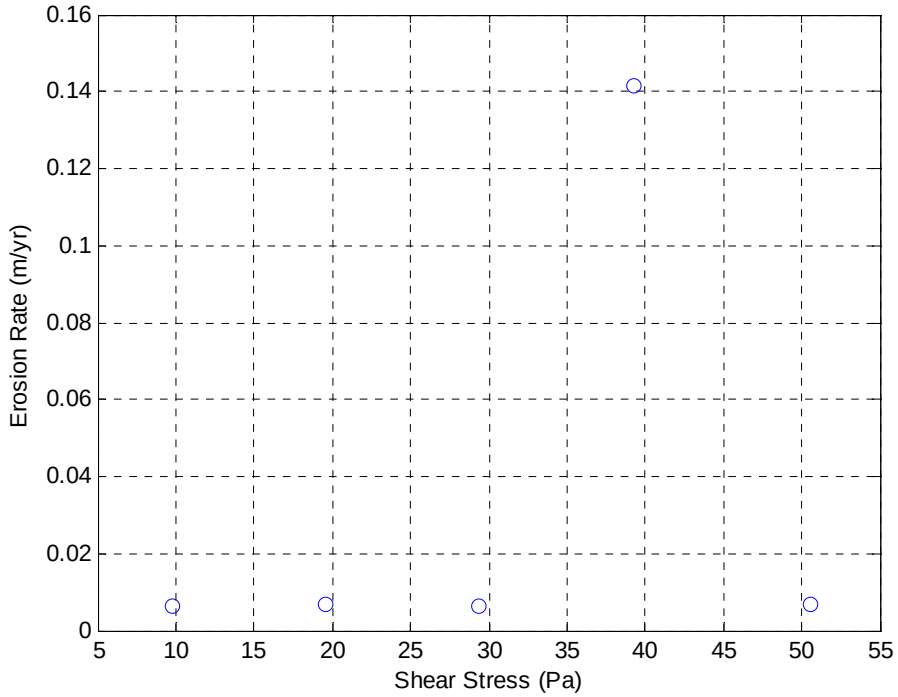

Figure 5-12. RETA Results from Batch 1, Round 2

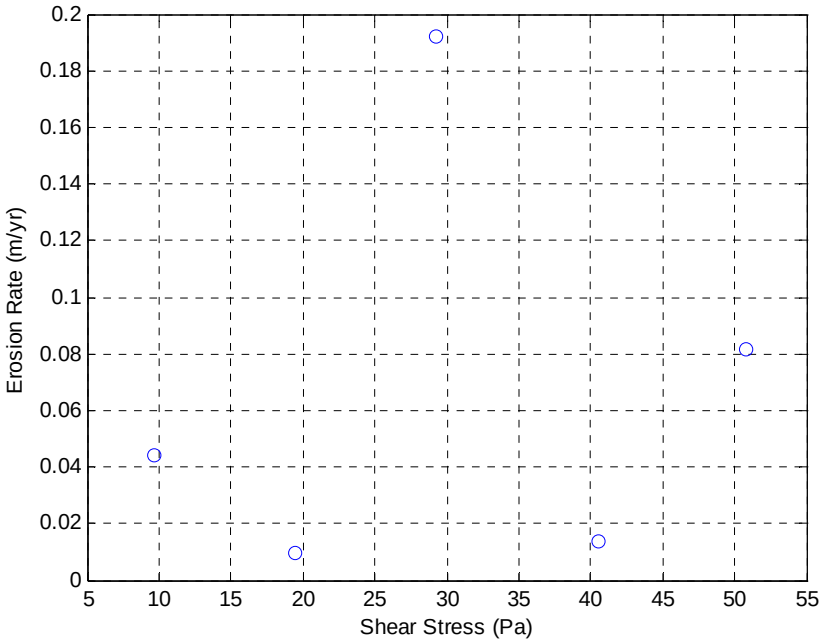

Figure 5-13. RETA Results from Batch 2, Round 2

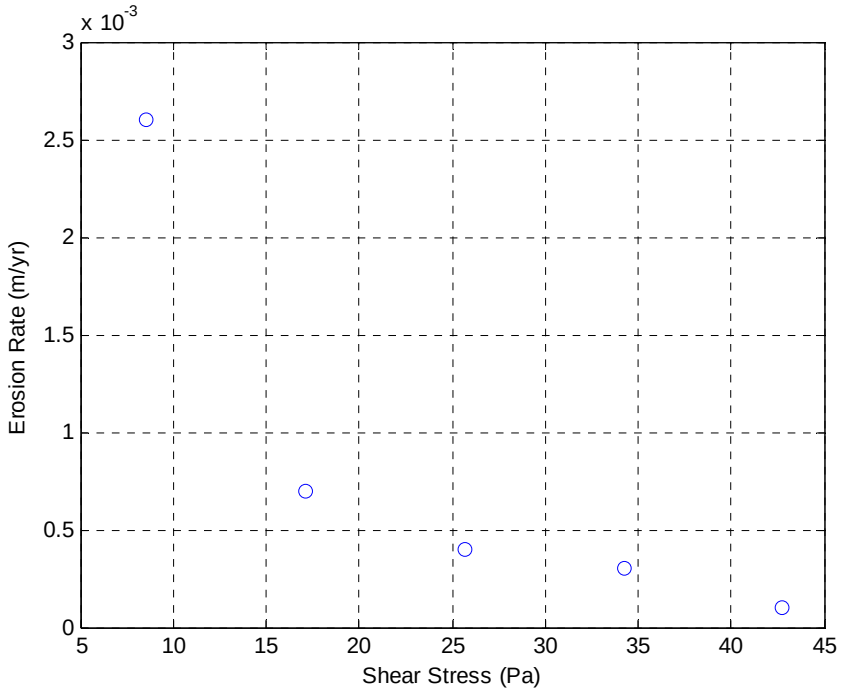

Figure 5-14. RETA Results from Batch 3, Round 2

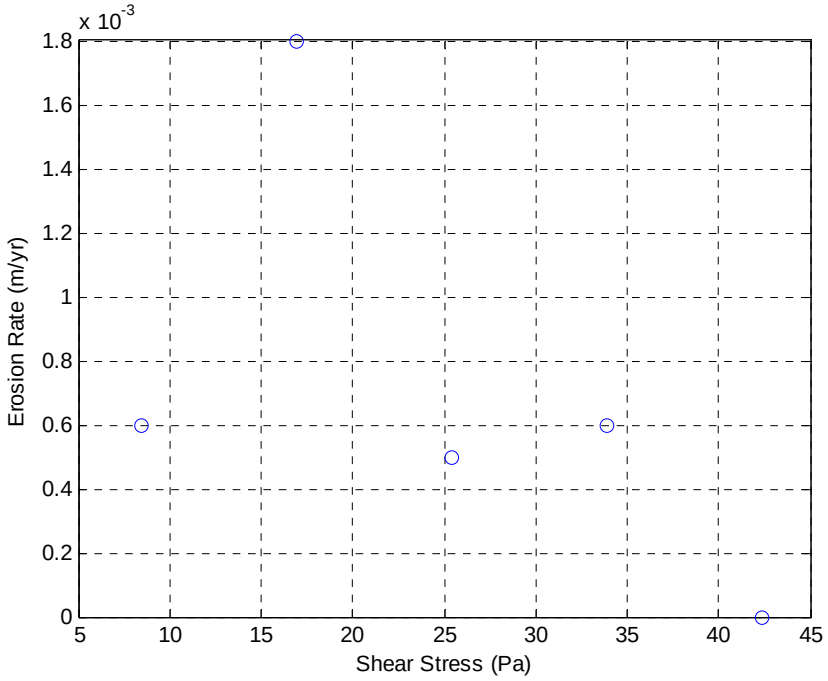

Figure 5-15. RETA Results from Batch 4, Round 2

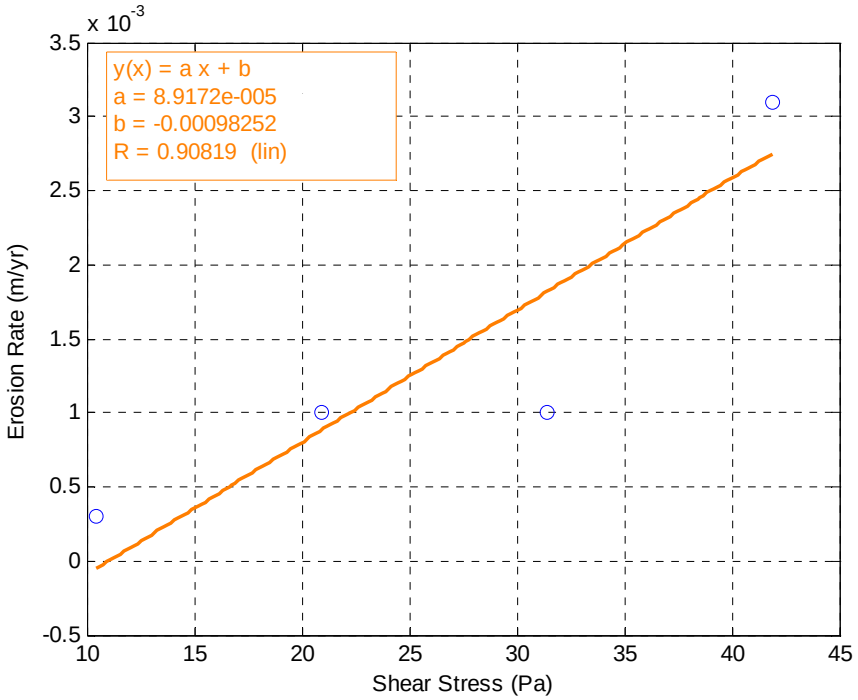

Figure 5-16. RETA Results from Batch 5, Round 2

As seen in these five graphs, results from the second round of tests differ from the first round of tests in that while during the first round, the sample from Batch 1 and the sample from Batch 2 failed at increasingly higher shear stresses, none of the samples from the second round of tests failed. While during the first round of tests, samples that made it through every test exhibited a pattern where increasing shear stress meant increasing erosion rate, during the second round of tests, only samples from Batch 1 and Batch 5 resembled this trend. Even these results needed to be modified to produce the expected erosion rate-shear stress results. During Batch 5 data analysis, the final 50 Pa erosion point was eliminated because it showed zero erosion rate; during Batch 1 data analysis, the ~40 Pa data point was eliminated for the sake of fitting a best-fit line to the data (although this data point is still shown in Figure 5-16).

The question became why the disparaging results between the data sets? To explain this phenomenon, multiple discussions between Crowley of UF and Pitocchi of FDOT were conducted. Pitocchi's exact words when describing the second data run was, "…we had problems…" (Pitocchi 2010). Pitocchi described how during tests several RETA control boxes broken. On one occasion a RETA was accidentally turned off. On a few others, the bottom plate

that holds the sample to the RETA annulus kept coming loose, etc. Essentially, he claimed that the entire dataset was not very good and should be repeated with new samples.

Pitocchi blamed the failure of the second run of Gator Rock samples on two factors:

1. Bull Gator Rock was still too resistant to erosion to give accurate RETA results.
2. Bull Gator Rock samples were slightly the incorrect diameter.

First, the latter point will be addressed. As noted in Section 5.4, when the first round of Bull Gator Rock samples was produced, it was designed using the SERF's sediment diameter. Because originally the goal was to make SERF and RETA samples that were as similar as possible, the smaller 2.30 inch diameter was chosen. Any deviation from a precise 2.40 inch diameter sample will force the RETA's motor to run harder than it normally would to produce a specified shear stress. At aggressive shear stresses – such as 40 Pa or 50 Pa – the motor was forced to work hard, and this led to some of the mechanical issues seen during the second round of tests. To address this problem, Pitocchi recommended creating a new Gator Rock batch with a slightly larger diameter.

The former point – the Gator Rock's resistance to erosion – also concerned Pitocchi. Pitocchi indicated that even if the diameter was modified, based on his experience he still doubted whether or not Bull Gator Rock could be expected to yield reproducible experimental results. Pitocchi said that Gator Rock, like most rock-like material exhibited a moderate to high degree of "blocking." In this paper, "blocking" is synonymous with previous words such as "chunking" or "pitting" in that it is a rudimentary description of rock-like erosion. Materials that exhibit even a moderate degree of rock-like erosion properties may not produce a regularly expected erosion rate vs. shear stress curve, especially when a relatively small amount of particle-like erosion is present. When erosion is small, the blocking mechanism becomes dominant, and it does not appear to occur at regularly expected shear stress intervals. Rather, it is the function of another property – perhaps normal stress – and therefore cannot be quantified using a RETA.

During both rounds of Gator Rock tests, a relatively small amount of material eroded from the Gator Rock surface. The most significant erosion rate was seen during Batch 2, Run 2, where 18 g of material were removed from the sample. This extreme erosion rate can be attributed to blocking for several reasons. First, this erosion rate is abnormally high when compared with erosion rates of similar materials at similar shear stresses. Secondly, this erosion

rate was produced during testing of a weak batch – Batch 2. At times, Batch 1 and Batch 2 exhibited characteristics like a compacted sand. For example, during SERF testing (to be discussed in Section 5.5.4) it was often impossible to secure the samples to the piston because as the samples' screws were driven into the plastic piston, the screws often broke loose while chunks of loose sand fell from the rock core. In other words, there was little "glue" or Portland cement physically holding the samples together – as evidenced in Table 5-2. As a result, when the screw offered any resistance, it would break free and spin within the sample. A similar lack of glue mechanism is probably to blame for the Bach 2, Round 2 data point.

If the Batch 2, Round 2 data point is taken as a sort of loose sand outlier, the next most significant erosion rate is found during the tail-end of Batch 5 testing during both rounds of tests where approximately 3 mm/yr. of erosion was seen. Extrapolating this back to a 24 hour test implies that during the test, only .008 mm of material was removed from the Gator Rock surface. Or, in terms of density, this means that only approximately 0.1 g of material eroded during the entire test. This is an incredibly small amount of material to accurately measure. Erosion quantities this small can easily be muddled due to simple effects such as not properly cleaning the RETA annulus. Further, this amount of material is extremely small when compared with the any block-material erosion that could occur. For example, if during an erosion test, 0.05 g of material "block" were to break due to pulsing action on the sample face (in a manner similar to Bollaert's 2003 mechanism), it would only take two of these "block failures" to equal the total amount of erosion resulting from the 3 mm/yr. presumed shear stress failure. And, making matters even more confusing, with a RETA test it is impossible to differentiate between the two modes of erosion failure because erosion rates so small and erosion as not measured continuously. If higher erosion rates could be produced with the Gator Rock, it was thought that it could be possible to isolate the particle-like erosion from the block-like mechanism. Rather than relying on pulsating impulse action, a steady tugging mechanism should force more, weaker, looser material to erode from the Gator Rock surface. This would allow for a better basis of comparison between the RETA and the SERF. Before this new Gator Rock mix is discussed however, testing on Round 1 Gator Rock should be analyzed.

5.5.4 SERF Tests

SERF tests were conducted concurrently with RETA tests. Results confirmed that a new Gator Rock mix was required.

5.5.4.1 Shear Stress Tests

The first question during Gator Rock SERF testing was how to accurately estimate the shear stress on the Gator Rock's surface at a given flow rate. Based on the Chapter 4 discussion, shear stress is dependent on roughness, and shear stress cannot be accurately estimated using a flat-walled assumption. An assumption was made where regardless of water/cement ratio, each Gator Rock batch was assumed to have approximately the same roughness. Intuitively, this is logical because for a given Gator Rock sample, the only thing that changes is the ratio between the limestone and the Portland cement. The determining factor in finding a sample's roughness should be dominated by the crushed limestone's grain size distribution, not the cement content.

Procedures for running a shear stress test are discussed in detail in the operations manual, but a brief synopsis will be given here. To produce a test-disc for use in the shear sensor, leftover Gator Rock aggregate was spread out on a counter. Four test-discs were coated with epoxy and pressed against the Gator Rock aggregate surface. The epoxied discs were allowed to dry overnight. The result was that four test discs were created such that random samples of the non-uniform Gator Rock aggregate were stuck to the discs' surfaces. These test-discs were subjected to three rounds of shear stress testing each. If the discs were a true random sampling of Gator Rock roughness conditions, shear stress values at the same flow rate should be close to one another from both an intra-disc and inter-disc perspective. Results from this round of tests are presented in Figure 5-17.

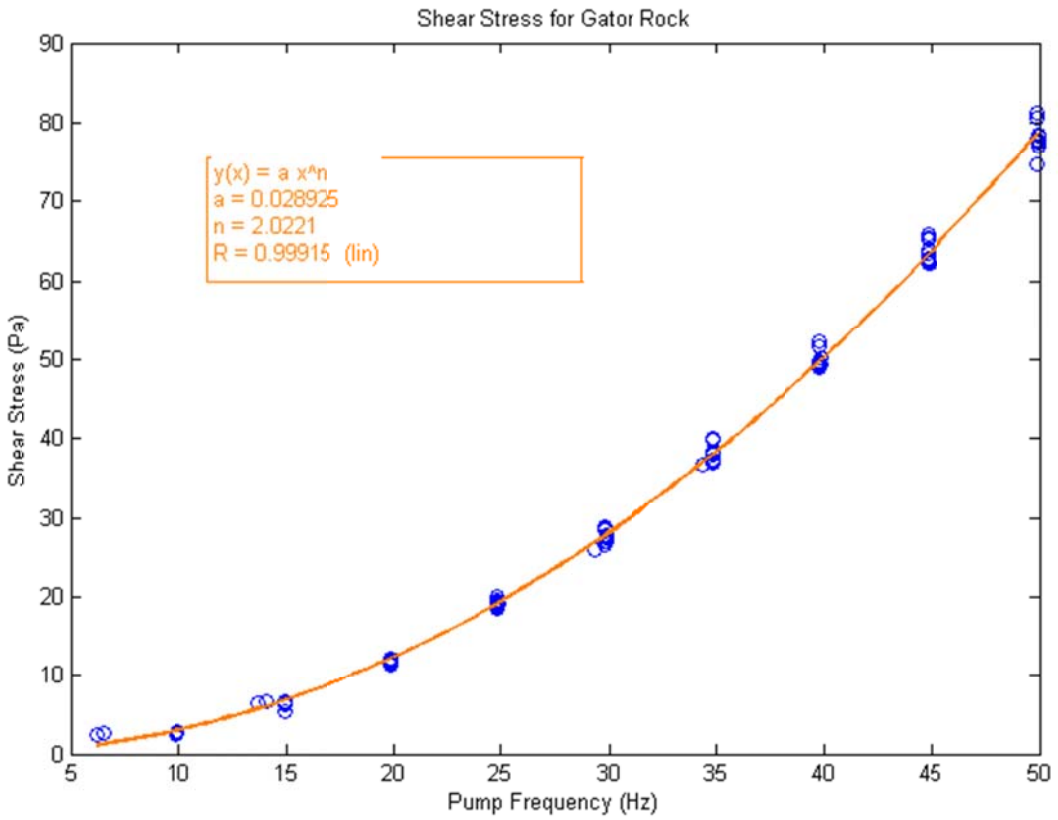

Figure 5-17. Gator Rock Test Disc Results

Figure 5-17 shows data points combined with one another; data time-series were similar to results shown in Chapter 4. Because of the tight-pack between data points, it appeared as though the true roughness of the Gator Rock surface had been captured. This shear stress vs. pump frequency curve was then used to define shear stress at varying flow rates in the SERF. For example, from Figure 5.5.14, a pump frequency of approximately 20 Hz corresponds to a Gator Rock shear stress of approximately 19 Pa. Values from this curve were used to match shear stress values – approximately 10 Pa, 20 Pa, 30 Pa, 40 Pa, and 50 Pa – that were used during RETA testing because the goal was to reproduce RETA data points as closely as possible using the SERF.

5.5.4.2 Erosion Tests

During SERF erosion tests, two experimental procedures were used. At first, the SEATEK ultrasonic ranging system was used in conjunction with the laser-leveling system as a redundant mechanism. The programs were manipulated such that for a sample to advance, two of the three

lasers needed to be uncovered and the SEATEK needed to determine that the sample was no longer level with the flume bottom.

SERF testing began with the mid-point sample, or Batch 3. During the Batch 3 test, no erosion was shown. While the SEATEK, which is more prone to errors than the lasers, would sometimes try to initiate the motor motion sequence, the lasers would block this from happening. After five days without sample advancement, the Batch 3 sample was removed from the device and replaced with a Batch 2 sample. Batch 2 also showed no sample advancement after five days, and eventually it was replaced with a Batch 1 sample. The Batch 1 sample also showed no advancement. In other words, the SERF was indicating that the sample was not eroding.

Visual observation of the samples, particularly the Batch 1 specimen, showed that a "no erosion" result must be incorrect. The Batch 1 sample visually showed some erosion along its front face and some pit-like localized erosion zones along its top surface. While the top of the sample hadn't eroded uniformly enough to warrant sample advancement, as per the stringent programming restrictions utilized in the SERF control programs, some material had been removed from it. The problem with the laser design is that it assumes the entire surface, from photoelectric sensor to light source, will erode. If edges erode faster than a sample's mid-section, the sample cannot advance until the midsection also erodes. Even a small block or chunk of material blocking the laser's light will preclude advancement. Small chunks blocking the laser's light were not observed often; rather, advancement was usually prevented because on average there was not enough erosion to warrant a full step's worth (a step equaling 1.0 mm) of advancement. Still, to say no erosion occurred would be incorrect.

Two options existed for finding a better method to measure erosion. The first option was to use a method similar to the RETA. Before and after testing, the sample could be weighed, and the weight difference should equal the erosion rate. There were issues with this method however. Similar to problems in the RETA, using this weight method would not give a top-to-bottom erosion time-series.

The second issue with weighing the sample is that because of the nature of the SERF testing, it is unclear and unlikely whether or not the correct results could be obtained. Two possibilities are present. One is that the sample fits snugly into the test cylinder. When the sample fits snugly, advancement often causes some erosion along the sample's edge due to friction between the sample and the test cylinder's side walls. Although normally during higher

erosion rates this erosion quantity is small when compared with the erosion of the sample's top-face, with Gator Rock, top-face erosion quantities are extremely small. The relative magnitude of side-wall sample-advancement friction is nearly the same or greater than friction due to fluid flow. Any weight measurement would take both erosion sources into account and not be an accurate representative of actual erosion conditions.

Even if sample advancement was precluded completely, as it was when the lasers were used, insertion of the sample into the test-cylinder produces some friction. Then, once the sample is placed in the cylinder, the piston must be attached to the SERVO motor, and the SERVO motor must be stepped forward so that the sample can be level with the flume's bottom. This causes friction, and the fear was that this frictional component to material lost during a SERF test would be on the same order of magnitude as actual fluid-flow erosion.

The second possibility is that a gap can be engineered between the sample and the test cylinder. This carries with it three underlying issues as well. First, if the gap between the sample and the sample cylinder is large enough, the sample itself will oscillate or rock back and forth as water passes over it. This cyclical knocking or rocking action will serve as another source of unnatural material loss, which again will be as high as or greater than the erosion rate due to fluid flow. The second issue with creating a gap between the sample and the test cylinder is that when small particles erode as part of the sample's bed load, they would fall into the gap. When the sample was weighed after the test, the total mass of the sample plus piston plus cylinder would be the same, yet particles would be removed from the sample's surface. Unlike the RETA, extracting a SERF sample is not easy, and doing so will cause friction which will result in material loss – so this is not an option either. Third, a gap will modify any fully developed flow pattern in the flume, which will also affect erosion rate. The SERF is designed to produce a fully developed velocity profile. Deviation from this velocity profile, especially at the sample interface, will change fluid conditions which will in turn produce non-natural erosion results.

The other solution was to take advantage of the fact that the SEATEK produces more errors than the lasers. The lasers were turned off and a test was run with just the SEATEK for 24 hours. On average the SEATEK readings were accurate. As typical with ultrasonic sensors such as the SEATEK, every ten readings or so, a value is returned that forces motor advancement/retraction, especially when there is little erosion. When this happens, the motor

slightly advances/retracts. This repeats itself several times during a test. Over the course of a 24-hour test, if one looks at a time series of motor position, an oscillating graph will be generated (Figure 5-18 and Figure 5-19).

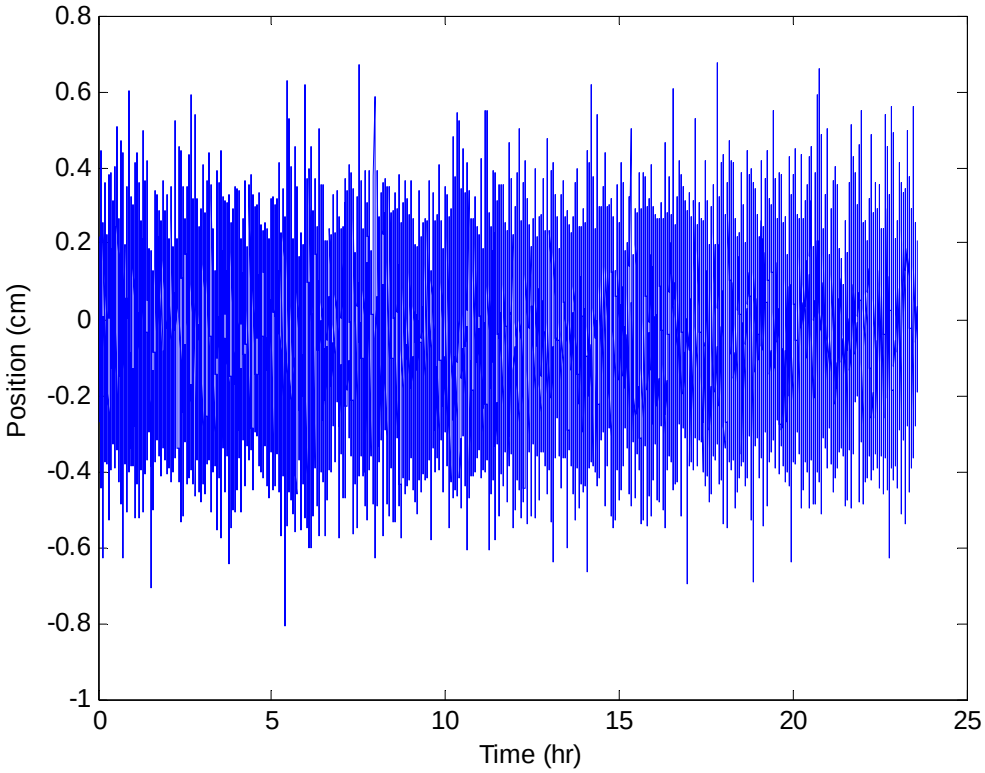

Figure 5-18. Time Series of Piston Position During Stand Alone SEATEK Test (Data from Batch 1 test at 50 Pa).

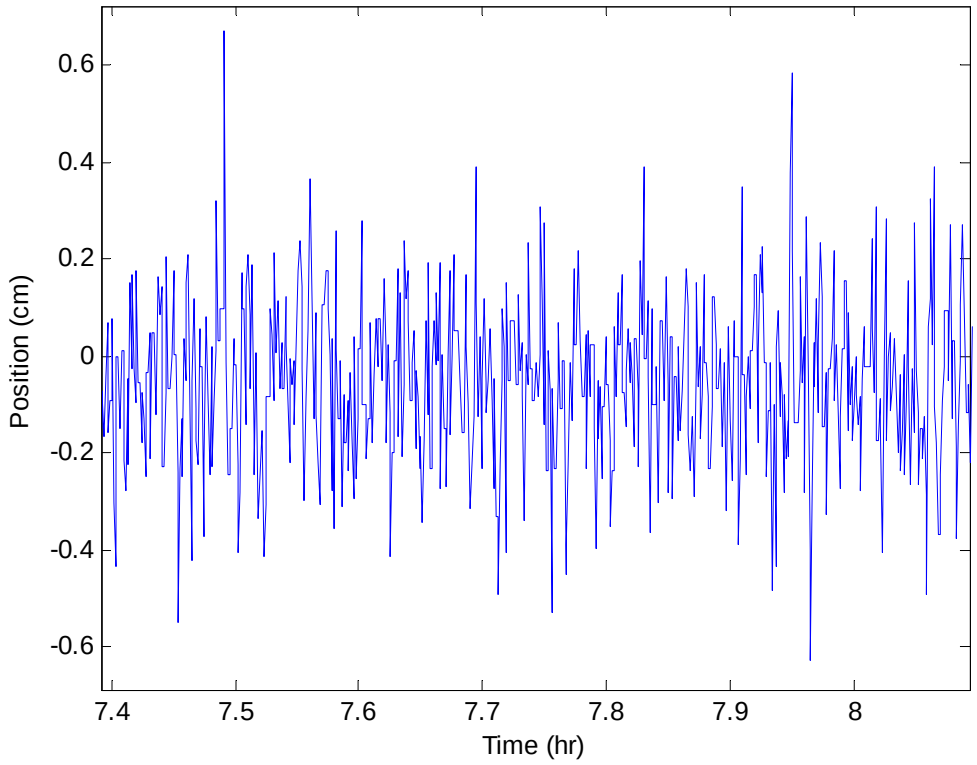

Figure 5-19. Zoomed-in Position vs. Time Graph from Batch 1, 50 Pa Data

One of the advantages to the SERF compared to the RETA is that the SERF measures erosion in real-time. Although one way to measure erosion rate is to take the difference between start position and end position, this method does not give real time erosion as a function of sample position. Using this method will give no information on a situation where the top of a sample erodes faster than the bottom or vice-versa. In the past, the final minus the initial position method was used exclusively by Trammel and Slagle during SERF analysis. Expressed mathematically, Trammel and Slagle's method for finding erosion rate was:

$$E = \frac{\Delta y}{\Delta t} \tag{5-5}$$

where Δy is the total sample position change and Δt is the total length of the SERF test. The method for computing erosion rate is crude; a better method is easily available. Instead of finding the average erosion rate using Equation 5-5, a better method for finding erosion rate is to take the differential limit and compute erosion rate as:

$$E = \frac{dy}{dt} \tag{5-6}$$

In other words, sample position and time should be plotted against one another. If a best-fit curve is plotted through the data set, then instantaneous erosion rate must (and average erosion rate if the curve is linear) be equal to the slope of this line. If the best-fit function through these data points is not linear, then it must mean that the sample is non-uniform from top-to-bottom because a portion of the sample must have eroded more quickly (or more slowly) than another portion. With Gator Rock, using this method can provide an erosion rate for even small values of material loss – even values smaller than those that would normally warrant a step. On average, the positive errors should cancel out with the negative errors. The overall slope of the best-fit line through the data points then should on average be representative of the sample slowly working its way upward throughout the test.

As implied in Figure 5-19, tests were repeated so that the SEATEK stand-alone method could be tried, and best-fit lines were produced using least-squares regression. Sometimes, the sample slowly worked its way down during a test. Under these conditions, the implication is that negative erosion occurred, which is not possible. Whenever this happened, erosion rate was defined as a 'no erosion' condition. Tests using the SEATEK stand-along method were conducted on two samples from Batch 1, one sample from Batch 2, and one sample from Batch 3 at 10 Pa, 20 Pa, 30 Pa, 40 Pa, and 50 Pa, and when possible, best-fit lines were computed through the data points. Figure 5-20 is shown as a typical sample position vs. time signal with the best-fit line while erosion rate vs. shear stress results are shown from Figure 5-21 through Figure 5-23.

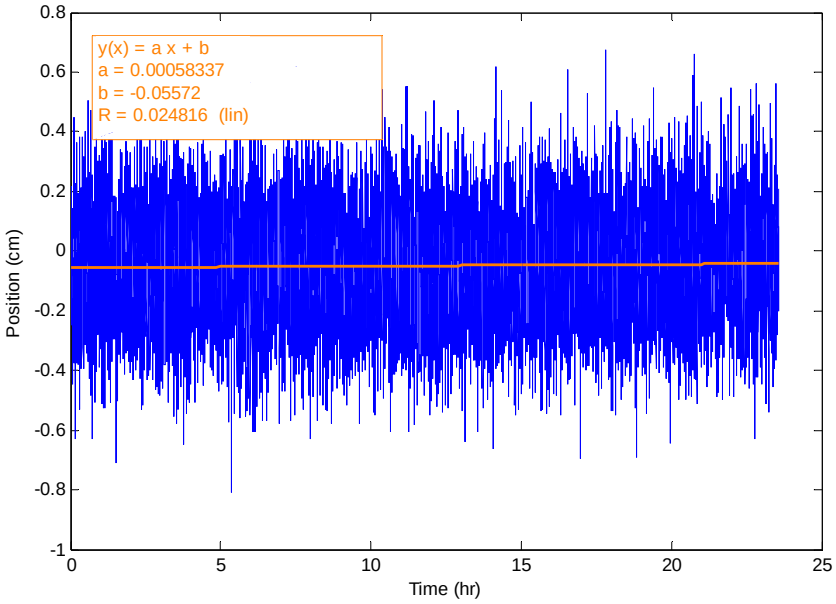

Figure 5-20. Batch 1 Sample Position vs. Time from SERF with Best-Fit Regression Line

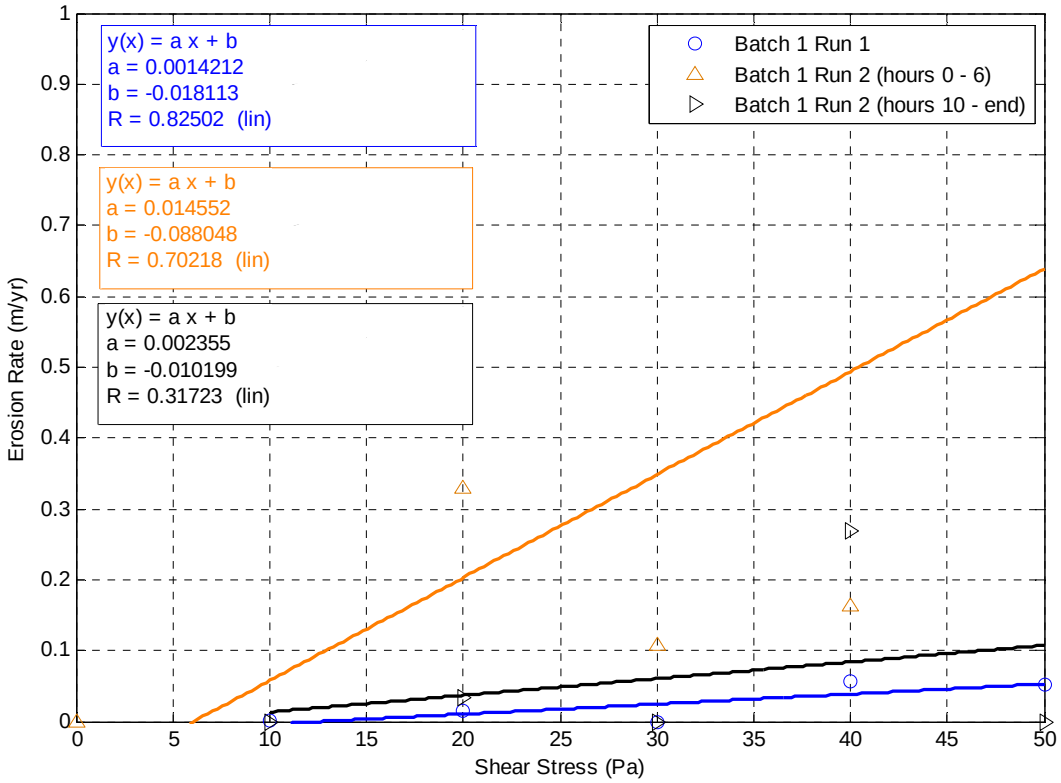

Figure 5-21. Erosion Rate vs. Shear Stress for Batch 1 in SERF Using First Round Mix

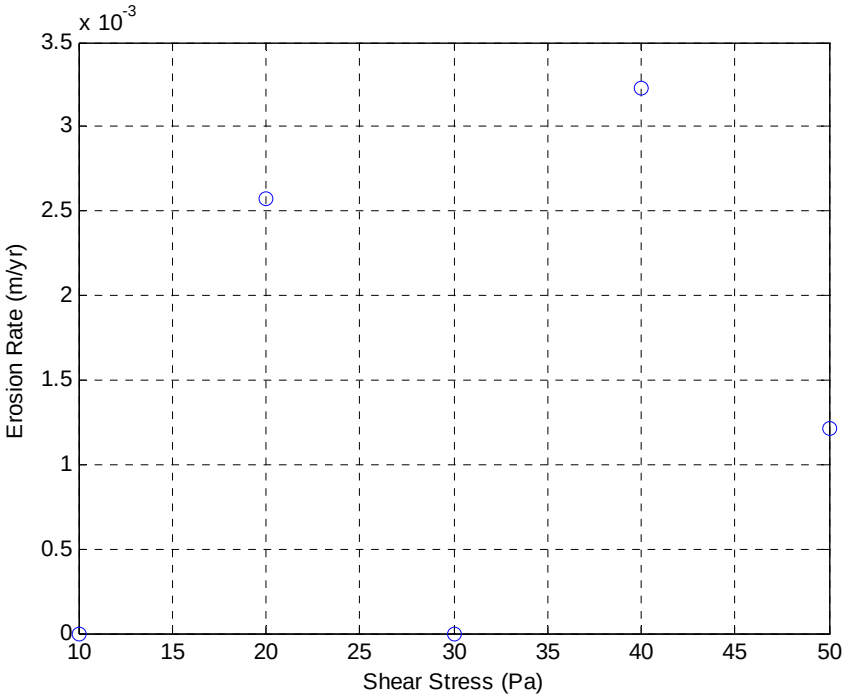

Figure 5-22. Erosion Rate vs. Shear Stress for Batch 2 from SERF

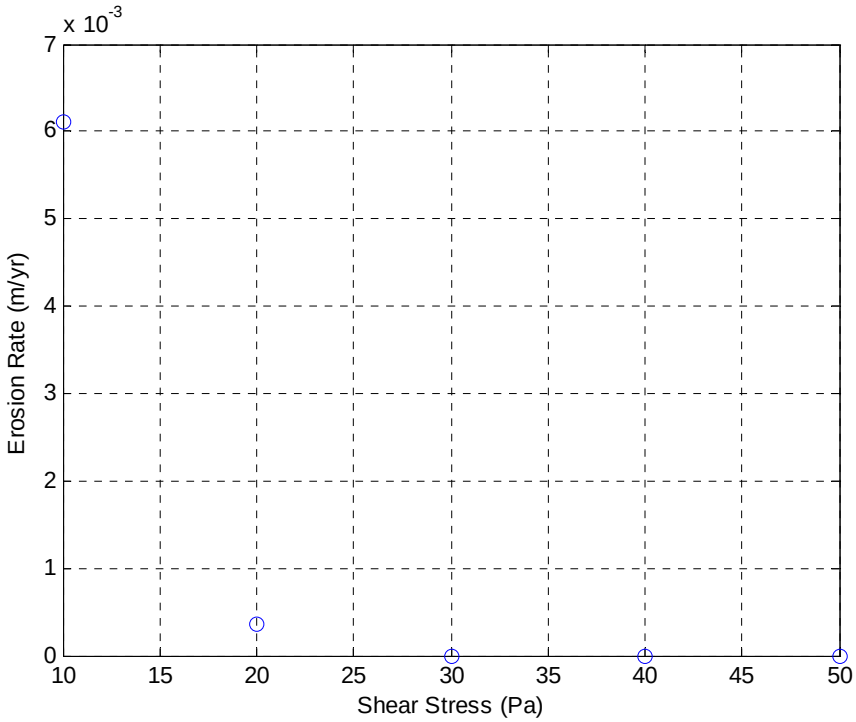

Figure 5-23. Erosion Rate vs. Shear Stress for Batch 3 from SERF

Since generally Batch 3 showed no erosion and Batch 4 and Batch 5 were shown to be stronger from the tensile and compressive strength tests, SERF tests were stopped after the Batch 3 data set was taken.

5.5.4.3 SERF Analysis

As shown, Batch 2 and Batch 3 produced poor SERF results. In these tests, an increase in shear stress did not show a corresponding increase in erosion rate. This poor performance is attributed to the same mechanism discussed already with the RETA tests – rock-like erosion. Visual observation of tests showed that generally it was common for small chunks of particulate to be removed from the material's surface. It was rare to find an instance where small particles eroded because a material's true critical shear stress had been achieved and incipient motion caused movement of several particles within the material matrix.

The Batch 1 results were similar in that rock-like erosion was present during testing, but the interesting thing concerning Batch 1 is the shear stress vs. time implication. During the first Batch 1 data run, erosion rate appeared to be relatively uniform throughout the course of the test at a given shear stress. During the second data run however, this was not the case. Figure 5-21 was generated by analyzing the Batch 1 data set in parts. During the first part of each Batch 1, Run 2 shear stress (generally approximately the first six hours), erosion rates were relatively high. As the Batch 1 sample eroded, erosion rate level off and becomes much closer to the erosion rate seen during the first data run.

This mechanism can be attributed to rock-like erosion. If one zooms in on a Gator Rock sample surface, there are localized sections that are bonded together more securely than others. In other words, there are certain particles within the Gator Rock matrix that are more likely to come off than others. A quick qualitative test that can be done to illustrate this is to scratch the Gator Rock's surface with a fingernail a few times. Scratching will show that certain particles are removed easily from the surface while other particles or chunks are more difficult to remove.

Under an erosion rate test, water is used to erode the material instead of a fingernail. Still, the erosion mechanism will be similar; sometimes it will be easy to remove chunks of material while other times chunks will remain for a given erosive effort. This effect must mean that some of the particles within the Gator Rock matrix are more securely bonded together than other particles. Under a rock-like erosion mechanism, cyclical impulse forcing along the material's

surface will weaken and eventually break the bonds holding the particles together. This cyclical forcing mechanism must act such that the looser bonds are broken first, and they are broken more quickly than the relatively strong localized particle bonds. For a given flow rate, and consequently a given normal force, these weaker particles will be vibrated out of position early on in the erosion test. The strong particles will remain because the normal forcing is not strong enough to break these relatively strong bonds. In other words, under a rock-like erosion event, the Gator Rock results from Batch 1 imply that whatever can erode for a given flow condition will erode relatively quickly. After this erosion has occurred, nothing else will happen at that specified flow rate. This result was thoroughly unexpected, and it deviates from particle-like erosion theory. Under particle-like erosion, a critical shear stress induces incipient motion, and then over time, erosion occurs as a function of shear stress vs. critical shear stress deficit. Batch 1 results defy this theory and show that another mechanism must be present, and interestingly this mechanism is not seen during the first data run indicating different behavior for two different samples.

5.6 Second Gator Rock Mix

If rock-like erosion is indeed present with Gator Rock, attempts of verifying the RETA by using a direct comparison with the SERF may not be possible. Based on this reasoning, and the rationale presented in Section 5.5.3, it was logical to try to design a material that would respond in a more particle-erosion-friendly manner.

To induce particle-like erosion, the goal must be to uniformly weaken the bonds holding the Gator Rock matrix together. Portland cement, or the glue that is used for Gator Rock, derives its strength from the amount of water used during mixing. Simply put, more water means less bond strength; less water means more bond strength. Meanwhile, the glue holding the Gator Rock together must be more homogeneous so to reduce the number of chunks that come from the material. Preparation of the first round of Gator Rock mix was performed using low cement ratios – so much so that as described, Batch 1 at times behaved more like compacted sand than a coherent rock matrix (this may explain the different behaviors seen during SERF tests). The theory behind the second Round of Bull Gator Rock mix was to use additional, weaker glue to hold the material together and see if that would help to induce particle-like erosion in the two instruments.

Using the same mixing procedures described in Section 5.3.4, a second round of samples was designed and prepared (Table 5-3). During this mixing procedure, the cement content was held steady at 4% while the water content and limestone content were varied.

Table 5-3. Water, Cement, and Limestone Composition for Second Round Gator Rock Mix

Batch Number	% Limestone	% Cement	% Water
A	78	4	18
B	76	4	20
C	74	4	22
D	72	4	24

Because the time between mixing the first round of Bull Gator Rock and the second round of Bull Gator Rock was over a year, the source of crushed limestone had changed. A similar sieve analysis was conducted on the new crushed limestone to be used in the Round 2 mixing procedure. The average value for the grain size distribution is shown in Figure 5-24. As before, the grain size analysis was conducted four times. Each grain size sieving run showed excellent agreement with one another. Maximum percent deviation between data points was 9.44% (seen with the No. 200 sieve). This grain size analysis shows that crushed limestone particles used for the second round of Gator Rock mixing are on average slightly larger than the particles used for the first round of tests (D_{50}'s of 0.5 vs. 0.25 respectively).

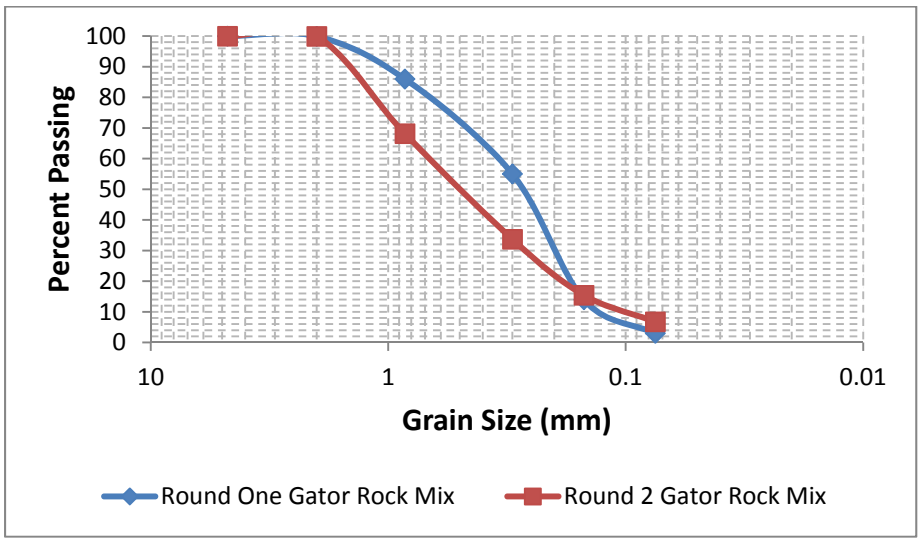

Figure 5-24. Grain Size Analysis for Round 2 Gator Rock Mix

5.6.1 Tensile and Compressive Strength Tests

As with the first round of Gator Rock tests, the first step in verifying sample-to-sample regularity was to conduct tensile and compressive strength tests. Tests were conducted on three randomly chosen samples from each of the four batches of Gator Rock. Results are presented in Table 5-4:

Table 5-4. Strength Test Results from Round 2 of Gator Rock Testing

SAMPLE NAME	SAMP. NO.	w (%)	DRY UNIT WT (pcf)	MAX. LOAD (lbs)	TENSILE STRENGTH (kPa)	COMP. STRENGTH (kPa)	DISPL. @ FAIL. (in)	STRAIN @ FAIL. (%)	TARE WT. (g)	WET WT. (g)	DRY WT. (g)
UC-A	1	16.31	105.1	677.5		978.0	0.0461	1.14	76.4	684.0	598.8
	2	14.82	103.7	1234.8		1781.8	0.0534	1.30	75.7	674.6	597.3
	3	13.21	102.0	382.8		552.4	0.0301	0.74	75.0	646.6	579.9
ST-A	4A	12.46	105.6	256.0	232.2		0.0196		74.3	365.0	332.8
	4B	12.43	102.8	214.3	194.8		0.0180		77.3	358.7	327.6
	5	14.33	105.8	321.3	237.7		0.0143		75.4	438.4	392.9
	6	13.38	106.9	362.1	269.4		0.0254		76.2	437.2	394.6
UC-B	11	15.96	103.9	603.3		866.8	0.0319	0.78	75.7	679.5	596.4
	12	15.07	103.9	578.1		830.0	0.0577	1.41	76.7	675.5	597.1
	13	14.81	103.6	608.7		870.1	0.0518	1.27	74.6	670.9	594.0
ST-B	14	15.80	106.6	277.0	201.7		0.0160		76.5	451.1	400.0
	15	9.62	104.0	345.4	260.5		0.0147		78.6	414.7	385.2
	16	14.56	104.2	222.3	165.6		0.0147		75.6	429.7	384.7
UC-C	21	10.83	101.1	850.4	376.8	1216.3	0.0354	0.87	77.5	633.2	578.9
	22	12.88	101.6	735.3		1058.2	0.0268	0.66	72.5	641.3	576.4
	23	10.96	102.4	922.2		1317.2	0.0338	0.83	76.9	642.9	587.0
ST-C	24	10.54	99.4	251.7	182.6		0.0161		81.1	416.8	384.8
	25	9.91	103.4	288.9	212.1		0.0163		75.1	416.7	385.9
	26	10.78	103.5	316.1	230.3		0.0164		75.1	423.4	389.5
UC-D	31	15.58	100.4	494.7	220.0	705.2	0.0313	0.78	77.1	651.3	573.9
	32	14.41	104.2	764.4		1087.1	0.0319	0.79	76.3	668.5	593.9
	33	13.48	102.0	698.5		995.5	0.0343	0.85	76.7	651.8	583.5
ST-D	34	14.52	103.6	250.2	188.2		0.0190		77.3	425.1	381.0
	35	12.62	105.8	325.6	243.7		0.0192		76.1	428.5	389.0
	36	14.79	102.6	240.1	177.2		0.0190		77.7	430.1	384.7

As demonstrated in this table, there was a high amount of variability among samples of the same batches during strength testing. The only batch that performed reasonably well was the Batch 2 specimen. There are two possible explanations that are related to one another that can be blamed for this poor strength testing behavior. The first is given in Figure 5-24. Explicitly, aggregate for the second round of Gator Rock mixing was larger and more non-uniform than

aggregate for the first round of Gator Rock tests. This is significant because of Gator Rock mixing procedure. During Gator Rock mixing, aggregate for samples are chosen at random, packed, and vibrated. If aggregate is more non-uniform, it stands to reason that each individual sample would likewise be more non-uniform. More non-uniformity within a sample implies more jagged edges between particles – or more precisely more voids in the Bull Gator Rock matrix. More non-uniformity also increases the chance that from a sample-to-sample perspective, one Bull Gator Rock sample from the same batch will be different from another sample from the same batch of aggregate/cement.

Bull Gator Rock is dependent on water's ability to work its way up through a sample. More, larger voids hinder capillary action. Even a small increase or decrease in voids size or frequency from a sample-to-sample standpoint could severely inhibit water transport up through the material – thereby creating slightly stronger or weaker samples. In other words, a variable void ratio from a sample-to-sample perspective affects strength test data. This effect was even greater than the water-to-cement ratio change that occurred from batch-to-batch.

There was some empirical evidence of this effect even before strength testing occurred, although at the time it was ignored and quantitative measurements were not obtained. When the Round 2 Gator Rock samples were done curing after 28 days, some of the samples had failed to absorb their water properly. Although the observation was qualitative, there did not appear to be a corresponding relationship between cement content and water absorption.

Although measurements were not conducted post-curing, measurements were conducted pre-break testing. Before each break-test, Gator Rock samples were saturated. As Gator Rock was saturated, different samples from the same batch took different water quantities. This indicates different void ratios for different samples from the same batch (same cement content). It also implies different water absorption rates during curing for different samples from the same batch.

The sample with the most uniform water absorption rate post-curing was Batch 2. It is not a coincidence that this round of tests was also the most regular from a sample-to-sample standpoint. To illustrate this phenomenon, a plot was made for Gator Rock batches created during the second round of tests (Figure 5-25).

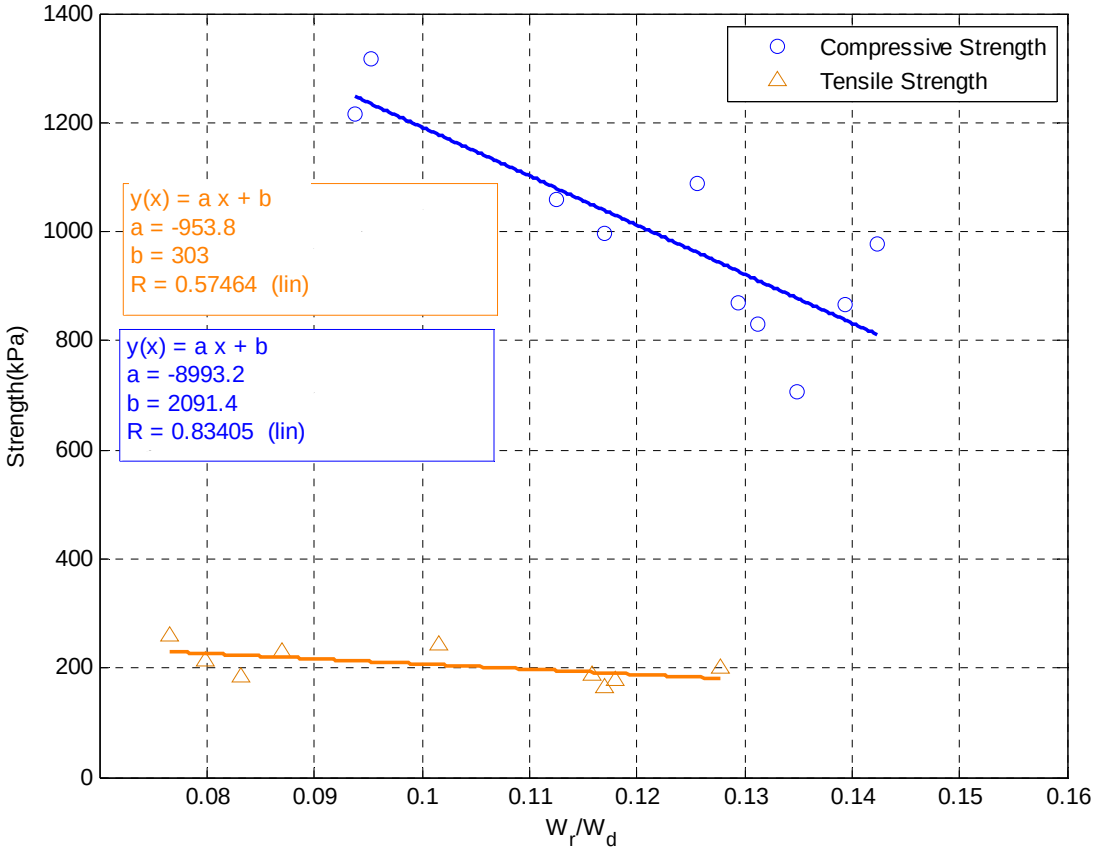

Figure 5-25. Non-Dimensionalized Water Retained vs. Strength (W_R is the weight of retained water after saturation; W_D is the dry sample weight).

This graph shows a trend whereby an increase in absorbed water during saturation yields a lower strength value during the break test. This relationship appears to supersede any relationship between cement content and strength. It also implies that different void ratios must be present from a sample-to-sample perspective, which again should be caused by more variability in limestone aggregate.

5.6.2 RETA Tests

The preceding discussion marked the first time in the history of Gator Rock that a series of Gator Rock samples failed to display regularity during compressive and tensile strength tests. Given the variability of strength data, it appeared unlikely that obtaining erosion data (which overall is generally even more variable than strength data) would be repeatable. Since there is only one SERF, testing time in it is at a premium. Before spending more time trying to compare

something that may be incomparable, with a SERF test, two sets of RETA tests were completed on two batches of material from the Round 2 Bull Gator Rock mix. Results are presented in Figure 5-26 and Figure 5-27:

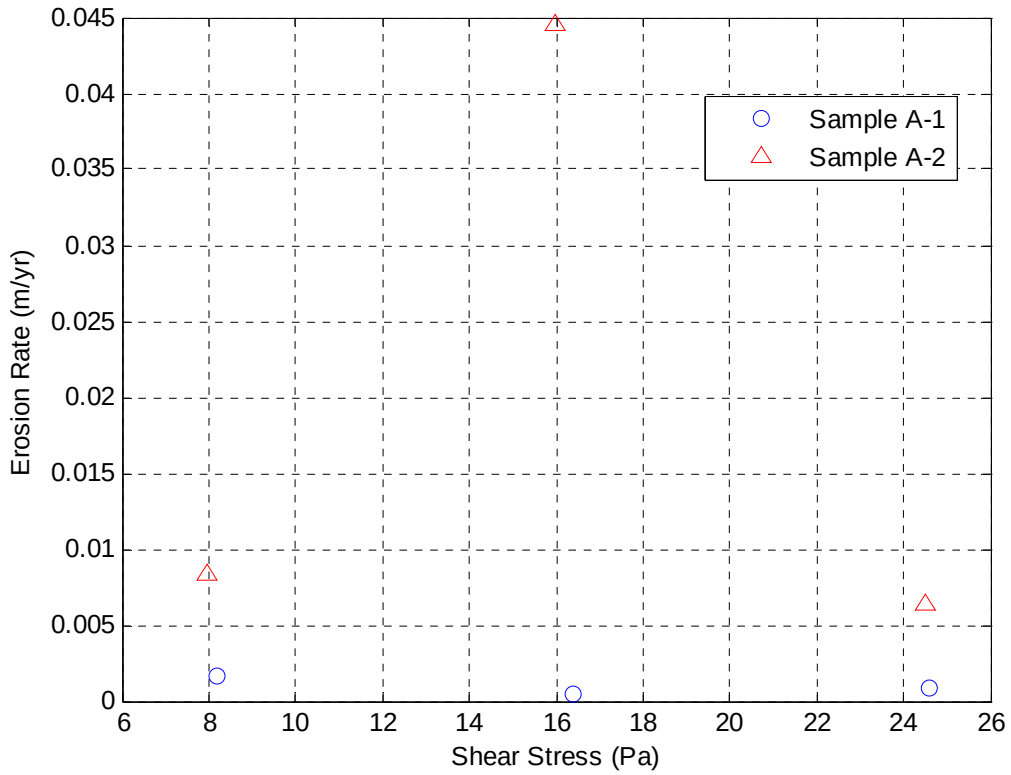

Figure 5-26. Batch A RETA Results

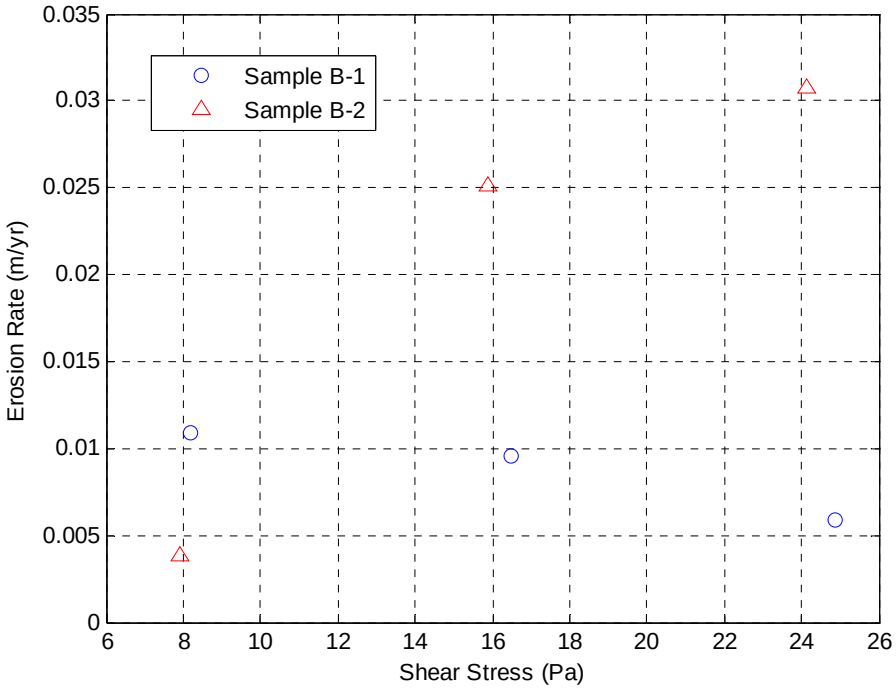

Figure 5-27. Batch B RETA Results

Of these four tests, only one showed a regular erosion rate-shear stress curve – sample B-2. This is not to say that if these tests were to be repeated several times, it would not be possible to generalize RETA results for one of these samples. After several repetitions, it may be possible to generalize a scenario where erosion rate increases with shear stress. Given these results though, the dataset is limited. These two graphs indicate that rock-like erosion is present, and it is of a similar order of significance as the particle-like erosion mode seen in Sample B-2.

Under ideal conditions, several tests (twenty or more) could be repeated with the Batch B mixing configuration. This would be the best-case scenario because Batch B showed the least strength test variability and it showed the ability to produce a regular erosion rate vs. shear stress relationship. If these tests were conducted repeatedly, they may show that on average shear stress and erosion rate can be correlated. Conversely, they may also show that rock-like erosion is dominant and that a regular erosion rate-shear stress curve cannot be developed for this material given current measurement limitations.

5.6.3 Absorption Limits

Once RETA tests and strength tests confirmed that repeatability for the second round of Gator Rock testing would not be achieved, investigation looked to further quantify why this could have occurred and determine whether or not the Bull Gator Rock was functioning as designed. During the second round of Gator Rock curing, investigators noticed that some water had not been absorbed by the dry limestone-Portland cement mixture. At higher water contents in particular, there were often significant amounts of water remaining in the samples' curing containers. The amount of remaining water for each sample batch, which was measured by mass and is presented as a function of the intended water content, is presented in Table 5-5:

Table 5-5. Actual W/C Ratios for Second Round of Gator Rock

Water Remaining (g)	Water Absorbed (g)	Cement (g)	Actual W/C Ratio
6.59	154.52	32.22	20.85%
29.14	148.08	32.22	21.76%
43.15	150.18	32.22	21.46%

As shown in this table, beyond about 20% water, the dry Bull Gator Rock mixture does not appear to be capable of absorbing any more fluid. In other words, by mimicking Niraula's (2004) original 20% water content during the first iteration of Gator Rock mixes, investigators had inadvertently stumbled upon the absorption limit for the bottom-up method of creating Gator Rock. The scatter seen then in Table 5-4 and in the RETA results is actually a representation of Gator Rock samples with similar water contents.

The implications of this are two-fold. First, it does not appear that creating a bottom-up version of Gator Rock with a higher water content than 20% is possible. Because of the rock-like erosion discusses in Section 5.6.2, this means that creating a weaker Gator Rock where particle-like erosion may be induced appears to require another method. Likewise, perhaps it would be better in further tests to use a different material; a sand-clay mixture for example. Secondly, if the distinctions between batches can be eliminated, the implication of this round of tests is that Gator Rock will often produce rock-like erosion at a 20% water content. As evidenced by Figure 5-26 and Figure 5-27, only once was a direct erosion rate vs. shear stress relationship developed.

5.7 Discussion

The problem with large-scale replication of this round of tests, and in general with RETA tests is time. Large-scale production of Bull Gator Rock is time consuming. Obtaining material, meticulously measuring out samples, mixing the samples, shaking the samples, measuring water, etc. is labor intensive. Mixing a large-scale batch takes between fifty and sixty man-hours. Then, the samples need to cure for 28 days, and even then there's no guarantee they're going to work; in fact, according to Section 5.6, it appears likely that particle-like erosion induction will fail. Finally, they must occupy a RETA for often weeks at a time. Although the first round of Bull Gator Rock testing in the RETA was completed using a 24 hour testing timeframe, the Round 2 mixes were tested with a 72 hour timeframe per shear stress because this is the standard in FDOT's RETA Florida Method. This translates to at least nine days of testing per dataset. FDOT has a limited number of RETA's and taxing one (or several) of these instruments for weeks on end increases the probability for breakage – which right now is nearly a certainty after a few weeks of testing. As discussed, control boxes often break, machines malfunction, equipment turns off, etc. These issues mean that from start to finish, development of one erosion rate vs. shear stress curve takes approximately a month. At RETA testing's present rate of success, developing an extensive dataset could take years.

Even with the most successful outcome possible after a string of RETA tests – a particle-like dominated erosion rate vs. shear stress curve – there is an additional need to compare results with SERF data. The SERF has its own set of issues, particularly with longer-duration erosion tests. Although the improvements chronicled in Chapter 3 now make longer-duration erosion rate tests possible, a SERF test too is labor intensive. Loading the sample into the SERF often makes samples break, samples often get knocked loose from the screw holding the sample to the piston, motors, which are a constant problem, get burned out after several hours of testing, etc. In short, although the device is much improved, and its present setup will allow eventually for a full-scale dataset to be taken, this in effect is a massive project in and unto itself.

Data discussed in this chapter was taken over the course of six months with little equipment downtime. During this timeframe, two SERF motors burned out (this is common for stepper motors), and three RETA's broke. Add to this mix-time, preparation time, false starts emanating from failed procedures and tests, implications from the absorption limit study, and it was fortuitous that it was even possible to obtain this limited dataset.

With the present setup, the RETA and the SERF can only measure shear stresses and erosion rate. Whenever erosion becomes dominated by rock-like erosion and a regular erosion rate vs. shear stress graph cannot be generated, the test is effectively useless as a basis for comparison between the two instruments.

Realizing these limitations, after the second Batch 2 Round 2 dataset was taken, particularly with respect to the absorption limit problem, the effort to verify RETA results via a direct comparison was effectively abandoned. SERF testing was not conducted on these materials because of variability seen during strength testing and rock-like erosion seen during RETA testing. Instead, the SERF was reserved for sand-clay tests (Chapter 7). It appeared unlikely that any dataset could be produced that would even closely mimic data coming from the B-2 RETA sample, and as per an FDOT proposal, sand-clay data needed to be taken.

Still, the effort to verify particle-like RETA results was not abandoned completely. As will be discussed in Chapter 6, there is another pseudo-analytical method that is available for both verifying RETA results somewhat and correlating RETA results to cohesion.

5.8 Summary and Conclusions

A summary of work completed in this chapter and a list of conclusions from work presented in this chapter is presented below:

1. A new method was invented for the creation of Gator Rock (Bull Gator Rock) where limestone and cement were mixed dry and water was slowly added to the limestone-cement mixture through capillarity.

2. Initial strength and erosion testing for Gator Rock was encouraging. The first Gator Rock mix showed little variability in strength tests. Erosion tests showed erosion rate vs. shear stress curves that indicated possible particle-like erosion.

3. Secondary testing for Bull Gator Rock showed issues with its initial design. Erosion tests showed rock-like characteristics. Repeatability was not shown between the first and second dataset indicating that although particle-like erosion may have been present the first time around, it may have been fortuitous.

4. Attempts were made to improve Gator Rock design. Improvements showed sensitivity to void ratio which led to variability in both strength and erosion testing.

5. The “improved” Gator Rock batch appeared to indicate that obtaining more than ~20% water content using the bottom-up water absorption method may not be possible.

Therefore, it appears unlikely that using this material as a standard of comparison between the RETA and the SERF will be successful because of the presence of rock-like erosion.

6. Variability in the strength and erosion results revealed that a comprehensive dataset was necessary for a direct RETA-to-SERF comparison.

5.9 Future Work

A direct comparison should be attempted between the RETA and the SERF, but the time-frame for production of such a dataset must be extensive (at least three years). During this time, there must be an investigator who is committed to producing a material to test in both devices and using the SERF exclusively for to produce an extensive dataset for this material. There must also be a RETA dedicated to production of a corresponding dataset. Because of the current limited amount of laboratory equipment, this is the only way to insure that enough data points are produced.

Based on lessons from the second round of the Bull Gator Rock mix, in the future a more uniform aggregate should be used when mixing Bull Gator Rock, or a new material/method for Gator Rock production should be developed. As shown during the second round of tests, obtaining a water content higher than 20% may not be obtainable using this method.

Although work for this chapter began as a method to provide definitive SERF-to-RETA answers, in the end, it had the net opposite effect, as more questions were generated:

1. Can Gator Rock be designed to induce particle-like erosion?
2. Might a different material be more appropriate?
3. Can either Gator Rock or a similar material be used to induce particle-like erosion?
4. Can either Gator Rock or a new material be designed to generalize SERF or RETA data?

CHAPTER 6
VERIFICATION OF THE ROTATING EROSION TESTING APPARATUS (RETA) AND USING RETA RESULTS TO PREDICT EROSION RATES AND SHEAR STRESSES OF ERODING BED MATERIALS USING COHESION

6.1 Executive Summary

In an effort to verify results from the Rotating Erosion Test Apparatus (RETA), a semi-analytical approach was used. Results from the RETA were filtered so that only data that exhibited a direct erosion rate vs. shear stress relationship was considered. Then, this dataset was fit to a shear stress deficit erosion rate formula. Results showed agreement between the formula and RETA results. Dimensional analysis was used to develop relationships for erosion rate constant and critical shear stress based on other geotechnical parameters. Based on Mohr's Circle reasoning, a cohesion term was added to non-dimensional parameters. Cohesion-based non-dimensional correlations were used to estimate erosion rate vs. shear stress curves and compared with RETA results. Data showed agreement between the empirical formulae and actual results, although the R^2 value when comparing these two parameters was low. Because the cohesive dataset was limited, it is thought that this is what led to these low R^2 values.

6.2 Review of Relevant Background

Development of an extensive RETA dataset is labor intensive. The same is true for a SERF dataset or any dataset in a flume-style device. Even if a comprehensive dataset could be generated for both instruments, there is no way to verify that the material tested in both machines is the same from one test to another. The first version of Bull Gator Rock was the most uniform, regular, and homogeneous manmade material found to date that would stand up to testing in both devices, and even Gator Rock tests in the RETA showed variability. Although the RETA's dataset was quite limited, for a comparison to be made between the RETA and the SERF, the testing material's results should be repeatable even with a small dataset. Faced with these difficulties for making a direct comparison between the RETA the SERF, another method was

investigated to determine whether or not the RETA was providing accurate erosion rate and shear stress relationships.

Since its inception, the SERF has been used limitedly because of issues associated with its operation. The RETA on the other hand has been used extensively for over five years. The FDOT SMO has a laboratory with several RETA's, and these machines are run often with a variety of soil, rock, and hybrid samples. Every time a test is run its results are added to FDOT's comprehensive RETA database. As of 2010, FDOT had conducted RETA testing on 83 different materials. Materials from both Florida and from out of state were tested. Some materials were manmade, while other materials were natural. During the SMO tests, at least three shear stresses were run during each test. Each test lasted for 72 hours. This database represents 6,000 hours of RETA testing, and it is the most extensive rotating erosion rate testing device database known to exist. It took years to generate this database, and it would take several more years to generate anything similar.

As it is set up, the RETA is designed to measure erosion rates and corresponding shear stress for particle-like erosion only. As discussed at several points throughout this report, particle-like erosion assumes that a gentle pull or tug removes a few outside particles from a sediment sample. This pull or tug is different than rock-like erosion in that during rock-like erosion, a pulsating impulse force removes chunks or blocks of material from the sediment sample. The overall goal of this project is to use erosion rate testing devices to measure the sediment transport function that is used in computing scour depth. Recall from Chapter 2 and Chapter 3 that particle-like erosion is generally defined by functions taking the following form:

$$E = C \cdot f(\tau) \tag{6-1}$$

where E is the erosion rate, C is an erosion rate constant, and $f(\tau)$ is a function of shear stress. Although more complicated computations for this function have been presented (for example Van Prooijen and Winterwerp 2008), they can be approximated by this generalized equation. Typically, following shields, the shear stress function is instead expressed as a deficit between bed shear stress and critical shear stress:

$$E = M \cdot (\tau_b - \tau_c) \tag{6-2}$$

where τ_b is the bed shear stress and M is the material specific erosion rate constant.

As discussed in Chapter 2, Equation 6-2 was discovered in the 1970's for particle-like cohesive erosion rates by Kandiah (1974) and Ariathurai (1974). This equation confirmed

analytical results from Einstein (1950), Partheniades (1965), and others. Equations of this form have been shown to work using a variety of erosion rate testing equipment. For example, Partheniades verified his equation for erosion rate by measuring sediment concentrations. Kandiah on the other hand used a device similar to the RETA to develop his expression. In general, equations similar to Equation 6.6-17 have shown global relevancy for the particle-like cohesive erosion problem.

If an equation of this form is valid and the RETA is measuring erosion rate vs. shear stress relationships correctly, RETA data should fit this form as well. Although a direct comparison between the RETA and the SERF proved difficult, a direct comparison between the RETA and equations of this form is possible because of the existence of the RETA database. The technique used for this analysis was to take the RETA database and try to fit data from it to Equation 6-2. This meant that instead of just comparing the RETA to one other dataset using one other erosion rate testing device, the RETA is compared with every other cohesive erosion study.

6.3 RETA Verification

The first step of RETA data analysis was to filter the RETA dataset so that only particle-like results were analyzed. For each material in the RETA database, erosion rate and shear stress were plotted against one another, and best-fit least squares regression line was fit to the data points. If the line had a positive slope, the material for which the curve was generated was used for overall analysis; if the line had a negative slope (or no slope), the material was ignored and rock-like erosion conditions were presumed to have dominated that particular RETA test. An example of one best-fit line for a RETA material exhibiting rock-like erosion is given in Figure 6-1 while a particle-like erosion line is shown in Figure 6-2:

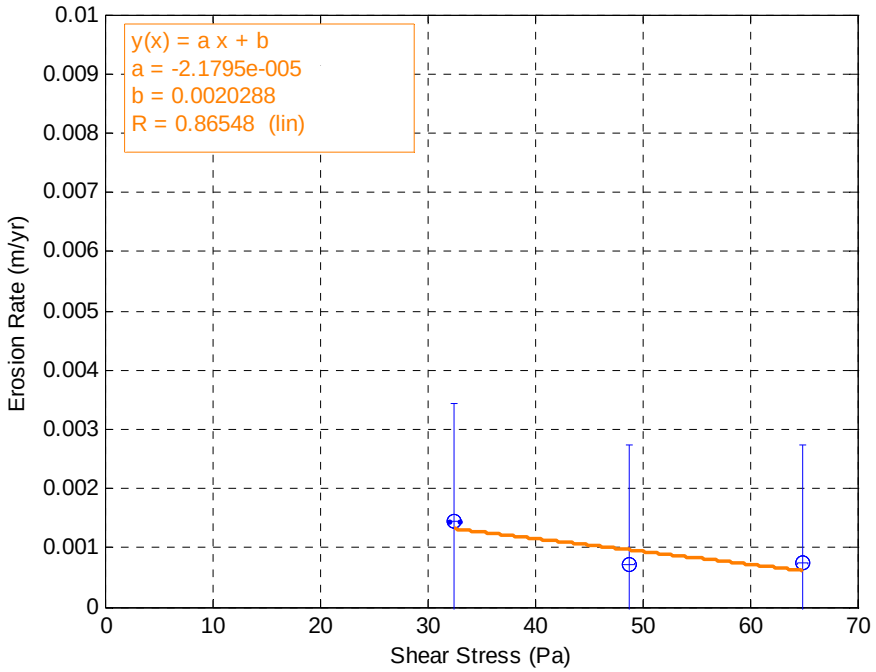

Figure 6-1. Example of a RETA Material with Rock-Like Erosion Properties

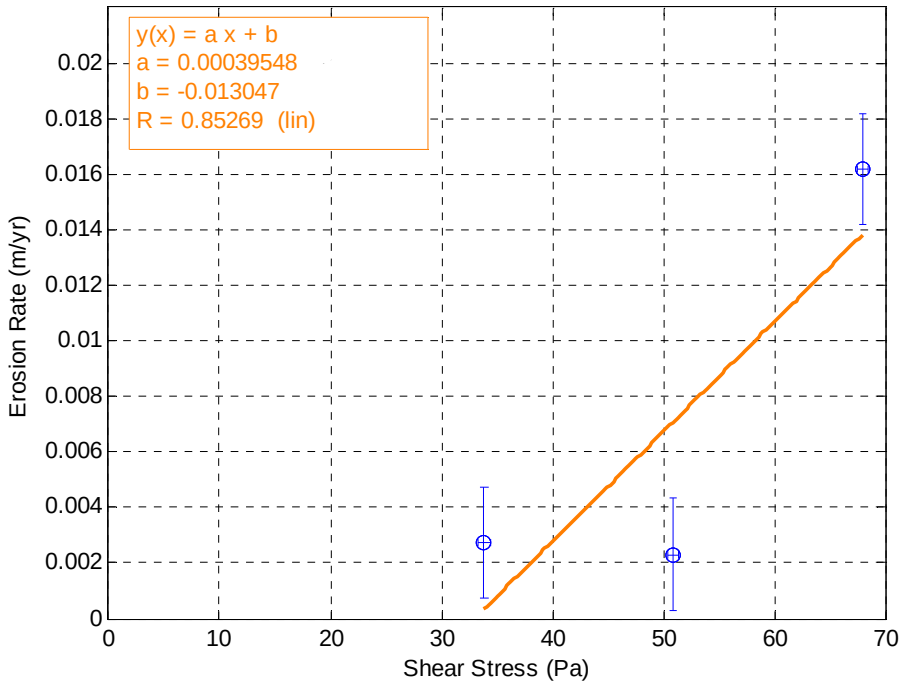

Figure 6-2. Example of a RETA Material with Particle-Like Erosion Properties

Filtering cut the number of samples used for analysis. Whereas the dataset started with plots relating erosion rate to shear stress for 83 materials, after filtering, only 32 materials fit the stringent erosion rate-shear stress curve criteria (approximately 40%). Although this looks like a great deal of data elimination, for a material to survive a RETA test, it must be resilient. Generally resilient materials are harder and stiffer than materials that crumble under the moment forcing associated with RETA testing. In other words materials that are able to withstand a RETA test are more rock-like, which implies that they are more likely to respond to erosion via a rock-like mechanism. In this context then, a 40% data recovery rate is actually quite precise. Once filtering was completed, a brief analysis was conducted to compare average rock-like erosion quantities with implied particle-like erosion quantities. In general, materials that exhibit direct shear stress to erosion rate relationship erode an order of magnitude faster than materials that do not exhibit a direct shear stress to erosion rate relationship. This fits with the overall rock-like erosion argument.

Once filtering had been completed, the next step in fitting a shear stress deficit equation to the RETA dataset was to find the critical shear stresses associated with each material. By definition, erosion rate below the critical shear stress point should equal zero. Therefore, the critical shear stress should be defined as the x-intercept corresponding to a material's erosion rate vs. shear stress line. For each case where a direct erosion rate vs. shear stress relationship was observed, the critical shear stresses were estimated using the corresponding best-fit least squares regression equation. Bed shear stress and erosion rate were measured directly during each RETA test. With critical shear stress estimated from the best-fit regression lines, the only unknown in Equation 6-2 was M, the erosion rate constant. For each erosion rate and shear stress point, the value of M was computed.

As a basis of comparison with the Equation 6-2 linear erosion approximation, the most recent analytical expression for erosion rate was also used (Van Prooijen and Winterwerp 2008). Van Prooijen explains that his expression for erosion rate can be approximated using a three-piece function that also utilizes a shear-stress deficit approach and an erosion rate constant. Erosion rate constant was also computed using Van Prooijen and Winterwerp's set of equations.

$$\frac{E}{M\tau_c} = \begin{cases} 0 \text{ if } \dfrac{\tau_b}{\tau_c} < 0.52 \\ -0.144\left(\dfrac{\tau_b}{\tau_c}\right)^3 + 0.904\left(\dfrac{\tau_b}{\tau_c}\right)^2 - 0.823\left(\dfrac{\tau_b}{\tau_c}\right) + 0.204 \\ \left(\dfrac{\tau_b}{\tau_c} - 1\right) \text{ if } \dfrac{\tau_b}{\tau_c} > 1.7 \end{cases} \tag{6-3}$$

These two approaches for solving for *M* differ only slightly – only by 0.984%. Results were non-dimensionalized, and a best-fit regression line was fit through the dataset (Figure 6-3).

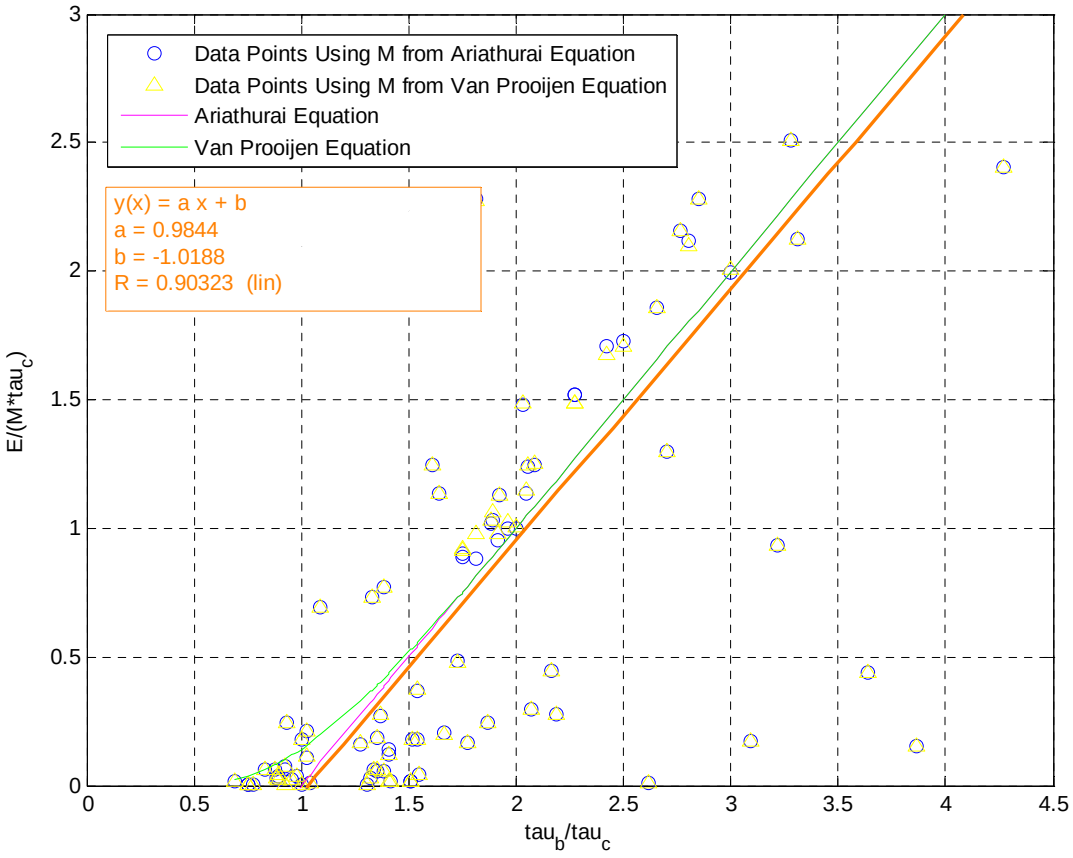

Figure 6-3. Non-Dimensional Erosion Results from RETA Data Set

Based on Equation 6-2, both the slope and the x-intercept of the regression line should have been 1.0. As shown, with a high R^2 value (0.8279), the slope and the intercept of the regression line are extremely close to where they should be. The x-intercept shows an error of 0.93% and the slope shows an error of 11.78%. Generally, the Equation 6-2 appears to be a somewhat conservative estimate of erosion rate. The Van Prooijen and Winterwerp Equation

appears to capture true erosion rates at lower shear stresses somewhat better than the linear approximation – particularly when bed shear stress approaches critical shear stress. Overall, from this analysis, data from the RETA appears to fit correctly. This implies that when a direct shear stress vs. erosion rate curve is developed, the RETA is providing accurate results.

6.4 Extending RETA Results – Predicting Erosion Rate as a Function of Material Strength

Based on the relatively small error associated with the preceding analysis, there was confidence behind RETA results. The next step in this study involved trying to find a way to correlate erosion rate constant and critical shear stress to another geotechnical property of rock-like bed materials. The goal of this phase of research was to eliminate or reduce the need for extensive RETA testing. If the need for RETA tests could be cut down – to a situation where a user simply had to run a RETA test to confirm or disprove a direct erosion rate vs. shear stress relationship – this would be invaluable. Based on the Mohr's Circle analysis in Chapter 2, if erosion rate is to be a function solely of shear stress, then the y-intercept of the Mohr's Circle failure line, or cohesion, should be correlated to erosion rate. This Section discusses attempts to use cohesion to approximate a material's erosion rate constant and critical shear stress.

6.4.1 Approximation of *M*

The first goal was to approximate *M* as a function of a bulk material property. Intuitively, as material gains strength, erosion rate should decrease. Likewise, as the material gains strength, its critical shear stress should increase, and therefore overall, the erosion rate constant, *M* should decrease.

A correlation was developed between erosion constant, *M* and material cohesion, or *C* (Figure 6-4). As shown, there appears to be a relatively strong correlation between these two parameters. Previously, for clay-like materials, attempts have been made to correlate *M* to critical shear stress, but for the materials tested in the RETA, no direct relationships could be computed between critical shear stress, erosion rate constant, or material strength. Figure 6-5 shows a plot of critical shear stress vs. *M*.

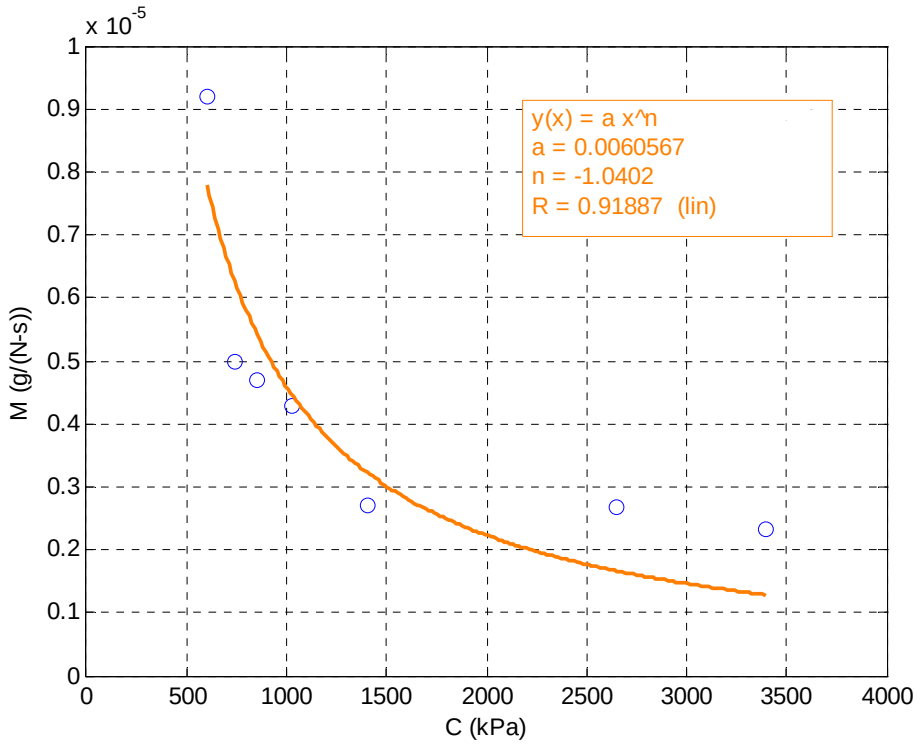

Figure 6-4. Relationship between Erosion Rate Constant and Cohesion

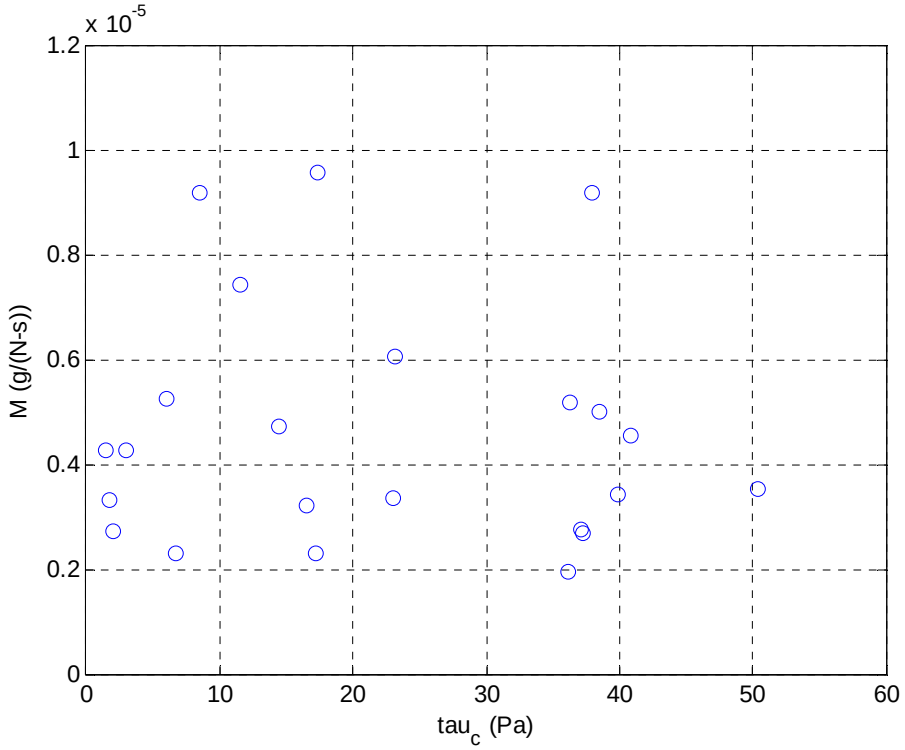

Figure 6-5. Relationship between Critical Shear Stress and Erosion Rate Constant

The relationship given in Figure 6-4 for *M* was compared with computed *M* values from erosion rate data. Although in Figure 6-4, the relationship between *M* and cohesion appears to be excellent, when comparing the equation from Figure 6-4's trend line with measured data (Figure 6-6), results start to deviate. Using the predictive equation shown in Figure 6-4, the R value between $M_{measured}$ and $M_{calculated}$ drops from 0.92 to 0.69 although even with this lower R value, the equation of the line is nearly where it should be (along y=x).

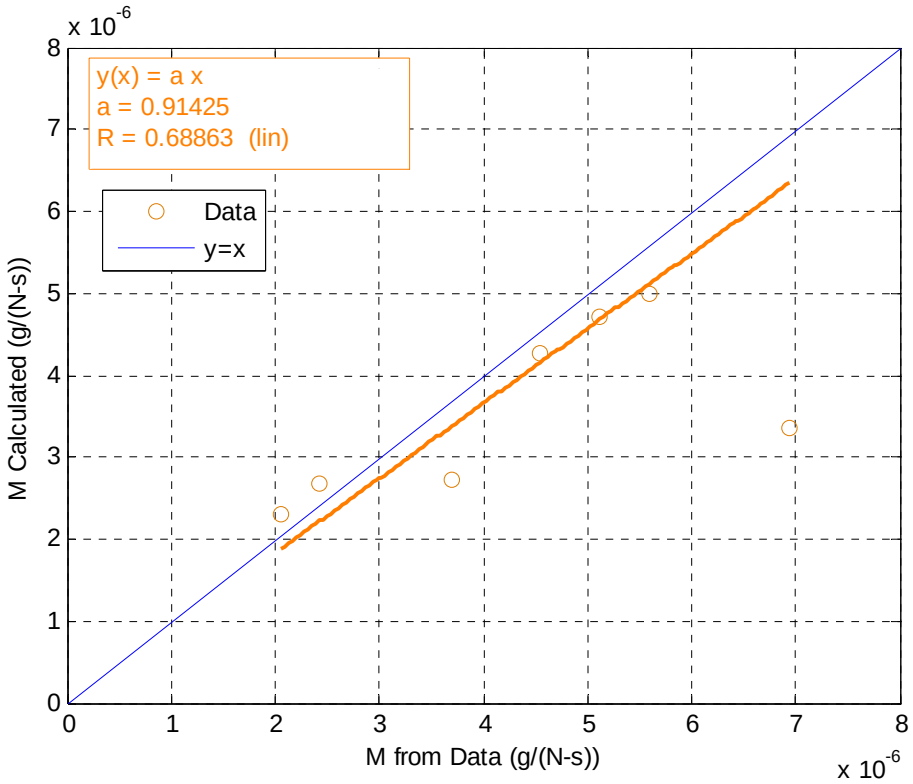

Figure 6-6. *M* from Cohesion based equation vs. *M* from Measured Data

If the relationship developed in Figure 6-4 is used to predict erosion rate and compared with measured data, results are still reasonable, even though *M* appears sensitive to cohesion (Figure 6-7). The best-fit line plotted for measured vs. predicted values of erosion rate lies within 10% of where it should be (along y = x). The magnitudes of measured erosion rate vs. predicted erosion rate are excellent, although the predicted erosion rate is on average lower than the measured value. Still, overall, when dealing with erosion rates on the order of magnitude of mm/year, this analysis should provide the correct order of magnitude for erosion.

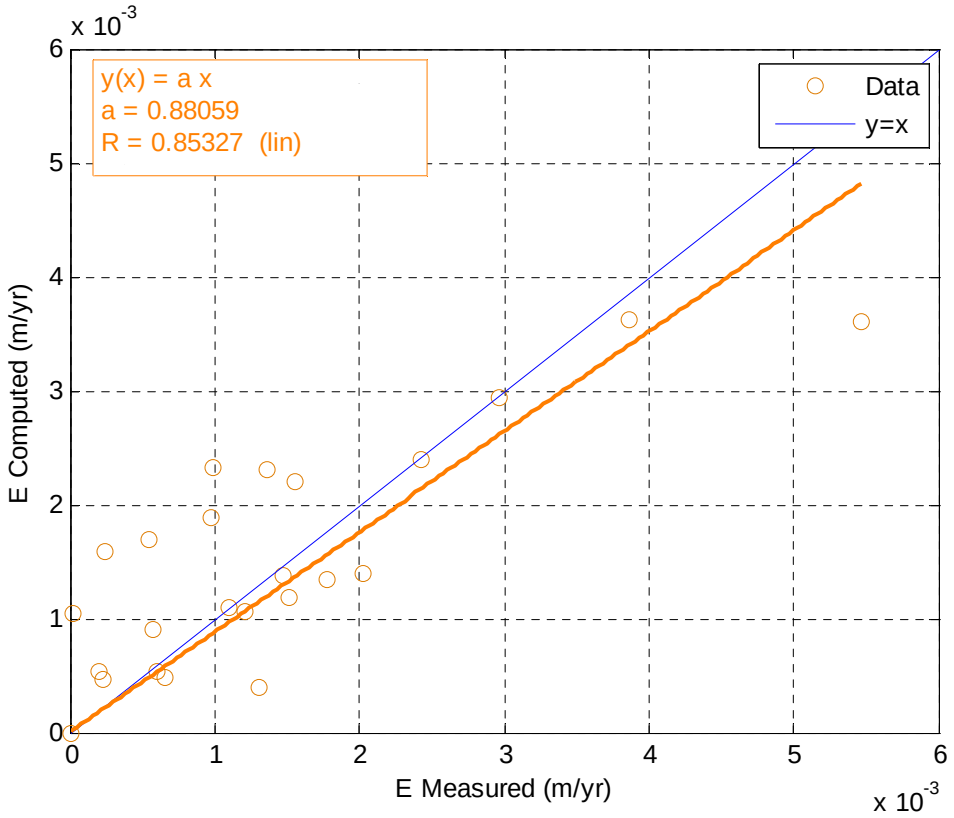

Figure 6-7. Predicted Erosion Rate vs. Measured Erosion Rate Using *M* Based on Material Strength

6.4.2 Dimensional Analysis

Because it looked as though it was possible to predict *M* from material strength, the next step was to non-dimensionalize this parameter. Based on dimensional analysis, it was hypothesized that erosion rate constant should be non-dimensionally depended on the ratio between material strength and critical shear stress such that:

$$\frac{MC}{u_*} = f\left(\frac{\tau_c}{C}\right) \tag{6-4}$$

In this expression, C is cohesion, τ_c is critical shear stress, M has been converted to m^2s/kg by dividing by material density, and u_* is the friction velocity associated with the critical shear stress such that:

$$u_* = \sqrt{\frac{\tau_c}{\rho}} \tag{6-5}$$

According to this argument then, as the ratio between material strength and critical shear stress increases, erosion rate constant should decrease. Intuitively, this appears to fit what Gordon's 1991 memo already stated – stronger materials tend to erode less quickly than weaker ones (Figure 6-8)

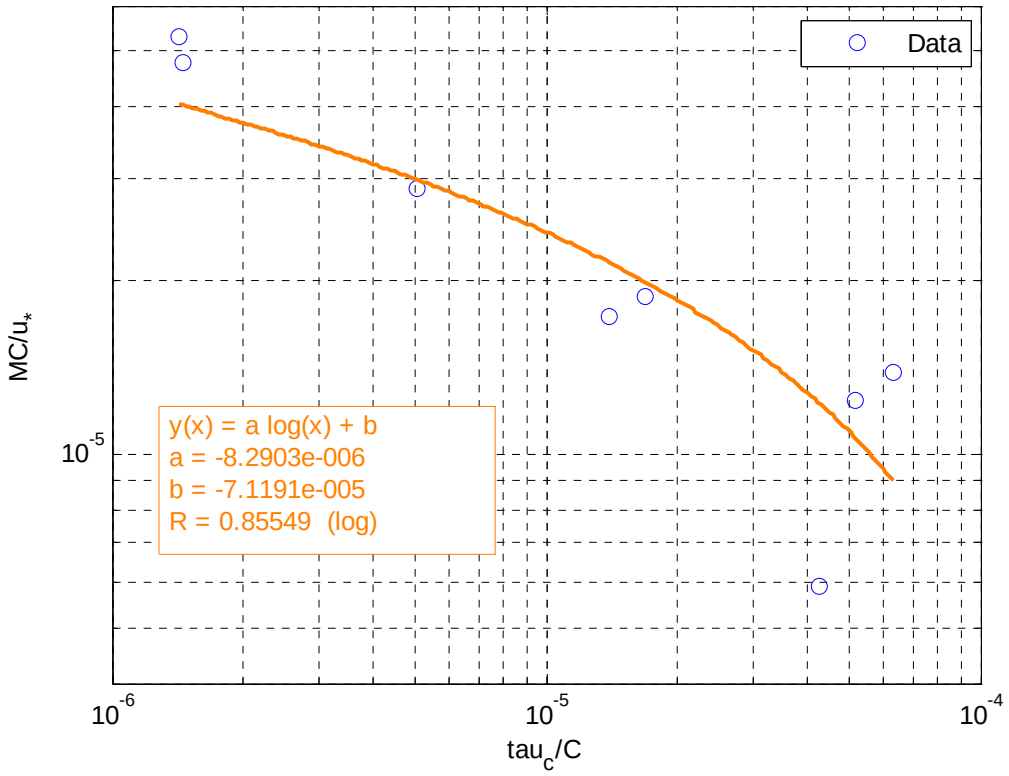

Figure 6-8. Non-Dimensional Erosion Constant vs. Non-Dimensional Material Strength

As demonstrated in this figure, the R value for this relationship is 0.86. More data is needed to shore up this relationship between material strength and erosion rate constant. This is emphasized when one uses the logarithmic expression in Figure 6-8 to estimate erosion rate directly. In contrast to Figure 6-7, erosion rate is not as accurate as it was when using the dimensional relationship between material strength and erosion rate constant (Figure 6-9). As shown, the *R* value drops to 0.86 when the non-dimensional expression is used, and the best-fit line through the data points under predicts the erosion rate by approximately 30% on average. As before, the same order of magnitude is recovered.

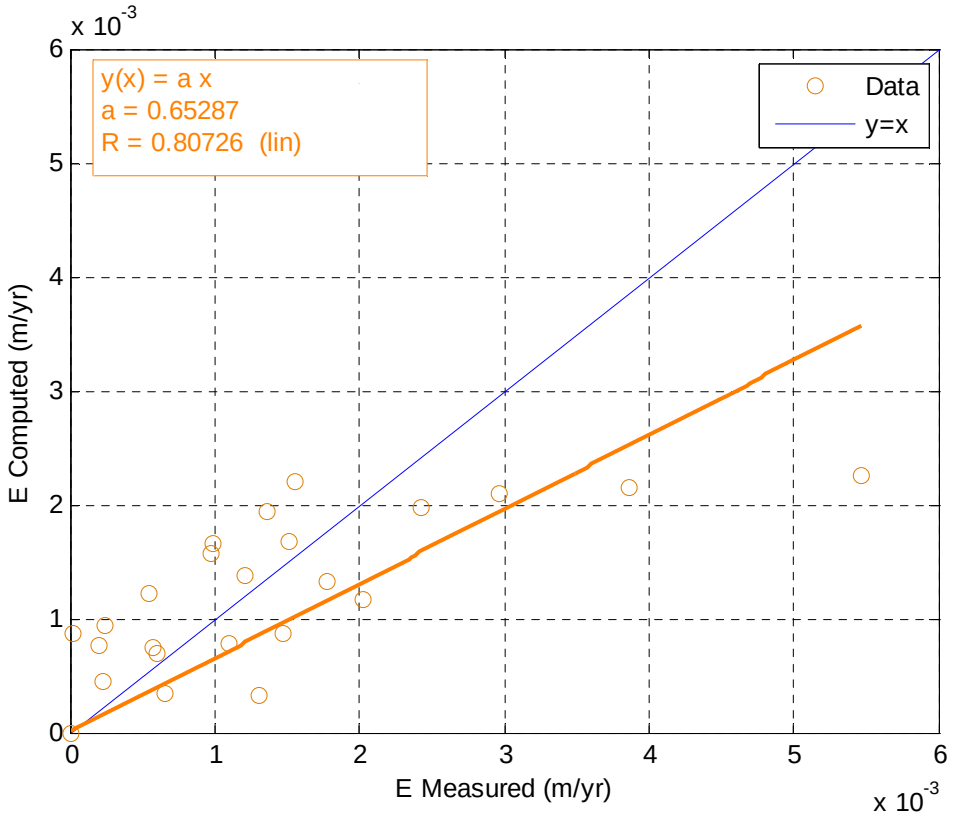

Figure 6-9. Graph showing computed value for *E* vs. Measured value for *E* when the Non-Dimensional Relationship for *M* is used.

6.4.3 Approximating τ_c

With a correlation developed between material strength and cohesion, the only remaining unknown in the Equation 6-2 (and the non-dimensionalized cohesion relationship) was critical shear stress. Development of a relationship between material strength and critical shear stress has been done before for clay-like particles. Migniot (1986) developed an expression that showed a relationship between upper Bingham yield stress and critical shear stress such that:

$$\tau_c = \begin{cases} 0.256\tau_y & \tau_y > 1.6\,\text{Pa} \\ 0.289\sqrt{\tau_y}; & \tau_y \le 1.6\,\text{Pa} \end{cases} \quad (6\text{-}6)$$

Migniot was dealing with much softer and weaker sediments than the sediments found in the RETA database. Migniot's critical shear stresses were four orders of magnitude higher than typical RETA critical shear stresses ($O(10^1)$ *vs.* $O(10^{-3})$). Based on this large difference for critical shear stress, it is not surprising that his correlations did not work for RETA materials.

Following the development for the non-dimensional expression for *M* as a function of the critical shear stress-cohesion ratio, another non-dimensional group was developed via dimensional analysis such that:

$$M\rho_s u_* = f\left(\frac{\tau_c}{C}\right) \tag{6-7}$$

where ρ_s is the bulk material density, *M* has once again been converted to m^2s/kg by dividing by the density, and previous terms have been already defined. A power-law regression line was fit to data (Figure 6-10). This predicted value for *M* was used to approximate erosion rate (Figure 6-11), and results show that although this relationship also under-predicts erosion rate, the relationship developed in Equation 6-4 appears to be more accurate than the relationship developed in Equation 6-7 because on average, it only under-predicts erosion rate by approximately 25%.

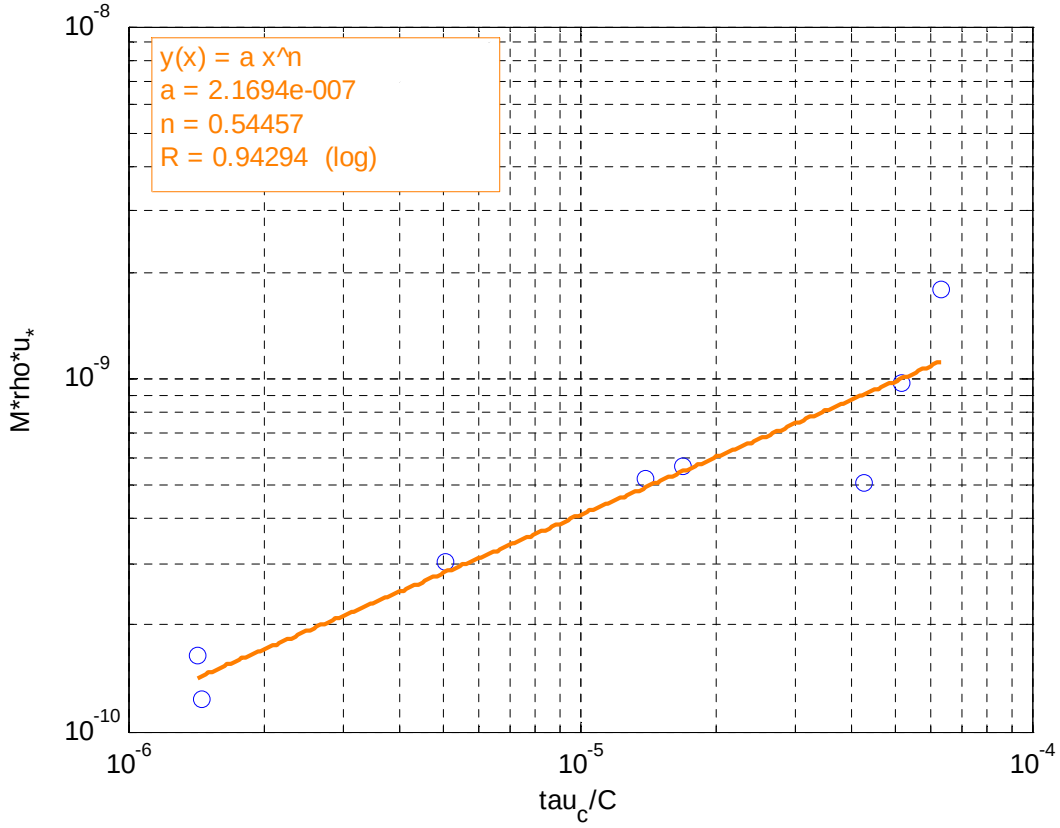

Figure 6-10. Non-Dimensional Critical Shear Stress vs. Non-Dimensional Material Strength

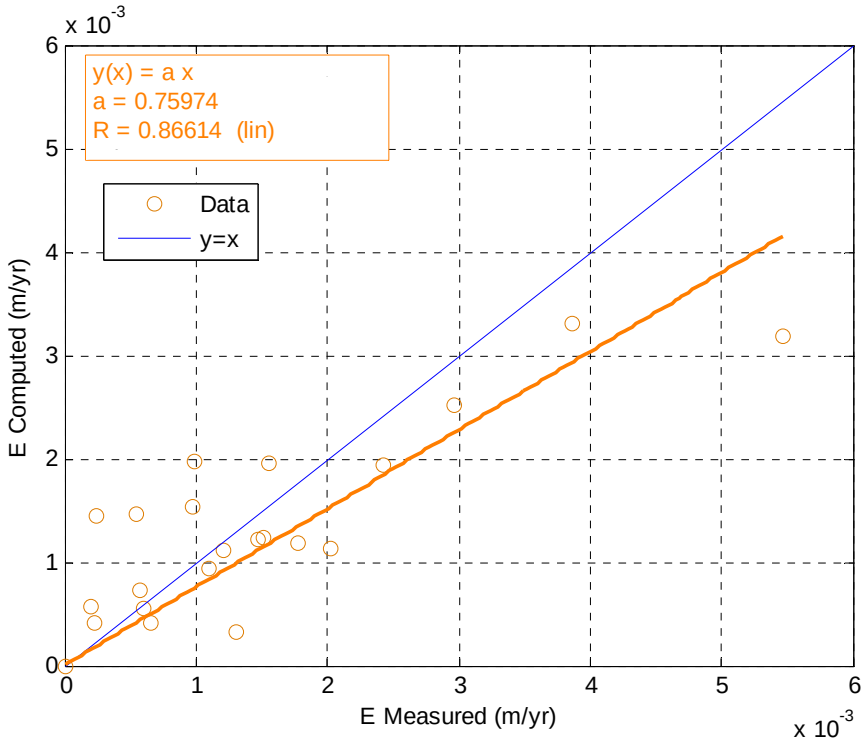

Figure 6-11. Measured Erosion Rate vs. Predicted Erosion Rate Using the Non-Dimensional Expression Developed in Equation 6.4-4.

With the development of Figure 6-3, Figure 6-8, and Figure 6-10, a non-dimensional method was finally available for estimating erosion for a given shear stress without development of an erosion rate-shear stress curve. Under field conditions using the Van Prooijen and Winterwerp expression, bed shear stress, or $\tau_{b,}$ is known from a hydrograph, and between Figure 6-8 and Figure 6-10, there are two expressions presented in terms of one another with two unknowns: M and τ_c. These two expressions, which are implicit in one another, can be combined and solved together to find erosion rate solely as a function of cohesion, or an interpolative solution can be found using the diagrams provided.

Combining the expressions from these two diagrams, an equation was developed for τ_c as a function of only cohesion such that:

$$\frac{A}{\rho_s u_*}\left(\frac{\tau_c}{C}\right)^k = \frac{u_*}{C}\left(a \ln \frac{\tau_c}{C} + b\right) \tag{6-8}$$

where A = 2.17x10^{-7}, a = -8.29x10^{-6}, b = -7.12x10^{-5}, and k = 0.545. Solving this equation for τ_c and comparing with measured values for τ_c led to development of Figure 6-12:

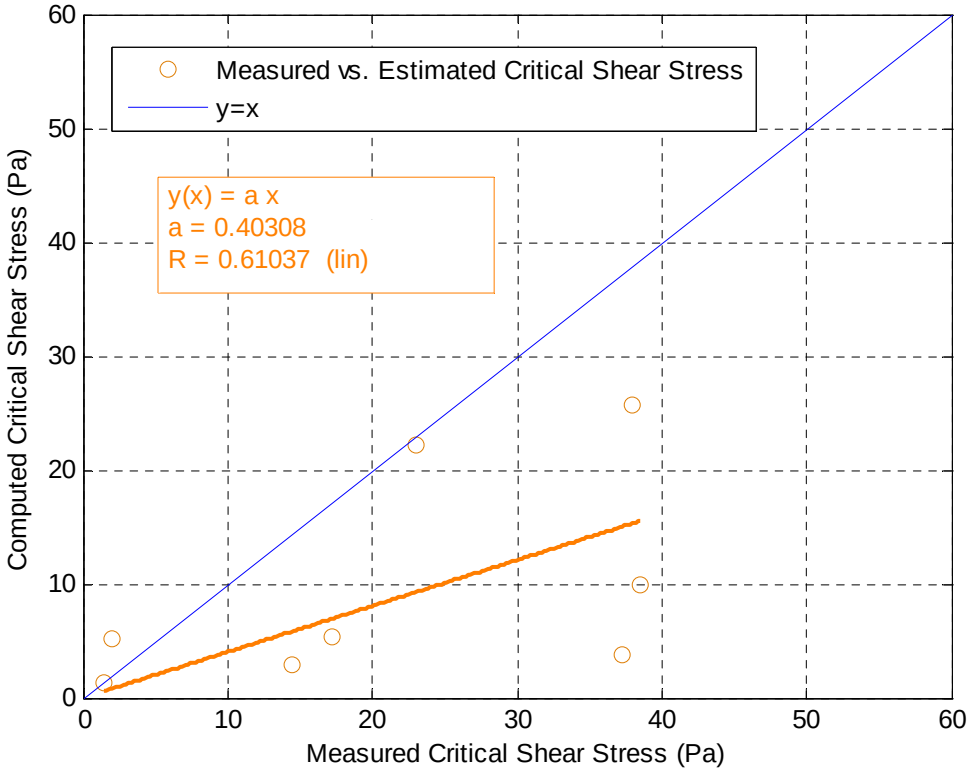

Figure 6-12. Measured vs. Computed Critical Shear Stress

As shown, the errors associated with the best-fit curves from the two non-dimensional groups appear to have compounded leading to a large error between actual and estimated critical shear stress estimates. This was expected since the sum of the errors of the two non-dimensional groups was on the order of 60%.

Using the predicted values for critical shear stress, new values of M were computed, and they in turn were used with the computed critical shear stresses to solve for erosion rate. The results are presented in Figure 6-13:

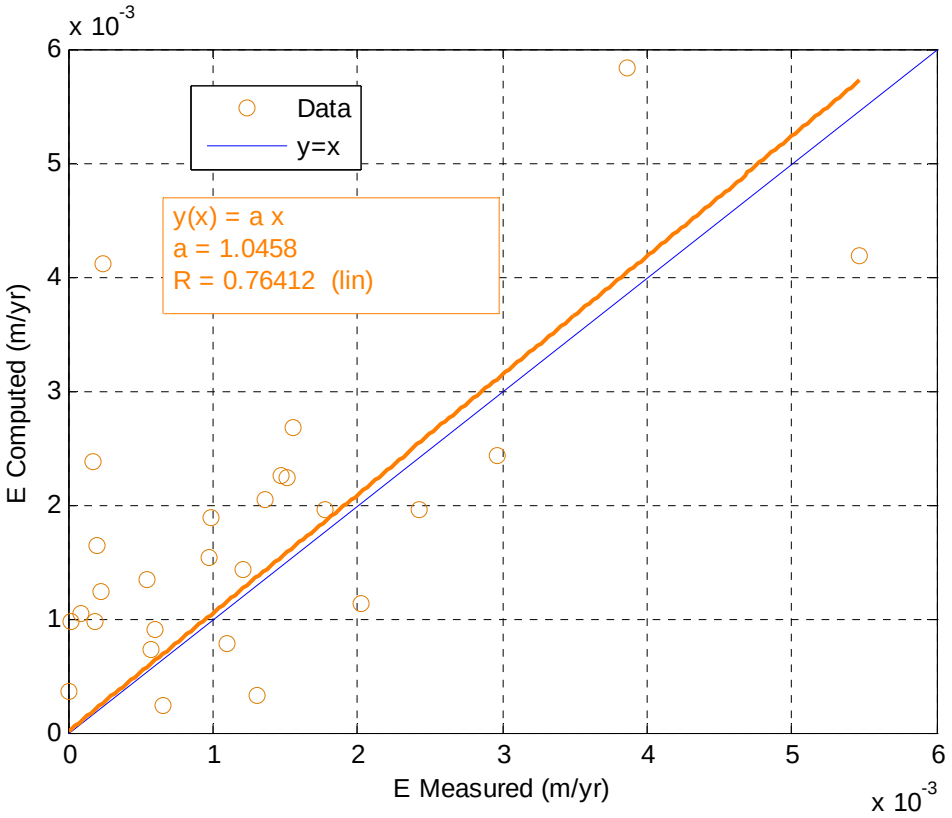

Figure 6-13. Predicted Erosion Rate Using Cohesion Computation vs. Actual Erosion Rate

6.5 Discussion and Future Work

The most significant result from this study is that data from the RETA database has been shown to fit a shear stress deficit equation. Several assumptions with the cohesion estimating method have been alluded to, but should be discussed explicitly. As shown in most of the cohesion plots, only eight cohesion data points are shown. Until 2006, no one had realized that cohesion could possibly be related to erosion rate. When RETA tests were conducted then, a separate cohesion test was not conducted on material before 2006. As a result, the number of cohesion points is limited. Combine the time-frame limits with initial filtering requirements, and the cohesion dataset is small compared with the overall usable RETA dataset. More research needs to be done to determine whether or not the correlations developed in Section 6.4 hold up when more data points are used to develop these curves.

The fundamental assumption in using cohesion as a correlating parameter with the RETA dataset is that the materials on which cohesion was measured are similar to the materials on

which erosion was measured. Quantifying a material's erosion rate vs. shear stress relationship and a material's cohesion value requires three sediment samples. During each test – tensile strength, compressive strength, and RETA – the sediment sample is destroyed. Using cohesion as the correlating factor assumes that unlike the Round 2 Bull Gator Rock samples, there is little variability among the three sediment cores. This assumption may or may not be true; a method for verifying sample uniformity should be developed if a method similar to this is to be used for design.

If the dataset used to construct these correlations can be extended though, and if uniformity between samples can be established, results from this study are promising, especially when examining Figure 6-13. Although the R value (which again is probably caused by a lack of data points) is poor (0.764), the slope of the best-fit line through the dataset is within 5.5% of where it should be. This indicates that, this method for predicting erosion rate based only on material strength has the potential to provide an accurate estimate of actual erosion rate. If the data set becomes more populated, more accurate critical shear stress estimates and more accurate erosion rate constant estimates would follow.

This method does predict the order of magnitude of erosion properly. On average, it also provides a slightly conservative estimate of erosion rate. Although the % error between this method and the actual erosion rate is relatively high, in terms of actual magnitudes of erosion rates, it is fairly low. On average, this method for predicting erosion rate over predicts erosion by 0.52 mm per year; the maximum error is 3.86 mm of erosion per year; and the minimum error is an under prediction of 1.28 mm of erosion per year. Although not perfect (as evidenced by the lower R value in Figure 6-13), this method will provide erosion rates with 5 mm of the actual conditions, and it can potentially lead to a reduction in the amount of SERF or RETA tests. If this method is to be used, a safety factor should be employed because of the uncertainty among the non-dimensional material strength relationships.

This method may be able to reduce the number of RETA testing. Even though this method was created using filtered data that represented a direct erosion rate vs. shear stress relationship, it was also found that data that did not exhibit a direct relationship was an order of magnitude higher than data that did exhibit a direct relationship. If then, this method is used and it turns out that the material in question exhibits an indirect erosion rate vs. shear stress relationship or no shear stress vs. erosion rate relationship, it can be inferred that it must erode less than it would if

it were to obey a direct distribution. Using cohesion to estimate erosion rate would be considered conservative. However, substantially more data are required to validate this theory.

6.6 Summary and Conclusions

A summary of work and a list of conclusions are presented below:

1. FDOT's RETA database was filtered so that only direct erosion rate vs. shear stress relationship data was considered.

2. Filtered data was used in development of erosion rate vs. shear stress best-fit regression lines. Regression lines were used to imply critical shear stress for the eroding material.

3. Implied critical shear stresses were used with erosion rate and actual shear stress data to solve for erosion rate constant.

4. Results were non-dimensionalized and plotted. RETA data showed excellent agreement with shear stress deficit analytical formulas.

5. Cohesion was used to develop two non-dimensional groups to estimate erosion rate constant and critical shear stress.

6. Using cohesion as a predictive erosion parameter shows some promise, although the cohesion dataset for RETA samples is quite limited.

7. More research should be conducted before any of these curves are used for design purposes. Specifically, the erosion rate vs. shear stress vs. cohesion database should be expanded.

CHAPTER 7
A STUDY OF EROSION RATES, SHEAR STRESSES AND DENSITY VARIATIONS OF SAND/CLAY MIXTURES

7.1 Executive Summary

In an effort to generalize sediment transport functions for sand-clay mixtures, a series of tests was conducted in the Sediment Erosion Rate Flume (SERF). Results from the tests show that shear stress on sand-clay mixtures corresponds to roughness such that as roughness (average sediment diameter) increases, shear stress increases. Work in this study provides some data for the question of suspended particle effects on shear stress. This study showed that for a smooth wall, as suspended particle concentration increases, shear stress does not necessarily correspondingly increase. Erosion rate testing was inconclusive. Generally, erosion rate testing showed that sand-clay mixtures' erosion response is sensitive to how the sand-clay mixtures are initially created. Changes in initial water content and compaction methods affect erosion rate as much as or more so than sand-clay ratio. More research, particularly on natural samples, is needed to generalize the erosive behavior of sand-clay mixtures.

7.2 Review of Relevant Background and Motivation for Research

As discussed in Chapter 2, the EFA-SRICOS method for predicting scour depth presumes that a relationship exists between erosion rate and shear stress for an eroding bed material. Some particle-like erosion models have been proposed over the years for cohesive bed materials. (Einstein 1950, Mehta and Lee 1992, Van Prooijen and Winterwerp 2008, etc.). Most of these erosion models presume a uniform sediment diameter. Some models have been developed for determining the critical shear stress of cohesive bed materials that are composed of mixed elements (Barry 2003, Sharif 2002), but sediment transport models for mixed-bed sediments have yet to be developed. If a direct erosion rate vs. shear stress relationship exists for mixed bed materials, then it may be possible to determine critical shear stress and use a particle-like stochastic erosion model. If a direct erosion rate vs. shear stress relationship does not exist for these materials however, application of a particle-like erosion model may be inappropriate.

The Rotating Erosion Test Apparatus (RETA) database described in Chapter 6 was obtained by running tests on materials that conform to the stringent guidelines associated with RETA testing. For a material to be tested in the RETA, it must erode nearly uniformly from top-to-bottom, it must be strong enough to stand up on its own, and it must be strong enough to withstand the forces associated with the RETA's spinning annulus. Generally speaking, materials that meet these requirements are stiff, hard, strong, rock-like earth materials. The Bull Gator Rock described in Chapter 5 was engineered to mimic the characteristics of hard, stiff, strong, rock-like materials that constitute successful RETA tests.

The distinction between rock-like cohesive sediments and weaker cohesive sediments is important. RETA database analysis showed a split between rock-like and particle-like erosive behavior for samples that are strong enough to withstand a test. For weaker cohesive bed material such as sand-clay mixtures, there is limited available data.

The goals then of this phase of research are then two-fold. First, is to determine how mixed-bed earth materials behave. Do they obey a direct erosion rate vs. shear stress relationship or do they exhibit more rock-like erosion qualities? If mixed-bed earth materials respond to a direct erosion vs. shear stress pattern, is it possible to generalize this behavior? For example, may it be possible to claim that an increase in clay content decreases the erosion rate? Barry and Sharif indicate that varying clay contents in a sand-clay mixture affect critical shear stress, so it may be possible that varying clay contents also affects erosion rate.

7.3 Materials and Procedure

The Sediment Erosion Rate Flume (SERF) was used exclusively to obtain erosion rates and shear stresses for a range of sand-clay mixtures. Although originally the plan was to conduct tests at 12.5% clay intervals from 0% clay to 100% clay, unexpected testing results forced investigators to limit to the SERF dataset to 0% clay, 25% clay, 50% clay, 75% clay, and 100% clay.

7.3.1 Materials

Edgar Plastic Kaolinite (EPK) and industrial sand were obtained from Edgar Minerals, Inc. of Edgar, FL. Grain size distributions for these materials are shown in Figure 7-1 and Figure 7-2:

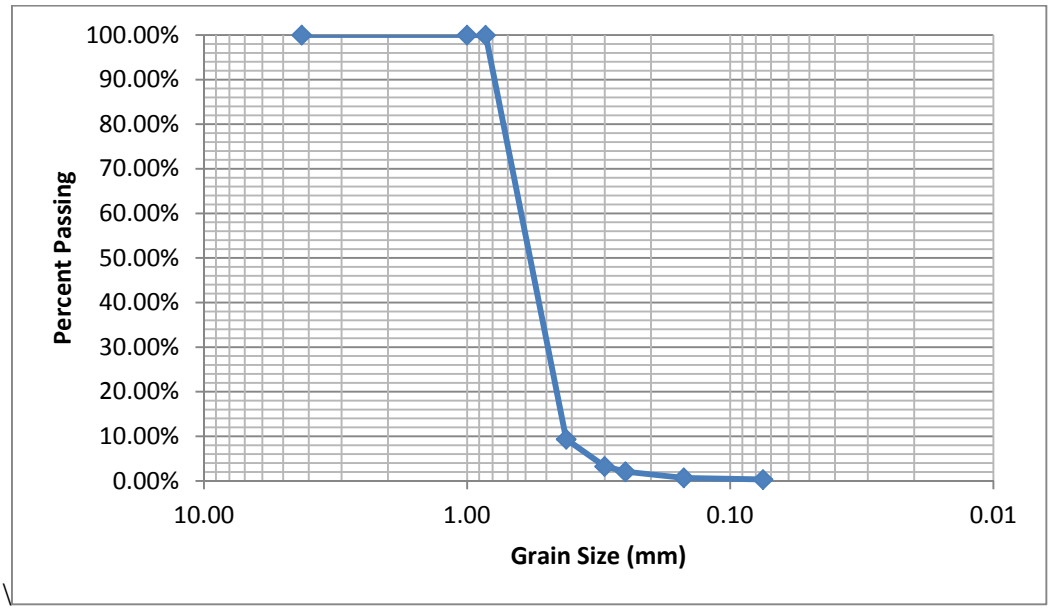

Figure 7-1. Grain Size Distribution for Sand Used During Sand-Clay Tests

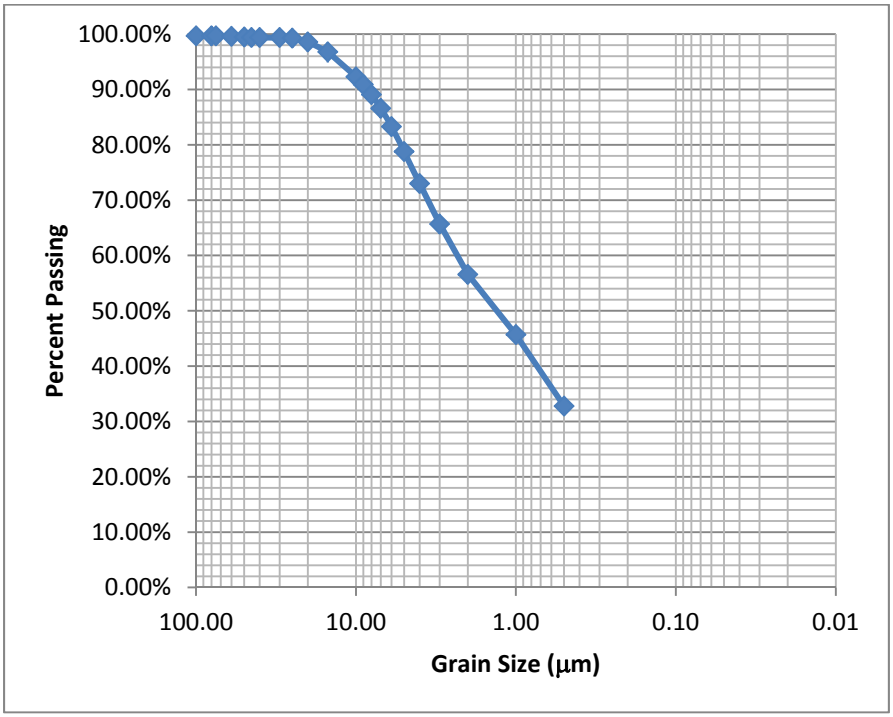

Figure 7-2. Grain Size Distribution for EPK Used During Sand-Clay Tests

7.3.2 Shear Stresses

Shear stresses needed to be determined for the bed materials to be used during the test. Recall from Chapter 4 that shears stress is dependent on roughness. Because of this, a similar series of shear stress tests was conducted on sand-clay mixtures using the shear stress sensor. Sensor discs were prepared at 12.5% clay increments from 0% clay to 100% clay so that a relationship between flow speed and sample roughness could be determined. This 12.5% distribution corresponds to the original testing plan.

Two different test-disc preparation procedures were used during shear stress testing. The first round of disc-preparation used the method described in Chapter 4. Sand and clay were weighed in the appropriate proportions and mixed as dry materials in a small Tupperware container. Plastic test discs were coated with JB Weld epoxy. Then, the sand-clay mixtures were spread out over a table and the acrylic test discs were pressed onto each of the sand-clay mixtures. At least three test discs were made for each sand clay mixture to insure that a true representative roughness was captured from each mixture batch.

When epoxy is spread on the plastic test discs, the goal is to spread it evenly, but despite best efforts, sometimes small ripples (thickness less than the diameter of the pinhead) will be formed as the epoxy is spread. When sand content is relatively high, these ripples are masked because the diameter of a sand grain is much larger than the diameter of a ripple. When sand content is low however, the diameters of clay particles are on the same order of magnitude as the size of the ripples. As a result, when the clay particles stick to the plastic test disc, small epoxy ripples are exposed, thereby slightly falsely increasing the test-disc's roughness. To combat this issue, a second disc-preparation method was invented. Fiberglas resin was poured into 50 mm molds. Then, the sand-clay mixtures were sprinkled onto the fiberglass before it dried. Because the planed fiberglass should be self-leveling, it was thought that pouring a sand-clay mixture onto the fiberglass before it dried would create a ripple-free sample.

This fiberglass method worked well when sand content was high, especially under 100% sand conditions. Unfortunately, as sand content was reduced and clay content increased, this method became much less successful. Under higher clay content conditions (anything above 12.5%), the presence of clay particles interfered with the fiberglass hardener. The result was that the test discs either did not dry properly, or the discs dried at differential rates. When differential drying occurred, the discs' edges dried much faster than the discs' mid-sections so that when the

discs were removed from the molds, some of the mid-section would "stick" to the molds' top, and a concave surface was created along the discs' front-face.

When put into the shear sensor, this concave disc surface could not be fully leveled with the flume bottom. If the bottom of the concave surface was leveled, the side walls would protrude into the flume such that when water was run through the flume, the shear sensor would also measure a normal component of force on the test disc. If the side walls were leveled with the flume bottom, the bottom would not be level, and the correct shear stress would not be measured either. Tests were conducted on the discs to see how much of an effect this concave surface had on overall results compared to the effect of epoxy ripples. In either fiberglass resin tests or epoxy-glued disc tests, testing on each test disc was repeated at least three times.

7.3.3 Mixing Procedure

Because the goal of this study was to determine sand-clay erosion behavior and attempt to generalize erosion behavior as a function of clay content, samples for testing had to be relatively uniform and repeatable. There was some question as to how to properly mix sand and clay together to produce uniform, repeatable samples. Previous research with sand-clay materials is limited. One reference (Barry 2002) indicates that when he conducted his tests, he made his samples by "adding tap water and working by hand." He does not indicate how much tap water, but he does describe his bulk density after the sample has been prepared.

Rather than use a target density procedure which would be difficult to duplicate, especially when making a SERF piston-cylinder sample, different procedures were developed. First, investigators tried to mix sand and clay dry and slowly add water to the samples from the bottom-up (as with Bull Gator Rock). The result was a soup-like mixture with little apparent bonding between sand grains and fine sediment. Eventually, investigators realized that if water was added to the sand-clay mixture as it was mixed, sand and clay began to flocculate. The obvious question became how much water to add during mixing? Rather than pick an arbitrary amount of water, investors settled on using an already established parameter – the optimum water content based on a Proctor Test (Figure 7-3).

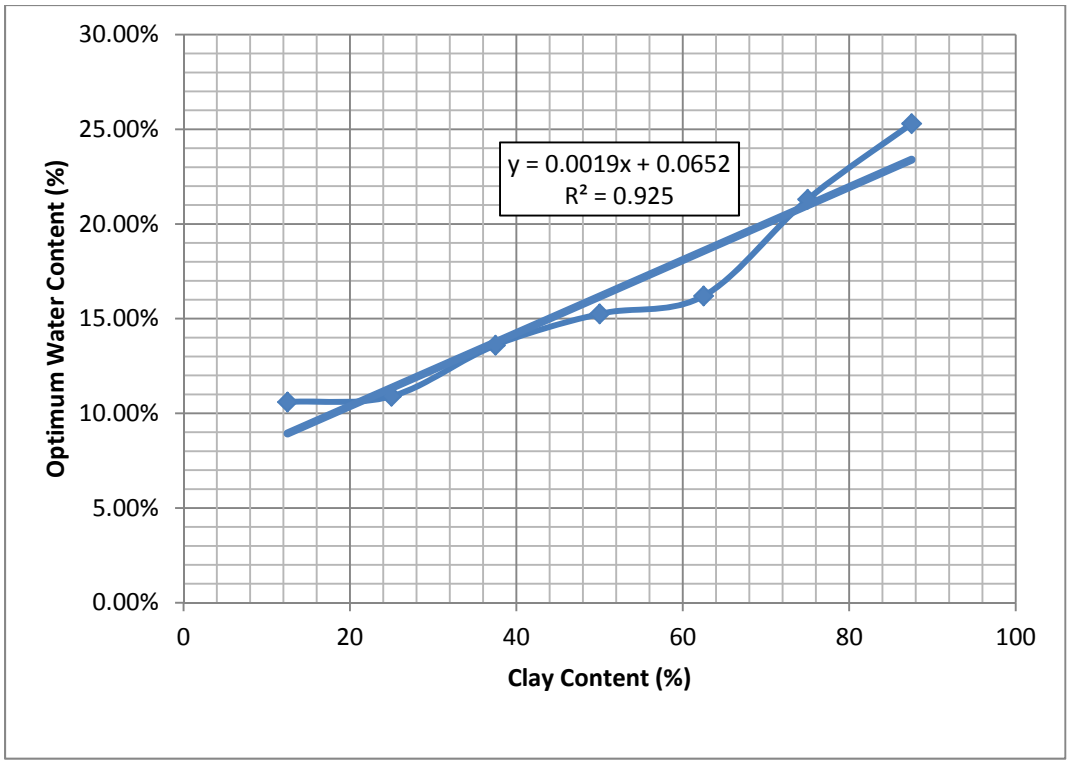

Figure 7-3. Optimum Water Content vs. Clay Content

Because the 100% sand sample does not have any cohesive material in it, optimum water content could not be obtained. Because of this, sand mixing procedure was slightly different from sand-clay mixing procedure. The sand mixing procedure and sand-clay mixing procedure are given below:

7.3.3.1 Sand Mixing Procedure

1. A SERF piston cylinder was thoroughly cleaned to eliminate contamination from other sand or clay particles. The piston was inserted into the cylinder and its O-rings were thoroughly greased.

2. The weight of the piston-cylinder was recorded.

3. The distance to top of sample was recorded and divided by 4. Then, the cylinder was filled ¼ of the way to its top.

4. A 2.5 lb. compaction hammer was used to deliver 17 blows to the sample. This blow count and hammer weight was based on the compactive effort delivered during Proctor tests. Because the SERF sample is smaller than the sample for a Proctor mold, calculations were developed to ensure that the same compactive effort was used under both conditions.

5. Once the first sample lift had been completed, a second, third, and fourth lift were added to the sample and compacted with the same blow count used in (3).

6. The 4th lift was planed with the sample-cylinder surface.

7. Water was slowly added to the sand-clay sample using a burette, a tube, and a small plastic pipe fitting. Water flow rate was less than 0.1 mL/sec.

8. Once the sample had been fully saturated (as evidenced by water coming out of the top of the sample), the sample was weighed so that its density was known.

7.3.3.2 Sand-Clay Mixing Procedure

1. The volume of the piston-cylinder was computed and multiplied by an assumed worst-case total density of 2.65 g/cm^3. This number was multiplied by the percent clay to get the required mass of clay and it was multiplied by percent sand to get the required mass of sand.

2. The appropriate mass of sand and clay were weighed using an electronic balance.

3. Sand and clay were evenly and slowly poured into a mixing bowl and the mixer was turned on "low" for approximately five min. Halfway through mixing, the mixer was stopped and the sides of the bowl were scraped so that any material on the sides would be moved toward the center of the bowl.

4. The mixer was turned on again, and half of the water required to achieve optimum water content was measured with a graduated cylinder and added to the mixing bowl.

5. Once the mixer had run for two minutes, it was stopped, scraped, and restarted. Then, the ¾ of the remaining water was added to the bowl.

6. After two minutes, the mixer was stopped and scraped again.

7. The mixer was restarted, set to "high," and the rest of the water was added. The mixer was allowed to blend for another 2 minutes.

8. The sand-clay mixture was added to the piston-cylinder until the piston-cylinder was ¼ full.

9. Using the modified 2.5 lb. Proctor hammer, 17 blows in a circular pattern were applied to the sample.

10. Steps (9) and (10) were repeated for lifts of ½ full and ¾ full. For the final lift, a collar was placed over the tube, and the tube was overfilled such that material extended approximately ¼ above the lip. Again, 17 blows were applied to the sample.

11. A metal screed was used to level the sample with the top of the piston-cylinder.

12. A small piece of remaining material was placed in a water content canister, and the canister was placed in an oven at 125^{o}F so that water content could be measured.

13. The sample was attached to a burette-valve device and filled from the bottom-up so that until it was saturated. Saturation was defined as water flowing out from the top of the sample.

14. The final mass of the sample was recorded.

15. The sample was placed in the SERF.

7.3.4 SERF Testing

The procedure for SERF testing is outlined in the operations manual, but in brief, the following procedure was used during tests:

1. The sample was loaded into the SERF such that the two 1.0 mm cutouts along the top of the sample cylinder lined up with the lasers.

2. The motor and motor platform were slowly moved into position.

3. The SERF was filled with water.

4. Once the flume had been pressurized, the sample was allowed to slightly protrude into the flume.

5. A high flow rate was used to re-level the sample with the flume's bottom.

6. The flume pumps were started at a low flow rate. Flow speed was incrementally increased until incipient motion was detected.

7. Because tests were run with sand-clay, the lasers needed to be used exclusively during SERF tests. Therefore, the lasers were turned on, and the test began.

8. At the end of the SERF test, once the sample was empty, a new sample was prepared, and steps 1-7 were repeated.

7.3.5 Procedural Variations

In the preceding SERF discussion, Step 7 is intentionally described vaguely. At first, the plan was to vary flow rates randomly from 0 Pa to a shear stress where erosion rate was approximately 1.0 mm/s. The 1.0 mm/s erosion rate criterion was chosen because the laser-motor system cannot keep up with erosion rates higher than this. At each flow rate and shear

stress, erosion rate would be recorded, then the flow rate would be changed, and the procedure would repeat.

This procedure assumes that a sample will erode uniformly from top-to-bottom. As will be described in Section 7.4, this did not happen. Instead, erosion rates varied as a function of sample depth. Because of localized hard patches where bulk density increased, which corresponded to depths at which the modified Proctor hammer was used, erosion was non-uniform. To capture this behavior, eventually instead of using several shear stresses on one sample, one shear stress was tested per sample.

Because of these differential erosion rates, investigators tried to develop samples that would respond more uniformly. During mixing, water contents were modified so that double the optimum water content was used to determine if mixed water content affects erosion behavior. For some clay contents, a third batch of samples were made where the number of lifts during mixing was reduced from four lifts to two, while the blow count delivered per lift was doubled to determine if lift height affected sample erosion or uniformity.

7.4.6 Density Profile Tests

Because of the differential erosion rates, a series of samples were prepared where density profiles were measured. To run these tests, the samples were mixed according to the procedure outlined in Section 7.3.3. Then, samples were extracted from their molds and cut into 1.5 cm segments using a modified coping saw. Instead of a typical saw blade, the modified coping saw used a three-strand braided 28-gauge wire. The sample segments were weighed, dried, and reweighed to give both dry and wet densities as a function of sample depth. Results were compared with lift depths recorded during sample preparation.

7.4 Experimental Results and Analysis

Experimental results are divided into three segments:

1. Results from shear stress tests
2. Results from SERF tests
3. Results from Density Profile Tests

7.4.1 Shear Stress Tests

Shear stress experimental results are divided into results from the epoxy-glued discs and results from the fiberglass resin discs.

7.4.1.1 Epoxy-Glued Discs

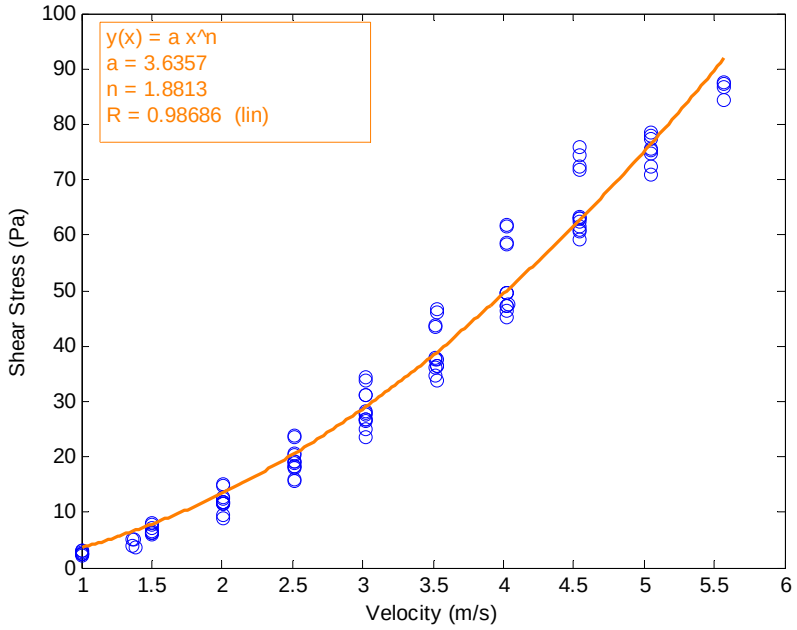

Figure 7-4. Shear Stress vs. Velocity for 0% Clay Epoxy Glued Disc

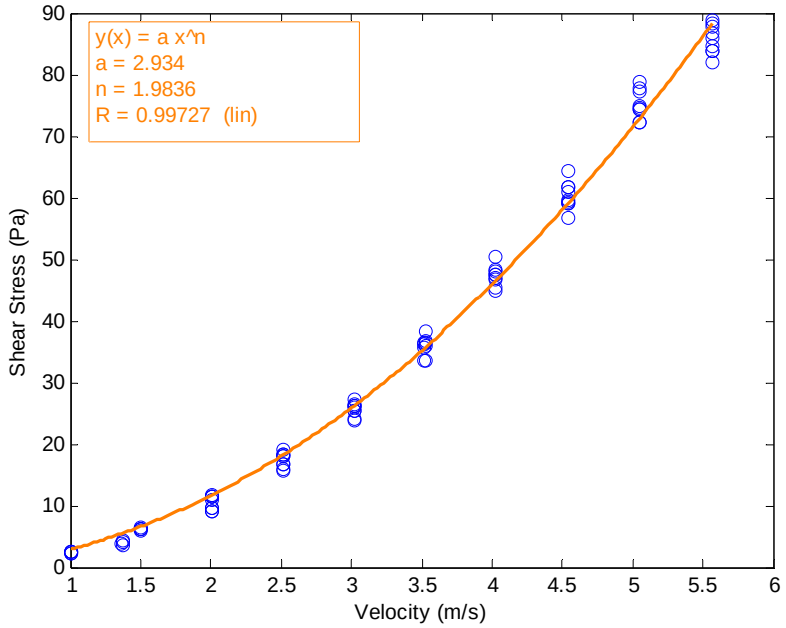

Figure 7-5. Shear Stress vs. Velocity for 12.5% Clay Epoxy Glued Disc

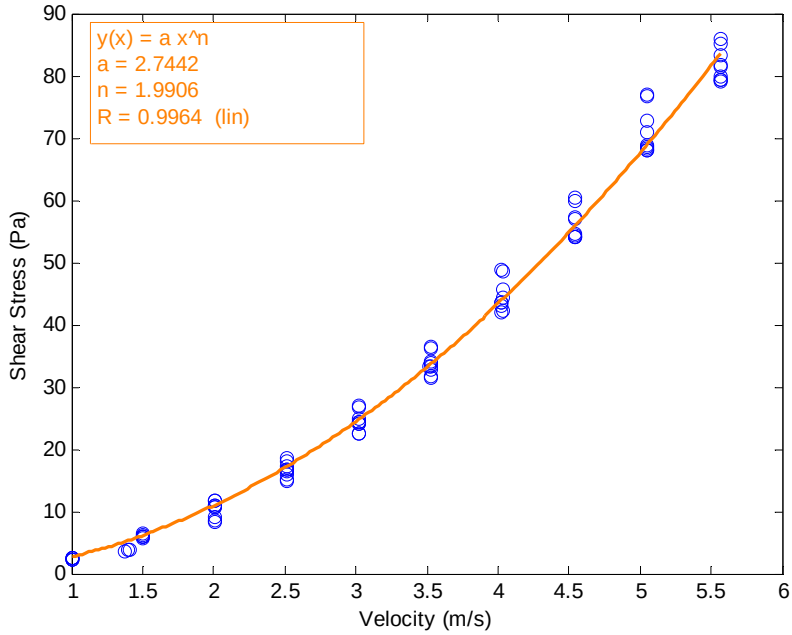

Figure 7-6. Shear Stress vs. Velocity for 25% Clay Epoxy Glued Disc

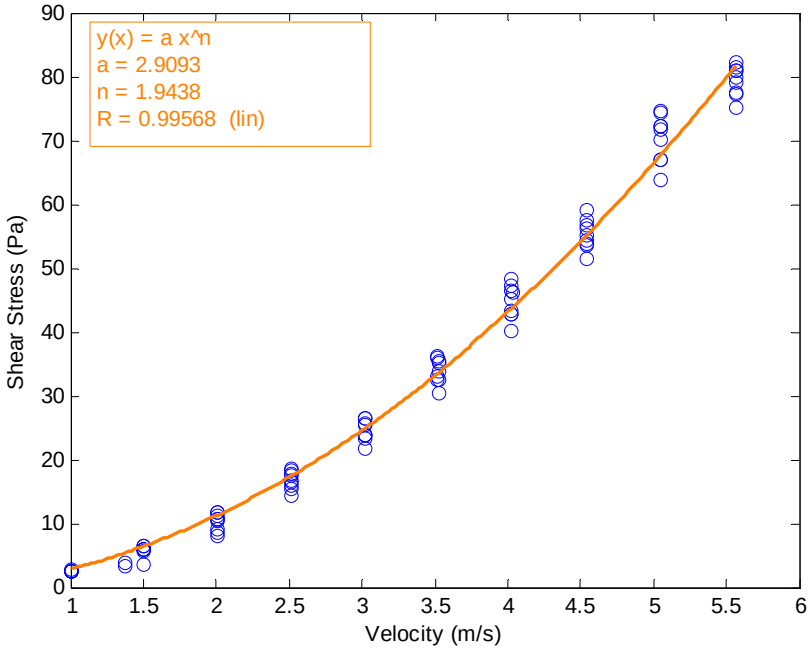

Figure 7-7. Shear Stress vs. Velocity for 37% Clay Epoxy Glued Disc

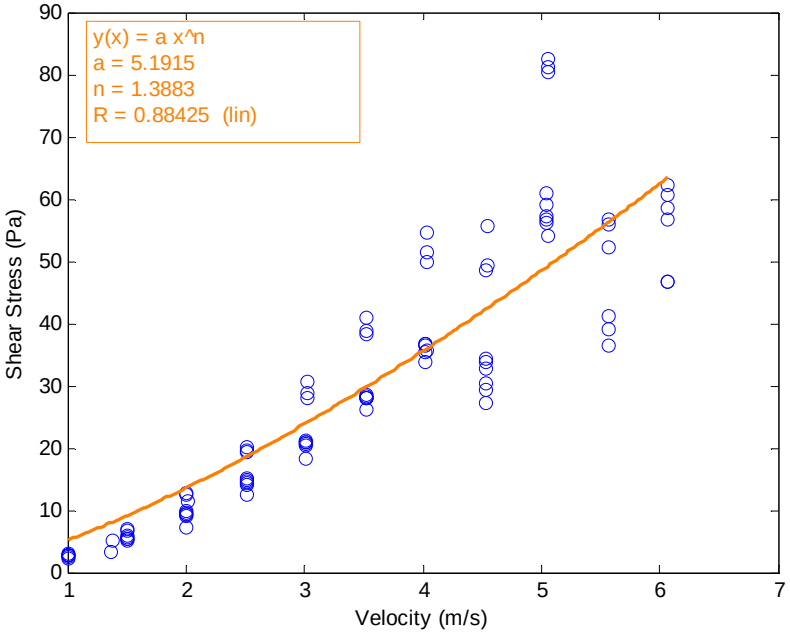

Figure 7-8. Shear Stress vs. Velocity for 50% Clay Epoxy Glued Disc

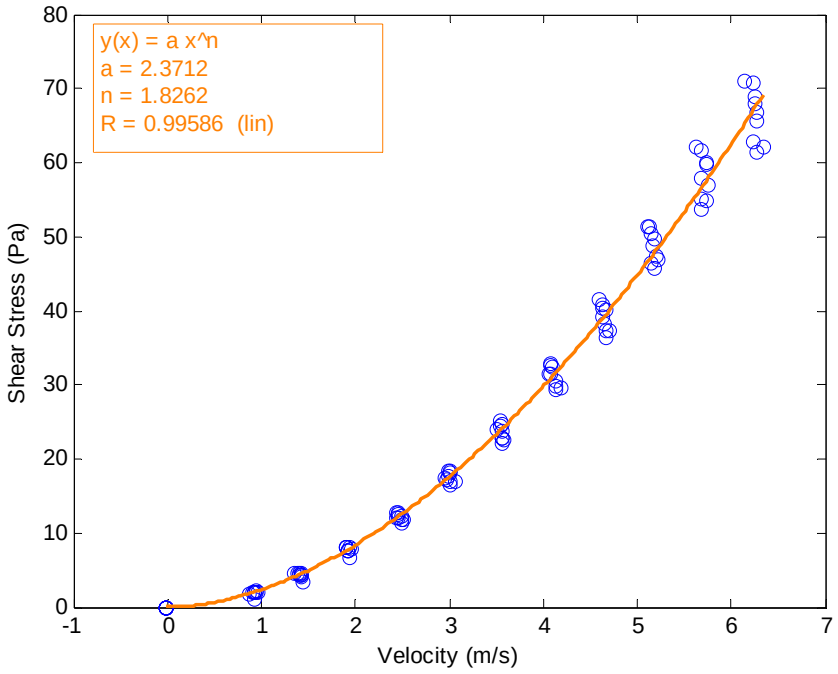

Figure 7-9. Shear Stress vs. Velocity for 62.5% Clay Epoxy Glued Disc

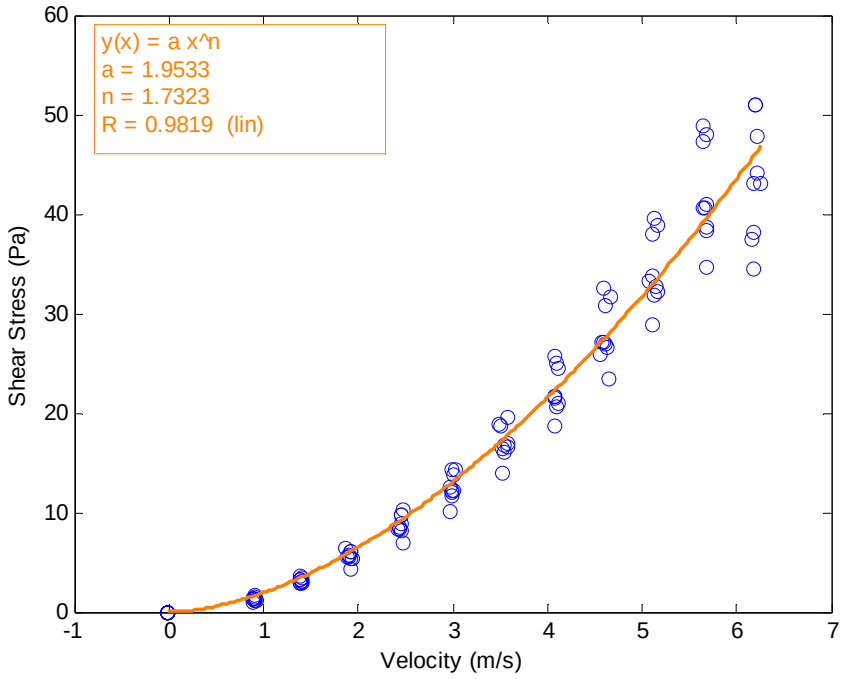

Figure 7-10. Shear Stress vs. Velocity for 75% Clay Epoxy Glued Disc

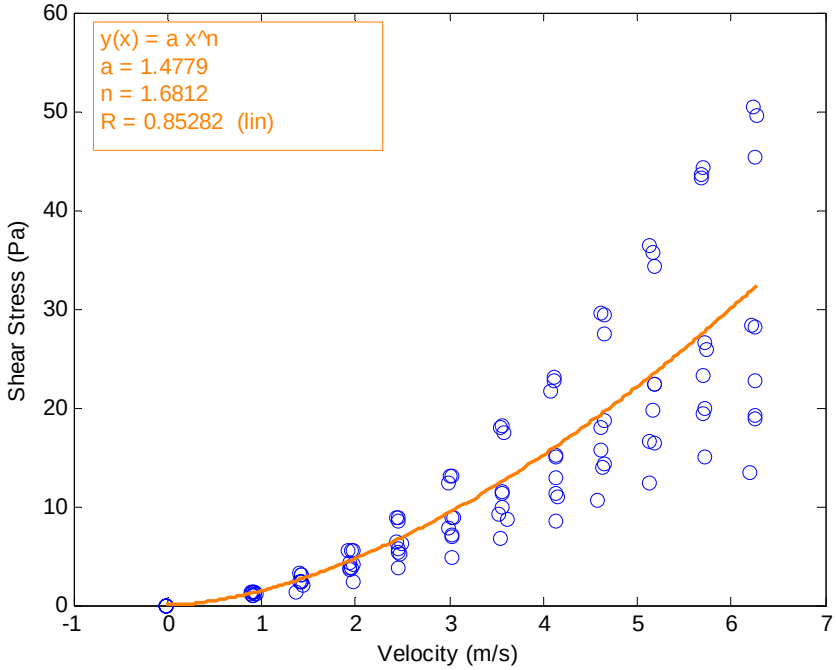

Figure 7-11. Shear Stress vs. Velocity for 87.5% Clay Epoxy Glued Disc

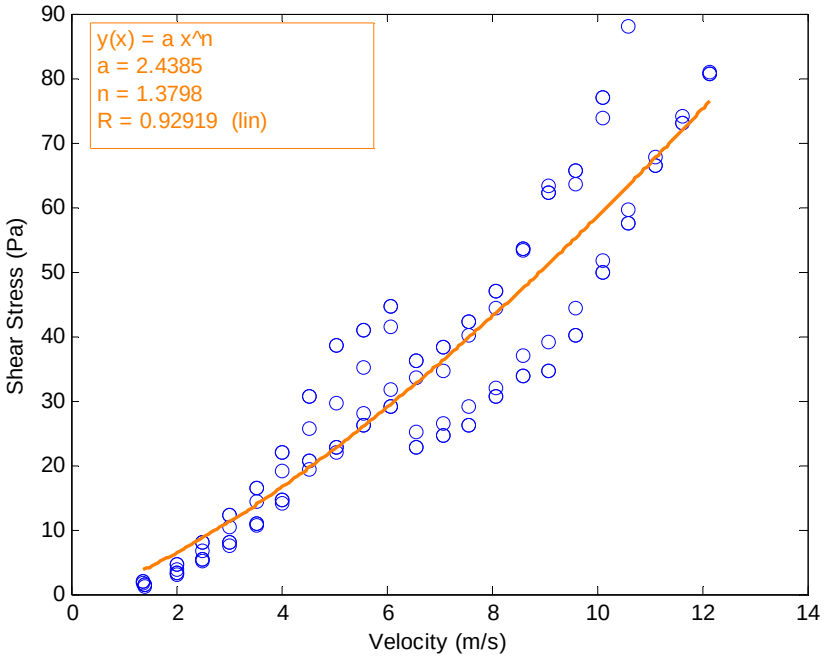

Figure 7-12. Shear Stress vs. Velocity for 100% Clay Epoxy Glued Disc

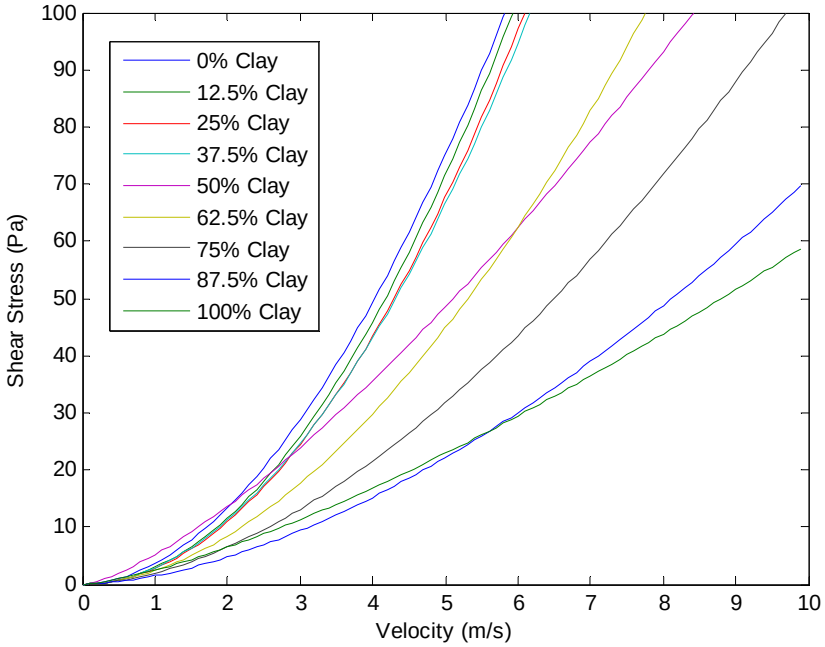

Figure 7-13. Summary Chart Showing Best-Fit Lines for Sand-Clay Epoxy Glued Discs

7.4.1.2 Fiberglass Resin Discs

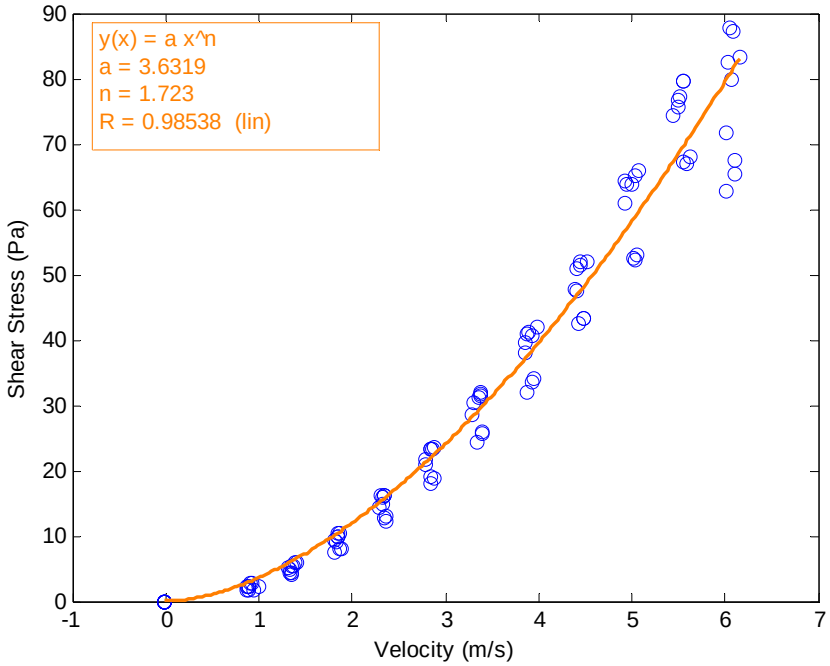

Figure 7-14. Shear Stress vs. Velocity for 0% Clay Fiberglass Resin Test Disc

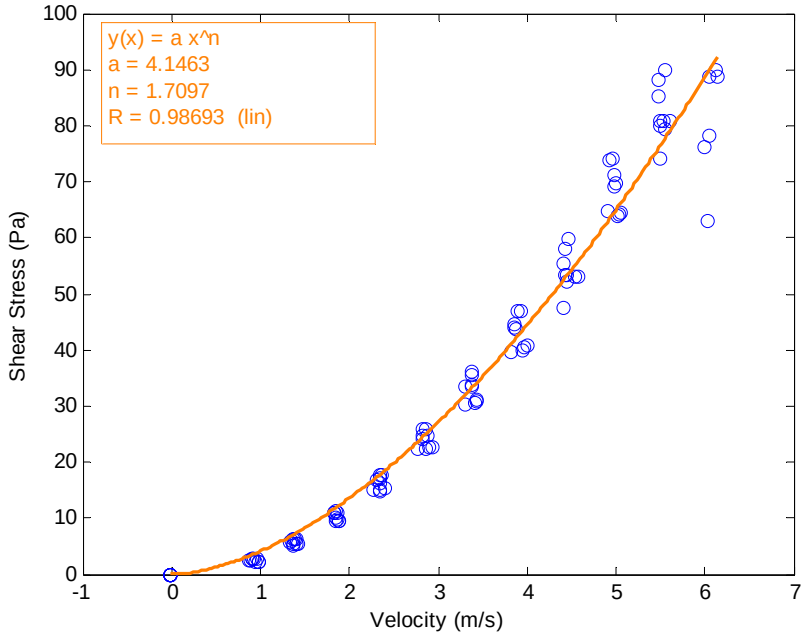

Figure 7-15. Shear Stress vs. Velocity for 12.5% Clay Fiberglass Resin Test Disc

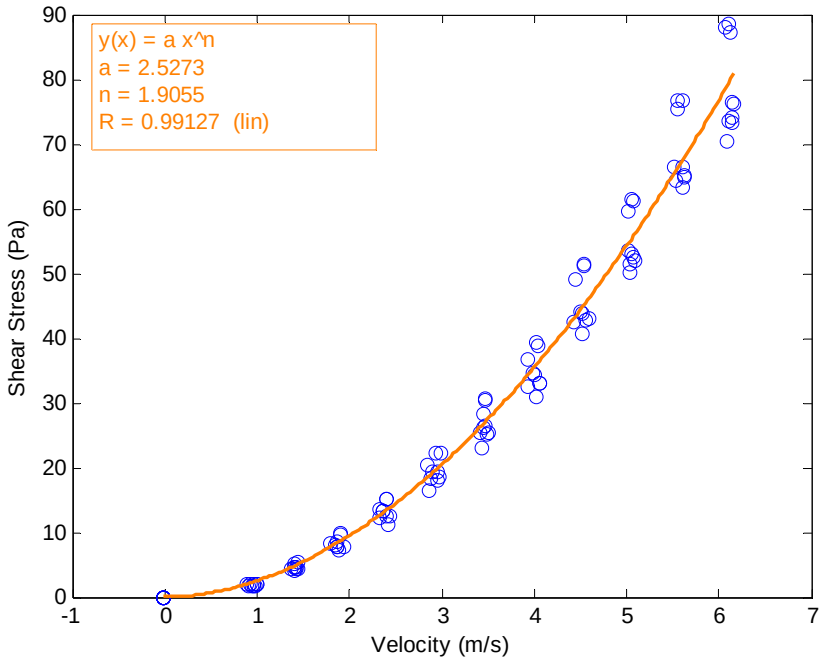

Figure 7-16. Shear Stress vs. Velocity for 25% Clay Fiberglass Resin Test Disc

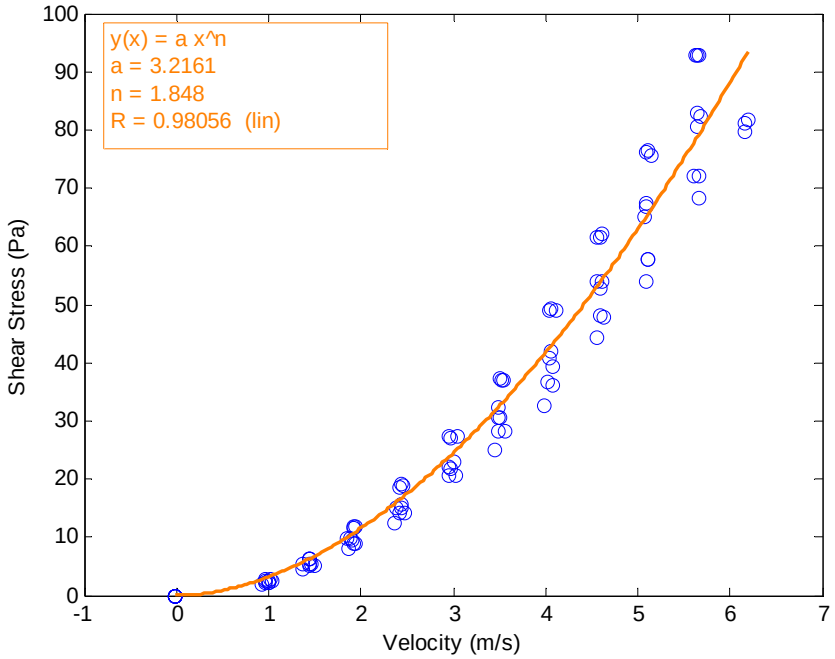

Figure 7-17. Shear Stress vs. Velocity for 37.5% Clay Fiberglass Resin Test Disc

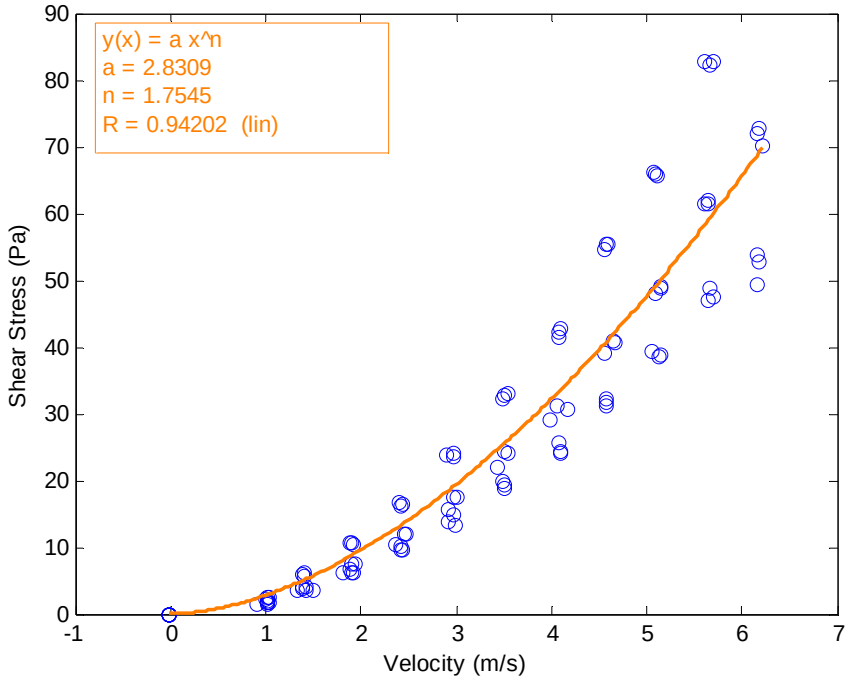

Figure 7-18. Shear Stress vs. Velocity for 50% Clay Fiberglass Resin Test Disc

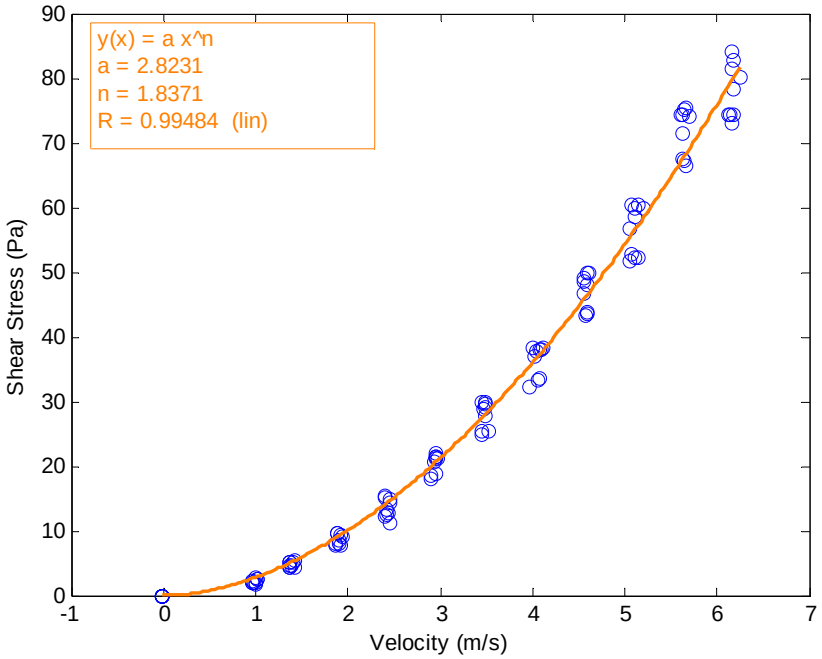

Figure 7-19. Shear Stress vs. Velocity for 62.5% Clay Fiberglass Resin Test Disc

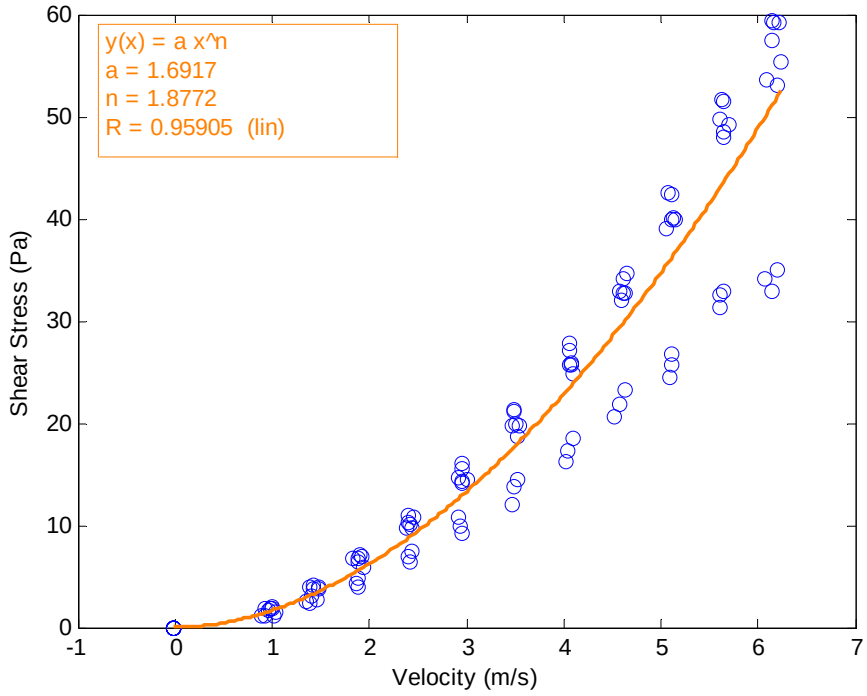

Figure 7-20. Shear Stress vs. Velocity for 75% Clay Fiberglass Resin Test Disc

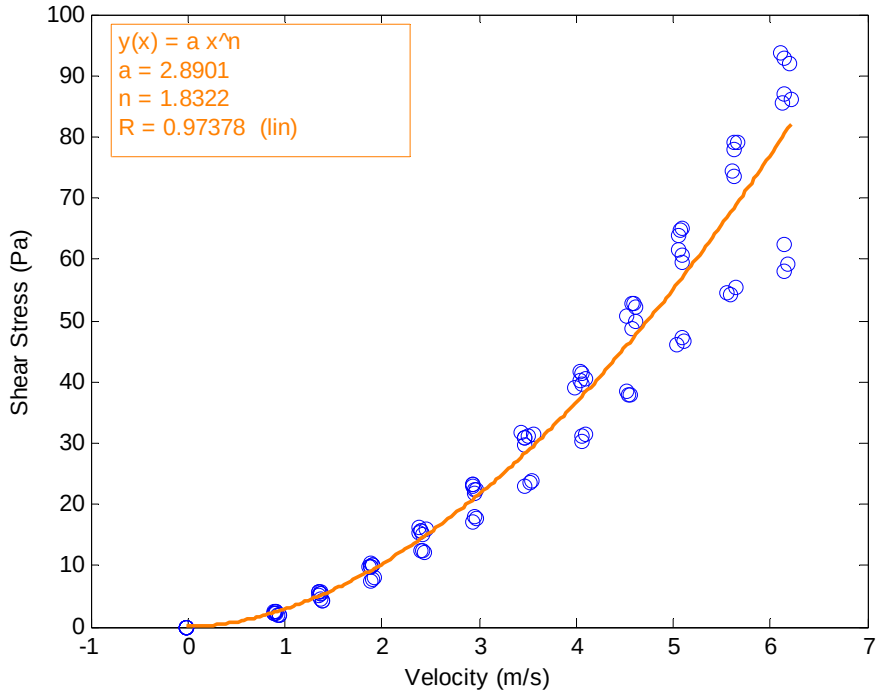

Figure 7-21. Shear Stress vs. Velocity for 87.5% Clay Fiberglass Resin Test Disc

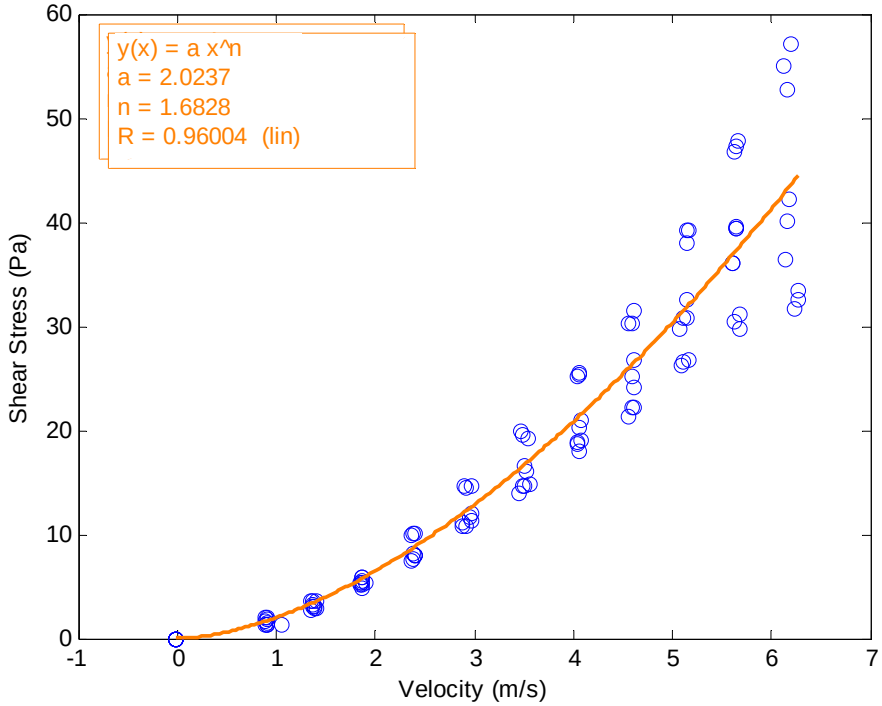

Figure 7-22. Shear Stress vs. Velocity for 100% Clay Fiberglass Resin Test Disc

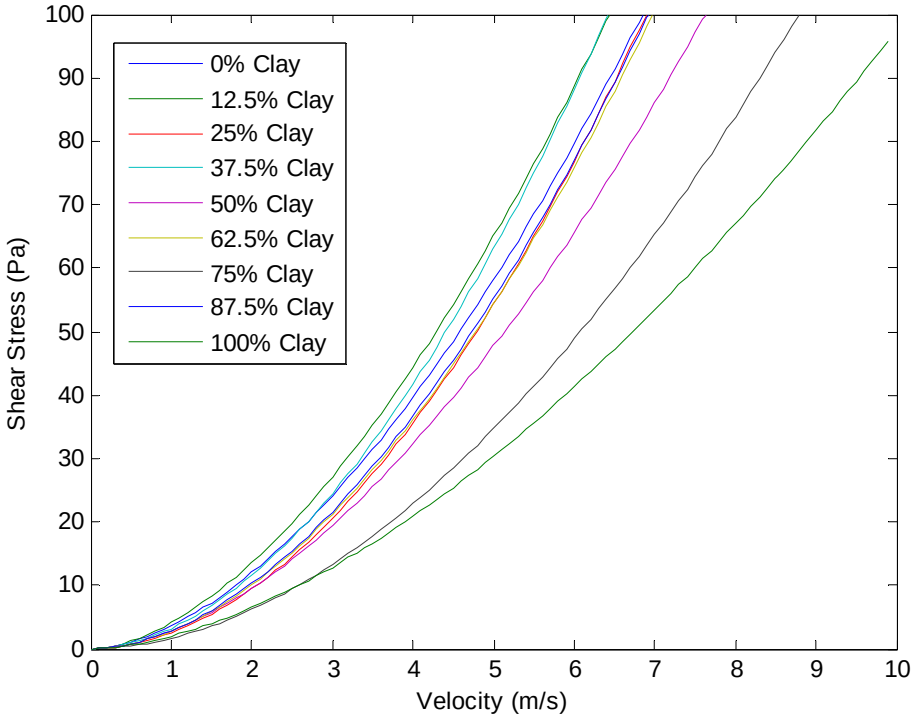

Figure 7-23. Summary Chart Showing Best-Fit Lines for Sand-Clay Fiberglass Resin Discs

Although Figure 7-23 shows that the 100% clay mixture does indeed have the lowest shear stress associated with it, this figure also shows that certain sand-clay percentages may produce higher shear stresses than the shear stresses seen under 100% sand conditions. This may be true under special circumstances, for example, when floc erosion instead of particle erosion is an important erosion mode, but as of yet, there is no known way to predict when this will occur and the purpose of this test was not to predict the floc size that would erode from a sample, but rather, to find the relative shear stress magnitudes along a sample face resulting from simple particle effects. Figure 7-23 shows that when clay content is at 87.5% and when clay content is at 62.5%, shear stress is higher than it would be when there is no clay in the sample. Based on a particle-based roughness rationale, this must be impossible.

These higher shear stress readings then can be attributed to the concave nature of the test-discs. Because an average leveling height was used even though the disc was not level, the discs protruded into the flume somewhat (~1 mm – 2 mm). Even this slight protrusion caused a large increase in the force on the disc because of the added normal component. During the epoxy testing, the discs were precisely level with the flume bottom, and there were no normal forces

acting on them. Figure 7-23 shows no discernable pattern that would indicate a decrease in shear stress that corresponds to a decrease in sand content. This appears to contradict the data shown in Chapter 4 which indicates that as roughness decreases (for a given flow rate), shear stress should also decrease – especially at higher flow rates.

Because of this, the data in Figure 7-23 must be rejected in favor of the shear stresses corresponding to the data shown in Figure 7-13. This conclusion has interesting implications regarding EFA testing because in the EFA procedure, a protrusion of 1 mm into the flume is specified. This data indicates that shear stresses are sensitive to any protrusion into a flume. Because the EFA uses a Moody Diagram to estimate shear stresses on its samples (Chapter 4 verified that this was an accurate method), the shear stress should not be underestimated using this device. But, because a 1 mm protrusion could cause a much higher actual stress on the sample compared with the stress than would be caused with a level sample, the actual stress on a sample would be greater because of the normal component. This in turn would produce a higher erosion rate than usual, and this could lead to an overly-conservative erosion rate-shear stress curve. For example, the protrusion caused by the wave-like 50 mm test disc under 87.5% clay conditions shows over a 100% increase in stress at a moderate velocity of 4 m/s. Because erosion rate-shear stress curves have thus far proven to be mostly linear, this should correspond to an over-prediction of erosion rate by over 100%.

7.4.2 SERF Tests

When investigation into erosion rates of sand-clay mixtures began, the hypothesis was that a repeatable mixing procedure modeled after the Proctor test would lead to samples that eroded uniformly from top-to-bottom. As testing moved from the 0% clay to the 25% clay sample, it became clear that samples were not responding this way. Instead, as clay was introduced, localized portions of samples eroded more slowly than other localized sample sections. Instead of attempting to generalize erosion rate as a function of shear stress and clay content then, research looked instead to explain these localized erosion variations. As a result of this, the same gambit of tests was not necessarily conducted for each sand-clay ratio. The following is a summary of results, some rationale behind the tests that were conducted, and some analysis to explain why results were found as shown.

7.4.2.1 Zero-Percent Clay Mixture

Shear Stresses

The first goal during sand-clay testing was to verify that the SERF was providing the correct experimental results based on historically accepted data – the Shields Diagram. Shields Diagram calculations showed that incipient motion should occur at a shear stress of approximately 0.25 Pa. Three critical shear stress tests were conducted on 100% sand samples using the procedure outlined in the operations manual. Average actual critical shear stress from tests was 0.43 Pa. At first, this looked like a discrepancy.

Analysis of the shear stress sensor shows why it may over predict critical shear stress values. Experience has shown the sensor to be accurate within 0.2 Pa of accuracy (+/-2% F.S.). At lower flow rates, the shear sensor appears to be less accurate than it is at higher flow rates. The strength of the shear sensor lies in its ability to accurately measure shear stresses that are still low at much higher flow speeds. In other words, if a creeping flow is moving past the sensor, it won't pick up this small deflection in the platform-test disc-leaf spring-Servo magnet system. This has to do with the mass of these moving parts, which relative to the small flow speed and the small associated shear stress, is large. Therefore, with the current setup it would be impossible to with 100% accuracy to measure shear stresses at such a low range. When dealing with a shear stress less than 1 Pa, accuracy within 2% is actually quite precise.

The next dataset to consider was Trammel's 2004 data. Here he attempted to verify the pressure drop system within 5% of accuracy by using a Shields Diagram. Chapter 4 shows that especially at higher flow rates, the pressure drop method does not accurately estimate shear stresses in the SERF. Because shear stress can be correlated to a power-law distribution with respect to velocity, at low flow speeds, the pressure drop readings do converge to a curve that appears to be the same.

Trammel verified the pressure drop method (again at low speeds) by measuring the pressure drop on samples that were 1.4 mm, 0.921 mm, 0.696 mm, and 0.508 mm in diameter. In terms of the tests run during this round of testing, the 0.921 mm data and the 0.508 mm data are of interest because they should closely correspond to 1.0 mm data and 0.50 mm data respectively as presented in Chapter 4. Figure 7-24 shows Trammel's data overlaid with data from this study:

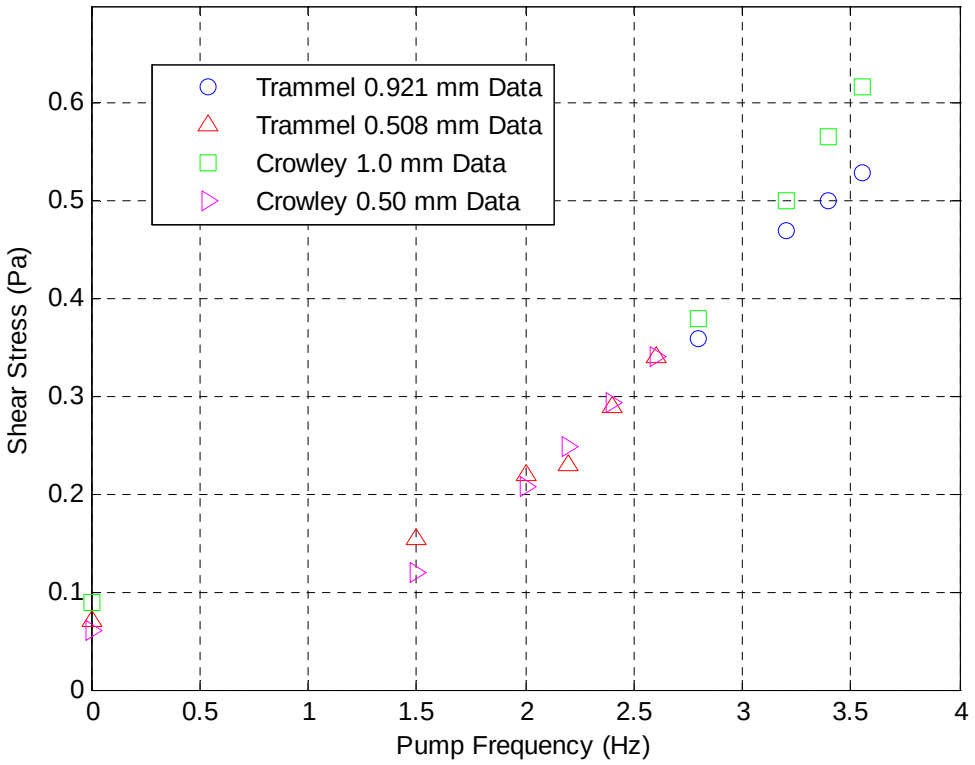

Figure 7-24. Trammel's 2004 Data Overlaid with Data from this Study

Figure 7-24 shows shear stress vs. pump frequency for shear stresses computed by Trammel overlaid against shear stress vs. frequency from the curves presented in Chapter 4. This diagram shows the readings from these two sets of tests are close – on average within 8.63% of one another. The Shields calculations however are extremely sensitive to shear stress values; any deviation – even an 8% deviation at such low shear stress magnitudes – will cause a large deviation in the shear stress entrainment function. This in turn causes a relatively large difference in the computed shear stress which in turn causes a large deviation in overall results.

Trammel's collected his pressure readings with a pressure transducer with +/-2.5psi range at 0.1% F.S. error. This means that Trammel was capturing pressure accurately within +/-0.0025psi or +/-17.24 Pa. Shear stress is related to pressure drop using the following equation:

$$\tau = \frac{\Delta p l w}{(2l + 2w)L} \tag{7-1}$$

In Trammel's case, he had pressure sensors spaced further apart than the current setup (4 ft. or 1.22 m). If one was to ignore the fact that with this setup most of the flume wall along this spacing length was smooth and therefore most of the pressure drop was be caused by smooth rather than rough conditions, the following accuracy calculation would follow:

$$\tau_{ERROR} = \frac{(\pm 17.24Pa)(0.0445m)(0.2032m)}{(1.22m)[(2)(0.0445m)+(2)(0.2032m)]} \tag{7-2}$$

$$\tau_{ERROR} = \pm 0.258Pa \tag{7-3}$$

This calculation shows that Trammel's measurements could only have been accurate within 0.26 Pa – which for some of his measurement shown in Figure 7-24 is less than the shear stress value than he was measuring. Chapter 4 showed how difficult it is to get accurate readings from the pressure drop method, and no spectral analysis or filtering of his data except for the installation of a hard-wired fourth order low-pass Butterworth filter was employed. The fact that because of his pressure port spacing, most of his pressure drop would have been influenced by smooth flume bottom and not the roughened sample portion of the flume. On the other hand, results from the shear stress sensor allowed investigators to conclude that shear stress results were accurate enough to proceed to erosion rate tests.

Erosion Rates

Based on the preceding analysis, an erosion rate vs. shear stress curve was developed based on the shear stress vs. flume velocity curve presented in Section 7.4.1 (Figure 7-25). Rather than use a simple final position minus initial position divided by time calculation to find erosion rate (as was used by Trammel and Slagle), a best-fit least squares regression line was fit to a sample position vs. time plot. Results in Figure 7-25 are developed from the slopes of these trend lines. Results from Figure 7-25 were non-dimensionalized in the same manner in which RETA database results were non-dimensionalized in Chapter 6 (Figure 7-26). A 100% sand sample was allowed to run at a moderate shear stress (3.0 Pa) to verify that erosion rate was the same from top-to-bottom throughout the sample. Since erosion rate was constant throughout the sample,

100% erosion data was taken such that multiple shear stresses were used on one sample. In total, erosion rate tests were conducted on five 100% sand samples.

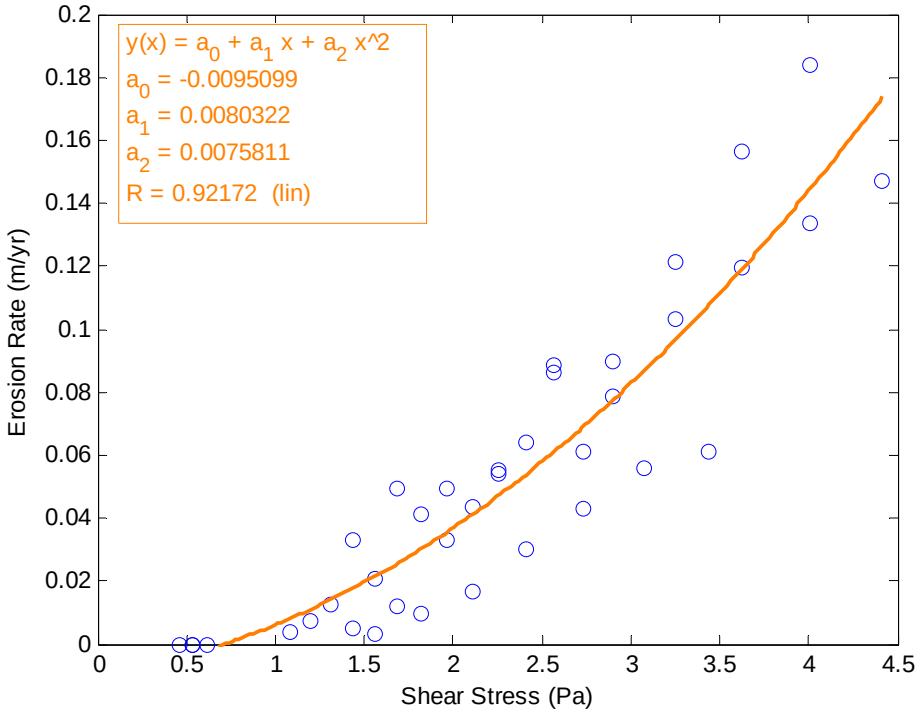

Figure 7-25. Erosion Rate vs. Shear Stress for 100% Sand Sample

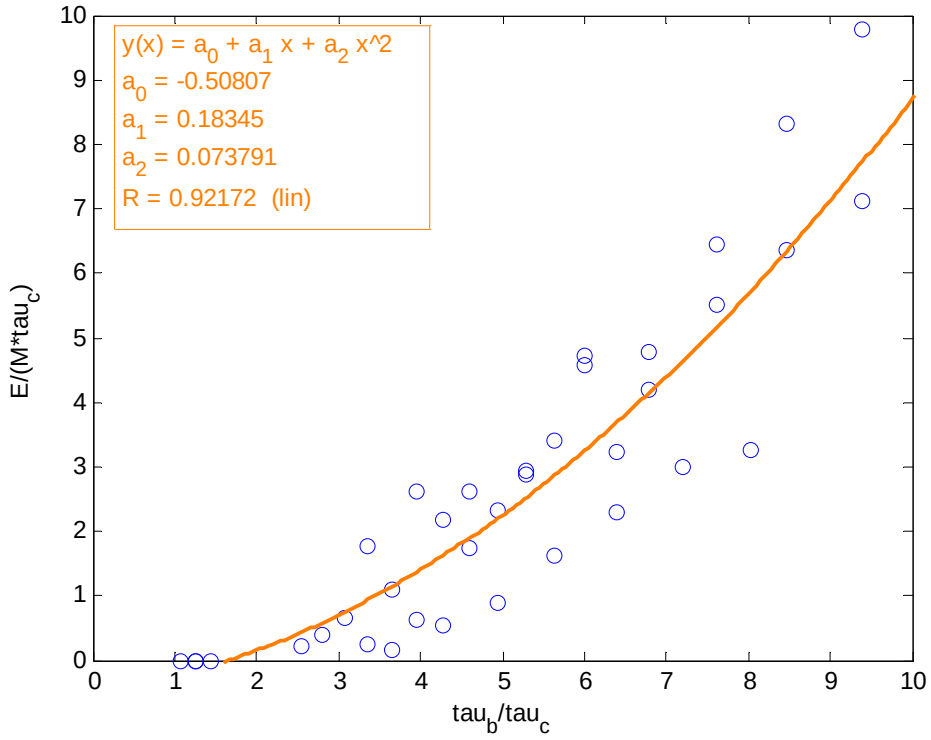

Figure 7-26. Non-Dimensionalized Erosion Rate vs. Shear Stress for 100% Sand Sample

7.4.2.2 Twenty-Five Percent Clay Samples

At first, when the sample mixing procedure presented in Section 7.3.3.2 was introduced, an additional step was added after Step 16. The sample was put into a bucket for 24 hours to insure saturation. However, by mistake, one time samples were prepared at the end of the day on a Friday and tested on a Monday. Over the weekend, it appeared as though consolidation had taken place, as erosion rates were much smaller than the erosion rates shown in previous tests. To determine if allowing the samples to sit upright for 24 hours or more played a role in erosion rate, a sample was prepared and inserted immediately into the SERF. This sample showed a much higher erosion rate than the erosion rates seen with previous samples that had been allowed to soak. Because of this then, a standard needed to be developed, and since investigating consolidation effects is not within the scope of this project, it was decided that zero consolidation would be used as the standard for future testing. In other words, for samples with clay, samples would be prepared and immediately put into the SERF.

The 25% sand-clay mixture was the first time that the lasers described in Chapter 3 were forced to perform sample advancement on their own. Because erosion rates were moderately quick, the issues that were found in using the lasers with the Gator Rock were nearly non-existent with the clays. The lasers worked as designed. The only downside to the lasers was that at higher flow rates, the motor could not keep up with the analog blips coming from the lasers. Therefore, sometimes when erosion rate was high, there would be a backlog of advancement that should have happened but could not. Once erosion rate leveled out, this would cause sample penetration into the flume, which in turn would cause the sample to erode even faster and exacerbate the problem. However, this was only an issue at high flow speeds (relative to the erosion rate), and if one extrapolates these erosion rates over a year, the result returns kilometers of erosion per year, which is not possible.

For the 25% clay data run, procedures remained the same as they had for the 0% clay data run as far as testing the effects of multiple shear stresses per sample. However, during testing, investigators noticed that with the 25% clay sample, as more of the sample eroded from the piston-cylinder, the sample appeared to exhibit hard layers. Whenever these hard layers were encountered, qualitatively it was observed that erosion rate slowed down. Eventually, these hard layers would erode, albeit through a more undercutting, normal stress induced, rock-like erosion mechanism, and once the layer had been removed from the sample, erosion would continue on as normal. Because of this layered effect, at first results were confusing because at first, before the layered effect was discovered, it appeared as though sometimes lower shear stresses caused higher erosion rates.

It was evident that the layers probably corresponded to the four-lifts that were used in sample preparation by analyzing a time-series of erosion data and allowing the same shear stress to be run over the entire length of a sample (Figure 7-27). The four-steps shown in this diagram should not be a coincidence, especially because this pattern was seen on the 25% clay samples. Of note though is that this four-step effect is only visible during moderately-paced erosion rates. When erosion rate is high (Figure 7-28) or erosion rate is low (Figure 7-29), the sample responds much more uniformly.

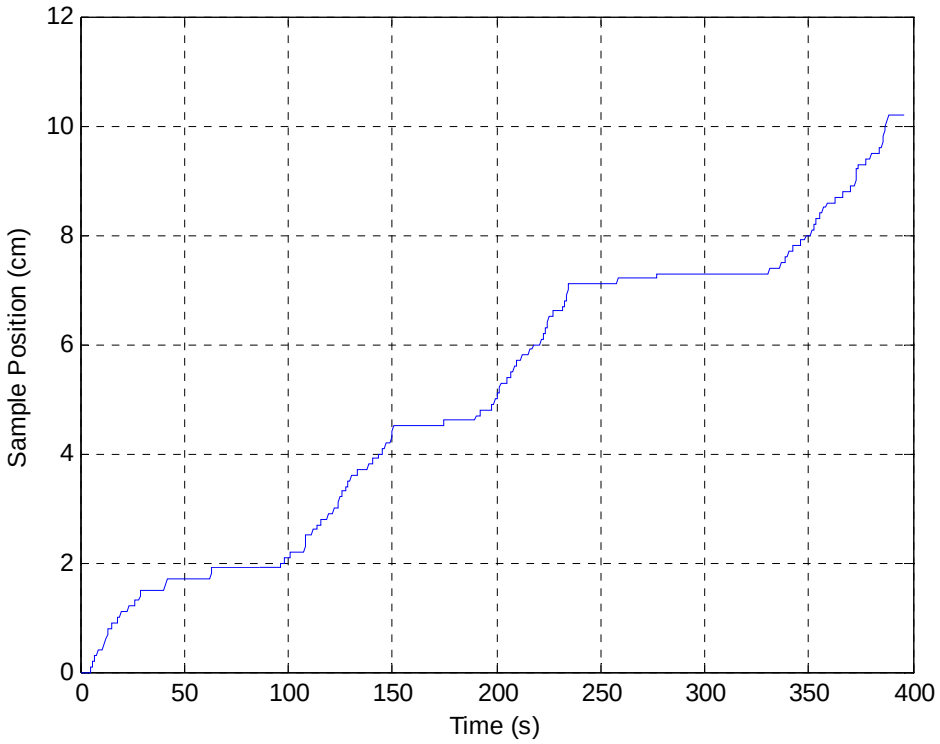

Figure 7-27. Sample Position vs. Time for 25% Clay Mixture at 13.4 Pa

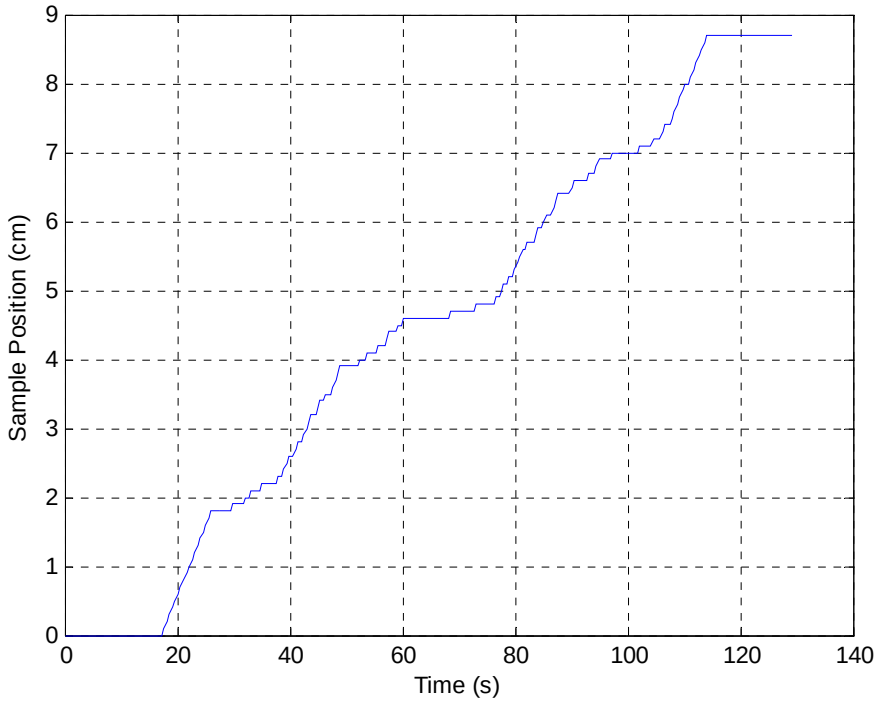

Figure 7-28. Sample Position vs. Time for 25% Clay Mixture at 40.0 Pa

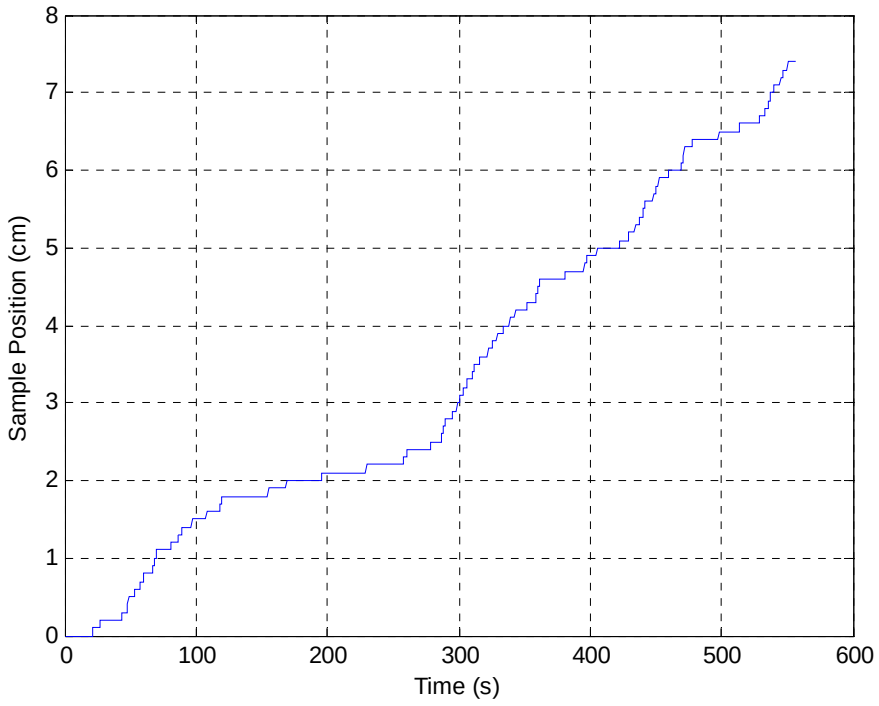

Figure 7-29. Sample Position vs. Time for 25% Clay Mixture at 3.37 Pa

The interesting thing regarding this pattern is that the best-fit line method for determining erosion rate, which was an effective indicator of erosion rate beforehand, is not necessarily relevant under these conditions even though the R^2 value is close to 1.0. Figure 7-27 shows two different erosion rates – one slow and one fast.

The slow erosion rate can be explained by the initial portion of a rock-like erosion mode. During the first part of rock-like erosion, little actual particle movement is seen. Rather, water flowing past the sample surface serves to weaken the top layer (which can be viewed as a large chunk of material) by loosening small localized portions of it. Eventually, channels developed along certain parts of the sample face, and once these channels developed, flow was concentrated into the sample through them. These channels are analogous to cracks or fractures that form on a rock face. Eventually, the undercutting flow caused by the channels causes a large chunk of material (or sometimes most of the sample surface) to erode, and once this happened, the rapid advancement of the sample into the flume would occur. During rapid advancement, additional chunks and blocks of material would be removed from the material surface as quickly as the material advanced. This would continue until another hard layer was exposed. Then, erosion rate slowed down and the beginning stages of rock-like erosion occurred again. The rapid

sample advancement portion of erosion is similar to a particle-like scenario. The critical shear stress for this relatively loose, relatively weaker material has already been exceeded, and because of this rapid erosion of large sections of material is seen. This back-and-forth particle-like vs. rock-like erosion pattern continued until the sample was gone.

In addition to the 3.37 Pa, 13.4 Pa, and 40.0 Pa results already presented using the first mixing procedures, experimental results were obtained at 30.0 Pa and 53.2 Pa (Figure 7-30 and Figure 7-31).

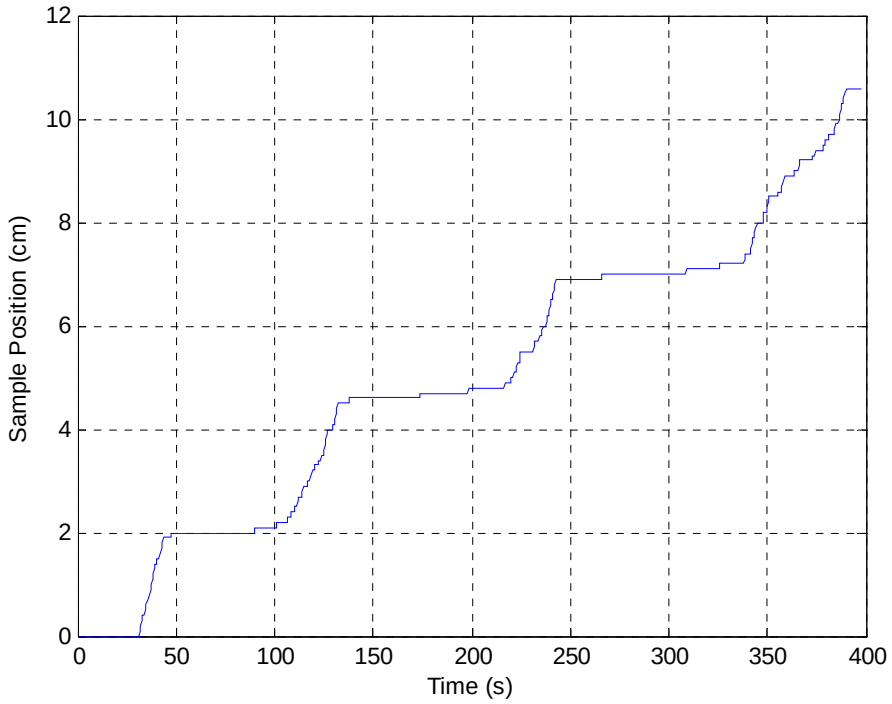

Figure 7-30. Sample Position vs. Time for 25% Clay Sample at 30.0 Pa

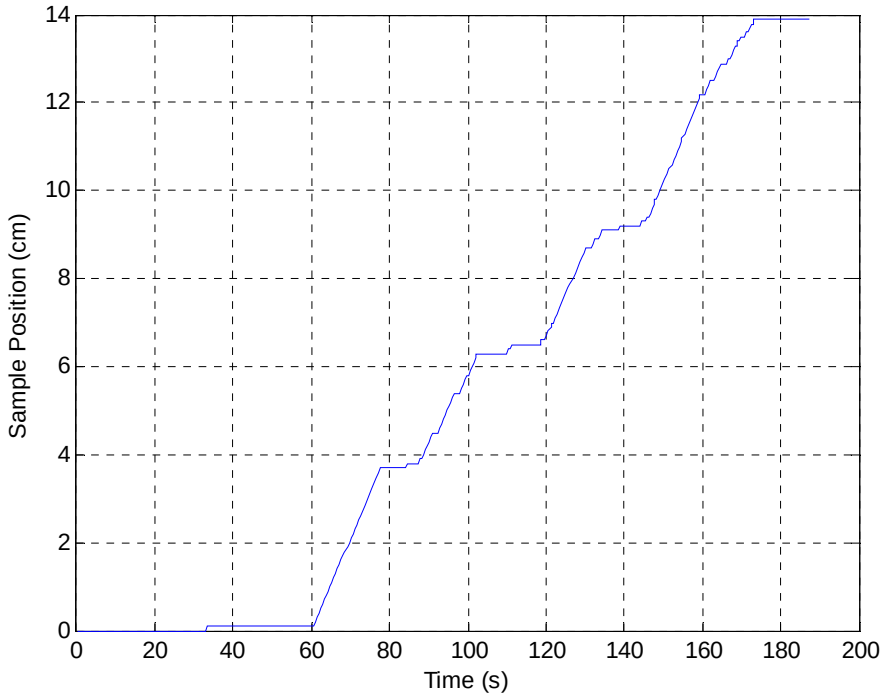

Figure 7-31. Sample Position vs. Time for 25% Clay Mixture at 53.2 Pa

If the hardened layers were caused by the initial stages of rock-like erosion, and the hardened layers were localized, the conservative solution to the problem should be to eliminate the hardened sections from the piston position curve and use the rapid advancement portions of the curve to define an erosion rate. This should give a generalized erosion rate vs. shear stress relationship. Figure 7-32 was developed by analyzing the flat sections of the five erosion rate shear vs. shear stress curves. Figure 7-33 was developed by analyzing the rapid advancement portions of the curves. In both cases, data was cut from the datasets into alternating flat and rapid advancement sections. Then, a best-fit line was fit to each data string. Since the best-fit line corresponds to $y = mx + b$, the average slope coefficient, m was found for each flat case and each rapid advancement case at each shear stress.

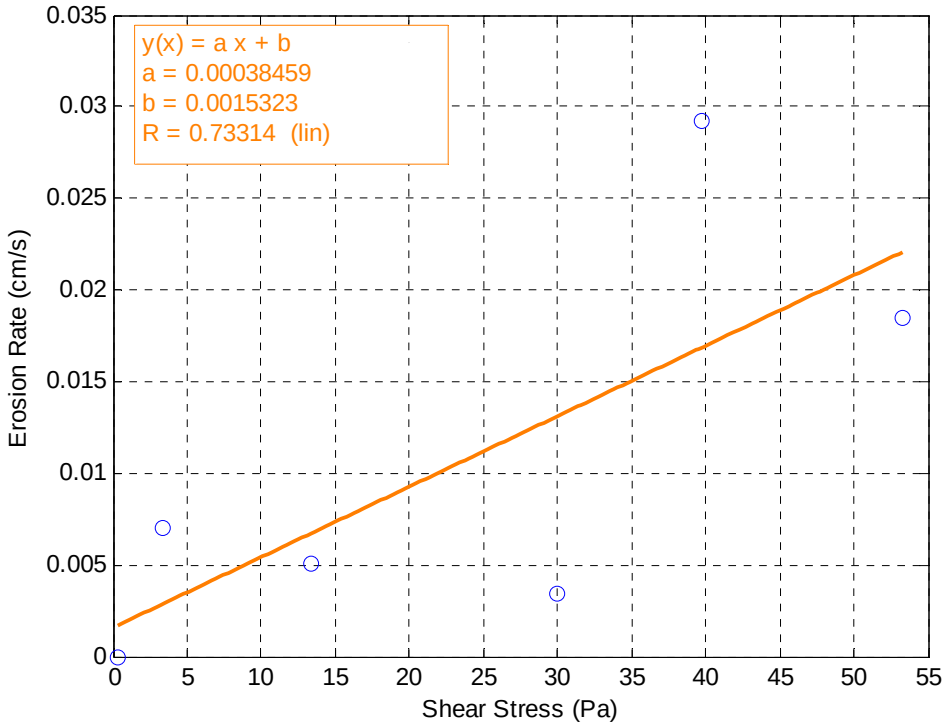

Figure 7-32. Erosion Rate vs. Shear Stress for Flat Portions of Sample Position vs. Time Curves

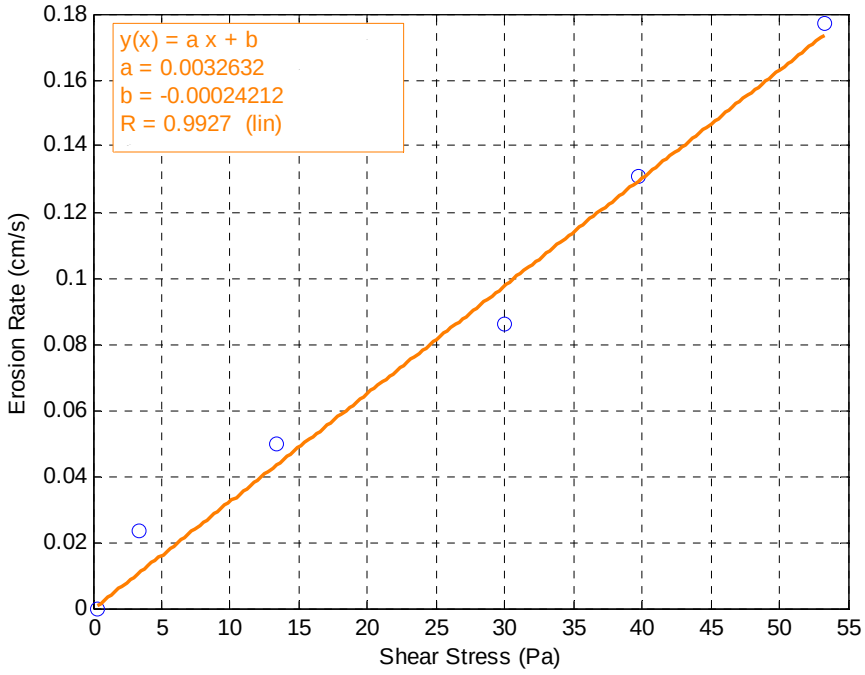

Figure 7-33. Erosion Rate vs. Shear Stress for Rapid Advancement Portions of Sample Position vs. Time Curves

Analysis of Figure 7-32 and Figure 7-33 show that the beginning stage of rock-like erosion hypothesis appears to be correct. In Figure 7-33, there appears to be strong erosion rate vs. shear stress relationship for the rapid advancement erosion sections of each of the five samples. Although there appears to be some relationship between erosion rate and shear stress for the flat portions of erosion as well, the correlation is not nearly as strong. This corresponds to the notion that rock-like erosion may have something to do with flow speed, but flow speed is not the only parameter that affects the normal stresses acting along the sample face. Comparison of these two figures also confirms what was hypothesized with the RETA database in terms of rock-like vs. particle-like orders of magnitude. Recall from the RETA database that generally, materials that did not respond to a direct erosion rate vs. shear stress relationship had erosion rates that were an order of magnitude lower than materials that did have a direct relationship between erosion rate and shear stress.

The question then became, how does one define the "correct" erosion rate? Should the erosion rate be defined conservatively by the rapid erosion portions of the signal, or is the hardened layer portion of erosion more valid? Or, are both of these erosion rate measurements bad estimates because of the way in which the sample was prepared?

According to a Westergard soil stress distribution, some sand-clay mixtures are assumed to be comprised of an infinite number of alternating layers of sandy soil and fine grained soil. In soils such as these, a vertical surface load leads to a lower vertical stress within the soil column than the stresses that would be seen using a Boussinesq approximation which assumes a uniform material. Presumably these materials should also exhibit differential erosion rates as observed in Figure 7-27. However, investigators had to verify that the four-layer erosion sequence did indeed respond to the sample preparation method. To do this, a test was run at 13.4 Pa where the sample was prepared using two lifts (Figure 7-34). Results appear to indicate that sample-preparation procedure is the same for the differential erosion rate behavior.

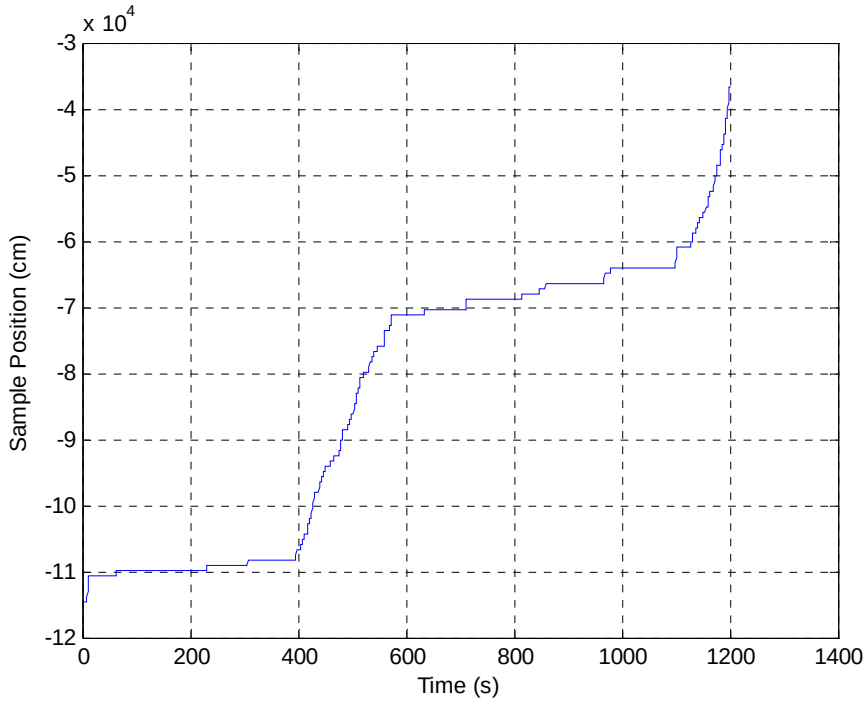

Figure 7-34. Two-lift test at 13.4 Pa.

After observing this behavior a hypothesis was made that lift-to-lift cohesive forces would be stronger if the top of the first lift is rougher. Essentially what was happening using an optimal water content approach was that doing this was like trying to glue two flat, slick, and smooth surfaces together using relatively small cohesive forces. Instead, what should have happened if samples were to be nearly uniform was that the compactive effort applied to the top lift should have been high enough to cause lift-to-lift particle interaction. This could only be achieved if the sample was allowed to slump more. In other words, allowing for a more easily deformable material would induce more particle-to-particle bonding per blow, which in turn would create a more uniformly "sticky" material that although weaker, should exhibit lower erosion qualities. Note that this notion contradicts the erosion as a function of cohesion theory as discussed in Chapter 6 because this method says that creating a weaker material will actually provide a lower average erosion rate due to the increase in vertical cohesive forces within the material matrix. This does not necessarily mean the discussion in Chapter 6 is incorrect; rather perhaps it only applies to stiffer materials. When unhardened sand-clay samples are present, another mechanism may be dominant.

Two more samples were prepared using double the optimum water content, and a time-series erosion test was run on them (Figure 7-35). As shown, the steps that were easily visible using the first sample preparation method disappear. However, Figure 7-35 shows that on average, erosion rates are slower than they would be using the preparation method outlined originally. Note that the samples that were prepared to create Figure 7-35 were mixed with the original four-lift mixing procedure.

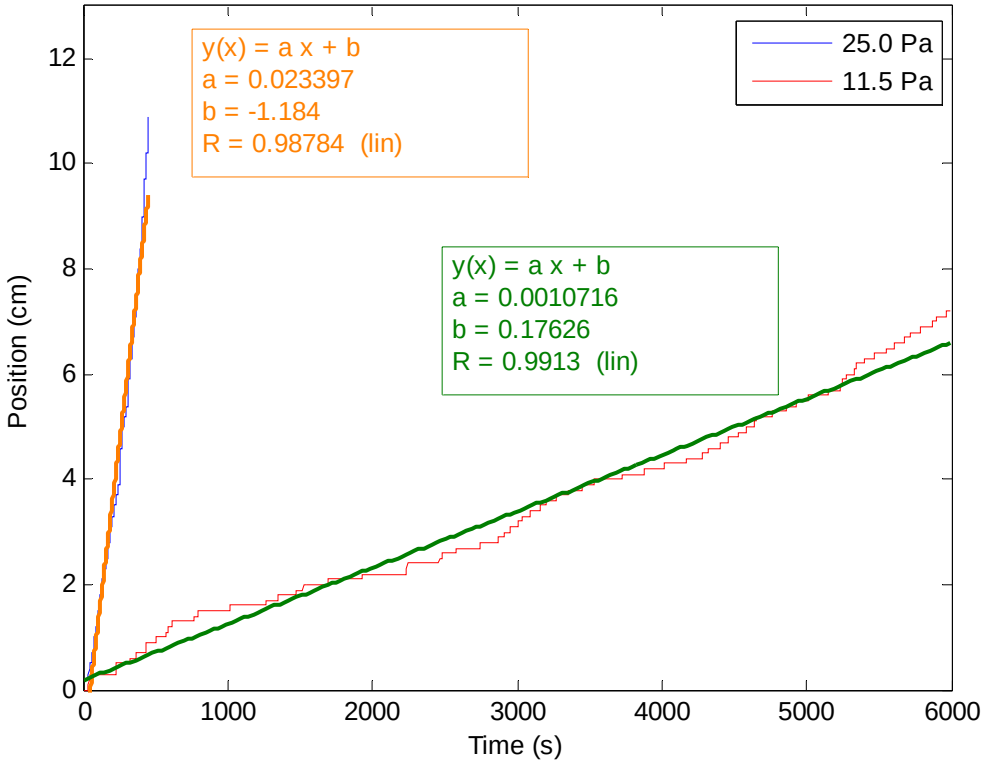

Figure 7-35. Sample Position vs. Time for 25% Clay Mixture Using Double Optimum Water Content

Development of Figure 7-35 shows that a change in the mixing water content changes erosion rate. This figure shows that weaker samples can erode more slowly than stronger samples. This was unexpected.

If Figure 7-33 is a conservative estimate of erosion rate vs. shear stress for a 25% clay sample when the sample is mixed at the optimum water content, Figure 7-35 shows that the estimate is only accurate under the special-optimum water content case. An interesting study would be to determine where the tipping point between the two curves is from a mix-perspective. In other words, if optimum water content produces a certain particle-like erosion rate, and an

increase in water content produces a slower erosion rate, at what point is erosion rate the maximum? And, is this maximum valid for any layered sediment? Or, does the amount of layers in the sediment strata play a role? Could layer thickness preclude the development of a particle-like erosion mode from taking place at all? Another interesting question was at what clay content does this layered effect become relevant? Although investigation started with the 25% clay sample, it may be possible that below a certain clay threshold, layering no longer has an effect.

At this point, it was obvious that substantial tests would be required to provide one data point for a 25% clay mixture. Even if the 25% clay mixture problem could be solved, it does not necessarily apply to other sand-clay ratios. Because the purpose of this project was to bound the sand-clay erosion problem, investigation into erosion rates for the 25% sand-clay mixture was stopped. The above analysis shows that a variety of erosion behaviors can be engineered by varying the initial water contents and lift-heights, but the real question is what do natural earth materials do? Both the slower layered rock-like erosion and the faster rapid-advancement particle-like erosion are valid erosion modes.

7.4.2.3 Fifty-Percent Clay Samples

Analysis of the 25% clay samples shows that an increase in the water content may eliminate the stepping behavior seen under optimum water content mix conditions. When investigation into the 50% clay samples began, investigators' first goal was to determine if the 50% sand-clay ratio behaved similarly. As with the 25% mixture, a series of erosion rate tests was conducted at a variety of shear stresses for the 50% mixture using the initial optimum water content mix approach (Figure 7-36).

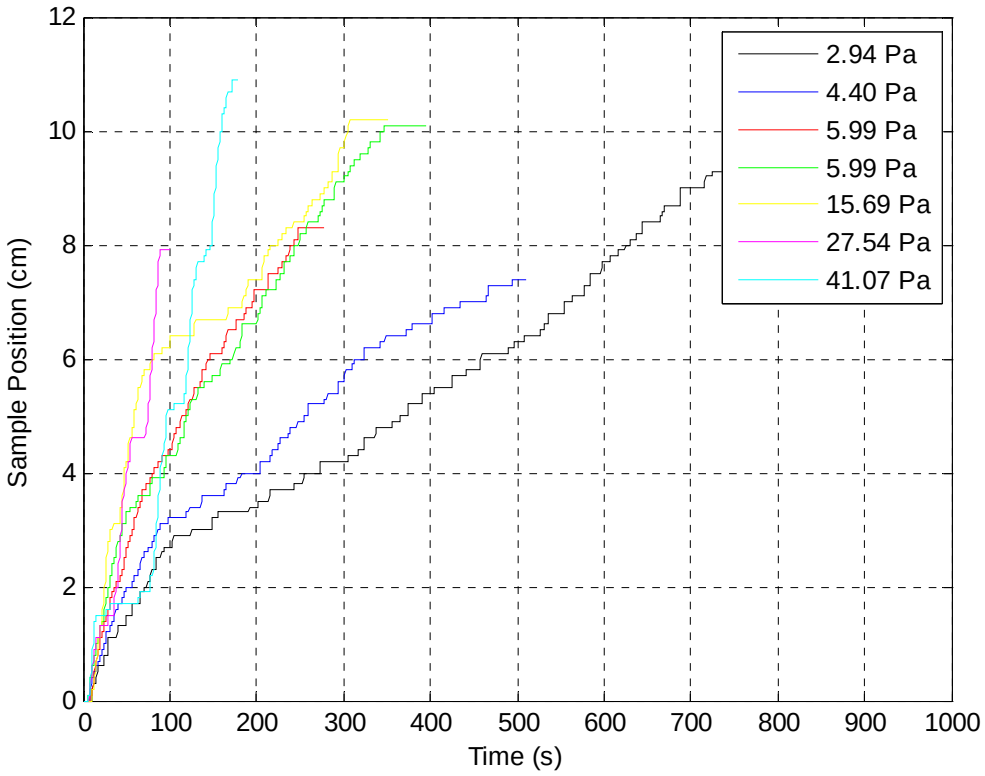

Figure 7-36. Sample Position vs. Time for 50% Clay Mixtures

Figure 7-36 shows that the step-like erosion behavior seen for 25% clay mixtures is not as apparent with the 50% samples. As flow rate (and subsequently shear stress) increases, the step-like erosion behavior becomes more apparent, but for lower flow rates and shear stresses, step-like erosion is nearly non-existent. Although perhaps not as obvious from Figure 7-36, when one zooms in on an erosion rate curve at a higher flow rate, the step-like erosion behavior is obvious (Figure 7-37).

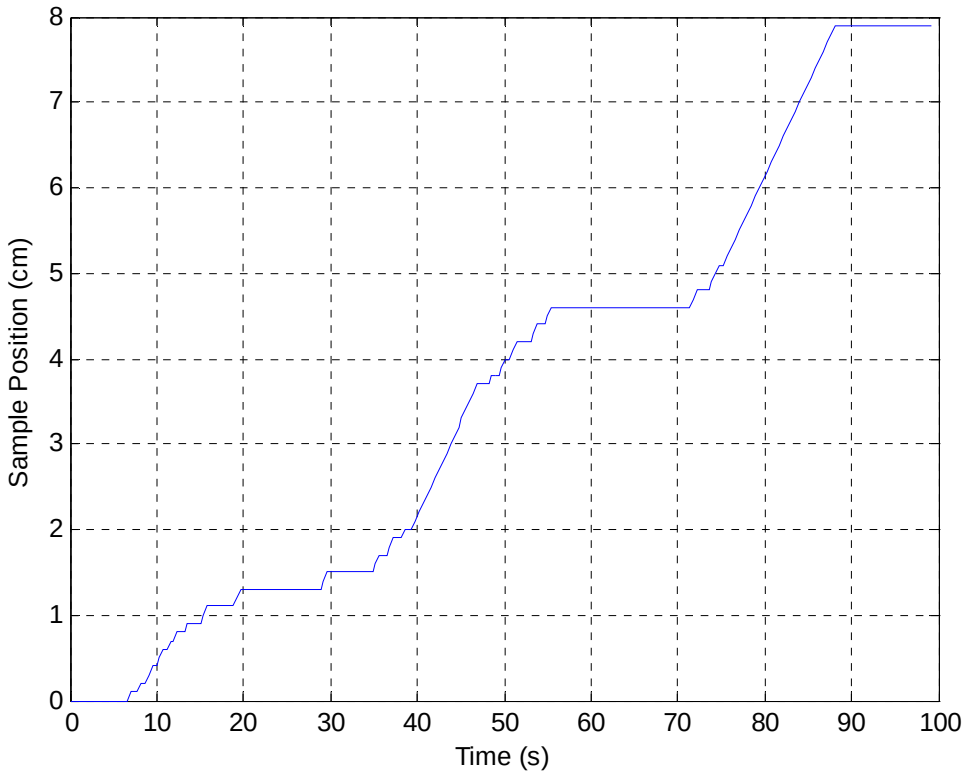

Figure 7-37. Sample Position vs. Time for 50% Clay Mixture at 27.54 Pa

Figure 7-37 also shows another interesting phenomenon. The top layer of each sample erodes much more quickly than other sample layer (Figure 7-38). As testing time and subsequently sample depth increases, erosion rates become much slower. This implies that the bottoms of the 50% samples are more erosion-resistant than the tops of the samples. This behavior was not seen with the 25% sand-clay mixtures.

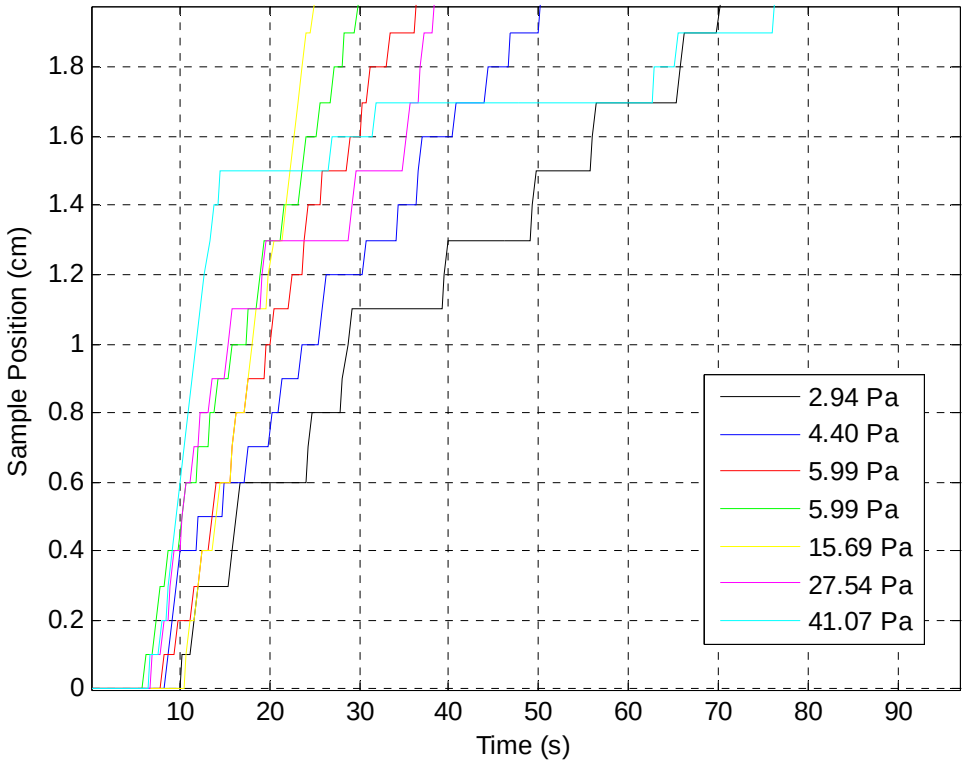

Figure 7-38. Zoom-in on First 90 Seconds of Sample Position vs. Time Curves

Water content was doubled to determine if a change in initial water content would affect erosion rate behavior. As with the 25% sand-clay mixture, an increase in water content made a much weaker sample that tended to slump much more easily. This weaker sample showed much greater resistance to erosion than the optimum water content mixture – so much so that to observe any erosion, shear stresses had to be increased from the values used for the optimum water content tests (Figure 7-39).

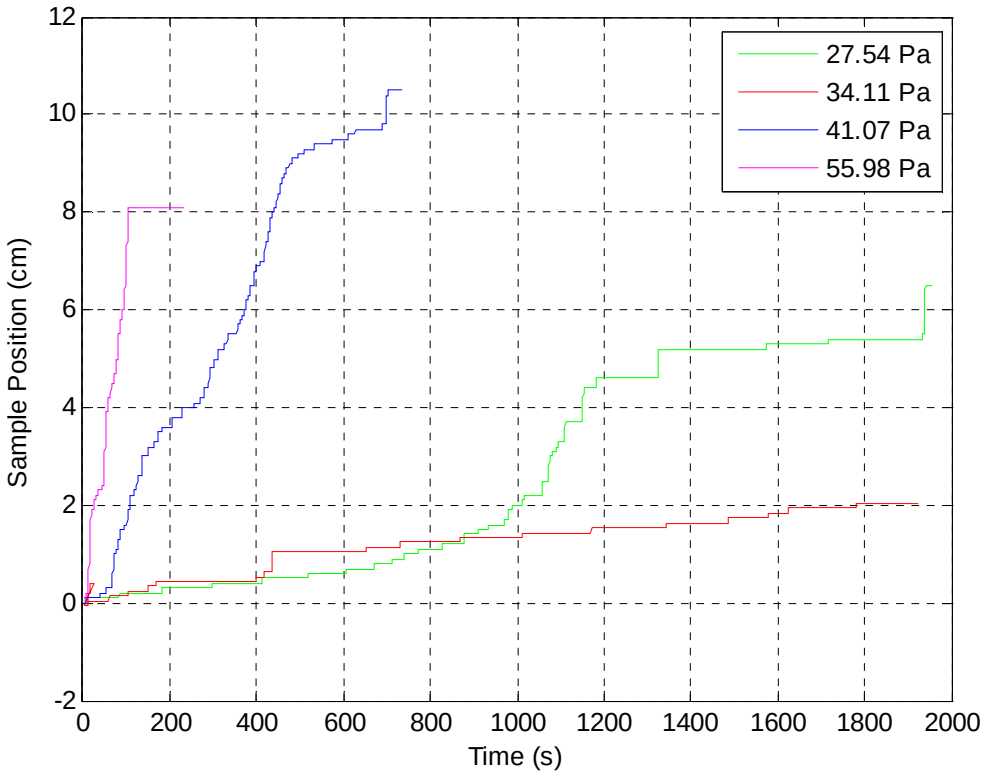

Figure 7-39. Sample Position vs. Time for 50% Clay Mixture at Double Optimum Water Content

Figure 7-35 and Figure7-39 show an interesting phenomenon for samples mixed at double the optimum water content. In Figure 7-39, a ~7 Pa increase in shear stress appears to cause a high increase in erosion rate. Likewise, Figure 7-35 shows that a 14 Pa increase causes a similar rise in the magnitude of erosion rate. Beyond this tipping point, erosion rate appears to increase relatively slowly; below this tipping point erosion rate behaves similarly. This behavior appears to suggest that for a certain shear stress, erosion rate will transform from a regular slow particle-like erosion pattern to a more chaotic floc-like erosion scenario.

Visual observation during the erosion rate test showed that the behavior seen below this tipping point is much different than erosion rate behavior above this tipping point. When erosion rate is relatively small (as it is at 30 Hz or 35 Hz in Figure 7-39), an observer can see individual flocs breaking from the sample's surface and moving downstream. Floc erosion is nearly uniform across the sample face, although the middle of the sample does erode somewhat more slowly than the sample's outsides (probably due to where most of the compaction is applied for a given sample). As erosion rate increases, erosion becomes much more irregular, and an observer

can see large chunks of material removed from the sample. When the flow rate becomes high enough, erosion transforms to an advanced stage of rock-like erosion. With the four-lift optimum water content samples the beginning stages of rock-like erosion were seen – with the hardened layers and subsequent rapid advancement once the layer was broken. When water content is doubled, layering does not have as much of an effect, yet beyond a certain point, instead of steady floc-flow, large-scale chunking is observed.

If samples with a higher water content are "more sticky" this phenomenon appears to make sense. Whereas for the optimum water content, individual flocs struggle to stick together, when water content is increased, the cohesive bonds holding flocs together have more of an effect. This inhibits the creation of hard layers. At the same time, once particle and floc vertical movement is initiated by the normal forces associated with rock-like erosion this increase in "stickiness" causes larger chunks of material to be removed.

Again, the question is how does one define a "proper" erosion rate for any sand-clay mixture? Once this behavior was observed for the 50% sample, the goal for the 75% sample and the 100% samples became to bound this "tipping point" between rapid erosion and slow erosion at higher optimum water contents. Additionally, the original 4-layered mix would be studied to verify that layering was an important erosion rate effect at certain initial water contents. This is done with the understanding that until tests are run on a series of natural samples, developing a generalized erosion rate vs. shear stress relationship for any sand-clay mixtures is premature.

7.4.3.4 Seventy-Five Percent Clay Mixture

As with the 25% mixture and the 50% mixture, the 75% mixture was studied using a four-lift mixing procedure. Both optimum water content and double the optimum water content were used during mixing. As before, samples were saturated before they were subjected to SERF testing. Results are presented in Figure 7-40 and Figure 7-41.

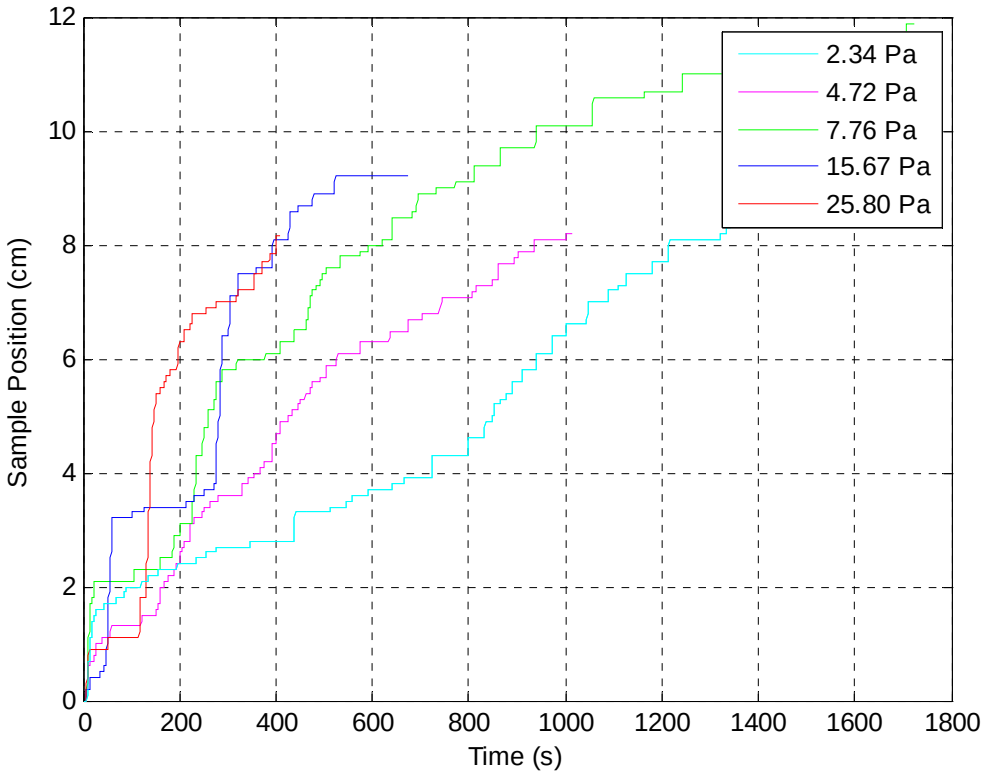

Figure 7-40. Sample Position vs. Time for 75% Clay Mixture Mixed at Optimum Water Content

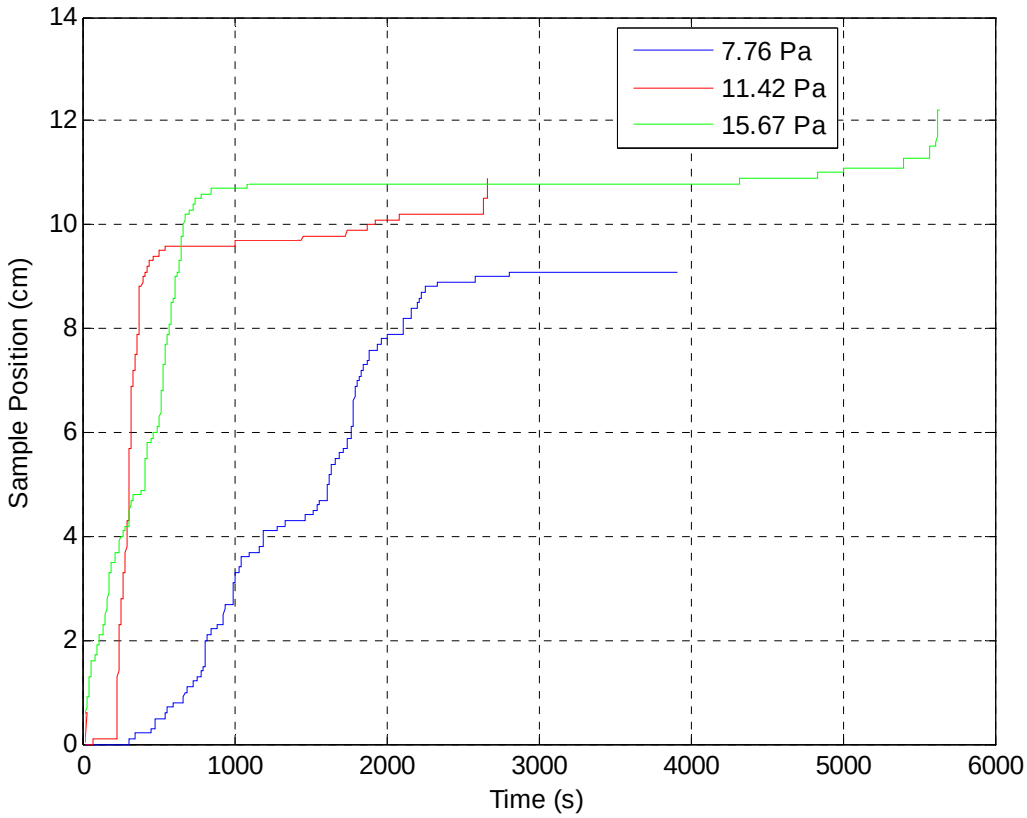

Figure 7-41. Sample Position vs. Time for 75% Clay Mixture Mixed at Double the Optimum Water Content

The 75% sand-clay mixture shows a tendency that was slight with the 50% sample. As shown in Figure 7-40, the relationship between sample position vs. time is not linear. The bottoms of the samples erode much more slowly than the samples' tops. As such, it would be inappropriate to fit an erosion rate line to the data. This tendency was shown with the 50% sample, although this non-linear behavior is much more apparent with the 75% mixture.

The 75% sample at optimum water content is similar to the 50% sample at optimum water content in that the step-like erosion behavior does not exist below a certain shear stress. However, above a certain flow rate/shear stress threshold, step-like erosion still occurs.

When water content is doubled, the bottom sample layer becomes much harder than the top sample layers (Figure 7-41). Rapid erosion is seen until this point, and beyond this point erosion is slow. This bottom layer approximately corresponds to the bottom sample-lift. In other words, for the first time at any sand-clay ratio, there appears to be some relationship between lift height and erosion behavior at the higher water content.

Below this slow erosion zone, erosion rate is approximately linear for the higher water content case. Erosion rate cannot be compared with the lower water content case since erosion at the lower water content is non-linear. Overall, the 75% sample is similar to the other sand-clay mixtures in that erosion is hypersensitive to the manner in which the sample was prepared.

7.4.3.5 One-Hundred-Percent Clay

As with the mixtures, two batches of 100% clay were prepared using both the optimum and double the optimum water contents. By the time testing reached this point, a pattern emerged. When the water content was doubled, the erosion rate decreased. At the higher water content, there was a tipping point between regular particle-like erosion and chaotic advanced rock-like erosion. At the optimum water content, erosion appeared to be step-like and/or non-linear. Therefore, fitting an erosion rate curve to a sample position vs. time graph is inappropriate because for a non-linear sample, erosion rate is more dependent on localized material properties. The 100% clay tests were run simply to confirm this pattern of behavior. Results are shown in Figure 7-42 and Figure 7-43.

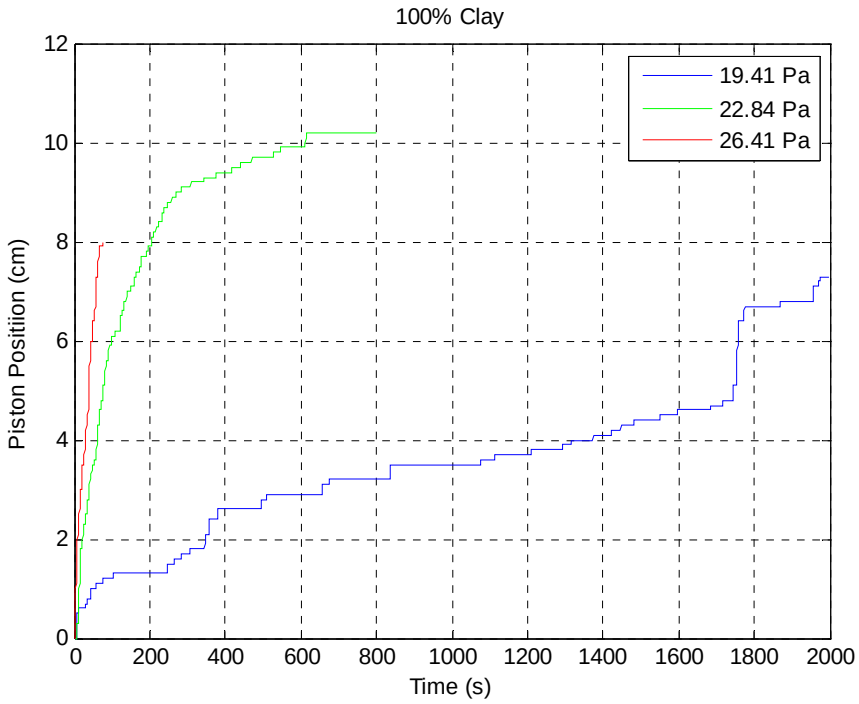

Figure 7-42. Sample Position vs. Time for 100% Clay Mixed at Optimum Water Content

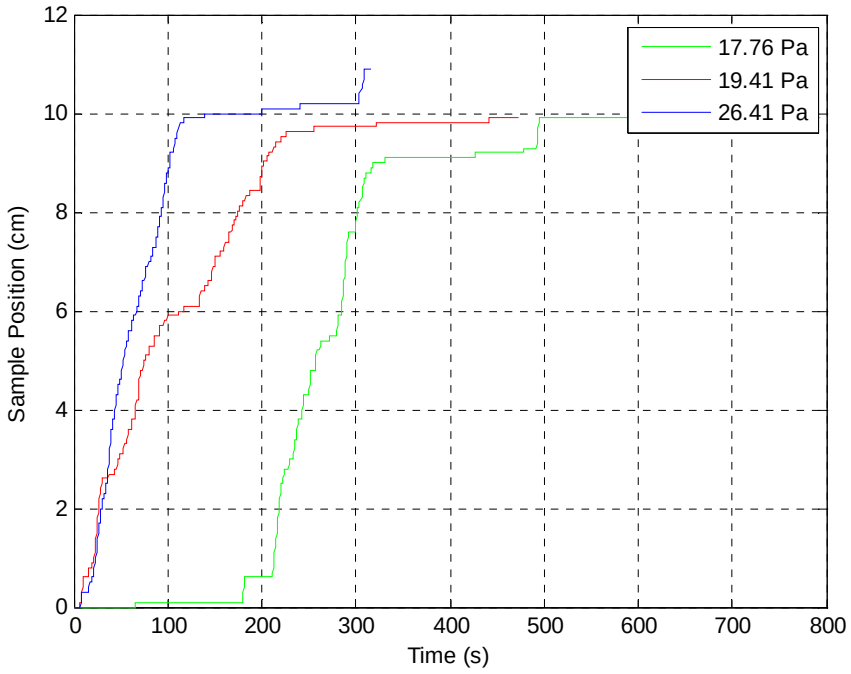

Figure 7-43. Sample Position vs. Time for 100% Clay Mixed at Double Optimum Water Content

The double optimum water content samples shown here appear to exhibit the pattern from highly regular particle-like erosion behavior to more chaotic behavior somewhere between 17.76 Pa and 19.41 Pa. Interestingly, the 100% clay sample at optimum water content also appears to show a tipping point to a more chaotic erosion behavior somewhere between 19.41 Pa and 22.84 Pa. Although this is the case, erosion rate appears to be highly non-linear as it was for the 75% sample. As more of the sample erodes, the bottom portion of the sample provides more erosion resistance.

7.4.3 Density Profile Tests

The goal of the density profile tests was to quantify density variability in the sand-clay mixtures and to compare localized density variations with hardened erosion rates observed during SERF testing. Results from the density profile tests are presented below. Where appropriate, the black lines represent lift interfaces measured during sample preparation. Since the most extreme erosion fluctuation with density variability occurred with the 25% sand-clay

mixtures (from a stepped-erosion perspective), most density profiles concentrated on this mixture concentration.

Table 7-1. Sample Density Profile Designations

Sample Designation	Water Content Times Optimum	Clay Content (%)	Number of Lifts	Average Dry Density (g/cm^3)	Average Wet Density (g/cm^3)	Dry Density Standard Deviation (g/cm^3)	Wet Density Standard Deviation (g/cm^3)
I	1x	25	1	1.70	1.91	0.070	0.077
II	1x	25	1	1.54	1.77	0.111	0.117
III	1x	25	2	1.53	1.76	0.125	0.133
IV	1x	25	2	1.53	1.84	0.213	0.234
V	1x	25	4	1.52	1.75	0.166	0.789
VI	1x	25	4	1.52	1.75	0.144	0.160
VII	2x	25	4	1.70	2.07	0.277	0.339
VIII	1x	25	8	1.58	1.81	0.074	0.089
IX	1x	50	4	1.44	1.83	0.162	0.175
X	1x	50	4	1.39	1.75	0.127	0.154
XI	1x	75	4	1.20	1.57	0.276	0.313

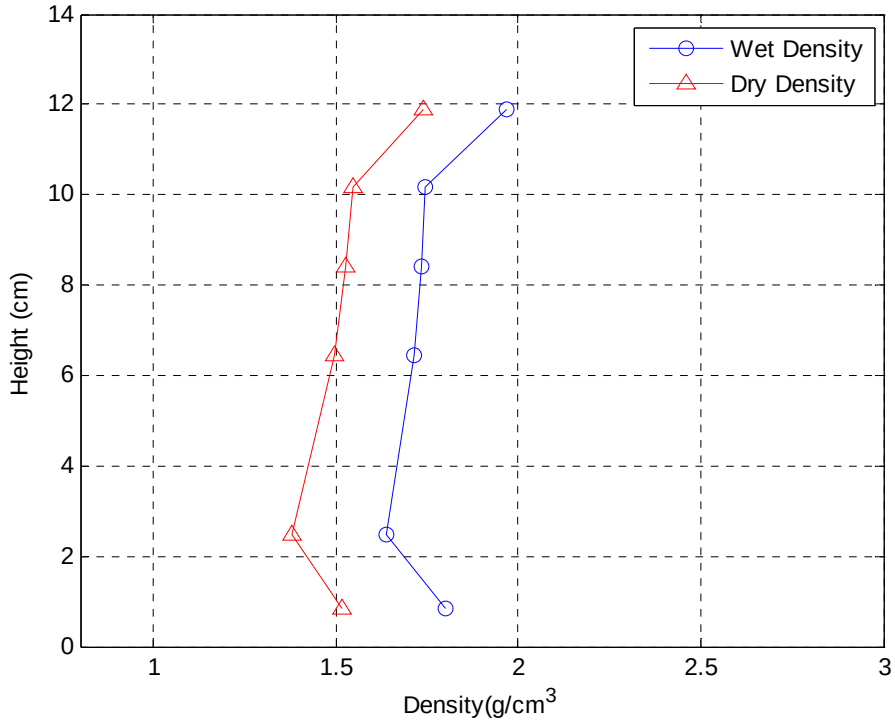

Figure 7-44. Density Profile for Sample I

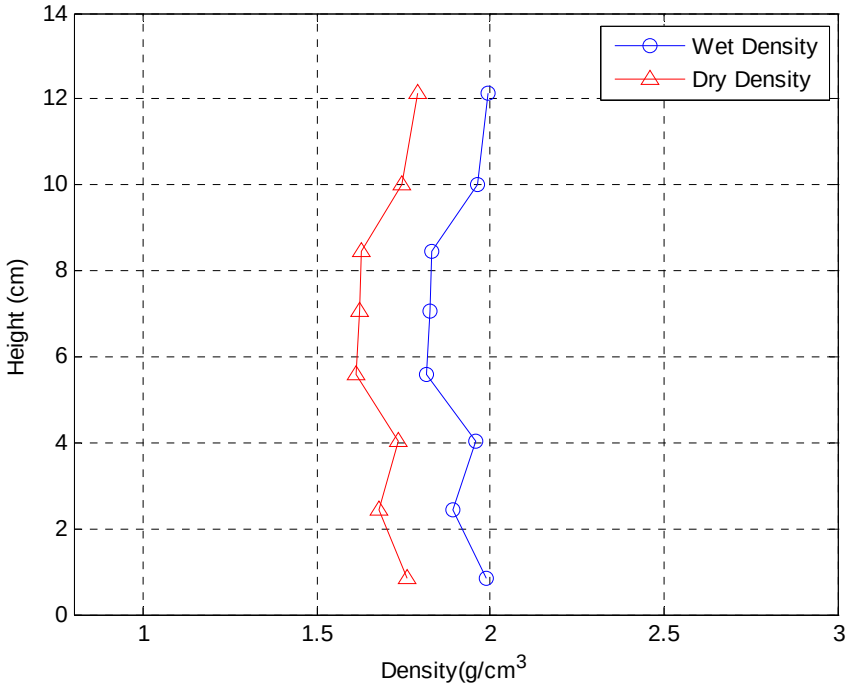

Figure 7-45. Density Profile for Sample II

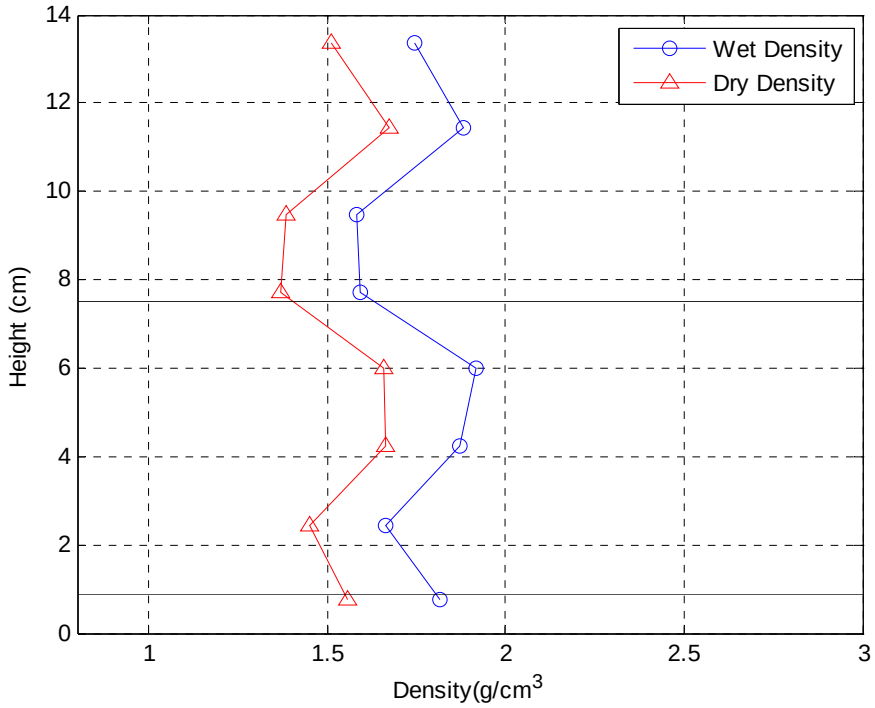

Figure 7-46. Density Profile for Sample III

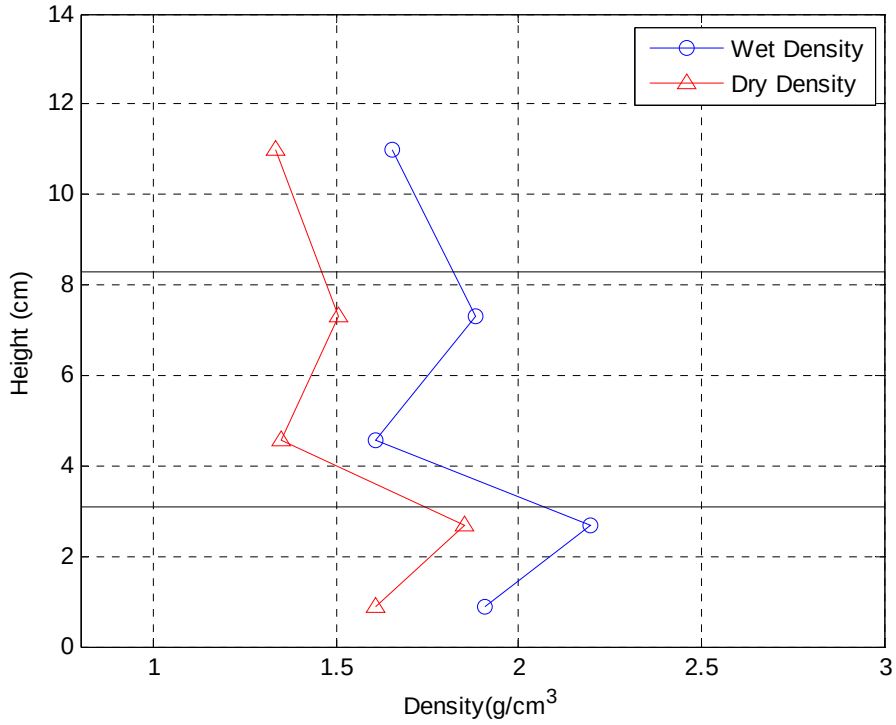

Figure 7-47. Density Profile for Sample IV

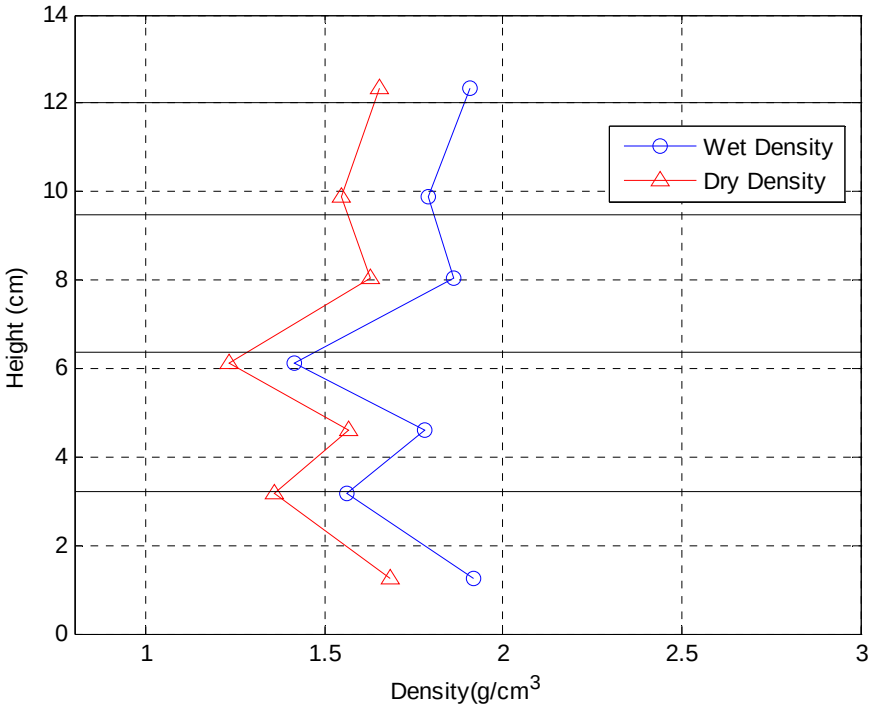

Figure 7-48. Density Profile for Sample V

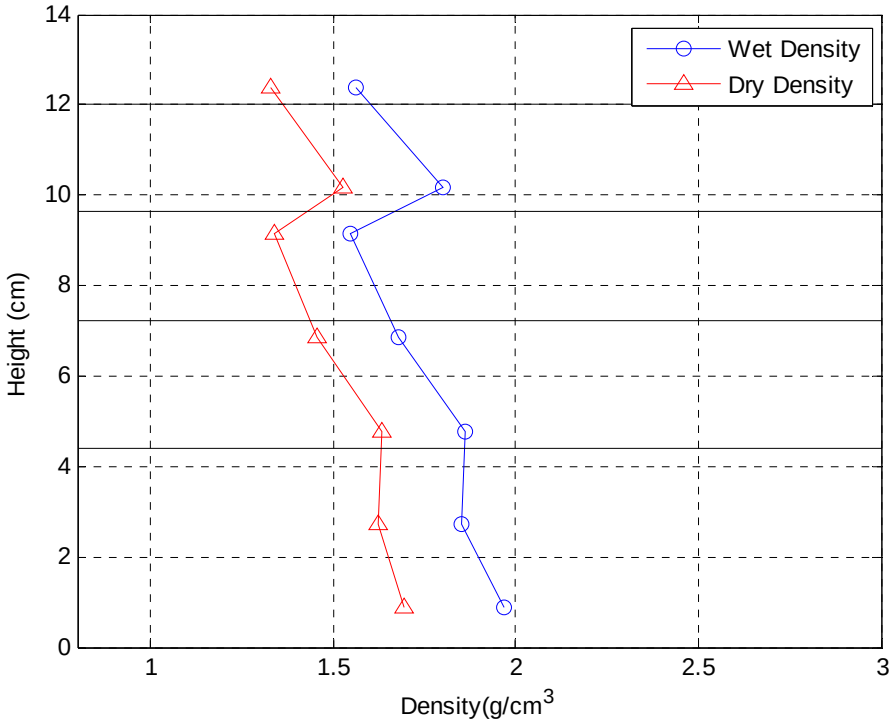

Figure 7-49. Density Profiles for Sample VI

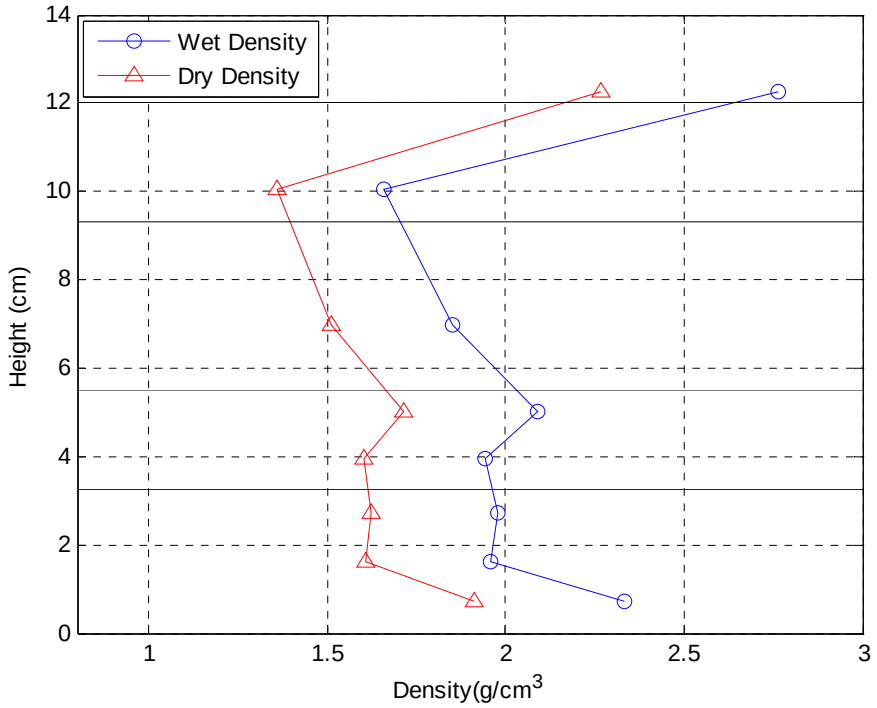

Figure 7-50. Density Profiles for Sample VII

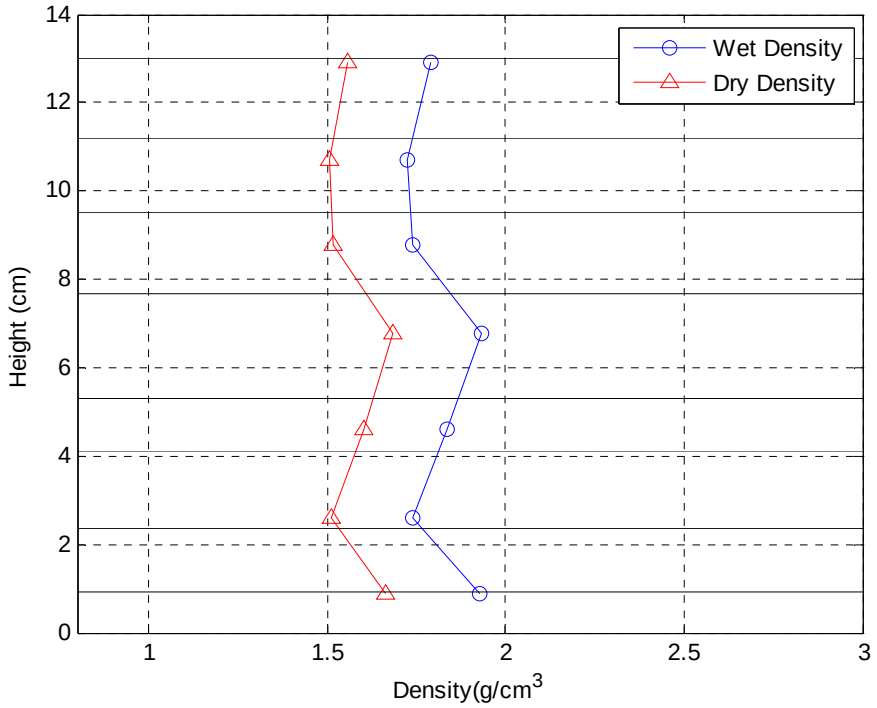

Figure 7-51. Density Profiles for Sample VIII

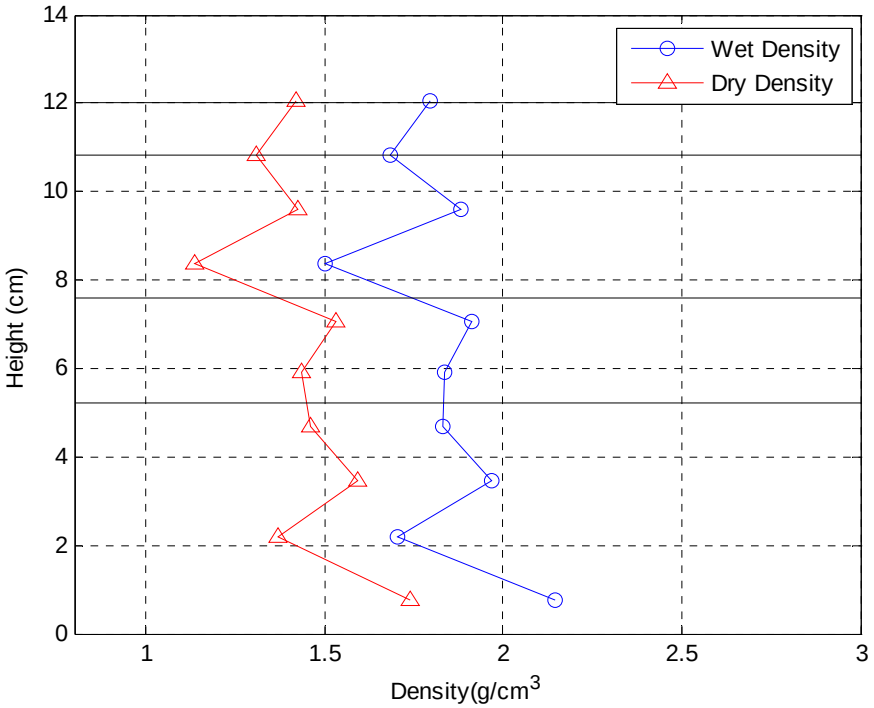

Figure 7-52. Density Profiles for Sample IX

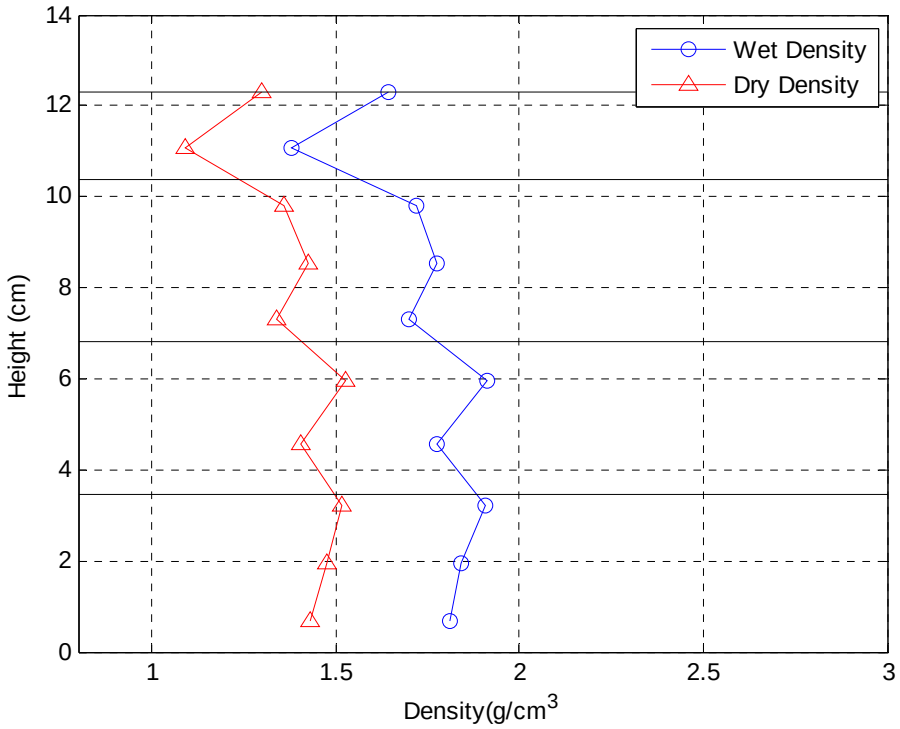

Figure 7-53. Density Profiles for Sample X

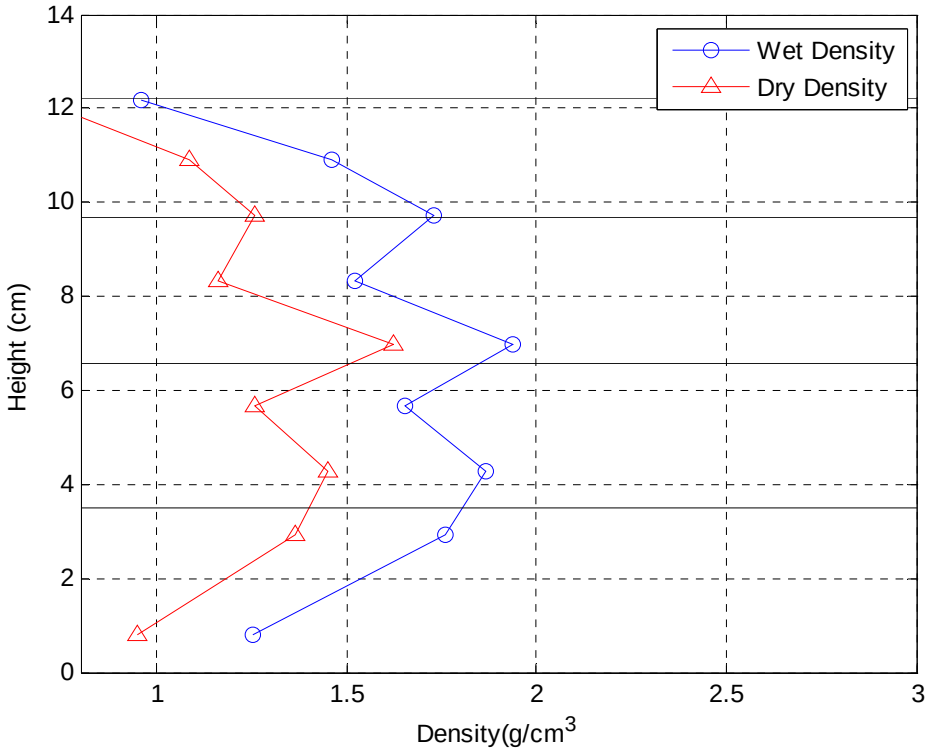

Figure 7-54. Density Profile for Sample XI

Generally speaking, a lift interval does not necessarily line up with localized density fluctuations. Sometimes a lift interface will line up with a higher density, while other times it will align itself with a lower density. Still, other times, lift interfaces do not align with any maxima or minima density measurements. This is not to say that the lift interfaces are not causing density variations. Whenever a lift is poured on top of a previous lift and compacted, some of the compactive effort on the new lift helps to densify the previous lift's interface further. This means that lift heights may not necessarily match up with density variations. Interestingly, the 75% sample shows the best alignment between lift height and density increases (which is what would be expected). This implies that under the 75% clay content scenario, the initial compactive effort per lift is sufficient to bury it to its ultimate depth.

The 25% clay sample showed generally, average bulk density ranged from ~1.50 - ~1.70 g/cm^3 with standard deviations on the order of 0.2 g/cm^3. In other words, the amount of average variability in the sample corresponds to the expected density range. Or, the density variation is within the range of averaged densities. This implies that the intra-sample density fluctuations are relatively low when compared with overall density. The eight-lift sample implies that using

more lifts may help to reduce the density variability, but it is equally possible that a second run of an eight-lift sample will yield similar results to the one-lift sample. During one one-lift sample, density variability was low but during another one, it was a little bit higher. This argument also ignores the fact that density variability is relatively low to average density regardless of what lift method is used.

This is not to say that larger localized maximum or minimum density changes do not exist. The density profiles were taken by cutting the samples into 1.5 cm sections. Visual observation of the samples after they were extracted from their molds showed that the lift interfaces could be plainly seen with the naked eye. Observation also showed that the lift interface was relatively small (1 mm – 2 mm) compared to the 1 cm sections that were used to make the density profile. Because of limits with available tools, investigators could not cut less than a 1.5 cm section of sample at a time. Cutting precise smaller sections would increase the resolution of the density profile, and this might reveal the expected localized density variability between lift sections. Unfortunately, an accurate method for cutting strips of sample that were thin enough to do this could not be found.

Analysis of the SERF results back up the notion that density fluctuations smaller than those picked up using the 1.5 cm strip method may exist. Generally, data shows that the localized hard patches seen during step-like erosion behavior are only 1 mm – 3 mm thick. If this is the case, then it implies the need to refine the density profile method.

It was hypothesized that it may be possible that density fluctuations are not the deciding factor. When the compaction hammer is applied to the top of the lift, it does two things:

1. It compacts the sample.
2. It presses protruding flocs into the top of the sample – thereby smoothing out the surface.

It was thought that it may be possible to visually see the lift interfaces because the top of the lift is smooth. If the top of the lift is smooth, the lift's top section may have trouble bonding to another lift's bottom section because of a decrease in relative surface area. To test this hypothesis, a 100% clay sample was prepared with 6 lifts. In between these lifts, the surfaces were roughened before the new lift was poured. Under these conditions, density variability was similar when compared with previous density profiles (standard deviation was 0.11). In addition to this quantitative test, a qualitative test was done where a sample was prepared by roughening

the surfaces between lifts and extracted. Visually, lift interfaces were still apparent, and this method was abandoned.

The most plausible hypothesis right now is that sample preparation causes localized density variability along a small length scale. This localized variability in turn causes localized changes in erosion rate. When density increases, eventually it induces a hardened surface that behaves similar to the way a rock-face behaves.

7.4.4 Effects of Sand Concentration on Shear Stresses

When this project was originally proposed, one of the goals of it was to determine the effect of suspended sediment on bed shear stress. While the sand injector could not be implemented (Chapter 3), another method for estimating bed shear stress became apparent during sand-clay tests. When the 100% sand samples were run through the SERF, investigators noticed that some sand particles were cycled back through the flume during operation. The filter system, which was primarily designed to protect the water chiller, did not work fast enough to filter out eroded material during an erosion test.

When clay was added to the sand during tests, conditions in the flume became even worse. Clay particles and mud-sand flocs were held in solution and suspension through the flume water. The result was that during some tests, operators could visibly see sand and sand-clay flocs being cycled back through the device. At times there was so much suspended material in the water column that the cameras could not see through it any longer. This corresponds to less than 3 inches of visibility.

A series of qualitative tests was conducted to determine whether or not recirculating sand would affect erosion rate-shear stress development. A flat disc was installed in the shear stress sensor, and an erosion test was conducted on a 50% sand-clay mixture. The 50:50 ratio was used because it was a logical midpoint. Once the erosion test was conducted, a shear stress test was run. Once this had been completed, an erosion test was run on another 50:50 sand-clay mixture, and then another shear stress test was run. This was repeated a third time so that by the end of the series of tests, the SERF water was cloudy. Investigators hesitated to run a fourth series of tests because they did not want to damage the primary pumps.

What resulted were shear stress readings for four conditions – clear water, after one data run, after two data runs, and after three data runs. Although sediment concentrations could not

be measured directly, they can be implied roughly by dividing the sample volume by the volume of the reservoir tank. If the results showed that shear stress varied from one sediment concentration to another, then it would call into question any result from SERF tests because as the test is run it would mean that shear stress is changing dynamically with time.

The result though varied from Sheppard's conclusions in a 2006 study. In it he was scour hole depths under field conditions and one day due to snow melt, the amount of suspended material in his water was abnormally high. This corresponded to abnormally low shear stress readings. Sheppard reasoned that suspended material should weaken turbulent eddies, which in turn should decrease bed shear stress. Results from this round of tests show something else (Figure 7-55).

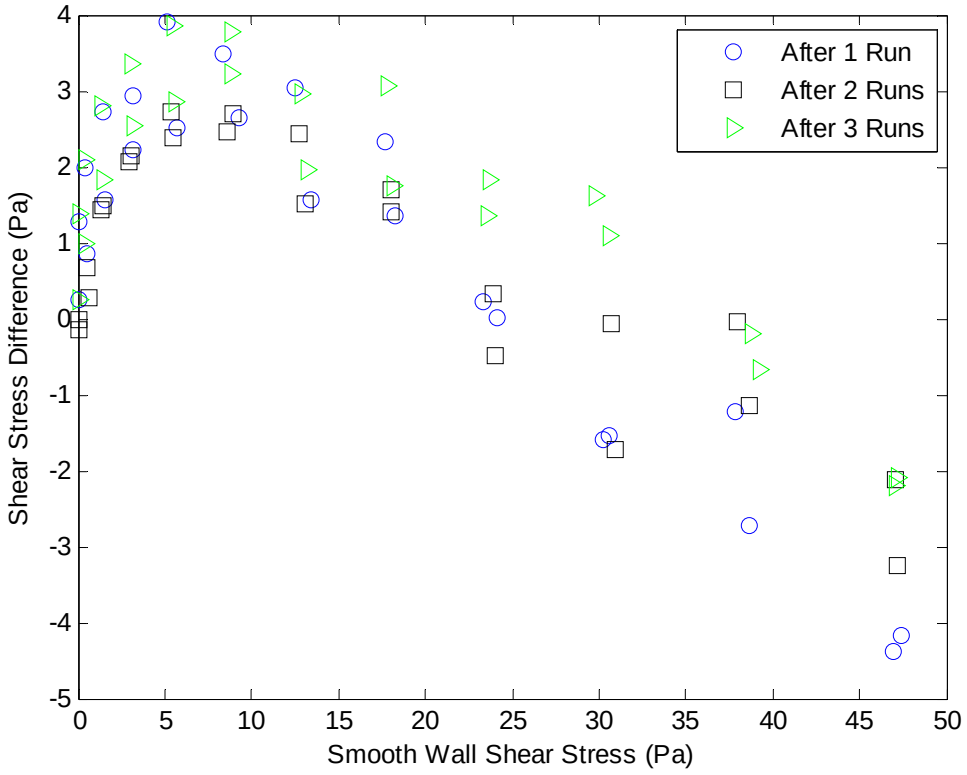

Figure 7-55. Shear Stress vs. Velocity for Different Sediment Concentrations

According to this figure, as sediment concentration changes, there does not appear to be a correlation between concentration and shear stress. Instead, similar shear stresses are recovered (+/-4 Pa) compared with shear stresses for a smooth wall. Sheppard (2010) speculated that at higher flow velocities (velocities greater than 1 m/s) as seen in the SERF, flow conditions would

become turbulence-dominant. In this case then, shear stress reduction infects from an increase in sediment concentration may be overridden by turbulence. It is also possible that during Sheppard et al.'s (2006b) work, the decrease in erosion rate that was seen during his tests was in fact the manifestation of an increase in sediment deposition. During Sheppard's tests, shear stress was not measured directly; rather scour depth was measured. It is possible that because Sheppard et al. measured depth, they were in fact measuring sediment aggradation. Both explanations are plausible, and since many of the SERF results were obtained at higher flow rates (velocities greater than 1 m/s), they do not necessarily contradict one another. During this series of tests, investigators did not want to overdo it, and therefore, they avoided running a comprehensive series of shear stress tests because they did not want to risk further damage to the pumps. Still, both explanations should be investigated.

7.4.5 Temperature Effects

As per the scope of the proposal for this project, a test was run at a different temperature to determine if temperature plays a role in determining erosion rate development. Because of the unexpected step-like behavior of previous sand-clay tests, most of the tests for this project involved explaining this behavior. As such, a comprehensive study could not be completed regarding temperature, and its effects on erosion rate. Rather, a mid-point shear stress was used as a basis of comparison between the two temperatures.

The temperature effect test was conducted toward the end of this project. During the test, operators noticed damage to one of the pump's mechanical seals. This damage is probably caused by the lack of a proper filtering mechanism. The temperature test was conducted on a 25% clay, 75% sand mixture at 45^{o}F (8^{o}C) at a shear stress of 30.0 Pa. Qualitatively, erosion was much slower when compared to erosion rate testing at standard temperature (70^{o}F or 21^{o}C). Because of the damage to the pump's mechanical seal, water leakage was present throughout the test. Not wishing to risk further damage to the pump the test was shut-down after thirty minutes. This data is presented in Figure 7-56.

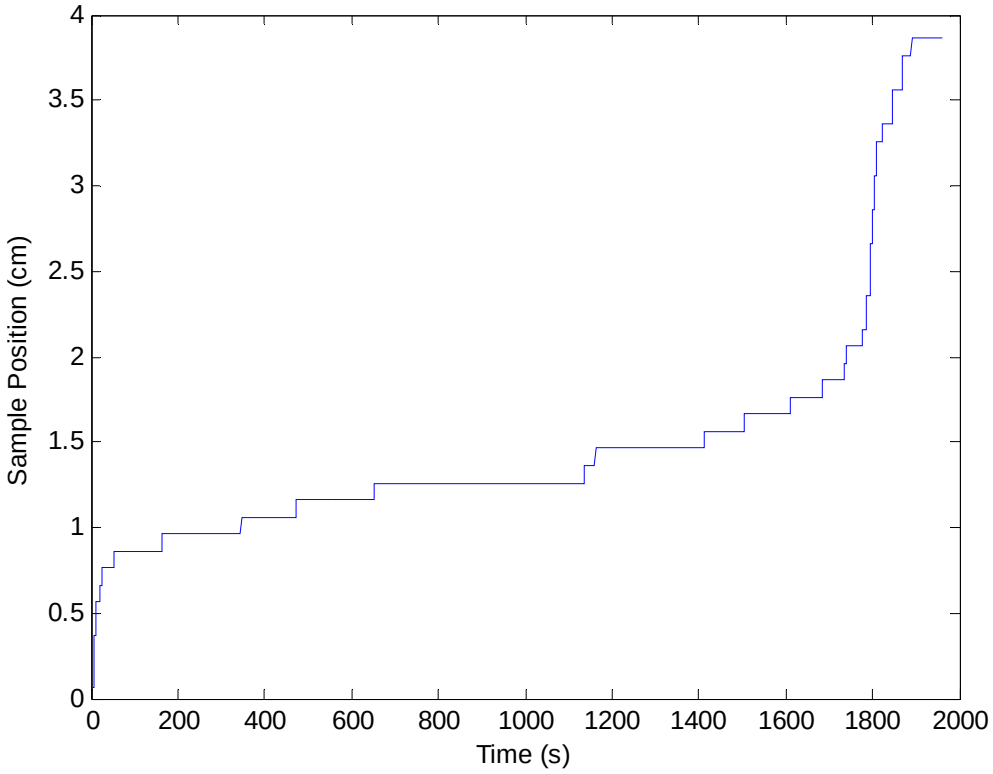

Figure 7-56. Sample Position vs. Time at 45°F (8°C)

This chart shows that temperature may play a role in determining erosion rates of sand-clay mixtures as this chart shows much slower erosion development compared with Figure 7-30. It would be beneficial to follow up on this experiment with a more comprehensive dataset. Although layering effects may continue to be more significant than temperature effects, it would be interesting to compare the two sets of data. As shown in Figure 7-56, layering still appears to occur, yet erosion overall – both during slow advancement and quick advancement – appears to slow down.

7.4.6 Compressive Strength Tests

In addition to erosion rate tests, a more "traditional" set of strength tests were conducted on a series of the sand-clay mixtures. The goal of these tests originally was to determine cohesion and use this variable to determine erosion rate similarly to the method shown in Chapter 6. As discussed, constant erosion rates at specified shear stresses could not be determined for these sand-clay mixtures because of the step-like erosion behavior shown during

erosion tests. Still, strength testing was valuable as it helped investigators to further understand the properties of these sand-clay mixtures.

7.4.6.1 Mix Procedure

Mix procedure was similar to the procedure discussed in 7.3.3.2, and therefore the procedure will not be repeated here except for where it differs from the previous discussion. Because triaxial testing molds are slightly larger (8 in. vs. 6 in.), eventually the four-lift technique was replaced with a six lifts procedure. Scarification was used between lifts for strength-test samples as per ASTM D-2850. Scarification was not repeated for SERF tests because it was thought that artificially creating more channels for water flow during rock-like and chunking erosion events would make the stepping issues seen in SERF tests even worse. Because strength testing occurred at FDOT's SMO and samples were prepared at UF, there was a lag-time between testing and mixing. To ensure SERF-similar conditions, once molds were prepared, they were sealed using plastic sheeting and a 2 mm silicon bead.

Because of the lag-time between sample preparation and testing, the samples needed to be preconditioned before they were tested. The samples were delivered to the SMO standing upright. This caused water to migrate toward the lower portions of the samples. To mitigate this, the bottom sheeting was removed before testing and the sample was placed on a porous stone so that water could seep from the bottom of the sample prior to removing the sample from the mold. Then the sample was trimmed so that an aspect ratio of 2-2.5:1 was achieved. Generally, more material was trimmed from the molds' bottoms or the portions of the samples where water had migrated so that more homogeneity would be achieved. Sample trimmings were weighed to determine water content and dry unit weight. When samples were extracted from their molds, investigators noticed voids in the specimens. During testing, different procedures were used to mitigate this effect.

7.4.6.2 Test Procedure

There are three options for triaxial testing: unconsolidated-undrained (U-U), consolidated-undrained (C-U) and consolidated-drained (C-D). Unconsolidated-undrained testing was selected because it is relatively faster than the other two versions of the triaxial tests. Testing procedure was as follows:

1. The sample was weighed for initial conditions.

2. A rubber membrane was placed around the sample to prevent water intrusion.

3. The top and bottom of the sample were sealed with a cap and a base using rubber o-rings.

4. The membrane-encased sample was placed in the triaxial chamber.

5. Sample was preconditioned by consolidating to approximately 5 psi chamber pressure and opening both the top and bottom drainage lines.

6. The sample was loaded at 0.3 in./min. until failure. During loading, confining pressure was maintained. Because the sample was undrained, pore water pressure increased as the sample was loaded.

7. Axial (deviator) stress and strain were recorded.

8. After testing, samples were removed from the loading device and triaxial chamber. The entire sample was oven dried to determine final water content.

7.6.6.3 Results

A summary of results is provided in Table 7-2 and Figure 7-57:

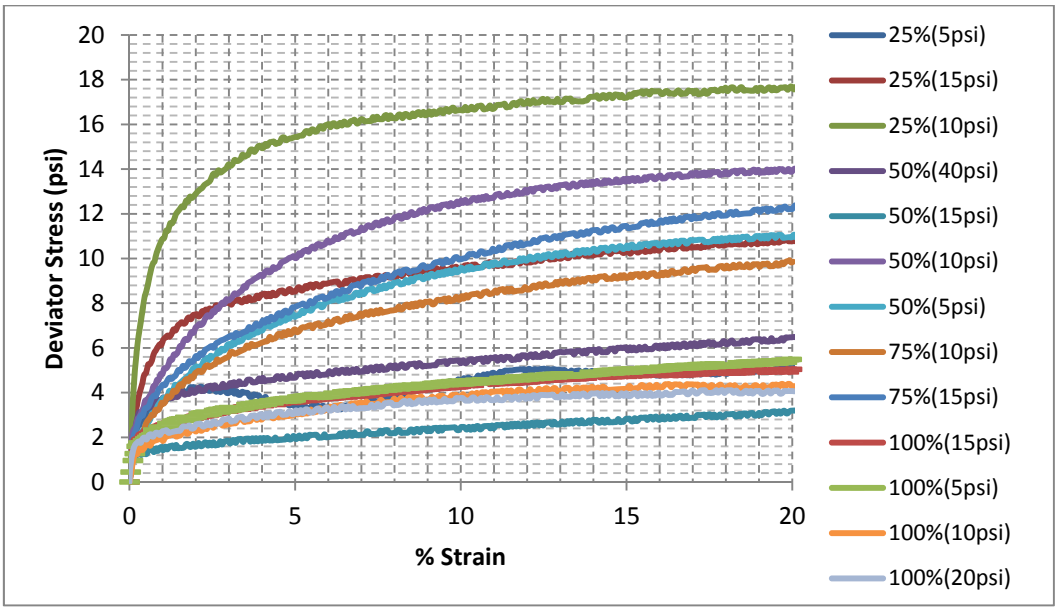

Figure 7-57. Graphical Summary of Triaxial Tests

Table 7-2. Tabular Summary of U-U Triaxial Test Data

Clay Content	Tube #	Confining Pressure (psi)	Max Dev. Stress (psi)	p (psi)	q (psi)	Dry Unit Wt. (pcf)	Initial w%	Final w%
100%	S-1	15	5.0	17.5	2.5	69.2	44.1	44.7
100%	S-3	5	5.8	7.9	2.9	69.3	43.8	43.3
100%	S-4	10	4.4	12.2	2.2	78.2	44.5	44.3
100%	S-5	20	4.2	22.1	2.1	74.0	44.8	43.5
75%	S-2	10	9.9	15.0	5.0	84.6	24.9	26.6
75%	S-3	15	12.4	21.2	6.2	93.1	24.3	26.7
50%	S-3	40	7.0	43.5	3.5	84.4	25.2	22.0
50%	S-2	15	3.4	16.7	1.7	85.5	25.9	21.5
50%	S-4	10	14.0	17.0	7.0	94.2	17.6	17.8
50%	S-5	5	11.1	10.5	5.5	97.6	17.7	18.6
25%	S-1	5	5.2	7.6	2.6	110.6	13.6	14.7
25%	S-3	15	11.2	20.6	5.6	106.6	13.2	14.0
25%	S-5	10	17.8	18.9	8.9	109.6	11.6	11.5

In addition to these numerical results, a series of visual observations were made after extracting the sand-clay samples from their molds. Often, even after fifteen (15) minutes of confining pressure, investigators still noticed layer demarcation lines when samples were cut in half (Figure 7-58):

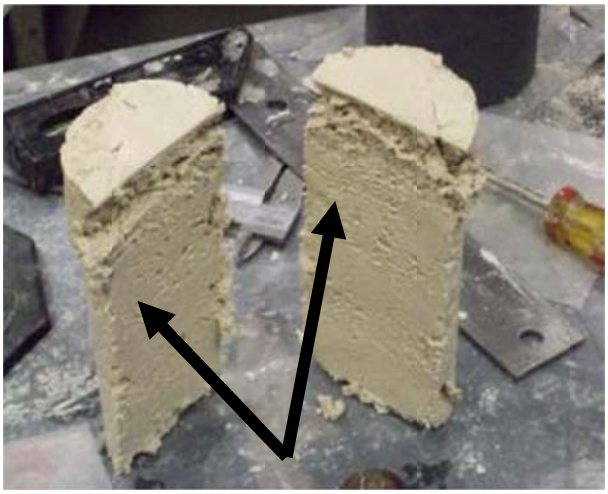

Figure 7-58. Extruded Sample. Arrows point to layer demarcation lines. Top of sample was damaged during cutting.

7.6.6.4 Analysis

Although Table 7-2 shows 4 tests at 50% clay and three tests at 25% clay, this table is misleading. The 25% sample labeled "S-1," the 50% samples labeled "S-2" and "S-3" were mixed using earlier mixing procedures. These samples were prepared similarly to Gator Rock where sand-clay was mixed dry and water was allowed to rise from the bottom-to-top through the sample. Results in Table 7-2 show that this mix procedure produces weaker materials. This backs up erosion-sensitivity arguments presented in previous sections of this report. Data is included here to show this dependence on mix procedure semi-quantitatively. After testing a series of Mohr's Circles was generated to develop values for cohesion (only standard mix procedure discussed in 7.6.6.2 is analyzed).

100% Clay

The mean *q*-value was 2.4 psi and was used to define the failure envelope with standard deviation of 0.34 psi. Of the four samples, samples S-1 and S-3 were made using four lifts and were saturated, and samples S-4 and S-5 were made using six lifts without saturation. Because of the stiffness of the samples, all exhibited noticeable voids, and lower unit weights than the other clay-sand compositions. This contributed to larger deformations at lower axial loadings. This combination of factors resulted in a lower cohesive strength trend than those for the other clay-sand compositions.

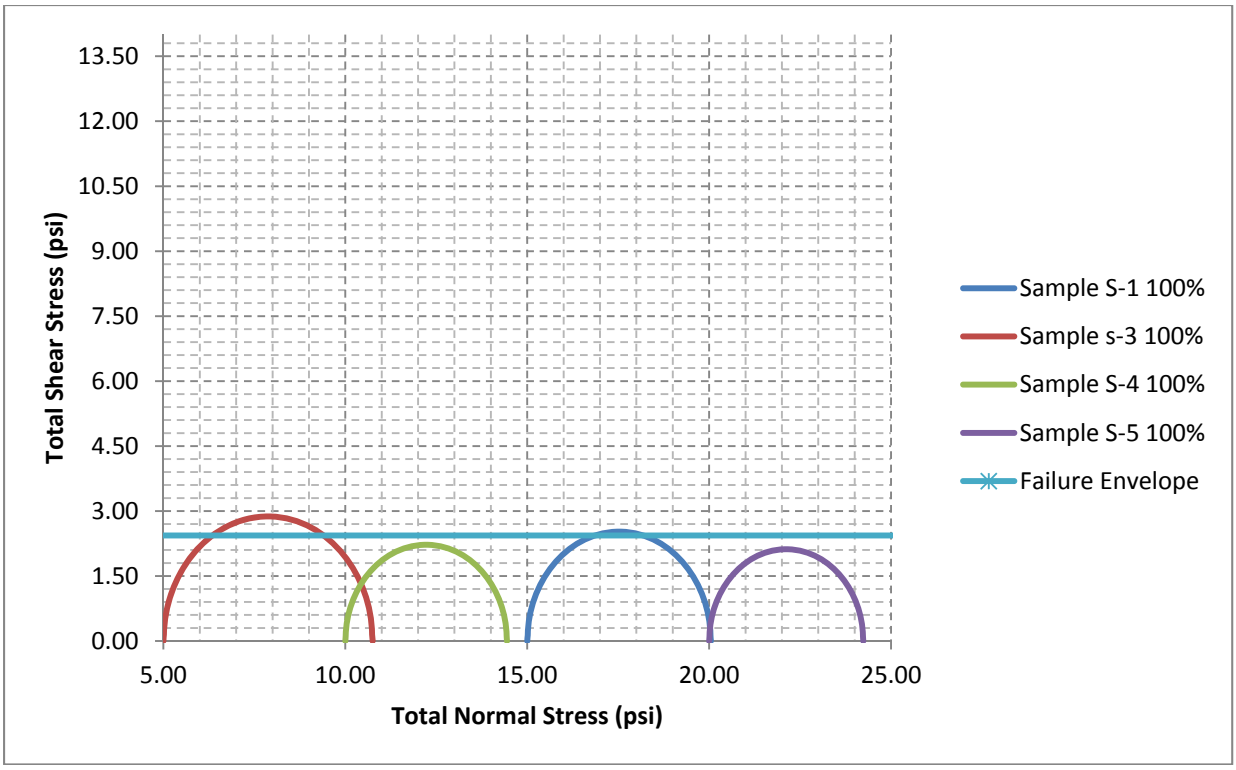

Figure 7-59. Mohr's Circles for 100% Clay

75% Clay

There were only two samples of the 75% clay composition that exhibited predictable behavior. Sample S-1 exhibited a cohesive strength (q-value) of 5.0 psi, and the cohesive strength of sample S-3 was 6.2 psi. The failure envelope was 5.6 psi. Several of the early 75% exhibited bulging in the uppermost layer with little deformation in lower layers and the lack of interlayer bonding resulted in tests that were not useful in strength analysis. These results are not included here.

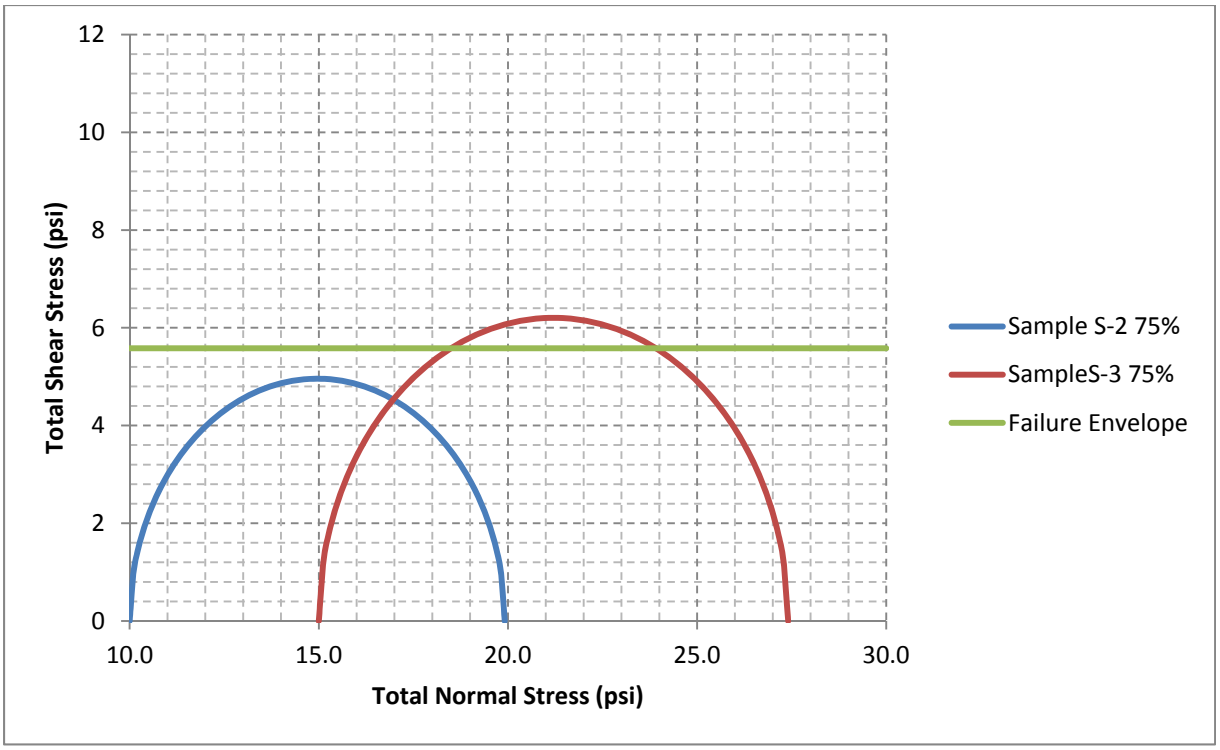

Figure 7-60. Mohr's Circles for 75% Clay

50% Clay

Two 50% clay mixtures were tested. The final values of q for the 50% clay content samples were 7.0 and 5.5 psi (mean 6.25 psi). Graphical results are similar to results shown in Figure 7-60.

25% Clay

Two 25% clay mixtures were tested. The value of *q* was 5.6 psi for sample S-3, and 8.9 psi for sample S-5 (mean 7.25 psi). Graphical results are also similar to results in Figure 7-60.

Discussion

As implied, there appears to be a correlation between clay content and strength. Generally, as clay content increases, strength tends to decrease (Figure 7-61).

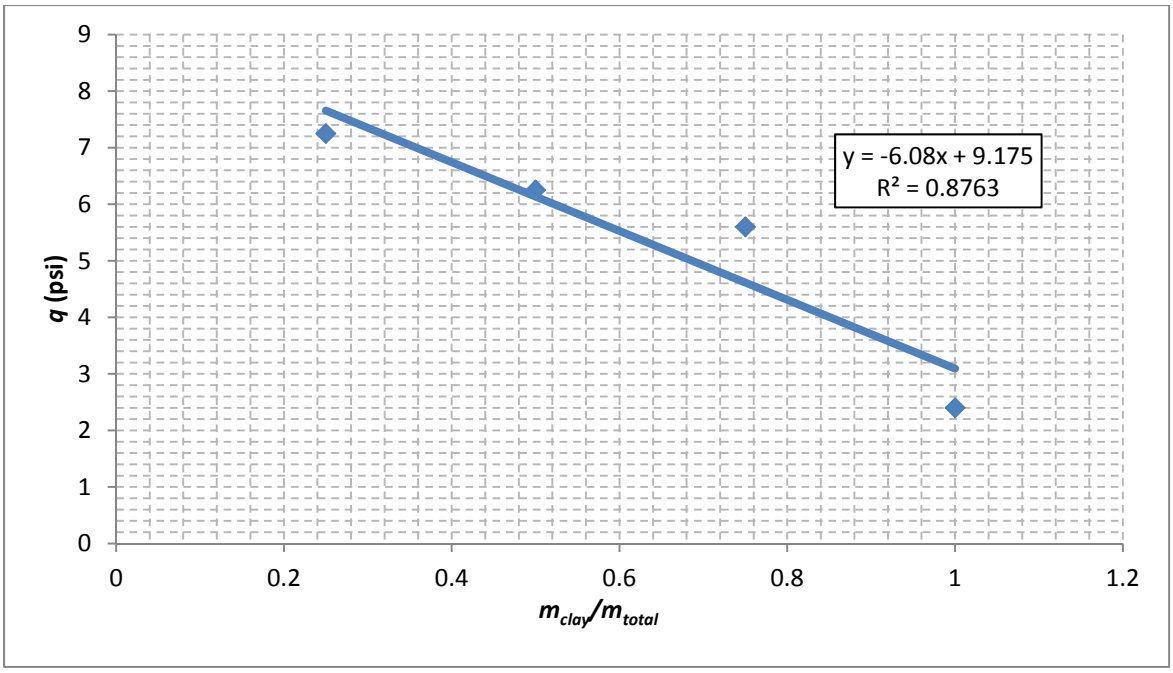

Figure 7-61. Clay-Sand Ratio vs. *q*

This apparent correlation between clay-sand ratio and material strength implies that if cohesion is related to material strength (as indicated Chapter 6), it may be possible to also relate sand-clay ration to erosion rate. This argument presumes that a layering-effect does not exist in natural sediments. If natural sediments can be shown to exhibit non-step-like behavior during erosion, this correlation between clay content and strength implies that erosion vs. cohesion correlations may be developed. This possibility should be investigated.

7.5 Summary and Conclusions

The purpose of this study was to generalize sand-clay erosion based on the sand-clay ratio. What was found was that this may not be possible without testing natural materials. Investigators expected to see regular, linear sample position vs. time signals from the SERF. Instead, what was found was for lower clay contents, a step-like behavior that corresponded to lift-heights existed. As clay content increased, the step-like behavior disappeared in some cases, but it was replaced with non-linear erosion behavior. A modification of water content to the samples helped to eliminate some of the step-like behavior, but it also induced a flow rate and/or shear stress dependent tipping point between regular particle-like erosion and more chaotic rock-like erosion. And, changes in water content changed average erosion rate.

In summation, sand-clay mixture response is sensitive to the manner in which they were created. Their behavior appears to result directly from the following factors:

1. Initial water content
2. Initial layer depth
3. Initial compaction

These variables appear to supersede variables that would be expected to govern the sand-clay erosion problem: the sand-clay ratio. The conclusion of this study is that it should be possible to engineer sand-clay materials to respond in a variety of different ways. The question is which one of these response mechanisms most effectively corresponds to natural conditions? Until this question is answered, further testing is not justified.

Other conclusions from this study are as follows:

1. Generally, it appears as though an increase in initial water content decreases erosion rate. It would be interesting to see if there is some threshold – i.e. does an increase in initial water content decrease erosion rate to a certain maximum and then does erosion rate increase again?
2. Likewise, is there a lower threshold limit? Below a certain initial water content, can a minimum erosion rate vs. shear stress relationship be found for sand-clay mixtures such that erosion rate is maximized for a given shear stress.
3. Solving (1) and (2) above may provide designers with an erosion rate range for a given shear stress based on sand-clay content. This could be useful for design purposes.
4. Although unintended, work during this study did provide information regarding the effects of suspended sediment on shear stresses. Shear stresses are not necessarily attenuated by the presence of suspended sediment. This may contradict earlier work by Sheppard et al. (2006b), and this discrepancy should be investigated.
5. Work during this study appears to preliminarily indicate that sand-clay mixtures may erode more slowly at lower temperatures. This effect should be compared with layering effects and quantified.
6. Shear stresses appear to correspond to the theory that increasing roughness causes an increase in shear stress. This confirms work in Chapter 4 and also shows that without a shear stress sensor, the Moody Diagram is the most effective method for estimating shear stress in a flume-style erosion rate testing device.
7. Sand-clay mixtures appear to correspond to a relationship where material strength decreases as clay content increases.

7.6 Future and Ongoing Work

One phase of study that should be investigated further is the question of the suspended sediment effects on bed shear stress. Results from this study contradict earlier work, and this discrepancy needs to be addressed. This could be due to lab scaling effects, the fact that a flat wall instead of a roughened surface was used during this study, or other unknown factors. Likewise, the effect of temperature on erosion rate should also be investigated and compared with layering effects.

The most important thing moving forward is to determine how actual sand-clay samples behave. Samples during this study appear to correspond to Westergard theory where individual layers are important. Do actual field samples behave similarly? The RETA cannot answer this question, but future SERF tests can. If actual sand-clay mixtures show a dependence on layering, using the RETA for development of sand-clay sediment transport functions is inappropriate. Similarly, strength-testing needs to be further investigated using other mixing recipes. As shown in Table 7-2, when mixing procedure deviates from a standard 6-lift technique, material strength changes. This may affect erosion rate, which also appears to be governed by mixing recipe, and needs to be investigated. Does a different mixing recipe similarly change erosion rate and material strength? If so, material strength vs. erosion rate curves may be appropriate. And, how do these curves relate to natural sand-clay samples? This is the most important factor to consider.

Another effect that was ignored during this study was the effect of consolidation. This needs to be examined as well. Does consolidation play any role in either suppressing or enhancing the layered-like behavior seen here? If it suppresses layered-like behavior, and it can do so rather quickly, perhaps the layered behavior is a moot point. For example, if 24 hours of consolidation reduces layering by a certain factor, this may show that there is no need to take layering into account.

This ignores the initial water content dependence seen during this study, but perhaps that is not that important either. Under natural conditions, sediment is saturated as it is deposited (under a stream erosion scenario). Perhaps, it would be beneficial to prepare samples as "naturally as possible." This means, mix sand and clay in water, let it sit for a while (30 days or more), and form a sample under its own self weight. Then, extract this sample, and test the

erosion rate on it. This may prove to be the most effective way to mimic field behavior in the future.

CHAPTER 8
SUMMARY AND FUTURE WORK

8.1 Summary

8.1.1 Review of Goals for This Study

The purpose of this research was to aid in the development of erosion rate functions for use in a similar-style Miller-Sheppard approach or EFA-SRICOS approach for predicting local scour depths. The specific goals for this were to:

1. Develop equipment to improve accuracy of erosion and shear stress measurements for a wide range of eroding bed materials.

2. Use these equipment upgrades and other analytical techniques to comment quantitatively on older methods for measuring these parameters by running a series of tests with the new equipment.

3. Use these new measurements and older results to determine if erosion rate can be related to any other existing common geotechnical parameters.

4. Use the new equipment to develop a series of erosion rate-shear stress curves for sand clay mixtures. Under natural conditions, it is rare to find a bed material that is purely cohesive or purely non-cohesive. Instead, usually sand is interspersed with clay particles or vice versa. Previous research has looked only to classify erosion rate-shear stress curves under conditions where a uniform material is present, but because this is rarely the case, erosion properties of mixtures are investigated.

8.1.2 Summary of Work

To achieve these goals, the following was accomplished during this project:

1. The Sediment Erosion Rate Flume (SERF) was enhanced and improved. Significant upgrades to the device include

    a. A laser system

    b. A new shear stress measurement system

    c. A vortex generation system

    d. Computer upgrades

e. Software upgrades

f. Additionally, a sand injection/control system was designed. Although funding for this system does not yet exist, when funding becomes available, installation of this system should be relatively straight-forward.

2. A series of tests were conducted with the new shear stress sensor in the SERF to determine the apparent most effective method for estimating shear stress in a flume-style erosion rate testing device.

3. A synthetic material, Bull Gator Rock, was designed so that it could be tested in both the SERF and the Rotating Erosion Testing Apparatus (RETA).

4. Bull Gator Rock testing revealed the presence of rock-like erosion, which is difficult to analyze with present equipment that is only designed to measure erosion rate and shear stress. Therefore, the entire RETA database was filtered and used in conjunction with analytical equations to verify whether or not the device was working properly.

5. A series of tests was run on a variety of sand-clay mixtures in an attempt to generalize sand-clay mixture erosion behavior as a function of sand-clay ratio.

8.2 Conclusions

The following is a list of conclusions from this project:

1. The laser-leveling system is an effective means of maintaining a sample level during an erosion rate test in a flume-style device, especially during clay and sand-clay tests.

2. The temperature control system in the SERF was effective at holding temperature within +/-2^{o}C.

3. The sediment control system was unable to keep up with rapid erosion rates.

4. Tests with the new shear sensor showed that as sample roughness increases for a given flow rate, corresponding shear stress also appears to increase.

5. In the absence of a shear stress sensor, the most effective alternative means for estimating shear stress on an eroding sample in a flume-style testing device is to use a Moody Diagram or Colebrook Equation. The roughness factor in the Colebrook Equation should be equal to one-half the median sediment diameter. Flat-wall assumptions for predicting shear stress under-predict shear stress, especially at higher roughness and flow velocities.

6. Bull Gator Rock may be a promising material for use in comparing results between different erosion rate testing devices if somehow water content can be increased. Currently, it appears that the bottom-up approach will produce a nearly-uniform material if limestone aggregate is similarly nearly uniform. However, Gator Rock tests also

showed that obtaining a water content greater than ~20% using a bottom-up technique may not be possible.

7. The RETA database showed that under special conditions where erosion conditions correspond to a direct erosion rate vs. shear stress relationship, results from the RETA correspond to results from equations that fit the Ariathurai equation form accurately.

8. RETA database analysis showed that there is an approximately even split between materials that behave with a direct erosion rate vs. shear stress relationship and materials that do not. For materials that do not obey a direct relationship, rock-like erosion described by the Stream Power Model is likely the culprit. When rock-like erosion is present, current equipment limitations do not allow for prediction or analysis of this erosion mode. This is significant because generally, rock-like erosion appears to occur an order of magnitude slower than particle-like erosion.

9. RETA database analysis showed that for the special case of particle-like erosion, correlations may exist between erosion rate constant, critical shear stress, and material cohesive strength.

10. Tests on sand-clay mixtures showed that sand-clay mixture erosion behavior is dependent on initial water content when the sample was formed, compactive effort as the sample was formed, and layering thickness as the sample was formed.

11. Sand-clay mixtures exhibit a combination of rock-like and particle-like erosion qualities even though sand-clay mixtures would usually not be described as rock-like materials.

12. Sand-clay mixtures tended to exhibit the opposite effect as stiffer RETA materials in terms of erosion rates for stronger materials. With sand-clay mixtures, when initial water content increased, samples were created that were qualitatively weaker in compression and tension. These samples exhibited more resistance to erosion than samples that were stiffer and stronger in compression and tension.

13. Recirculating sand in suspension in the SERF does not appear to affect shear stresses on a smooth plate compared to what shear stresses would have been under clear water conditions.

8.3 Future Work

The following is a proposed progression of future work. Proposed work discussed here will help to further improve the SERF, aid in developing erosion rate and shear stress relationships, and help to predict when (or if) particle-like or rock-like erosion will occur.

8.3.1 Essential Final Improvements to the SERF

Before the rock-like vs. particle-like erosion question can be answered, essential final improvements need to be made to the SERF. As discussed, when an erosion rate test is run, the eroded material recirculates back through the flume; this issue is common with recirculating flumes with a relatively small (1,100 gal.) reservoir tank.

This recirculating particle issue is troublesome for three reasons. First, due to the number of variables associated with the erosion rate problem, researchers need to isolate them from one another. The second and more important reason to add a high-capacity filter is that without it, the SERF will probably be damaged. The pumps will be damaged because these sand-clay flocs are essentially sand-blasting the centrifugal pumps' impellers. Sometimes when the reservoir tank is drained, rust particles are often seen interspersed with the sand-clay flocs. Since the flume is made of aluminum, the rust particles must be from the cast iron pumps. This proves that damage is already occurring. Towards the end of this project, one of the pumps' mechanical seals began leaking – which appears to indicate that damage due to recirculating sediment has occurred.

The third reason to add a high-capacity filter is so that the sand injector can be installed, tested, and used during tests. Installation of the sand injector will allow investigators to follow up on tests shown in Section 7.4.4 so that definitive results can be obtained for the effects of suspended sediment on shear stress.

If the filter is installed in the SERF, it makes sense to extend the device. Given the present setup, the sand injector cannot be installed anywhere else other than where the paddlewheel flowmeter is currently located. Presumably, a filter would have the same problem – the PVC run-up to the rectangular portion of the flume is not long enough to accommodate more than one device. Therefore, PVC pipes leading into the rectangular portion of the device should be extended in conjunction with the filter installation so that as water passes through the flume it passes through the pumps, through the filter, past the flowmeter, through the sand injector, and finally into the rectangular portion of the flume.

8.3.2 Non-Essential Final Improvements to the SERF

Although the following improvements to the SERF are listed as "non-essential" their inclusion is beneficial because these improvements will improve the accuracy of the device.

From 2003-2006, three of the twelve crystals in the SEATEK array broke; it is unclear why this happened, but what is clear is that the array should be replaced or fixed so that the crystals work properly. It may be advantageous to replace the array completely so that a faster mechanism can be installed. Computer technology has advanced in the past ten years, and the current ultrasonic array is only capable of sending an output signal once every second. A faster digital signal will allow for less time in between steps, which in turn will allow for a more level sample at the bottom of the SERF.

Secondly, the three-laser leveling system should be replaced with a light-sheet design. When certain materials erode under rock-like conditions, often differential erosion rates are present such that the back-face of the sample erodes faster than the front or vice-versa. When the lasers are used as a stand-alone mechanism for measuring sample flushness (as is necessary with clays), a simple array of three lasers is not enough to account for this. A better design would be to illuminate one side of the sample with a light sheet and install corresponding photoelectric sensors on the other side. Then, when a certain percentage of the light is seen (such as 50%), the sample would advance. This would provide a much more accurate method of leveling sand-clay mixtures with the flume's bottom.

The third improvement is quite simple: a new computer should be added to the SERF control room. The present computer system is old, and sometimes it cannot keep up with a rapidly eroding sample. A new computer running on a 64 bit operating system with more memory is needed.

The fourth improvement that should be made to the SERF is that the stepper motor assembly needs to be redesigned. The current design uses a stepper-motor assembly where the maximum force against the piston is approximately 400 lb. Over time, due to normal wear and tear, the amount of force that can be applied to the piston decreases. Eventually, the motor cannot provide enough force to overcome the friction between the piston's O-rings and the side walls of the piston-casing. What makes matters worse is that during an erosion test, small pieces of sediment get stuck in the tiny gap between the piston and its housing. Although these pieces of sediment are tiny, they are large enough to increase the friction factor between the piston and its housing to the point where the piston can no longer move. When this happens, the motor's gears begin to grind against one another, and eventually the motor burns out. During longer-duration testing (as seen with rock-like material and Gator Rock), this is especially an issue,

because as this is happening the motor heats up rapidly. To prevent this, the motor needs to be replaced by a heavy duty linear actuator. These devices are designed for repeated loading, and will be better able to apply a higher force to the piston. Since 2006, three motors have burned out during SERF testing due to normal motor usage combined with harsh experimental conditions. Rather than spend money on new motors every 18 months, an improvement should be implemented.

The fifth improvement that should be made to the SERF is to install an ultra-sonic Doppler radar (UDV) system for measuring velocity profiles in the device. This system will allow researchers to verify that flow conditions in the SERF are fully developed.

8.3.3 Determine Erosion Patterns for Natural Sand-Clay Mixtures

Once final improvements and enhancements have been made, the next step is to determine how natural sand-clay mixtures behave when subjected to SERF testing. As discussed, sensitivity exists between erosion rates and sample preparation methods. Rather than engineer a series of materials to behave differently, it makes more sense to mimic natural erosion patterns during future tests. Therefore, natural materials need to be obtained and tested in the flume to see how they react to erosion rate testing. These materials should be subjected to a series of tests under clear water and simulated live-bed conditions. Because the filter will have been installed, these tests will now be possible. These samples also should be subjected to tensile and compressive strength testing (if strong enough) to determine if the relationships developed for erosion rate as a function of cohesion presented in Chapter 6 is still valid.

8.3.4 Roughness Number Tests or Improved Testing Apparatus

As discussed in Chapter 3, shear stress is sensitive to sample roughness. Because it is not yet possible to measure shear stress at the same time as erosion rate, the question as to how to properly measure erosion rates and shear stresses of natural samples is difficult to answer. If it continues to be impossible to measure erosion rate and shear stress at the same time, then the most effective alternative is to measure a sample's roughness and use that to approximate the shear stress on it.

Curves have already been developed for shear stress as a function of flow rate and sediment diameter. Using high-resolution photography (UF has a device that can do this), it should be possible to measure the roughness associated with these samples. Then, given a natural sample, the cameras can be used to approximate its roughness and existing shear stress curves can be used to determine shear stresses associated with given flow rates.

Alternatively, using the principles from the shear stress sensor, it may be possible to engineer a device that can measure erosion rate and shear stress at the same time. Both approaches should be investigated.

8.3.5 Normal Stress Measurements in SERF

Preceding discussion assumes particle-like erosion, but as discussed several times, for cohesive material, a strict particle-like erosion mode is hardly ever seen. The next research step hinges on how natural sand-clay bed materials behave. Hence, first one needs to measure the normal stresses on different sand-clay mixtures to determine under what conditions rock-like erosion dominates. Presumably, if rock-like erosion were to dominate, the normal stresses on a sample should be larger than they would be under particle-like conditions.

If this is not the case, then it may be possible to find a sediment property that would indicate whether or not rock-like erosion is likely. For example, it should be possible to prepare a series of sediments at the same sand-clay ratio, same lift-heights, and different water contents. Based on results presented in Chapter 7, eventually at a certain initial water content, rock-like erosion should become important. Likewise beyond this water content, rock-like erosion may become less important. Similarly, there may be a threshold clay content where rock-like erosion also begins to take an effect. Right now, it is obvious that rock-like rock erosion does not and cannot occur for a 100% sand bed. At what clay content does it begin to become an issue? Finding these threshold values specifically (this report simply defined this as an important variable and helped to bound the problem) may hold the key to explaining when rock-like erosion will occur for a sand-clay mixture.

8.3.6 Normal Stress Measurements under Field Conditions

Because normal stress is caused by the fluctuating velocity component, and the turbulent eddy mixing length is much shorter in the SERF than it is in nature, normal stress measurements

must be compared with normal stress measurements under field conditions to test their validity. A field device or devices should be designed to measure both normal and shear stresses in an actual streambed to answer these questions. Additionally, an upstream Acoustic Doppler Current Profiler (ADCP) probe should be installed in this stream so that conditions can be monitored continuously.

8.3.7 Computer Model

If researchers find that normal stresses are significant, then these field results should be used to calibrate a computer model similar to Briaud's model. The difference between this model and Briaud's is that instead of just returning a maximum shear stress value, this new model may be able to return a normal stress value as well.

8.3.8 Summary of Proposed Future Progression

The preceding discussion is not a comprehensive discussion regarding the cohesive erosion rate problem. Predicting erosion rate for cohesive sediments is complicated and the discussion serves as a logical series of steps based on research presented in this report.

APPENDIX A
SCOUR DEPTHS IN NON-COHESIVE SOILS

A.1 Introduction

As discussed in Chapter 2, erosion of non-cohesive materials is a mode of particle erosion. Erosion processes such as these may be analyzed using a simple force balance relationship. When a non-cohesive particle is resting on the bed and water passes over top of it, the particle is subjected to a drag force, F_D and a lift force F_L where the magnitude of these forces is a function of the particle's geometry. An expression for drag forces and lift forces has been developed such that:

$$F_D = 0.5 C_D \rho A_{yz} u^2 \tag{A-1}$$

$$F_L = 0.5 C_L \rho A_{xy} u^2 \tag{A-2}$$

where A_{xy} is the planform area of the particle, A_{yz} is the cross-sectional area of the particle, ρ is the density of water, u is the fluid velocity, and C_L and C_D are experimentally determined drag and lift coefficients.

Under non-erosion conditions, these drag forces and lift forces, plus the buoyant weights of the particle are balanced by bed friction and the force of gravity. Under erosion conditions, the flow velocity, u, must become high enough to cause the lift force, F_L to overcome the force of gravity; or u must become high enough for the drag force on the particle, F_D to overcome the force of static friction between the particle and the bed. When the lift force becomes larger than the drag force, the particle is said to go into suspension whereas when the drag force overcomes the friction force, the particle is said to be moving as part of the bed-load.

In 1936, Shields studied the minimum velocity required to initiate incipient motion of bed particles of various sizes, and he developed a diagram similar to Figure A-1.

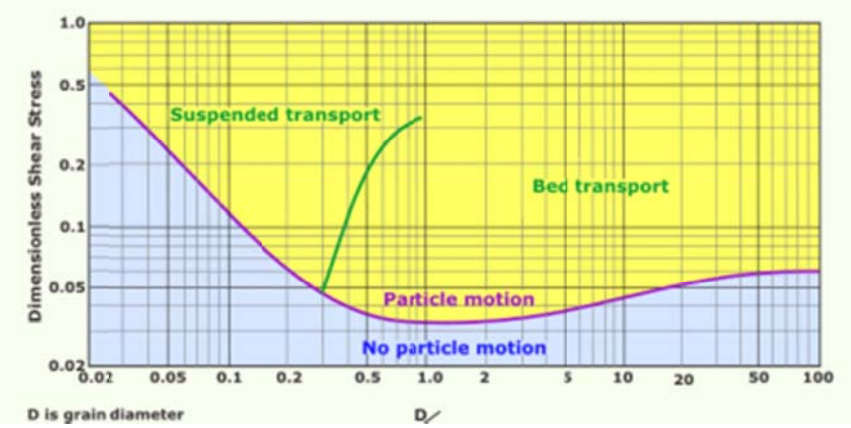

Figure A-1. Shields Diagram (Lemke 2010)

where below the purple line, there is no sediment motion and above the line, sediment will erode. The green line (Developed by Bagnold in 1966) divides the bed load from the suspended load.

Although this analytical approach to solving the erosion problem is elegant, the hydrodynamics in the vicinity of a scouring structure are complicated, and to date, a comprehensive theoretical solution to the scour problem could not be found. To solve analytically, flow conditions in the vicinity of a complex pier would need to be solved so that one could determine when flow velocity exceeded the critical velocity of the bed material.

Because of the difficulties associated with solving for these hydrodynamic conditions, an empirical approach has been used when solving for particle scour. The following is an analysis of the existing empirical standards for estimating scour depths due to non-cohesive sediment transport.

A.2 HEC-18: Basic Principles (Richardson and Davis 2001)

HEC-18 instructs an engineer to compute the scour effects from aggradation/degradation, general scour, contraction scour, and local scour. Then, the effects from each of these parameters are added and the total scour depth is computed.

A.2.1 HEC-18: Long Term Aggradation and Degradation (Richardson and Davis 2001)

Long term aggradation and degradation are computed by using a three-level fluvial system approach. First, a qualitative determination regarding long-term stream stability is established using general geomorphic and river mechanics relationships. Then, engineering analyses follow

where the probable behavior of the stream system is estimated. Finally, physical models or computer models are to be used to predict quantitative changes to the streambed elevation. According to HEC-18, acceptable computer models include Bridge Stream Tube Model for Alluvial River Simulation (BRI-STARS) and USACE HEC-6, Scour and Deposition in Rivers and Reservoirs computer model (Richardson and Davis 2001).

A.2.2 HEC-18: Contraction Scour (Richardson and Davis 2001)

To find the design contraction scour depth, first an engineer must determine if flow upstream from a bridge or an obstruction is already transporting bed material. Therefore the critical velocity for incipient motion, V_c, needs to be computed based on the upstream bed material's mean diameter, D_{50}. According to HEC-18, critical velocity is computed using the following equation:

$$V_c = K_u y^{1/6} D^{1/3} \tag{A-3}$$

where K_u is a constant that is dependent on English or SI units (6.19 for SI units, 11.17 English units), y is the average flow depth upstream from the bridge or obstruction, and D is the average particle size. Once critical velocity is known, the engineer can compute determine whether clear water ($V < V_c$ and there are no particles in suspension) or live-bed ($V > V_c$ and there are particles in suspension) conditions are present.

For clear water conditions, contraction scour is computed using Equation A-4:

$$y_2 = \left[\frac{K_u Q^2}{D_m^{2/3} W^2} \right]^{1/7} \tag{A-4}$$

where y_2 is the equilibrium scour depth after contraction scour, Q is the discharge through the obstruction, D_m is the diameter of the smallest nontransportable particle in the bed material ($1.25D_{50}$) in the contracted section, W is the bottom width of the contracted section minus the pier widths, and K_u again is a constant that is unit dependent (0.025 for SI units and 0.0077 for English units).

For live-bed conditions, contraction scour is computed using Equation A-5:

$$\frac{y_2}{y_1} = \left(\frac{Q_2}{Q_1} \right)^{6/7} \left(\frac{W_1}{W_2} \right)^{k_1} \tag{A-5}$$

where y_1 is the average depth in the upstream channel, y_2 is the average depth in the contracted section, Q_1 is the flow in upstream channel, Q_2 is the flow in the contracted channel, W_1 is the width of the upstream channel, W_2 is the width of the contracted section, and k_1 is an exponent based on shear velocity in the upstream section and fall velocity of the bed material. k_1 can be determined via Table A-1 and Equation A-6:

Table A-1. Values for k_1

V^*/ω	k_1	Mode of Bed Transport
<0.50	0.59	Mostly contact bed material discharge
0.50 to 2.0	0.64	Some suspended bed material discharge
>2.0	0.69	Mostly suspended bed material discharge

$$V^* = \left(\frac{\tau_0}{\rho}\right)^{1/2} = (gy_1 S)^{1/2} \tag{A-6}$$

where V^* is the shear velocity, g is the acceleration due to gravity, τ_0 is the shear stress on the bed, ρ is the density of water, ω is the fall velocity as determined from Figure A-2, and S_1 is the slope of the energy grade line of the main channel.

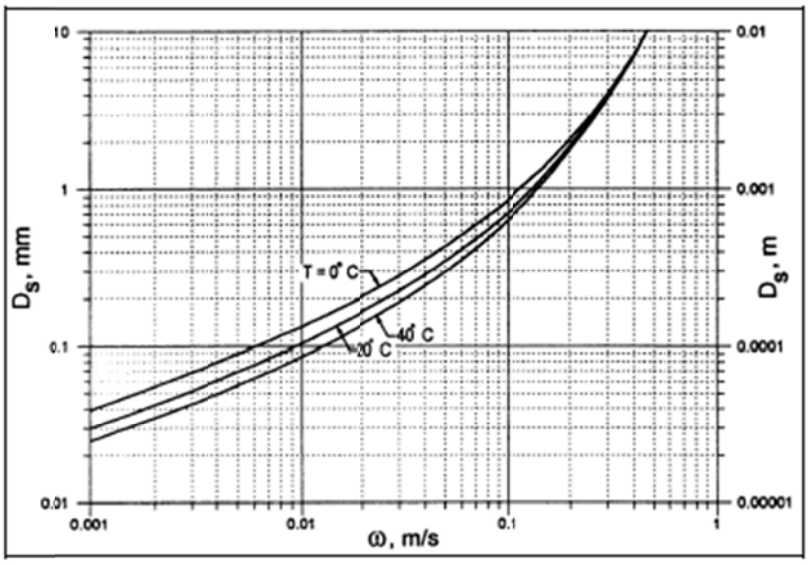

Figure A-2. Fall Velocity vs. Grain Size (Richardson and Davis 2001)

A.2.3 HEC-18: Local Scour (Richardson 2001)

Local scour is computed with the underlying assumption that each parameter that affects the final depth of the scour hole is independent of the other parameters. In other words, the effects of angle of attack, shape of the pier, spacing between pier piles, bed conditions, and armoring are computed separately. Then, these parameters are fit together with the following equation:

$$\frac{y_s}{a} = K_1 K_2 K_3 K_4 \left(\frac{y_1}{a} \right)^{0.35} Fr_1^{0.43} \tag{A-7}$$

where K_1, is the correction factor due to pier shape, K_2 is the correction factor for angle of attack, K_3 is the correction factor for the bed conditions (live bed or clear water), and K_4 is the correction factor for armoring; y_s is the depth of the scour hole, a is the pier width and Fr_1 is the Froude Number defined by

$$Fr_1 = \left(\frac{V_1}{g y_1} \right)^{1/2} \tag{A-8}$$

where V_1 is the velocity upstream from the pier and y_1 is the depth upstream from the pier (Richardson 2001).

The correction factor, K_1 is calculated using Figure A-3 and Table A-2:

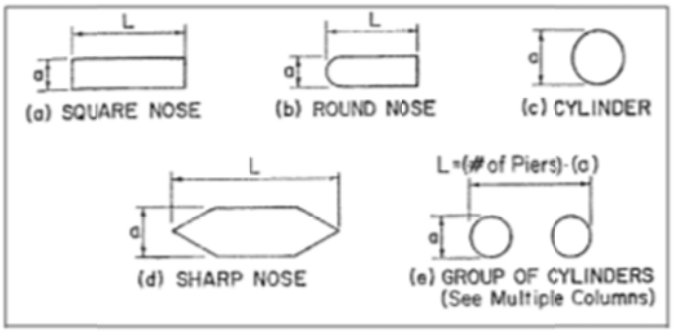

Figure A-3. Common Pier Shapes (Richardson and Davis 2001)

Table A-2. Pier Nose Shape Correction Factors (Richardson and Davis 2001)

Correction Factor K_1 For Pier Nose Shape	
Shape of Pier Nose	K_1
(a) Square nose	1.1
(b) Round nose	1.0

(c) Circular nose	1.0
(d) Group of cylinders	1.0
(e) Sharp nose	0.9

The correction factor K_2 is computed using Equation A-9:

$$K_2 = \left(\cos\theta + \frac{L}{a \sin\theta} \right)^{0.65} \tag{A-9}$$

where θ is the attack angle, and L and a were previously defined as the length and width of the pier respectively.

The correction factor K_3 is found using Table A-3:

Table A-3. Bed Condition Correction Factors

Increase in Equilibrium Pier Scour Depths, K_3, for Bed Condition		
Bed Condition	Dune Height (m)	K_3
Clear-water scour	N/A	1.1
Plane bed and antidune flow	N/A	1.1
Small dunes	3 > H ≥ 0.6	1.1
Medium dunes	9 > H ≥ 3	1.2 to 1.1
Large dunes	H ≥ 9	1.3

Finally, the correction factor K_4 is computed using a series of equations:

$$K_4 = 0.4(V_R)^{0.15} \tag{A-10}$$

$$V_R = \frac{V_1 - V_{icD_{50}}}{V_{cD_{50}} - V_{icD_{95}}} > 0 \tag{A-11}$$

$$V_{icD_x} = 0.645 \left(\frac{D_x}{a} \right)^{0.053} V_{cD_x} \tag{A-12}$$

$$V_{cD_x} = K_u y_1^{1/6} D_x^{1/3} \tag{A-13}$$

In these equations, V_{icDx} is the approach velocity required to initiate scour at the pier for a given grain size, D_x, and V_{cDx} is the critical velocity for incipient motion for the grain size, D_x; y_1 is the depth of flow just upstream of the pier; V_1 is the velocity of approach flow upstream of the pier,

and K_u us a constant that is unit-dependent (6.19 for SI and 11.17 for English). HEC-18 recommends a minimum value of K_4 of 0.4.

The preceding equations assume a narrow pier. For wide piers, or piers that have multiple piles or pile caps, the equations become somewhat more complicated. To compute scour for a wide pier, an additional correction factor, K_w is introduced and Equation A-7is modified:

$$\frac{y_s}{a} = K_w K_1 K_2 K_3 K_4 \left(\frac{y_1}{a}\right)^{0.35} Fr_1^{0.43} \tag{A-14}$$

$$K_w = 2.58\left(\frac{y}{a}\right)^{0.34} Fr^{0.65} \text{ for } \frac{V}{V_c} < 1 \tag{A-15}$$

$$K_w = 1.0\left(\frac{y}{a}\right)^{0.13} Fr^{0.25} \text{ for } \frac{V}{V_c} \geq 1 \tag{A-16}$$

When computing scour when there are multiple piles, a pile cap, and/or a pier involved, scour is computed by adding the effects of scour due to these three components:

$$y_s = y_{spier} + y_{spc} + y_{spg} \tag{A-17}$$

where y_{spier} is the scour component from the pier stem, y_{spc} is the scour component due to the pile cap and y_{spg} is the scour component due to the pile group. The equation for computing y_{spier} is similar to Equation A-18:

$$\frac{y_{spier}}{y_1} = K_{hpier}\left[2.0 K_1 K_2 K_3 K_4 \left(\frac{a_{pier}}{y_1}\right)^{0.65} \left(\frac{V_1}{\sqrt{g y_1}}\right)^{0.43}\right] \tag{A-18}$$

The difference between Equation A-18 and Equation A-14 is the introduction K_{hpier}, which is the coefficient used to account for both the height of the pier stem above the bed and the shielding effect by the pile cap overhanging distance *f* in front of the pier stem. K_{hpier} is found by using Figure A-4:

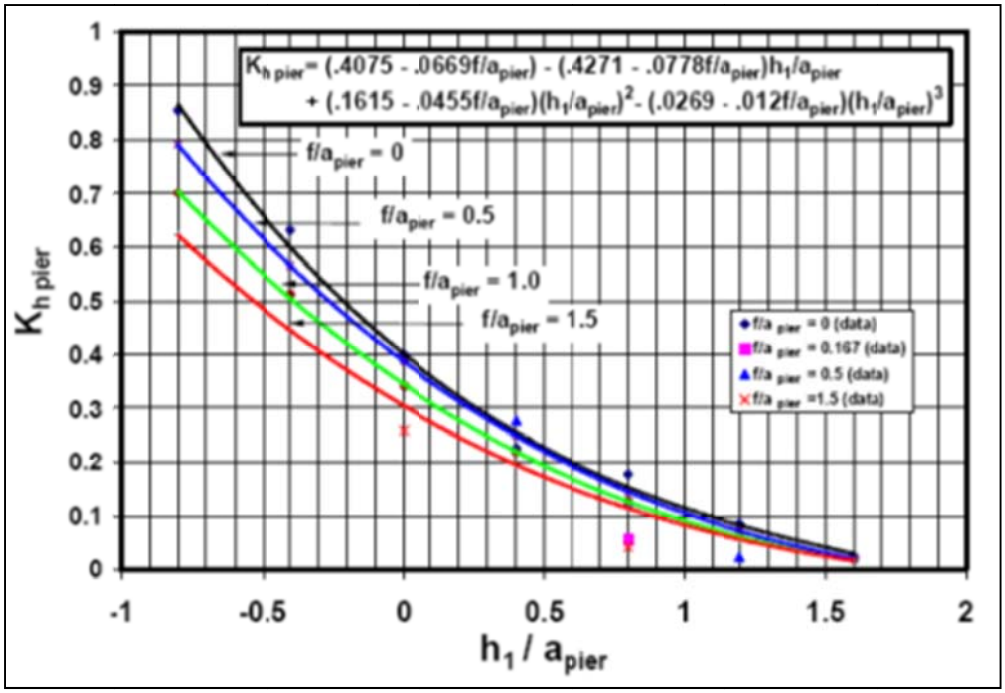

Figure A-4. Diagram used to determine K_{hpier} (Richardson and Davis 2001)

Scour from the pile cap is divided into two scenarios. On one hand, the bottom of the pile cap may be above the bed and in the flow path. On the other hand the pile cap may be located on or below the bed. When the pile cap is above the bed, the technique for computing scour is to reduce the pile cap width to an equivalent pier depth and width, a^*_{pc}, using Figure A-5:

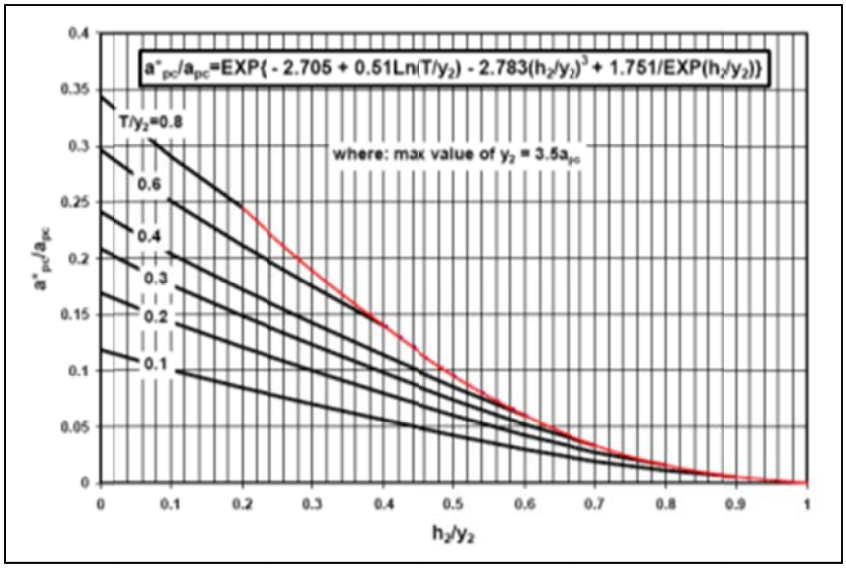

Figure A-5. Diagram used to determine a^*_{pc} (Richardson and Davis 2001)

Then, scour for the pile cap component is computed using Equation A-19:

$$\frac{y_{spc}}{y_2} = 2.0K_1K_2K_3K_4K_w\left(\frac{a^*_{pc}}{y_2}\right)^{0.65}\left(\frac{V_2}{\sqrt{gy_2}}\right)^{0.43} \quad \text{(A-19)}$$

Under the scenario where the pile cap is on or below the bed, a slightly different series of equations, Equation A-20, Equation A-21, and Equation A-22 are used instead:

$$\frac{y_{spc}}{y_2} = 2.0K_1K_2K_3K_4K_w\left(\frac{a_{pc}}{y_2}\right)^{0.65}\left(\frac{V_f}{\sqrt{gy_f}}\right)^{0.43} \quad \text{(A-20)}$$

$$\frac{V_f}{V_2} = \frac{\ln\left(10.93\frac{y_f}{K_s}+1\right)}{\ln\left(10.93\frac{y_2}{K_s}+1\right)} \quad \text{(A-21)}$$

$$y_f = h_1 + \frac{y_{xpier}}{2} \quad \text{(A-22)}$$

In these equations, V_f is the average velocity in the flow zone below the top of the footing and y_f is the distance from the bed to the top of the footing. Figure A-6 is an illustration of these parameters:

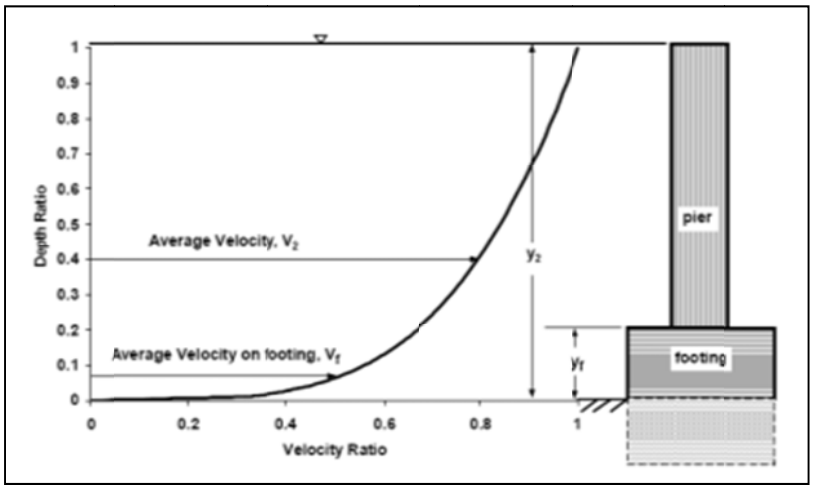

Figure A-6. Illustration sketch for computing scour when a pile cap is above the bed (Richardson and Davis 2001)

When the footing is on or above the bed, there is no need to compute the scour effect from the pile group. Therefore, under this scenario, Equation A-22 can be modified:

$$y_s = y_{spier} + y_{spc} \quad \text{(A-23)}$$

The strategy for finding the scour component that results from a pile group is to represent the pile group by an equivalent solid pier width, a^*_{pg}, which is found using Equation A-24:

$$a^*_{pg} = a_{proj} K_{sp} K_m \quad \text{(A-24)}$$

K_m is the number of rows factor, and it is equivalent to 1.0 for the general case of skewed or staggered rows of piles. When piles are aligned, K_m must be determined from Figure A-7:

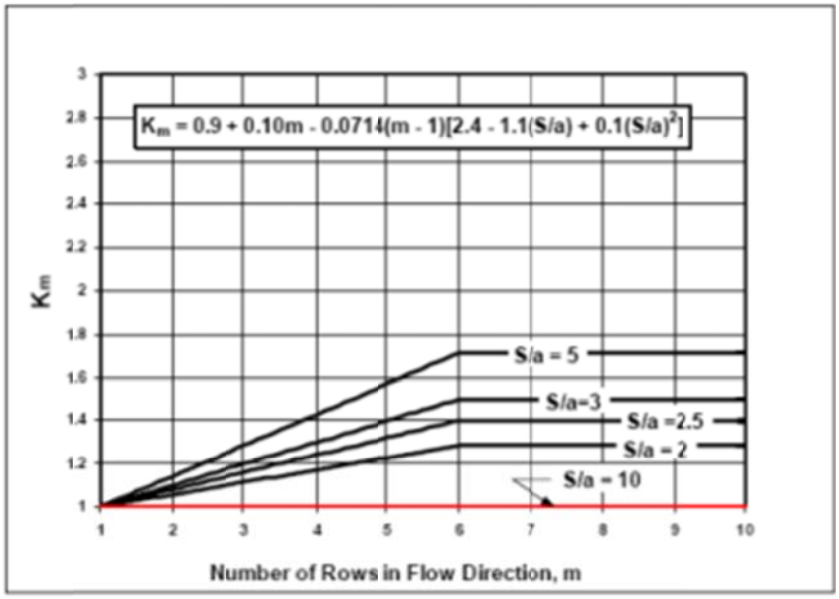

Figure A-7. Diagram for computation of correction factor, K_m (Richardson and Davis 2001)

To illustrate how to compute the projected pile group equivalent pier width, Figure A-8 is useful:

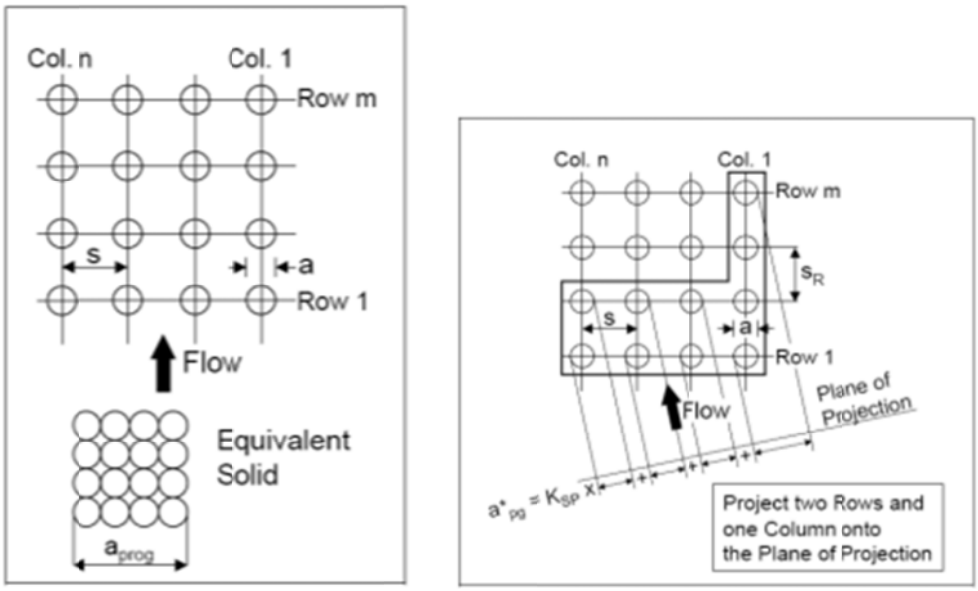

Figure A-8. Diagrams used to illustrate computation of equivalent pier width (Richardson and Davis 2001)

The coefficient of spacing, K_{sp} is found using Figure A-9:

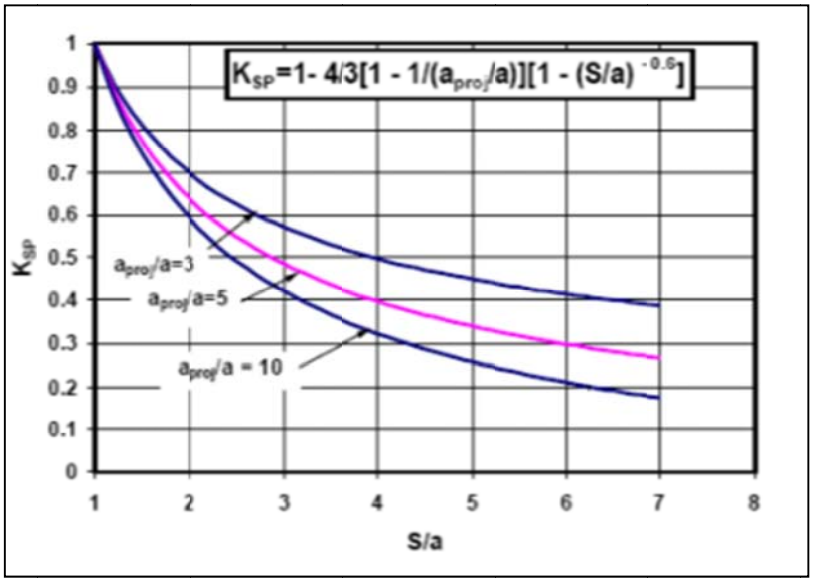

Figure A-9. Diagram used to compute the spacing coefficient, K_{sp} (Richardson and Davis 2001)

Finally, the scour component from the pile group is computed using Equation A-25, Equation A-26, and Equation A-27:

$$y_3 = y_1 + \frac{y_{spier}}{2} + \frac{y_{spc}}{2} \tag{A-25}$$

$$V_3 = V_1\left(\frac{y_1}{y_3}\right) \tag{A-26}$$

$$h_3 = h_0 + \frac{y_{spier}}{2} + \frac{y_{spc}}{2}$$

$$\frac{y_{spg}}{y_3} = K_{hpg}\left[2.0K_1K_3K_4\left(\frac{a^*_{pg}}{y_3}\right)^{0.65}\left(\frac{V_3}{\sqrt{gy_3}}\right)^{0.43}\right] \tag{A-27}$$

The pile group high factor, K_{hpg} is given in Figure A-10:

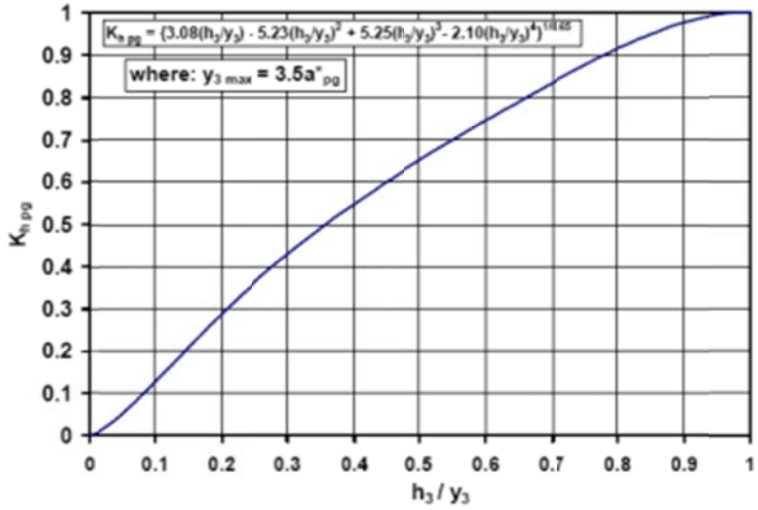

Figure A-10. Diagram used to compute the pile group height adjustment factor, K_{hpg} (Richardson and Davis 2001)

A.2.4 HEC-18: Brief Discussion

The local scour equations from HEC-18 are based on a series of tests at CSU, and they are empirical. Because these equations are empirical, after they were introduced, there was some concern that they may need to be slightly adjusted. This will be discussed in the subsequent section.

A.3 The Florida DOT Bridge Scour Manual

The FDOT Bridge Scour Manual (FDOTBSM) was published in 2005, and it is another source that can be used to compute design scour depth. This document is similar to HEC-18 in many respects; in both documents the scour component associated with long-term

aggradation/degradation, contraction scour, general scour, and local scour are computed independently and added together. To compute total scour, the FDOTBSM uses the same equations and recommendations as HEC-18 for scour components except for local scour.

A.3.1 Local Scour: Motivation for a Different Computation Algorithm

Computation of local scour is different in the FDOTBSM than it is in HEC-18. The FDOTBSM argues that because the CSU equations (HEC-18 equations) are empirical and based on small-scale laboratory data, they may yield different results when they are applied to prototype scale structures. The hydrodynamics surrounding the scour problem would appear to indicate that this is a valid concern, and an order of magnitude analysis can be used to illustrate this point:

1.) Under field conditions: assume a typical bridge pier width of 1.0m and a typical grain size of $1x10^{-4}$m; the ratio of grain size to pier width is on the order of $1x10^{-4}$m.
2.) Under laboratory conditions: grain size of sand cannot change because if the sand were smaller, it would no longer be a sand. Instead, it would be a cohesive material like a silt, and it would be affected by associated cohesive forces. However laboratory pier width may be on the order of 1 cm. Therefore the ratio of grain size to pier width is two orders of magnitude smaller – $1x10^{-2}$.

In 1988, Melville proposed a design method that allowed the designer to follow flow charts to calculate the limiting armor velocity and the local scour depth. According to this study, the maximum scour depth that can occur equals 2.4 times the pier diameter. However, when the designer is dealing with shallow water, larger sediment grain sizes, and clear water conditions, Melville proposed that this 2.4 factor should be reduced based on dimensionless flow velocity, V/V_c; the ratio of flow depth to pier diameter, y_0/D_{50}; the ratio of pier diameter to sediment grain size, b/D_{50}; and shape and alignment factors (Melville and Sutherland1988).

In the early 2000's, Dr. Sheppard of UF conducted three series of prototype-scale tests under both clear-water and live-bed conditions (Sheppard, et al. 2004). The first series of tests, which were conducted in Turners Falls, MA, tested scour depths of three pier sizes and three sediment sizes over a range of depths and velocities under clear water conditions. An interesting phenomenon was noticed during this study. The water supply for this flume study was taken from a hydroelectric power plant reservoir, and there was no control over the amount of

suspended sediment in it. During testing, Sheppard noticed sudden increases in shear stresses that were attributed to reduced levels of turbulence from increased suspended sediment load during high runoff events such as snow melt. Sheppard reasoned that these suspended sediments slowed or stalled the formation of equilibrium scour depths because the sediment helped to dampen the turbulence. The implication here is that under live-bed conditions the equilibrium scour depth may be lower than it would be under clear water conditions (Sheppard et. al. 2004).

In 2004, Sheppard launched a second study concerning an additional pressure gradient factor affecting the formation of local scour (Sheppard 2004). According to Sheppard, the pressure field adjacent to the bed is determined by the pressure field in the main flow. When a pier or another structure interrupts the flow, pressure gradients near the structure will impose forces on sediment particles of a greater magnitude than drag forces because of the water flowing around the sediment particles. Sheppard mathematically explored these pressure gradient forces and their dependence on the D/D_{50}; and he found that the magnitude of these forces caused by this pressure gradients decreased as this ratio increased (Sheppard 2004). This observation agreed with his previous experimental work (Slagle 2006).

Sheppard's third study was conducted at the University of Auckland and its purpose was to investigate live-bed local pier scour for a circular pile and compare calculated equilibrium scour depths with those that are physically measured. Sheppard observed a decreased dependence of normalized equilibrium scour on D/D_{50} at higher values of V/V_c where D is the pier width, D_{50} is the median sediment grain size, V is the upstream flow velocity, and V_c is the sediment critical velocity (Sheppard 2006b).

The combination of these tests helped in development of the equations in the FDOTBSM for local scour. According to Slagle, these equations are the most successful at predicting the local scour depth. Slagle says that the average percent difference in results between computed scour depth and measured scour depth was 16.6%; the standard deviation was 18.2% (Slagle 2006).

A.3.2 FDOTBSM: Local Scour Equations (Florida DOT Bridge Scour Manual 2005)

For computing the design scour depth of a pier under clear-water conditions, pier, Equation A-28 is used:

$$\frac{y_x}{D^*} = 2.5 \tanh\left[\left(\frac{y_0}{D^*}\right)^{0.4}\right]\left\{1 - 1.75\left[\ln\left(\frac{V}{V_c}\right)\right]^2\right\}\left[\frac{D/D_{50}}{0.4\left(D^*/D_{50}\right)^{0.5} + 10.6\left(D^*/D_{50}\right)^{-0.13}}\right] \quad \text{(A-28)}$$

Equation A-28 is only appropriate when ($0.47 < V/V_c < 1$). Under live-bed conditions ($1 < V/V_c < V_{lp}/V_c$), Equation A.3-2 is used to compute the design scour depth up until the live-bed peak:

$$\frac{y_x}{D^*} = \tanh\left[\left(\frac{y_0}{D_{50}}\right)^{0.4}\right] \times \left[\begin{array}{l} 2.2\left(\dfrac{V/V_c - 1}{V_{lp}/V_c - 1}\right) \\ + 2.5\left\{\dfrac{D^*/D_{50}}{0.4\left(D^*/D_{50}\right)^{1.2} + 10.6\left(D^*/D_{50}\right)^{-0.13}}\right\}\left(\dfrac{V_{lp}/V_c - V/V_c}{V_{lp}/V_c - 1}\right) \end{array}\right] \quad \text{(A-29)}$$

Beyond the live-bed peak, Equation A-30 is used to compute local scour for a pier:

$$\frac{y_x}{D^*} = 2.2 \tanh\left[\left(\frac{y_0}{D^*}\right)^{0.4}\right] \quad \text{(A-30)}$$

In these equations, D^* is the effective diameter of the pier, and it is given in Figure A-11,

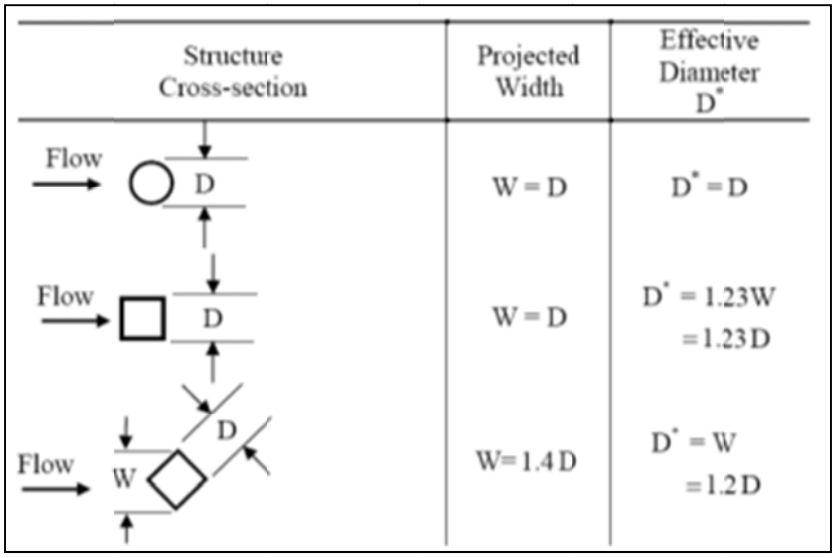

Figure A-11. Effective Diameter for Different Pier Shapes (Richardson and Davis 2001)

y_s is the equilibrium scour depth, V is the water velocity just upstream from the pier, V_c is the critical velocity, V_{lp} is the live-bed scour peak velocity, and y_0 is the initial water depth. Critical velocity is computed using Equation A-31 through Equation A.3-35; live-bed scour peak velocity is computed using Equation A-36 through Equation A-39.

$$V_c = 2.5u_{*c}\ln\left(\frac{y_0}{2.72z_0}\right) \tag{A-31}$$

$$u_{*c} = \sqrt{\frac{\tau_c}{\rho}} = \text{critical friction velocity} = \sqrt{\Theta_c(sg-1)gD_{50}} \tag{A-32}$$

$$\Theta_c = \begin{cases} 0.25 - 0.1\sqrt{d_*} \text{ for } 0.01 < d_* < 3 \\ 0.0023d_* - 0.000378d_*\ln(d_*) + 2.23/d_* - 0.005 \text{ for } 3 < d_* < 150 \\ 0.0575 \text{ for } d_* > 150 \end{cases} \tag{A-33}$$

$$d_* = D_{50}\left[(sg-1)g/\upsilon^2\right]^{1/3} \tag{A-34}$$

$$z_0 = \begin{cases} \upsilon/(9u_{*c}) \text{ for } 0 < \mathrm{Re}_c \le 5 \\ k_s 10^{-3}\left[-6 + 2.85\,\mathrm{Re}_c - 0.58\,\mathrm{Re}_c \ln \mathrm{Re}_c + 0.002\,\mathrm{Re}_c^2 + 111/\mathrm{Re}_c\right] \text{for } 5 < \mathrm{Re}_c \le 70 \\ k_x/30 \text{ for } \mathrm{Re}_c > 70 \end{cases} \tag{A-35}$$

$$k_s = \begin{cases} 2.5D_{50} \text{ for } D_{50} \ge 0.6mm \\ 5D_{50} \text{ for } D_{50} < 0.6mm \end{cases} \tag{A-36}$$

$$V_1 = 0.8\sqrt{gy_0} \tag{A-37}$$

$$V_2 = 29.31u_{*c}\log(4y_0/D_{50}) \tag{A-38}$$

$$V_{lp} = \begin{cases} V_1 \text{ if } V_1 \ge V_2 \\ V_2 \text{ if } V_1 < V_2 \end{cases} \tag{A-39}$$

To compute the design scour depth for a complex pier, the FDOTBSM uses a similar approach to HEC-18: the effects of scour of the pier, the pile group, and the pile cap are computed separately and added together. This assumes that these three components of scour act separately and do not interact. The difference between HEC-18 and the FDOTBSM is that the FDOT Manual looks for an effective pier diameter for each of these three shapes and then it uses this diameter to compute the scour depth. Conversely, HEC-18 applies a correction factor, K_x to the scour parameter instead of the effective diameter parameter.

Explicitly, the total scour of a complex pier in the FDOTBSM is computed by:

$$D^* = D^*_{col} + D^*_{pc} + D^*_{pg} \tag{A-40}$$

To compute the effective column (pier) diameter, Equation A-41 through Equation A-46 are used:

$$D_{col}^{*} = \begin{cases} K_s K_\alpha K_f b_{col}\left[0.1162\left(\frac{H_{col}}{y_{0(\max)}}\right)^2 - 0.3617\left(\frac{H_{col}}{y_{0(\max)}}\right) + 0.2476\right] \text{for } 0 \le \frac{H_{col}}{y_{0(\max)}} \le 1 \\ 0 \text{ for } \frac{\mathrm{H_{col}}}{\mathrm{y_{0(max)}}} > 1 \end{cases} \quad \text{(A-41)}$$

$$y_{0(\max)} = \begin{cases} 5b_{col} \text{ for } y_0 \ge 5b_{col} \\ y_0 \text{ for } y_0 < 5b_{col} \end{cases} \quad \text{(A-42)}$$

$$K_s = \begin{cases} 1 \text{ for circular columns} \\ 0.86 + 0.97\left|\alpha \frac{\pi}{180^o} - \frac{\pi}{4}\right|^4 \text{ for rectangular columns} \end{cases} \quad \text{(A-43)}$$

$$K_\alpha = \frac{b_{col}\cos\alpha + l_{col}\sin\alpha}{b_{col}} \quad \text{(A-44)}$$

$$f = \begin{cases} \frac{3f_1 + f_2}{4} \text{ for } \alpha \le 45^o \\ \frac{3f_2 + f_1}{4} \text{ for } \alpha > 45^o \end{cases} \quad \text{(A-45)}$$

$$K_f = \begin{cases} -.0.12\left(\frac{f}{b_{col}}\right)^2 + 0.03\left(\frac{f}{b_{col}}\right) + 1 \text{for} \left(\frac{\mathrm{f}}{\mathrm{b_{col}}}\right) \le 3 \\ 0 \text{ for} \left(\frac{f}{b_{col}}\right) > 3 \end{cases} \quad \text{(A-46)}$$

To illustrate b_{col}, the column width, and f, the side overhangs, a definition sketch has been provided (Figure A-12).

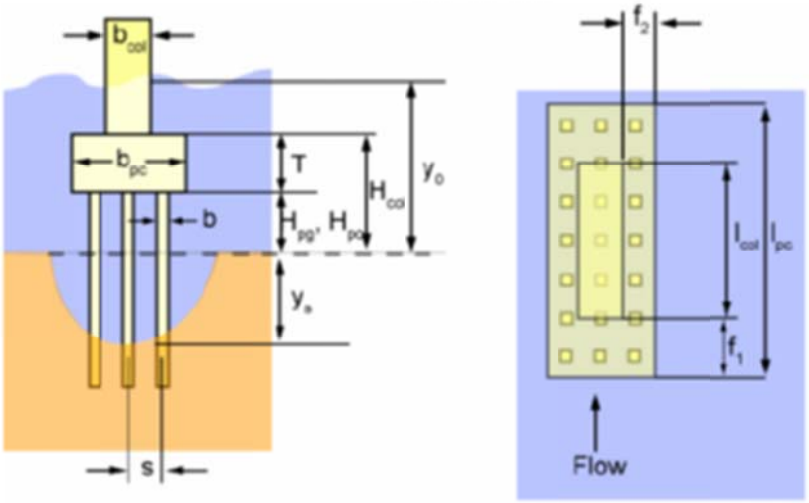

Figure A-12. Definition Sketch for Scour Around a Complex Pier (Richardson and Davis 2001)

To compute the effective pier diameter of the pile cap, Equation A-47 is used:

$$D_{pc}^{*} = K_s K_\alpha b_{pc} \exp\left[-1.04 - 1.77\exp\left(\frac{H_{pc}}{\bar{y}_{0(\max)}}\right) + 1.695\left(\frac{T}{\bar{y}_{0(\max)}}\right)^{0.5}\right] \quad \text{(A-47)}$$

K_a is the same as it was when it was computed for a column except that the pile cap's b is used instead of the column's b; K_s is the same as for a column; $y_{0(max)}$ is computed using Equation A-48

$$y_{0(\max)} = \begin{cases} 1.64\left[T\left(K_x b_{pc}\right)^{2.5}\right]^{2.7} \text{ for } y_0 < 1.64\left[T\left(K_x b_{pc}\right)^{2.5}\right]^{\frac{2}{7}} \\ y_0 \text{ for } y_0 < 1.64\left[T\left(K_x b_{pc}\right)^{2.5}\right]^{\frac{2}{7}} \end{cases} \quad \text{(A-48)}$$

To compute the effective pier diameter for the pile group, Equation A-49 through Equation A-55 are used:

$$D_{pg}^{*} = K_{sp} K_h K_m K_s W_p \quad \text{(A-49)}$$

$$K_s = \frac{K_{s(pile)} - K_{s(pilegroup)}}{9}\left(\frac{s}{b}\right) + K_{s(pile)} - \frac{10}{9}\left(K_{s(pile)} - K_{s(pilegroup)}\right) \quad \text{(A-50)}$$

$$K_{s(\text{pile or pile group})} = \begin{cases} 1 \text{ for circular piles or pile group arrays} \\ 0.86 + 0.97\left|\alpha\frac{\pi}{180} - \frac{\pi}{4}\right|^4 \text{ for square piles or rectangular pile groups} \end{cases} \quad \text{(A-51)}$$

$$K_{sp} = 1 - \frac{4}{3}\left(1 - \frac{w_{pi}}{W_p}\right)\left(1 - \frac{1}{\left(\frac{s}{w_{pi}}\right)^{0.6}}\right) \quad \text{(A-52)}$$

$$K_m = \begin{cases} 0.045m + 0.96, |\alpha| < 5 \;\&\; m \le 5 \\ 1.19, |\alpha < 5 \;\&\; m > 5| \\ 1, |\alpha > 5| \end{cases} \quad \text{(A-53)}$$

$$\bar{y}_{0(\max)} = \begin{cases} \bar{y}_0, \bar{y}_0 \le 2K_s W_p K_{sp} K_m \\ 2K_s W_p K_{sp} K_m, \bar{y}_0 > 2K_s W_p K_{sp} K_m \end{cases} \quad \text{(A-54)}$$

$$K_h = \begin{cases} 1.5\tanh\left(0.8\sqrt{\dfrac{\overline{H}_{pg}}{\overline{y}_{0(\max)}}}\right) \text{ for } 0 \le \dfrac{\overline{H}_{pg}}{\overline{y}_{0(\max)}} \le 1 \\ 0 \text{ for } 0 \le \dfrac{\overline{H}_{pg}}{\overline{y}_{0(\max)}} < 0 \\ 1 \text{ for } 0 \le \dfrac{\overline{H}_{pg}}{\overline{y}_{0(\max)}} > 1 \end{cases} \quad \text{(A-55)}$$

2.2.2.4 FDOTBSM: Brief Discussion

As briefly mentioned in Section A.3.1, these series of equations have been the most successful equations for predicting bridge pier scour depths. An example of predicted vs. measured scour depths is presented in Figure A-13:

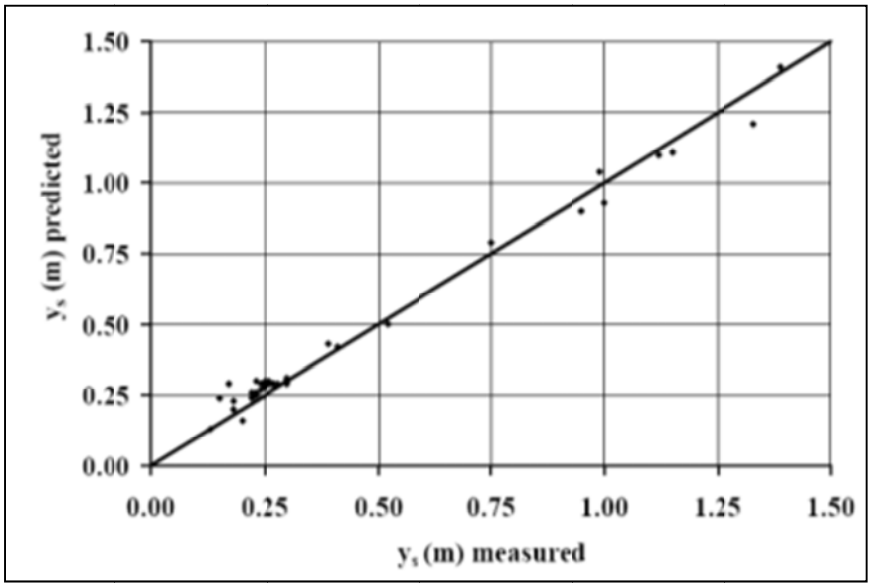

Figure A-13. Measured vs. computed scour depths (FDOT Bridge Scour Manual 2005)

These equations in the FDOT Bridge Scour Manual are considered by many to be the state of the art with the regard to predicting scour depths for a cohesionless sediment. They appear to provide excellent results, and although they are somewhat complicated, they are easily programmed into a computerized algorithm. Unfortunately, the FDOTBSM does not give any recommendations as far as designing scour depths for rock or cohesive sediments. Therefore, an

engineer has no choice but to refer back to HEC-18 for guidelines when designing for these bed materials.

LIST OF REFERENCES

Annandale, G. W., Smith, S.P., Nairn, R. and Jones, J.S. (1996). "Scour power." *Journal of Civil Engineering*, July, 58-60, cited in Slagle, P.M. (2006).

Annandale, G.W. (2005). *Scour technology*. McGraw-Hill, New York.

Ariathurai, R. (1974). "A finite element model for sediment transport in estuaries." Ph.D. dissertation, University of California, Davis, CA.

Bagnold, R. A. (1956). "An approach to the sediment transport problem from general physical." Professional Paper, No. 442-1, USGS, Washington, D.C.

Barry, K. M. (2003). "The effect of clay particles in pore water on the critical shear stress of sand." Ph.D. dissertation, University of Florida, Gainesville, Florida.

Barry, K. M., Thieke, R. J., and Mehta, A. J.(2005). "Quasi-hydrodynamic lubrication effect of clay particles on sand grain erosion." *Estuarine and Coastal Shelf Science* 67, 161 – 169.

Bloomquist, D (2010). Personal conversations and correspondence. Associate Professor, University of Florida, Gainesville, FL.

Bollaert, E. and Schleiss, A. (2003). "Scour of rock due to the impact of plunging high velocity jets part I: a state-of-the-art review." *Journal of Hydraulics Research*, 00(0), 1 – 14.

Bollaert, E. and Schleiss, A. (2003). "Scour of rock due to the impact of plunging high velocity jets part II: experimental results of dynamic pressures at pool bottoms in one- and two-dimensional closed end rock joints." *Journal of Hydraulics Research*, 00(0), 1 – 16.

Briaud J. L. (2004). "Scour#1 killer of bridges." *Geostrata*, The Geotechnical Institute of the American Society of Civil Engineers, Fall.

Briaud, J. L., Chen, H. C., Li, Y. and Nurtjahyo, P. (2004a). "The SRICOS-EFA method for complex piers in fine-grained soils." *Journal of Geotechnical and Geoenvironmental Engineering*, 130(11), 1180 – 1191.

Briaud, J.L., Chen, H. C., Li, Y., Nurtjahyo, P., and Wang, J. (2004b). "Pier and contraction scour in cohesive soils." *NCHRP Report 516*, Transportation Research Board, Washington, D.C.

Briaud, J. L., Chen, H. C. and Ting, F. (2010). "The, EFA, erosion function apparatus: an overview." http://tti.tamu.edu/conferences/scour/sample_paper.pdf, March 23, 2010.

Briaud, J. L., Ting, F. C. K., Chen, H. C., Gudavalli, R., Perugu, S., and Wei, G. (1999). "SRICOS: Prediction of scour rate in cohesive soils at bridge piers." *Journal of Geotechnical and Geoenvironmental Engineering*, 125(4), 237 – 246.

Christensen, B. A. (1972). "Incipient motion on cohesionless channel banks." *Symposium to Honor Professor H. A. Einstein*, edited by H. W. Shen, Colorado State University, Fort Collins, CO, 1 – 22.

Christensen, B. A. (1975). "On the stochastic nature of scour initiation." *Proceedings of the 16th International Association for Hydraulic Research Congress*, Sao Paulo, Brazil (2), 65 – 72.

Cokljat, D., Carter, J. G. and Emerson, D. R. (1996). "Calculation of flow in transition duct using second- order closure and wall functions." *American Instittue of Aeronautics and Astronautics*, 34(11), 2437 – 39.

Cornett, A., Sigouin, N., and Davies, M. (1994). "Erosive response of Northumberland straight till and sedimentary rock to fluid flow." *National Research Council of Canada, Institute for Marine Dynamics*, TR-1994-22, September, Ottowa, Canada, 1 – 15, 26 – 27.

Crowley, R.W. (2008). "Drag forces on pile groups." M.S. Thesis, University of Florida, Gainesville, FL.

Dade, W. B. and Nowell, A. R. M. (1991). "Moving muds in the marine environment." *Proceedings of the 1991 Conference on Coastal Sediments*, ASCE, New York, NY, 54 – 71.

Dade, W. B., Nowell, A. R. M., and Jumars, P. A. (1992). "Predicting erosion resistance of muds." *Marine Geology*, 105, 285 – 97.

Dyer, K. R. (1986). *Coastal and estuarine sediment dynamics*. Wiley Interscience, Chichester, United Kingdom.

Einstein, H. A. (1943). "Flow on a movable bed." *Proceedings from the Second Hydraulics Conference*, Iowa City, 27, 332 – 46.

Einstein, H.A. (1950). "The bed-load function for sediment transportation in open channel flows." *US Department of Agricultural Technologies*, 1026, Washington.

Englund F. and Hansen, E. (1972). *A monograph on sediment transport in alluvial streams*. Technial Press, Copenhagen, Denmark.

"Florida department of transportation bridge scour manual (2005)." <http://www.dot.state.fl.us/rddesign/dr/Bridgescour/FDOT-Scour-Manual-6-2-2005-Final.pdf>, Sept. 2, 2008.

Fukada, M. and Lick, W. J. (1980). "The entrainment of cohesive sediments in fresh water." *Journal of Geophysical Research*, 85(C5) 2813 – 2824, cited in McNeil, J. (1996).

Gessner, F. B., and Emery, A. F. (1980). "The numerical prediction of developing turbulent flow in rectangular ducts." *Journal of Fluids Engineering*, 103, 445 – 455.

Gordon, S. (1991). "Scourability of rock formations." Federal Highway Administration Memorandum, July 19, Washington, D.C.

Hanson, G. J. and Simon, A. (2002). "Discussion of erosion function apparatus for scour rate predictions by J.L. Briaud, F. C. Ting, H. C. Chen, Y. Cao, S. W. Han, and K. W. Kwak." *Journal of Geotechnical and Geoenvironmental Engineering*, 627 – 628.

Henderson, M. R. (1999). "A laboratory method to evaluate the rates of water erosion of natural rock materials." M.S. Thesis, University of Florida, Gainesville FL.

Hofland, B. and Battjes, J. A. (2006). "Probability density function of instantaneous drag forces and shear stresses on a bed." *Journal of Hydraulic Engineering*, 132, (11), 1169 – 1175.

Hjorth, P (1975). "Studies on nature of local scour." *Bulletin Series A, No. 46, Department of Water Resources Engineering, Lund Institute of Technology*, University of Lund, Sweden.

Jepsen, R., Roberts, J. and Lick, W. (1997). "Effects of bulk density on sediment erosion rates." *Water, Air, and Soil Pollution*, 99, 21 – 31.

Jepsen, R., Roberts, J. D. and Gailini, J. (2004). "Erosion measurements in linear, oscillatory, and combined oscillatory and linear flow regimes." *Journal of Coastal Research*, 20(4), 1096 – 1106.

Jones, J. S., Alqalam, Kamel, Gratton, Buddy, Summers, Brian (1995). "Effect of the 1994 southeast flooding on the highway system in Georgia." *Handout from presentation at the 1995 American Society of Civil Engineers Water Resources Engineering Conference*, San Antonio, TX., cited in Mueller, J., "Field based research on channel scour at bridges," <http://water.usgs.gov/osw/techniques/workshop/Mueller.html>, March 22, 2010.

Judson, S., Kaufman, M. E. and Leet, L. D. (1987). *Physical geology*. Prentice-Hall, Englewood Cliffs, NJ.

Kandiah, A. (1974). "Fundamental aspects of surface erosion of cohesive soils." Ph.D. dissertation, University of California, Davis, CA.

Kerenyi, K. (2010). Personal conversations. Lead researcher, FHWA Hydraulics Laboratory, McLean, VA.

Kerr, K. (2001). "A laboratory apparatus and methodology for testing water erosion in rock materials." M.E. thesis, University of Florida, Gainesville, Florida.

Laufer, J. (1954). "The structure of turbulence in fully developed pipe flow." *Report no. 1174, National Advisory Committee for Aeronautics*, Washington, D.C.

Lemke, K. A. (2010). "Stream sediment." University of Wisconsin-Stevens Point, http://www.uwsp.edu/geo/faculty/lemke/geomorphology/lecture_outlines/03_stream_sediment.html, Sept. 14, 2010.

MacIntyre, S., Lick, W. and Tsai, C. H. (1990). "Variability of entrainment of cohesive sediments in freshwater." *Biogeochemistry*,9, 187 – 209, cited in McNeil, J. (1996).

Mantz, P. A. (1977). "Incipient transport of fine grains and flakes by fluids." *Journal of Hydraulics Division of ASCE,* 103(6), 601 – 615.

McLean, S.R. (1975). "Theoretical modeling of deep sediment transport." *Marine Geology*, 66, 243 – 265.

McNeil, J., Taylor, C., and Lick, W. (1996). "Measurements of erosion of undisturbed bottom sediments with depth." *Journal of Hydraulic Engineering*, 122(6), 316 – 324.

Mehta, A. J. (2007). "An introduction to hydraulics of fine sediment transport." *OCP 6297 class notes draft*, University of Florida, Gainesville, Florida.

Mehta, A. J. and Lee, S. C. (1994). "Problems in linking the threshold condition for the transport of cohesionless and cohesive sediment grain." *Journal of Coastal Research*, 10(1), 170 – 177.

Mehta, A. J., Parchure, T. M., Dixit, J. G., and Ariathuri, R. (1982). "Resuspension potential of deposited cohesive beds." *Estuarine comparisons*, edited by V.S. Kennedy, Academic Press, New York, N.Y, cited in McNeil, J. (1996).

Mehta, A. J. and Parachure, T. M. (2000). "Surface erosion of fine-grained sediment revisited." *Muddy coast dynamics and resource management*, edited by: Belmming, B. W., Delfontaine, M. T. and Liebezeit, G., Elsevier, Amsterdam, The Netherlands, 55 – 74.

Melling, A. and Whitelaw, J. H. (1976). "Turbulent flow in a rectangular duct." *Journal of Fluid Mechanics*, 27(2), 289 – 315.

Melville, B. W. and Sutherland, A. J. (1988). "Design method for local scour at bridge piers." *Journal of Hydraulic Engineering, ASCE,* 125(1), 59 – 65, cited in Slagle, P.M. (2006).

Melville, B. W. " Scour at bridge sites." *Civil engineering practices, vol. 2*, edited by Cheremisinoff, N. P., Technomic Publishing, Lancaster, PA, cited in Slagle, P. M. (2006).

Meyer-Peter E. and Mueller, R. "Formulations for bed-load transport." *Proceedings for the 2nd Meeting International Hydraulics Research*. Stockholm, 39 – 64.

Migniot, C. (1989). "Tassement et rheologie des vases, lere partie." *La Houille Blanche*, 1, 11 – 29, cited in Mehta, A. J. (2007).

Miller, R. L. and Byrne, R. J. (1966). "The angle of repose for a single grain on a fixed rough bed." *Sedimentology*, 6, 303 – 314.

Miller, William Jr. (2003). "Model for the time rate of local sediment scour at a cylindrical structure." Ph.D. dissertation, University of Florida, Gainesville, Florida

Mitchener, H. and Torfs, H. (1996). "Erosion of mud/sand mixtures." *Coastal Engineering*, 29, 1 – 25.

Molinas, A (2003). "Bridge scour in nonuniform sediment mixtures and in cohesive materials: synthesis report." *FHWA Report Number FHWA-RD-03-083*, Washington, D.C.

Murillo, J.A. (1987). "The scourge of scour." *Civil Engineering*, American Society of Civil Engineers, 57(7).

Naimi, M. and Gessner, F. B. (1993). "A calculation method for developing turbulent flow in rectangular ducts of arbitrary aspect ratio." *Journal of Fluids Engineering*, 117, 249 – 258.

Nalluri, C. and Alvarez, E. M. (1992). "The influence of cohesion on sediment behavior." *Water Science and Technology*, 25(8), 151 – 164.

Neilsen, P. (1992). *Coastal bottom boundary layer and sediment transport.* World Scientific Publishing, River Edge, NJ.

Niraula, L. D. (2004). "Development of modified T-Z curves for large diameter piles/drilled shafts in limestone for FB-Pier." M.E. Thesis, University of Florida, Gainesville, FL.

Obi, K., Inoue, T. S., Furukawa, T., and Masuda, S. (1996). "Experimental study on the statistics of wall shear stress in turbulent channel flows." *International Journal of Heat and Fluid Flow*, 17(3), 187 – 192.

Papanicolaou, A. N., Diplas, P., Dancey, C. L., and Balakrishnan, M. (2001). "Surface roughness effects in near-bed turbulence: implications to sediment entrainment." *Journal of Engineering Mechanics*, 127(3), 211 – 218.

Panagiotopoulos, I., Voulgaris, G., and Collins, M. B. (1997). "The influence of clay on the threshold of movement of fine sandy beds." *Coastal Engineering*, 32, 19 – 43.

Partheniades, E. (1965). "Erosion and deposition of cohesive soils." *Journal of Hydraulics Division of ASCE*, 91(1), 105 – 138.

Pitocchi, D. (2010). Personal correspondence. Research engineer FDOT State Materials Office, Gainesville, FL.

Placzek, G. and Haeni, F. P. (1995). "Surface-geophysical techniques used to detect existing and infilled scour holes near bridge piers." *U.S. Geological Survey Water Resources Investigation Report 95-4009*.

Raudkivi, A. J. (1990). *Loose boundary hydraulics*. 3rd Edition, Pergamon Press, Oxford, United Kingdom.

Reichardt, H. (1951). "Vollstandige darstellung der turbulenten geschwindig-keitsverteilung in glattern leitungen." *Z. Angew. Math Mech*., 31(7) 208 – 19 (in German), cited in Barry, K. (2003).

Richardson, E. V. and Davis, S. R. (2001). "Evaluating scour at bridges fourth edition." *Publication No. FHWA NHI 01-001 hydraulic engineering circular no. 18*. http://isddc.dot.gov/OLPFiles/FHWA/010590.pdf, Sept. 2, 2008.

Roberts, J., Jepsen, R., Gotthard, D., and Lick, W. (1998). "Effects of particle size and bulk density on erosion of quartz particles." *Journal of Hydraulic Engineering*, 124, 1261 – 1267.

Roberts, S. K., and Yaras, M. I. (2006). "Effects of surface roughness geometry on separation-bubble transition." *Journal of Turbomachinery*, (128)349, 349 – 356.

Rokni, M., Olsson, C., and Sunden, B. (1998). "Numerical and experimental investigation of turbulent flow in a rectangular duct." *International Journal for Numerical Methods in Fluids*, 28, 225 – 242.

"Scour Plan of Action (2009)." http://www.dot.ca.gov/hq/structur/strmaint/scour.htm, December 14, 2009.

Schlichting, H. (1979). *Boundary layer theory*, 7th Edition. McGraw-Hill, New York, NY.

Sferrazza, L and Williams, M (2002). "Pressurized drums, what every handler should know." *Department of Defense Radioactive Waste Generators Conference*, May.

Shah, F. D. (2009). "Development and testing of uniform synthetic limestone samples for the calibration of equipment used to determine erosion rates." Honor's thesis, University of Florida, Gainesville, FL.

Sharif, A.A. (2002). "Critical shear stress and erosion of cohesive soils." Ph.D. dissertation, State University of New York at Buffalo, New York.

Sheppard, D. M. (2004). Personal correspondences and communications. Professor Emeritus, University of Florida, Gainesville, FL.

Sheppard, D. M. (2004). "Overlooked local scour mechanism." *Journal of the Transportation Research Board No. 1890*, TRB, National Research Council, Washington, D.C., 107 – 111.

Sheppard, D. M., Bloomquist, D. and Slagle, P. M. (2006a). "Rate of erosion properties of rock and clay (correlation of erosion rate-shear stress relationships with geotechnical properties of rock and cohesive sediments)." *FDOT Report for Project Number BD-545, RPWO #3.*

Sheppard, D. M. and Miller, W. (2006b). "Live bed and local pier experiments." *Journal of Hydraulic Engineering*, 132(7), 635 – 642.

Sheppard, D. M., Odeh, M., and Glasser, T. (2004). "Live-bed local pier scour experiments." *Journal of hydraulic engineering, ASCE,* 130(10), 957 – 963, cited in Slagle, P. M. (2006).

Shields, A (1936). Application of similarity principles and turbulence research to bed-load movement. *Mitteilunger der Preussischen Versuchsanstalt fur Wasserbau und Schiffbau*, 26, 5 – 24.

Slagle, P. M. (2006). Correlations of erosion rate-shear stress relationships with geotechnical properties of rock and cohesive sediments. M.S. thesis, University of Florida, Gainesville, Florida.

Sumer, M. and Fredsoe, J (2006). *Hydrodynamics around cylindrical structures*. World Scientific Publishing, Hackensack, NJ.

Suntoyo, and Tanaka, H. (2009). "Effect of bed roughness on turbulent boundary layer and net sediment transport under asymmetric waves." *Coastal Engineering*, (56)9, 960 – 969.

Ting, F. C. K., Briaud, J. L., Chen, H. C., Gudavalli, R., Perugu, S., and Wei, G. (2001). "Flume tests for scour in clay at circular piles." *Journal of Hydraulic Engineering*, 127(11), 969 – 978.

Torfs, H. (1996). "Erosion of mud/sand mixtures." Ph.D. Thesis, Catholic University of Leuven, Leuven, Belgium.

Torfs, H., Jiang, J., and Mehta, A. J. (2000). "An assessment of erodibility of fine/coarse sediment mixtures." *Coastal and estuarine fine sediment transport processes*, edited by: McAnally, W. H., and Mehta, A. J., Elsevier, Amserdram, 109 – 123.

Trammel, M. A. (2004). "Laboratory apparatus and methodology for evaluating water erosion rates of erodible rock and cohesive sediments." M.S. thesis, University of Florida, Gainesville, Florida.

Tsai, C.H. and Lick, W. (1988). "Resuspension of sediments from Long Island Sound." *Water Science Technology*, 20(6/7) 155 – 164, cited in McNeil, J. (1996).

Van Prooijen, B. C. and Winterwerp, J. C. (2008). "A stochastic formulation for erosion of cohesive sediments." *Journal of Geophysical Research*, Draft Copy, December 9, 2008.

Van Rijn, L.C. (1992). *Principles of sediment transport in rivers, estuaries, and coastal seas*, Aqua Publications, Amsterdam, The Netherlands.

Wei, G., Chen, H. C., Ting, F., Briaud, J., Gudavalli, R., and Perugu, S. (1997). "Numerical simulation to study scour rate in cohesive soils." *Report for Texas Department of Transportation, Department of Civil Engineering*, Texas A&M University, College Station, TX.

Wiberg, P. L. and Smith, J. D. (1987). "Calculations of the critical shear stress for motion of uniform and heterogeneous sediments." *Water Resources Research*, 23(8), 1471 – 1480.

Yalin, M. S. (1972). *Mechanics of sediment transport*. Pergamon, New York, NY.